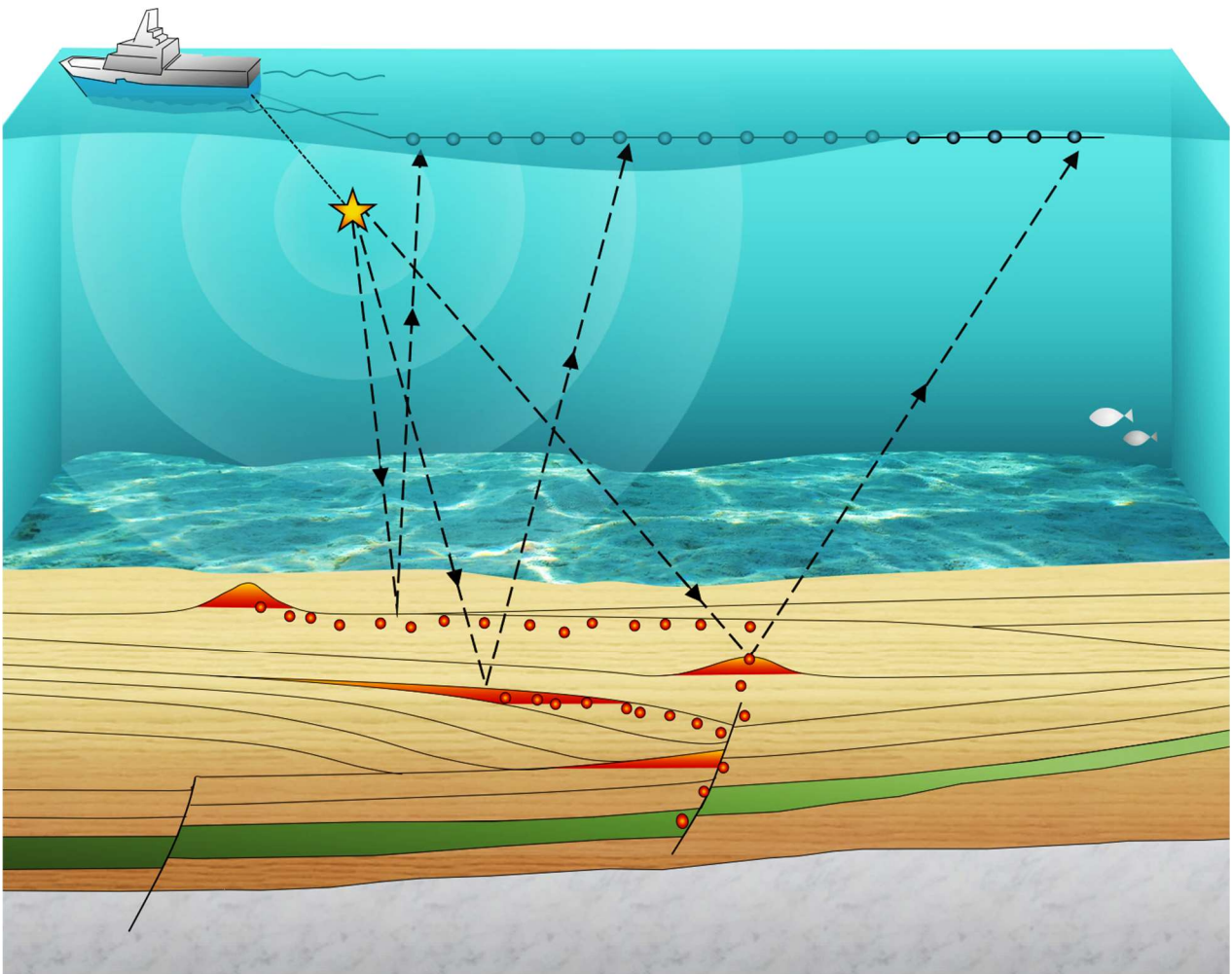


# Seismic sequence analysis and petroleum system indicators at the Oligocene-Miocene level in the southern North Sea

*Johanne Schøning Poulsen*





In cooperation with Lundin Norway

*Johanne Schøning Poulsen*

## **Abstract**

A thorough review of the Oligocene-Miocene stratigraphic evolution and depositional environments in the Norwegian part of the southern North Sea is presented and considered alongside observations of petroleum system indicators, from seismic-, core- and well-data. The reconstructed paleo-environments show a trend of fluctuating eustatic sea-levels, controlled by basin subsidence and uplift of the Fennoscandian Platform in the north, coupled with growth and melt of the Antarctic Ice Sheet. Stages of rising sea-level are reflected by low-angle, sigmoidal clinoforms with ascending shelf-break trajectories deposited simultaneously to rapid basin subsidence. Periods of a relative fall in sea-level are characterized by complex-oblique clinoform stacking patterns, with a distal displacement of the shelf and descending shelf-break trajectories. Falling stage system tracts are dominated by the evolution and progradation of complex channel systems and erosion of the exposed shelf. Lowstand system tracts are recognized where coarser, sand-rich material was deposited towards the distal basin margins.

The results provide new insight on the subsurface drainage system, as well as an evaluation of a potential Oligocene reservoir rock, the Vade Formation, which in general showed good reservoir properties. This work proposes an updated depositional model for the sandstone, with a newly defined lateral reach, extending beyond the previously established boundaries of this formation. The suggested model describing the petroleum system favours lateral drainage with migration focused sub-horizontally through the permeable Vade Formation which is capped by transgressive, sealing lithologies. Here a persuasive correlation to a Jurassic source rock, the Mandal Formation, is outlined, providing a tentative basis on which to endorse a thermogenic origin of the observed hydrocarbon indications with long distance lateral migration enabling accumulations to form far from the petroleum kitchen area. A differential entrapment model alongside potential leakage and well-information, provides an explanation for the dry wells adjacent to possible hydrocarbon accumulations in the region. The evaluation of the petroleum system sheds new light on the potential for several hydrocarbon filled structures in the subsurface of the Norwegian southern North Sea.

## **Acknowledgements**

Først og fremst vil jeg takke Lundin Norge for den flotte muligheten til å tolke et stort og veldig interessant seismisk datasett i Nordsjøen. Tusen takk til Harald Brunstad for godt engasjement og oppfølging til logging av kjerne. Ditt bidrag settes stor pris på. Tusen takk til Tom Arne Rydningen ved UiT for at du tok deg verdifull tid til å komme med innspill i sluttfasen av prosjektet. I tillegg vil jeg takke Iver Martens og Jan-Erik Lie for deres bidrag i oppstartsfasen.

En spesiell takk går til den fantastiske Vegard for lærerike diskusjoner, innspill og en enorm innsats til oppussing av hus i Harstad – det har vært et innholdsrikt år! Til alle venner jeg har fått på Svalbard og i Tromsø, dere er rå! Kristine, Eirin, Birgitta, Sofie, Siri, Tonje, Frank, Leif og Truls! Vi holder kontakten.

Alex Rolland – thanks for all the tricks and tips you have showed me in Petrel. Your contribution is invaluable!

# TABLE OF CONTENTS

<b>1</b>	<b>INTRODUCTION AND GEOLOGICAL BACKGROUND</b>	<b>1</b>
1.1	AIMS AND OBJECTIVES	1
1.2	STUDY AREA: SOUTHERN NORTH SEA	3
1.3	GEOLOGICAL SETTING	5
1.3.1	MESOZOIC	6
1.3.2	CENOZOIC	7
1.4	CENOZOIC STRATIGRAPHY IN THE NORTH SEA	8
1.4.1	THE HORDALAND GROUP	9
1.4.2	THE NORDLAND GROUP	10
1.5	PETROLEUM POTENTIAL OF THE SOUTHERN NORTH SEA	10
<b>2</b>	<b>THEORETICAL FRAMEWORK</b>	<b>12</b>
2.1	SEISMIC REFLECTION THEORY	12
2.1.1	SEISMIC RESOLUTION	13
2.2	SEISMIC SEQUENCE ANALYSIS	16
2.2.1	SHELF TERMINOLOGY AND PRINCIPLES	16
2.2.2	SYSTEM TRACTS	18
2.3	SEISMIC FACIES PARAMETERS	23
2.4	SEDIMENTARY STRUCTURES FROM CORE OBSERVATIONS	26
2.5	FAULT CONFIGURATIONS AND SEISMIC IMAGING	27
2.6	THE PETROLEUM SYSTEM	28
2.6.1	PRIMARY/SECONDARY/TERTIARY MIGRATION	30
2.6.2	TRAPS	31
2.7	DIRECT HYDROCARBON INDICATORS	35
2.7.1	SEISMIC RESPONSE OF GAS	35
<b>3</b>	<b>DATA AND METHODS</b>	<b>37</b>
3.1	DATA	37
3.2	METHODS	38
3.2.1	SOFTWARE	38
3.2.2	WORKFLOW	38
<b>4</b>	<b>RESULTS</b>	<b>45</b>
4.1	PRESENTATION OF RESULTS	45
4.2	SEISMIC FACIES	47
4.3	GENERAL CHARACTERIZATION OF THE SEQUENCES	48
4.3.1	REFLECTION TERMINATIONS	48
4.3.2	STRUCTURAL CHARACTERIZATION	49
4.4	SEQUENCE 1	52
4.5	SEQUENCE 2	58
4.5.1	CORE OBSERVATIONS	62
4.6	SEQUENCE 3	64
4.7	SEQUENCE 4	70

<b>4.8</b>	<b>SEQUENCE 5</b>	<b>72</b>
<b>4.9</b>	<b>SEISMIC HYDROCARBON INDICATORS</b>	<b>74</b>
4.9.1	ZONE 1	74
4.9.2	ZONE 2	75
4.9.3	ZONE 3	78
<b>5</b>	<b>DISCUSSION</b>	<b>83</b>
<b>5.1</b>	<b>A GENERAL CHARACTERIZATION OF THE SHELF</b>	<b>84</b>
<b>5.2</b>	<b>RECONSTRUCTING THE PALEOENVIRONMENTS</b>	<b>87</b>
5.2.1	EARLY OLIGOCENE (RUPELIAN) – S1	87
5.2.2	LATE OLIGOCENE (CHATTIAN) – S1/S2	91
5.2.3	LATE OLIGOCENE (LATE CHATTIAN) - MIDDLE MIOCENE (SERRAVALIAN)	97
5.2.4	LATE MIOCENE (TORTONIAN/MESSINIAN)	102
<b>5.3</b>	<b>PETROLEUM SYSTEM INDICATORS</b>	<b>106</b>
5.3.1	SUBSURFACE DRAINAGE SYSTEM	106
5.3.2	PETROLEUM POTENTIAL	113
<b>6</b>	<b>CONCLUSIONS</b>	<b>119</b>
<b>7</b>	<b>DIRECTING FUTURE WORK</b>	<b>121</b>
<b>8</b>	<b>REFERENCES</b>	<b>122</b>
<b>9</b>	<b>APPENDICES</b>	<b>127</b>
<b>9.1</b>	<b>APPENDIX 1 – EQUATIONS</b>	<b>127</b>
<b>9.2</b>	<b>APPENDIX 2 – OVERVIEW OF ALL SEISMIC DATA</b>	<b>128</b>
<b>9.3</b>	<b>APPENDIX 3 – COMPLETION LOGS AND REPORTS FROM WELLS</b>	<b>130</b>
<b>9.4</b>	<b>APPENDIX 4 – FREQUENCY SPECTRUMS</b>	<b>131</b>
<b>9.5</b>	<b>APPENDIX 5 – WELL PICKS OLIGOCENE/MIOCENE (LUNDIN)</b>	<b>132</b>
<b>9.6</b>	<b>APPENDIX 6 - CORE 2/2-2</b>	<b>133</b>

# **1 Introduction and geological background**

## **1.1 Aims and objectives**

The North Sea is a well explored petroleum province where abundant oil and gas accumulations of commercial quantities have been identified. The North Sea Basin forms a large epicontinental basin with a mosaic rift-structure forming ideal hydrocarbon traps (Ziegler, 1975). Whereas deeper layers of Mesozoic and Cenozoic age have been carefully investigated, the shallower parts of the basin are far less thoroughly explored, both with respect to hydrocarbon potential as well as seismic stratigraphic analysis. Laterally drained petroleum systems usually show a trend of oil accumulations occurring in thermally immature strata located far from the pod of active source rock (Magoon & Beaumont, 2003), thus investigation of the shallower parts could turn out to be of significant economic interest to the petroleum industry.

The Oligocene-Miocene sequence forms the middle part of the North Sea Cenozoic stratigraphy, and is situated in relatively shallow regions with regards to hydrocarbon exploration. In this study, a detailed reconstruction of the depositional environment is presented based on a seismic sequence analysis, along with variations in seismic facies, and a core log observation of core from well 2/2-2. Conceptual models and paleo-geographic maps are presented based on the seismic interpretation coupled with information from well completion logs and reports from the area. Emphasis is given to the late Oligocene depositional environment, where a sand unit, the Vade Formation, was deposited. The extent, depositional environment, and potential reservoir quality of the formation is discussed and presented through paleogeographic maps.

Through seismic interpretation methods, abundant hydrocarbon indicators observed in 2D and 3D data of the Oligocene-Miocene sequences are examined alongside the regions structural and stratigraphic controls, in order to better understand the evolution of, and interplay between, these features (Table 1.1.1). Gas accumulations in shallow sediments are often of particular interest to hydrocarbon exploration and production not only for commercial reasons but also because they represent a potential risk during drilling operations (Andreassen et al., 2007). Shallow hydrocarbon accumulations have gained more recent focus in the petroleum industry, since they highlight the nature of the subsurface plumbing system and so reveal unprecedented insight into hydrocarbon plays (Eriksen et al., 2010). Also, smaller accumulations of oil and gas are becoming more important in areas with a well-developed production infrastructure, as the costs of producing is reduced by utilizing the already established pipelines and fields.

Amplitude anomalies initiated by hydrocarbon-saturated sediments are mapped throughout the Oligocene-Miocene sequences in the seismic data. A migration model for the region is established, along with an evaluation of the various trapping mechanisms. In conjunction, information from wells and literature is used in order to better understand the different elements of the petroleum system, such as the Jurassic source rock. The Vade Formation in the southern North Sea is considered as an important part of the migration model.

Table 1.1.1. Summary of the key aims and objectives of this study.

Aim	Key objectives
(1) Stratigraphically characterise the Oligocene-Miocene sequences in the southern North Sea	<ul style="list-style-type: none"> <li>(a) A brief structural mapping, seismic sequence analysis, facies description, describe depositional trends such as e.g. system tracts, clinoform geometries, progradation patterns, etc.</li> <li>(b) Log core from well 2/2-2 and correlate with seismic interpretation</li> <li>(c) <b>Review and reconstruct the depositional environment during Oligocene-Miocene times as conceptual models and paleogeographic maps.</b></li> </ul>
(2) Understand the occurrences and distributions of petroleum system indicators with respect to the structural and stratigraphic controls.	<ul style="list-style-type: none"> <li>(a) Map amplitude anomalies from attributes in relation to previously defined structural and stratigraphical elements</li> <li>(b) Investigate migration pathways and drainage system in the region.</li> <li>(c) Use well information from the region to evaluate the hydrocarbon potential.</li> </ul>
(3) Consider the implications of the results from (1) and (2) on exploration in the region.	<ul style="list-style-type: none"> <li>(a) <b>Develop a migration/accumulation model for the petroleum system.</b></li> <li>(b) <b>Assess the relationship of hydrocarbons with potential source intervals in the region.</b></li> <li>(c) Evaluate the discussed results in a regional context.</li> </ul>



## 1.2 Study area: southern North Sea

The seismic data utilized in this study encompasses the Norwegian part of the southern North Sea situated approximately between 56-58°N ( Figure 1.2.1), south of mainland Norway.

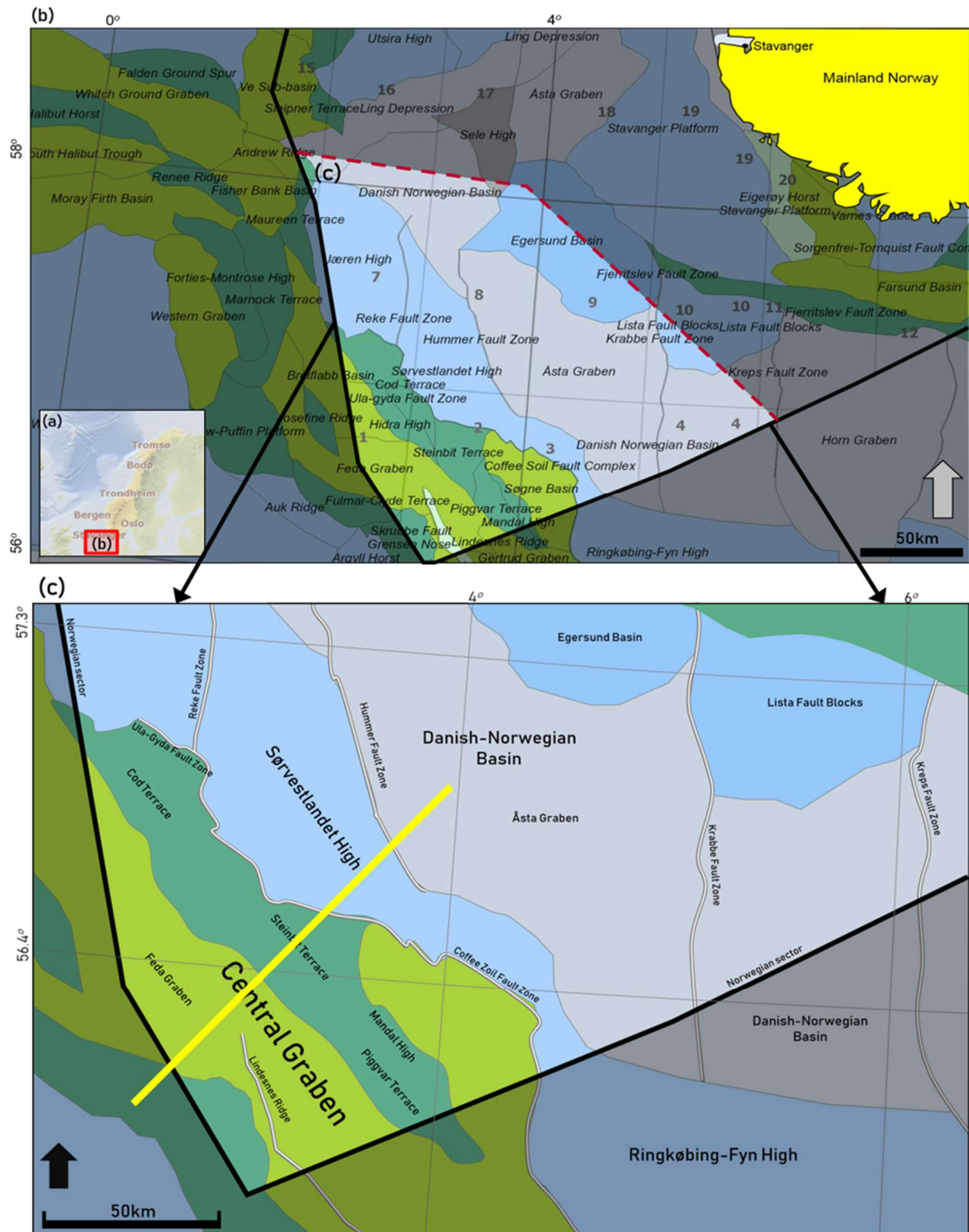


Figure 1.2.1. (a) The study area indicated on a miniature map of mainland Norway. (b) The study area covers the Norwegian part of the southern North Sea between approximately 56-58°N, encompassing structural elements such as the Permian Danish-Norwegian Basin, the Jurassic Sørvestlandet High and the Cretaceous Central Graben. Map modified from the NPD Factmaps service (2011). (c) The yellow line indicates the location of cross-section presented in figure 1.2.2.

The North Sea constitutes a large epicontinental basin where unfaulted Late Cretaceous to recent sedimentary fill is overlying Jurassic-Early Cretaceous graben systems and continental crust of Paleozoic age (Sclater & Christie, 1980). The region comprises several structural highs and basins formed during episodes of extensive rifting and subsidence/uplift.

Considering the extensive lateral extent of the study area, several structural elements of different ages are present, and it is therefore a comprehensive geological history for the region. The following chapter emphasizes tectonic and stratigraphic events important for understanding the formation of the geological setting up to and beyond the Oligocene-Miocene level. Other tectonic events will only be briefly explained in order to focus on the objectives for this study.

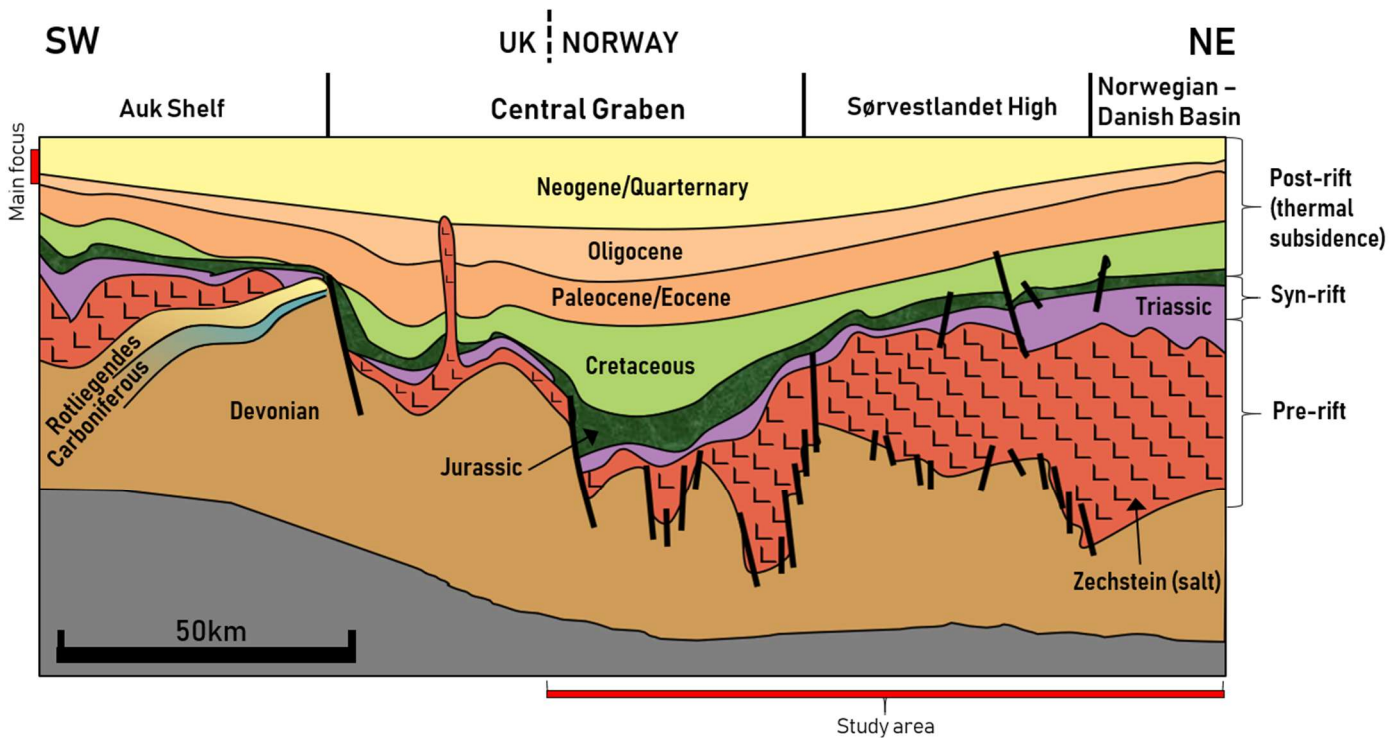


Figure 1.2.2. Geological cross-section of the southern North Sea, displaying the structural outline across the Norwegian-Danish Basin, the Sørvestlandet High, the Central Graben and the Auk Shelf in the UK sector. The Paleozoic basement including the Zechstein salt is underlain by Mesozoic syn-rift sediments (comprising the Jurassic source rock) subsequently buried by basin infill on late Cretaceous-Cenozoic age. Constructed based on sketch from Cornford (1994).

### 1.3 Geological setting

Figure 1.3.1 outlines a summary of significant tectonic events and the coeval stratigraphic deposits in the North Sea region from Paleozoic to Recent times. The Cenozoic era is emphasized in the following chapter.

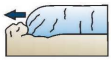











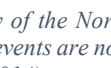

Era	Period	Epoch	Tectonic events	Illustration	Stratigraphy	Formations in study area	
Cenozoic	Quaternary	Holocene	GLACIAL EROSION OF MAINLAND NORWAY		FLUVIAL DEPOSITS GLACIAL DEPOSITS - ICE RAFTED DETRITUS (IRD)	THE NORDLAND GROUP	
		Pleistocene		UPLIFT OF NORWEGIAN MAINLAND			SEDIMENT SOURCE FROM THE NORTH
				UPLIFT OF THE FENNOSCANDIAN AREA			WETSWARD PROGRADATION OF DELTAIC SYSTEMS IN SOUTHERN NORTH SEA
	Neogene	Pliocene	POST-RIFT SUBSIDENCE		MAINLY SHALLOW-MARINE SHALES	(SKADE & UTSIRA FM)	
		Miocene	UPLIFT NORTHERN NORTH SEA - INVERSION CAUSED BY UPLIFT IN THE WEST - MAJOR SEDIMENT SOURCE FOR SUBMARINE FANS		DEPOSITION OF SUBMARINE FANS INTERFINGERING WITH MARINE SHALES	THE HORDALAND GROUP (VADE FM)	
	Paleogene	Oligocene	NORTH ATLANTIC DRIFTING STAGE - SEPERATION BETWEEN TH EUROPEAN AND NORTH-AMERICA		FILL IN SAUCER-SHAPED BASIN BY CHALKS, SANDSTONES, SHALES AND MUDSTONES	THE ROGALAND GROUP (FISKEBANK, SELE, LISTA & VÅLE FM)	
		Eocene					
		Paleocene					MAINLY DEEP-MARINE SHALES
	Mesozoic	Cretaceous	Upper	SUBSTANTIAL UPLIFT		SHALLOW-MARINE CARBONATE DEPOSITS	THE SHETLAND GROUP (Ekofisk, TOR & HOD FM)
			Lower	THIRD/LAST STAGE OF JURASSIC-CRETACEOUS RIFTING		CHALK DEPOSITS	
Jurassic		Upper	PARTLY ACTIVE VOLCANISM RELATED TO RIFTING IN CENTRAL GRABEN		DEEP MARINE CLASTICS, MOSTLY SHALE	THE VIKING GROUP (DRAUPNE/TAU/MANDAL FM - SOURCE ROCK)	
		Middle			SECOND STAGE OF JURASSIC-CRETACEOUS RIFTING CONTINUATION OF BASIN FORMATION		ANOXIC BASIN CONDITIONS THICK SHALE SEQUENCES
		Lower			FIRST STAGE OF JURASSIC-CRETACEOUS RIFTING		COASTAL, DELTAIC, FLOOD-PLAIN DEPOSITS
Triassic		Upper	MAJOR TRANSGRESSION		SHALLOW WATER SANDSTONES IN CENTRAL GRABEN - MAJOR MESOZOIC OIL RESERVOIR	THE STATFJORD GROUP (GASSUM & SKAGERRAK FM)	
		Middle			HALOKINETIC MOVEMENTS SUBSIDENCE/THERMAL COOLING		CLASTIC CONTINENTAL DEPOSITS, SANDSTONES, SHALE AND SILTSTONES
		Lower			DIVERGENT FORCES - RIFTING RELATED TO THE NORTH ATLANTIC RIFT ZONE		FLUVIAL DEPOSITION OF SEDIMENTS ALONG RIFT MARGINS
Paleozoic		Permian	RIFTING AND VOLCANISM		ROTLIEGEND EOLIOAN DEPOSITS SALT (HALITE) - EVAPORITES VOLCANIC DEPOSITS	ZECHSTEIN SALT UPPER ROTLIEGEND	
		Carboniferous	VARISCAN OROGENY		OLD RED SANDSTONES		
	Devonian						
	Silurian	EXTENSION OF CALEDONIAN CRUST					
	Ordovician	EROSION		METAMORPHIC BASEMENT	METAMORPHIC BASEMENT		
	Cambrian	CALEDONIAN OROGENY					

Figure 1.3.1. The structural and sedimentary history of the North Sea region from Paleozoic to Recent times. Constructed based on Chapter 1.3 in this study. The Paleozoic key events are noted from Ziegler (1975). The era/period/epoch configuration is modified from the NPD lithostratigraphic charts (2014).

### **1.3.1 Mesozoic**

At the onset of the Mesozoic era, the North Sea area was exposed to divergent forces resulting in massive rifting to dominate the paleotopography and sedimentation. The Triassic period was characterized by a continental depositional regime in the larger parts of northwestern Europe. Permian basins were progressively modified by the superimposition of a graben system caused by extensive rifting related to movements along the Arctic-North Atlantic rift zone (Ziegler, 1975; Coward et al., 2003). The Graben system transected the Northern Permian Basin and breached the Mid-North Sea-Ringkøbing-Fyn High, of Permian age. The structural high was gradually buried towards Jurassic times. Towards the end of the Triassic period, halokinetic movements were triggered and Zechstein salt deposited in the Permian basins began to ascend upwards through the overburden.

A major transgression associated with sea-floor spreading in the Central Atlantic and thermal subsidence marks the onset of the Jurassic period where Triassic basins were flooded (Ziegler, 1975; Doré, 1992). The continued northward drift of Europe along with the collapse of the Variscan mountain belt led to a rapid change from red to grey sedimentary beds as the climate increasingly became humid. Through the Jurassic and Cretaceous periods, several stages of rifting where graben systems came into place from downfaulted blocks, coupled with uplifting of the rift margins heavily affected the tectonic framework of the North Sea. Additionally, the halokinetic movement of Zechstein salt which was triggered during Triassic times continued as sediments were deposited into subsiding grabens and the pressure increased (Sclater & Christie, 1980). There are three main stages of rifting identified in the region which took place during respectively 1) Early Jurassic, 2) Middle to Late Jurassic / Callovian-Oxfordian phase, and lastly 3) Late Jurassic-Early Cretaceous (Ziegler, 1975; Færseth, 1996). The third rifting phase is considered as the most important rift phase, establishing the basic structural framework of the North Sea Basin with normal faults trending northeast. The rifting was accompanied by periods of tectonic quiescence providing a fundamental control on the regions sedimentation (Ziegler, 1975; Coward et al., 2003).

The Viking and Central grabens developed further in the Jurassic into major structural elements of the North Sea (Sclater & Christie, 1980). Rifting along the Central graben cut as deep as the Zechstein salt, and locally also into the Devonian sandstones and Paleozoic basement, which exposed these layers to erosion along the flanks of the graben (Ziegler, 1975). The Sørvestlandet High represents one of the major structural elevations within the study area and was formed during the Jurassic rift episodes. Volcanism was partly active during the rift phases, but mainly

restricted to the Central Graben where a volcanic dome built up as a result of a mantle hot spot (Underhill & Partington, 1993). Anoxic conditions prevailed in the rift basins caused by the heavy rifting, where thick shale sequences of high total organic content (TOC) were deposited (Coward et al., 2003).

### **1.3.2 *Cenozoic***

The Mesozoic rifting gradually ceased, and passive thermal subsidence began. The syn-rift topography was covered by transgressive sediments to form the so-called Base Cretaceous Unconformity in the North Sea (Ziegler, 1975; Coward et al., 2003). Basins were deformed by tectonic inversion, and a substantial uplift prevailed at the onset of the Cenozoic (Ziegler, 1975).

#### **1.3.2.1 *Paleogene***

The Cenozoic North Sea Basin forms a part of the larger Northwest European Basin that extends from the Atlantic shelves of Norway and Shetland in the northwest, to the Carpathian Mountains in the southeast (Fyfe et al., 2003). The taphrogenic stage of the North Sea that prevailed during the Mesozoic came to an end in the late Paleocene, at the onset of the Paleogene period (Jordt et al., 1995; Coward et al., 2003). The drifting stage in the Arctic North Atlantic was initiated by crustal separation between the European and the North-American-Greenland plate during the late Paleocene and Eocene epochs. Earth's crust experienced major movements, related to the north Atlantic sea floor spreading, but also to the mountain building in the Himalaya and Alps. The opening of the Arctic North Atlantic is generally believed to be the result of a sea-floor spreading along the Reykjanes and Mohns Ridges (Ziegler, 1975). The North Sea tectonic framework was further influenced by regional subsidence which was widespread and uniform, and resulted in the formation of a large, symmetrical, intracratonic basin, where accommodation space was created (Sclater & Christie, 1980). The semi-enclosed basin of the Norwegian North Sea that persisted during late Palaeocene-Eocene gradually changed during Oligocene into a more open basin with seaway connections to the Arctic Sea in the northeast (Rundberg & Eidvin, 2005).

Paleogene succession of up to 3.5km is present in the central North Sea (Ziegler, 1975). The basin was filled successively by chinks, sandstones, shales and mudstones. The subsidence and basin formation is suggested to have resulted from thermal relaxation of the lithosphere during an ongoing thinning of the crust from Middle Jurassic to Middle Cretaceous (Sclater & Christie, 1980). Series of submarine fans were transported and deposited from the East Shetland Platform in the west, as a result of inversion caused by uplift of the basin margins during the Early

through Middle Palaeogene (Jordt et al., 1995). The sandy submarine fans coalesce and interfinger with marine shales in both the Rogaland and Hordaland groups (Figure 1.4.1).

Uplift in the northern North Sea prevailed during Eocene and the Early Oligocene, and was followed by marked post-rift subsidence in the basin and along the Atlantic margin in late Miocene-Pliocene times. The subsidence history of the basin have been discussed by a number of authors (Wold, 1994; Wright & Miller, 1996; Rundberg & Eidvin, 2005).

### ***1.3.2.2 Neogene***

During the Oligocene-Early Miocene, the Northern North Sea progressively shallowed (Rundberg & Eidvin, 2005). The development of the Southern North Sea during these periods nonetheless remains far less explored. The climatic conditions were relatively warm. The basin development was influenced by dual controls of the closing of the Tethys Ocean to the southeast, and the opening of the North Atlantic Ocean to the northwest. The connection between the two respective oceans is termed as both the Moravian Gateway and the North Polish Strait. Tectonic movements influenced the oceanic circulations, and caused a local hiatus in the central North Sea region during the Early to Middle-Oligocene, which also has been attributed to a fall in eustatic sea level (Bukovics & Ziegler, 1984; Jordt et al., 1995).

### ***1.3.2.3 Quaternary***

Uplift of the Fennoscandian Platform during the Neogene caused an increased sediment flux and a consequent overall westward progradation of the deltaic systems in the south-eastern North Sea (Fyfe et al., 2003). Following in the Neogene period, the Norwegian mainland experienced a major uplift and accordingly became the next sediment source. Ensuing the uplift-subsidence events during the Eocene-Miocene, Quaternary glacial erosion and processes caused the deposition of thick sequences into the North Sea along with fluvial deposits from a large drainage area to the east (Jordt et al., 1995).

## **1.4 Cenozoic stratigraphy in the North Sea**

The lithologies of the Paleogene and Neogene sequences in the North Sea are characterized by shales and sandstones (Figure 1.4.1). This study will focus on the Oligocene and Miocene part of the stratigraphy, i.e. the Hordaland and Nordland groups, which are separated by the Mid-Miocene Unconformity (MMU).

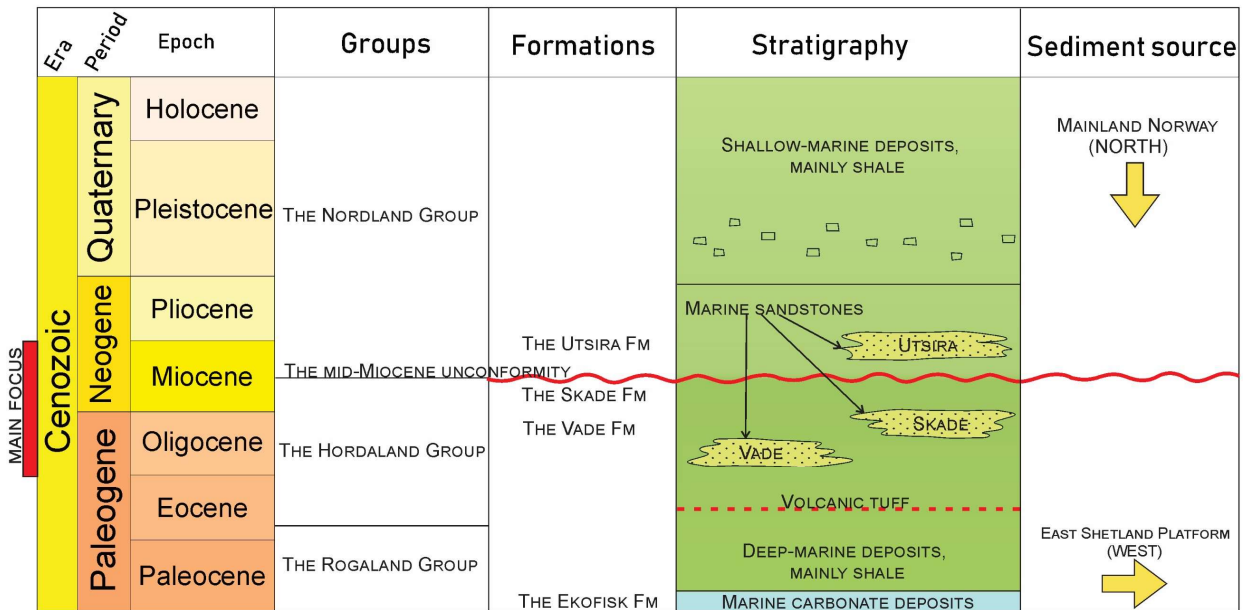


Figure 1.4.1. Stratigraphic units from the central North Sea, Danish-Norwegian Basin and the southern Viking Graben conjugated into one chronologically order from the Cenozoic stratigraphy in the study area. Constructed based on Chapter 1.2 and the NPD lithostratigraphic charts (2014).

### 1.4.1 The Hordaland Group

#### Eocene to Middle Miocene

Sediments deposited during the Early Eocene epoch were mainly derived from the East Shetland Platform located west of the North Sea, with two main depocenters along the Viking and Central Graben. The subsequently deposited Middle-Upper Eocene succession mainly built out from a coastal plain or deltaic systems in the west and north-west, and the depositional unit is characterized by cyclic occurrences of sand interrupted by thin clay intervals.

Post-rift subsidence continued after Eocene times, causing the deposition of up to 3000m of Oligocene to Holocene sediments (Fyfe et al., 2003). Three major sandy systems were deposited in the Norwegian North Sea during the Oligocene-Miocene periods, respectively the 1) Lower Oligocene sandy system, 2) Lower Miocene sandy system and 3) Upper Miocene-Lower Pliocene sandy systems (Rundberg & Eidvin, 2005). Isaksen and Tonstad (1989) recognized a sandy formation within the Oligocene sequence; the Vade Formation. The Vade Formation consists of shallow marine sandstones that occurs in the southern part of the Norwegian North Sea (Isaksen & Tonstad, 1989; Fyfe et al., 2003). The erosive Mid-Miocene Unconformity forms the top of the Hordaland Group (Rundberg & Eidvin, 2005).

The Skade and Utsira Formations, along with the Upper Pliocene sands of the Nordland Group, form the outer part of a large deltaic system sourced from the East Shetland Platform, which is linked to the described uplift in the west (Chapter 1.3.3; Jordt et al., 1995). The proximal parts of the deltaic system are mainly situated in the UK sector.

#### **1.4.2 *The Nordland Group***

##### **Early Miocene – Recent**

The margins of the North Sea was uplifted during the Mid- to Late Miocene, accompanied by climate cooling which lead to a restricted connection between the Norwegian-Greenland Sea and the North Sea. In turn this shallowing led to the development of sandy river systems on the shelf and progradation of deltaic complexes, depositing sediments from the drained Shetland Platform and Scandinavia (Fyfe et al., 2003). The Mid-Upper Miocene succession onlaps the underlying Lower Miocene in the northern North Sea, where the angular discordance represents the Mid-Miocene Unconformity (MMU) – the basal part of the Nordland Group (Rundberg & Eidvin, 2005). The sequence is underlain by the Upper Miocene-Lower Pliocene Utsira Formation, encompassing a large sandy system with subordinate intercalated mudstones (Rundberg & Eidvin, 2005). The formation forms an elongated sandbody mainly deposited in the center of the northern North Sea and the Viking Graben, and is lacking or only partly present within the study area. The Utsira Formation is the only formation to this date defined in the Nordland Group in the North Sea.

### **1.5 Petroleum potential of the southern North Sea**

The North Sea petroleum province comprise oil and gas which originates from three major petroleum systems: a dry gas system in the south and at least two oil systems in the north. The northern North Sea petroleum province involves the Viking, Witch Ground and Central grabens, which straddle the U.K. – Norway – and Denmark offshore boundary (Cornford, 1994). In the Central Graben, the oil-prone source rock named the Mandal Formation has charged mostly Upper Cretaceous-Paleocene reservoir rocks (Cornford, 1994). The source rock was deposited in anoxic rift basins as described earlier. The study area comprises the petroleum system of the Central Graben, which has been termed as the Mandal-Ekofisk petroleum system.

The Mandal-Ekofisk petroleum system in the North Sea is named based on the oil-prone source rock, the Mandal Formation, and the Ekofisk chalk which is the reservoir containing the larger parts of the migrated hydrocarbons from the Mandal Formation. The geographic extent of the



oil-prone source rock, Mandal Formation, is eroded north of the Forties field and is preserved in the Central Graben. Towards the southeast, the source rock extends across the Norwegian-Danish border, where it is recognized as the Bo Member within the Farsund Formation (Cornford, 1994; Petersen et al., 2010). The source rock is of Late Jurassic age of mainly type II kerogen (Figure 1.5.1), primarily oil-prone but also gas prone, with good-excellent TOC content (Petersen et al., 2010).

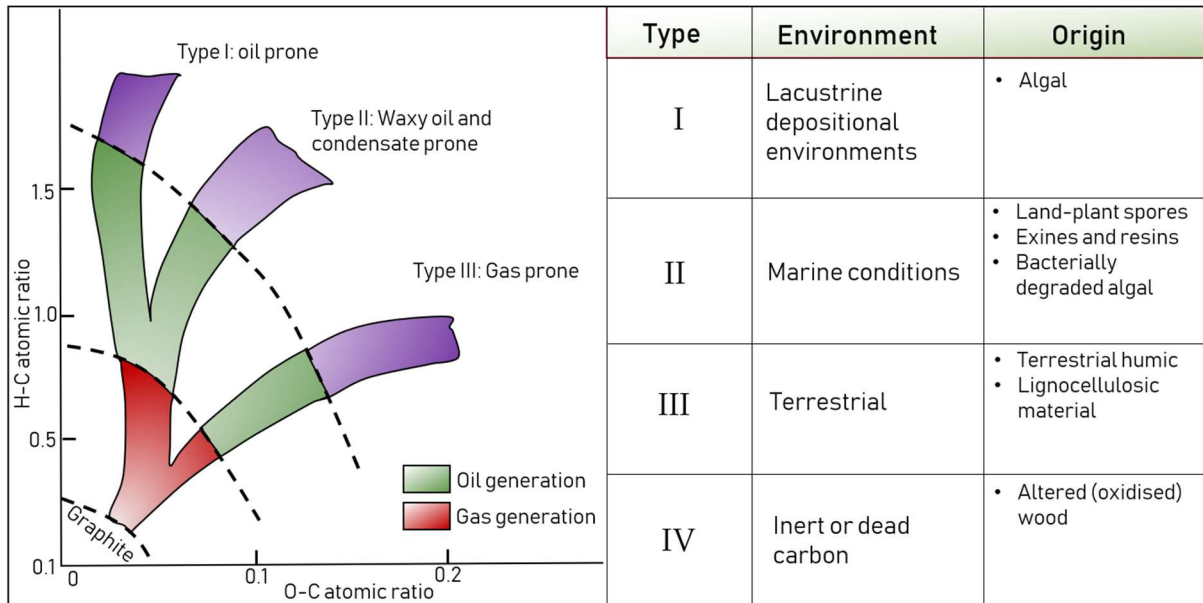


Figure 1.5.1. Van Krevelen diagram showing the different types of kerogen and their respective origin. Modified from Selley & Sonnenberg (2015).

Cornford (1994) listed some of the major fields and discoveries within this petroleum system, and only one was situated at the Oligocene or Miocene level; the Gyda discovery. Shallow-gas within the post-Eocene sediments has so far only had considerable significance as a drilling hazard to exploration and development. Furthermore the sandstone bodies, such as the Utsira Formation, has been found to be suitable for re-injection of CO<sub>2</sub> gas (Fyfe et al., 2003).

## 2 Theoretical framework

### 2.1 Seismic reflection theory

This study relies mainly on the seismic reflection method but additionally combines information from well-logs and one logged core in the region. The seismic reflection method enables identification and recognition of different depositional system tracts and fluid contents within the pores of sediments in the subsurface.

The application of geophysical principles is important in order to interpret seismic reflection data. These principles cover the acoustic properties of layers and the corresponding behavior and expression of the seismic wave. The reflection coefficient at a lithological interface describes the amplitude of a given reflected wave at a boundary (Reynolds, 2011) and is dependent on the acoustic impedance of the two contacting lithologies. Different rock types and pore-fill induces different geophysical criterias, such as density and velocity, and provides information about whether the energy moved through a harder towards a softer rock, or the other way around (Kearey et al., 2002). The seismic response of a host rock may however be altered depending on the pore-fill (e.g. water vs. gas, Figure 2.1.2). The different trace expressions depending on the relative acoustic properties are demonstrated in Figure 2.1.2.

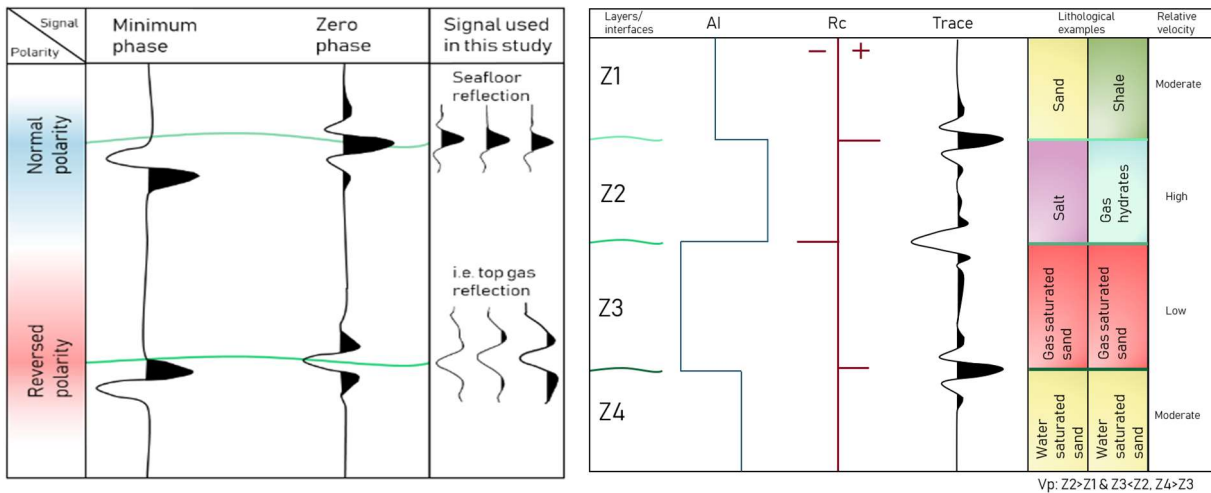


Figure 2.1.1. The polarity and phase conventions for plotting seismic signals, following the SEG standard. Modified from Sheriff (2002).

Figure 2.1.2. Example of geophysical properties for four given layers with different acoustic properties in the subsurface. The given seismic velocity ( $V_p$ ) is changing with depth, and is higher/lower following the different lithologies and fluid contents. e.g. salt or gas hydrates usually show high velocity, whereas gas saturated sediments have a relatively low velocity.

The phase configuration of seismic traces is essential to keep in mind when working with seismic data, in order to understand the observed amplitudes and patterns. A minimum phase configuration is displayed by a trough (white, left) right below the interface, followed by a peak

(black, right). A zero phase (as for this study) is illustrated by a trough right above the interface, followed by a peak located central to the interface, and then again followed by a trough (Figure 2.1.1). Normal polarity indicates e.g. that softer rocks overlie harder rocks, while the other way around is represented by a reversed polarity. The polarity may also be a result of the fluid content within the porespace of a rock.

## 2.1.1 Seismic resolution

In seismic interpretation, the resolution of a survey makes out the largest restriction. The resolution for each seismic survey is defined as the limit to detect structures of certain extents (Kearey et al., 2002), and is understood by the ability to distinguish and differentiate points and objects in the subsurface, such as lithological layers with different acoustic properties. Hence, resolution is a physical size measure of how large the features in the subsurface necessarily have to be in order to be visible on the seismic data. The resolution of seismic data comprises both vertical and horizontal aspects, both dependent on the dominant seismic wavelength ( $\lambda$ ), and is the product of velocity ( $v$ ) and frequency ( $f$ ) (Figure 2.1.3). The different equations for calculating the wavelength of a seismic pulse, and the vertical and horizontal resolution, is presented in Appendix 9.1.

Energy propagating through the subsurface spreads over an expanding wavefront due to the natural spherical divergence of a wave, causing the resolution to decrease with depth. Additionally, the energy is to some degree absorbed by the subsurface rocks which forms a constraint on the resolution of the seismic data. The velocity of lithological layers nevertheless increases with depth, on account of the compaction caused by the increasing weight of the overburden (Kearey et al., 2002). Deep-travelling seismic waves tend to have lower dominant frequencies as the higher frequencies of a seismic signal are absorbed progressively, and thus the resolution decreases with depth (Kearey et al., 2002, Veeken, 2007).

### 2.1.1.1 Vertical resolution

Vertical resolution is a measure of the ability to identify and recognize individual, closely-spaced reflectors in the subsurface and is determined by the pulse length on a recorded seismic section (Kearey et al.,

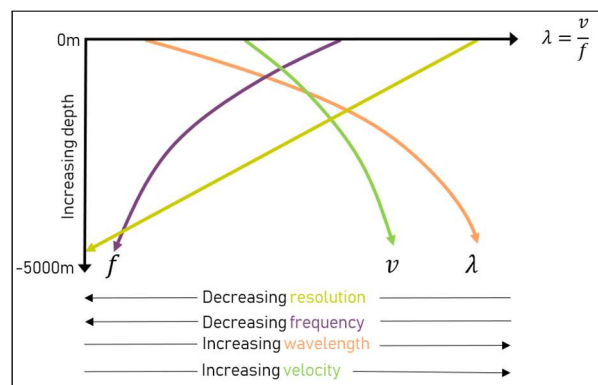


Figure 2.1.3. Aspects of seismic resolution with depth. Modified from Brown (1999).

2002). In terms of vertical resolution, the limit of separability is central for determining how thick a layer must be in order to be seen in seismic data. Below the limit, seismic pulses will overlap in time in the seismic recording (Kearey et al., 2002). The limit of separability is dependent on the wavelength ( $\lambda$ ) and equals the bed thickness of a layer, corresponding to the closest separation of the wavelets and can be derived from Equation 2.2. (Appendix 9.1). Towards one quarter of the wavelength, the top and base of reflections are visible but progressively attenuates until the limit is reached. This is exemplified in Figure 2.1.4, where a wedge pinchout of sandstone is disappearing from the synthetic seismic section below the limit of visibility.

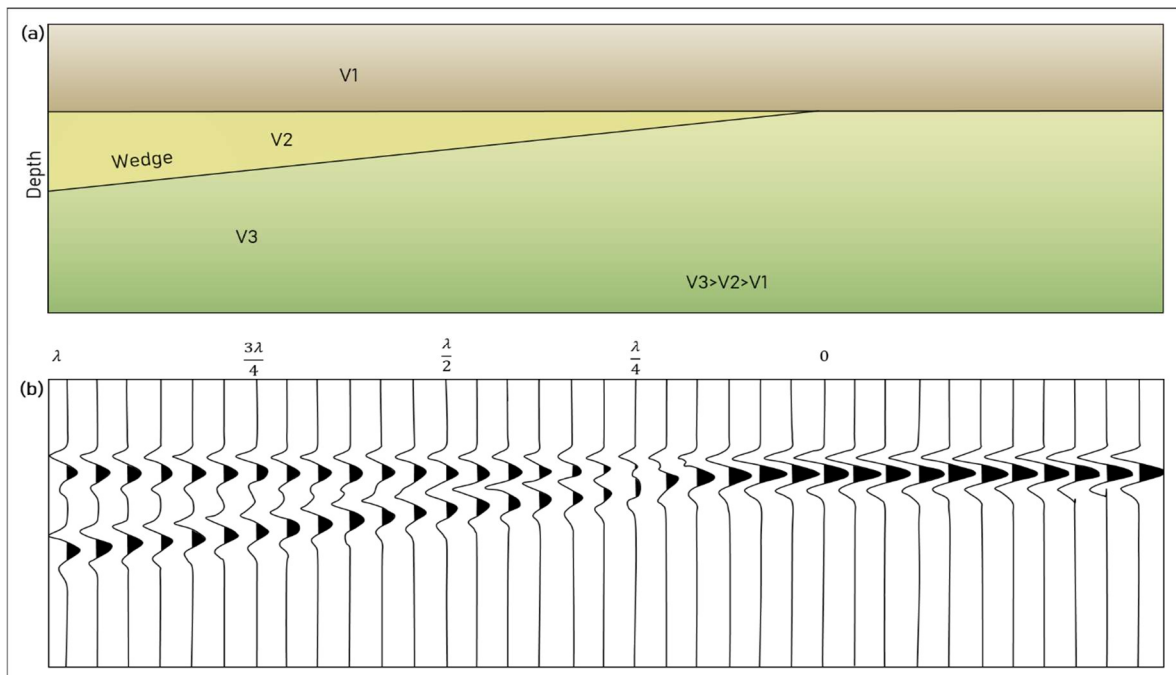


Figure 2.1.4. (a) Geological model showing a sedimentary wedge/pinchout and the relative velocity of the layers (increasing with depth). (b) Corresponding seismic response, showing the limit of separability and the seismic trace configuration. The example is illustrated using the zero-phase, normal polarity following the SEG standard. Constructed based on theory from Badley (1985), Sheriff (2002) & Andreassen et al. (2007).

### 2.1.1.2 Horizontal resolution

The horizontal resolution is defined as the possibility to identify laterally displaced objects and separate them as individual events in the subsurface (Chopra et al., 2006). The lateral measurement is derived from the Fresnel Zone. Caused by the spherical divergence of energy from a seismic source, the seismic wave affects an area and not a single point. Energy is returned to source from all points on a reflector. The horizontal resolution has mainly two controls in a reflection survey, one being intrinsic to the reflection process of a wave, and one by the detector spacing when gathering the seismic survey (Kearey et al., 2002).

Regarding the first control, objects in the subsurface with lateral extent which is less than the Fresnel Zone will not be visible in the seismic data (Figure 2.1.5.b). However, the horizontal resolution is a matter of three dimensional understanding, since the wave-fronts propagate in a spherical movement. It is thus important to consider the resolution of both pre- and post-migrated seismic data. The migration process is the principal processing technique for enhancing horizontal resolution, where there are three main aspects; (1) repositioning of out-of-place reflections caused by e.g. dipping interfaces, (2) focusing energy spread over a Fresnel Zone and finally (3) collapsing diffraction patterns from points and edges (Brown, 1999). Collapsing the Fresnel Zone is done only in the inline direction for 2D-data, whereas for 3D the zone is reduced to a small circle (yellow) which corresponds to the vertical resolution of the seismic survey (Figure 2.1.5). The measure of the unmigrated Fresnel Zone can be derived from Equation 2.3, and the post-migrated radius can be approximated from Equation 2.4 (Appendix 9.1). When the radius of the Fresnel Zone decreases, the horizontal resolution increases.

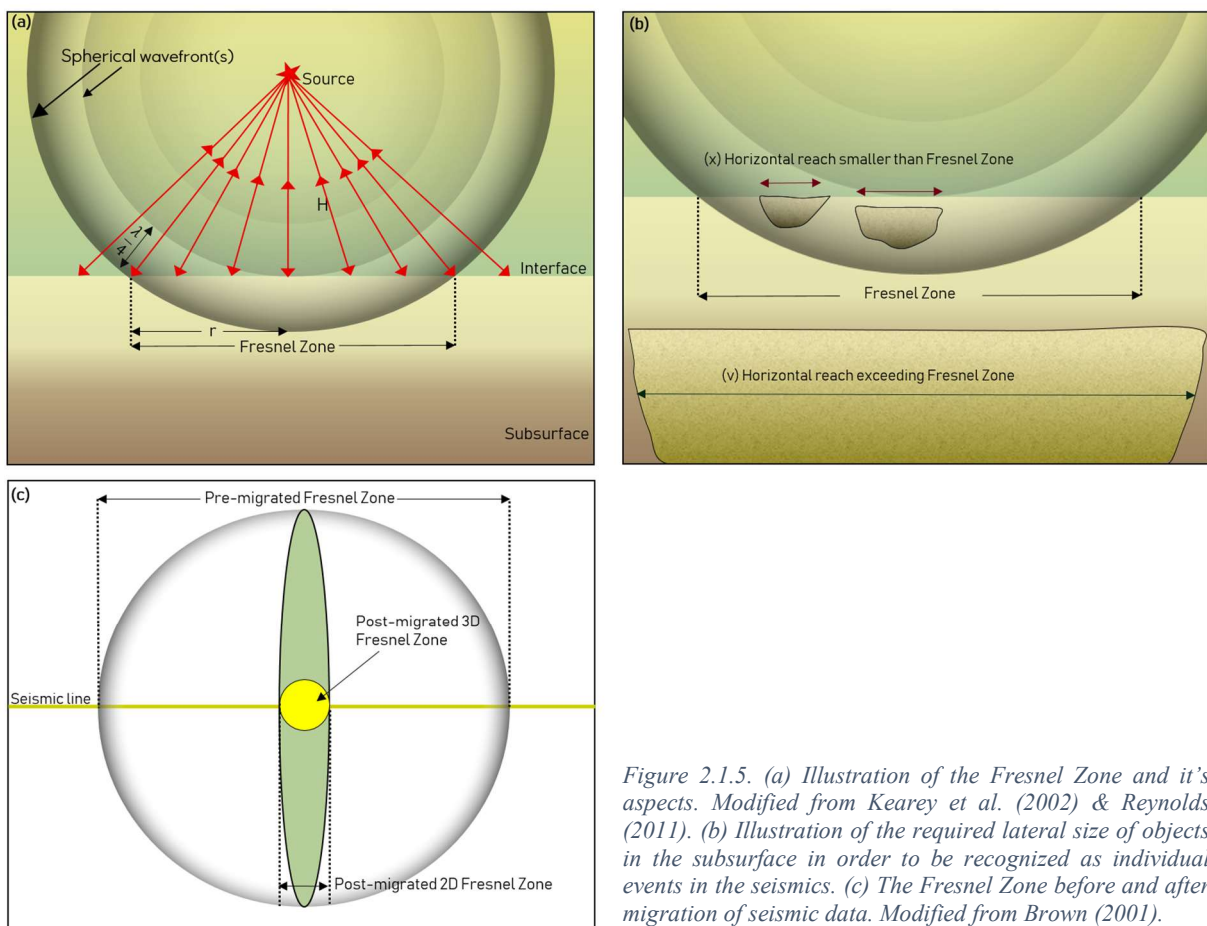


Figure 2.1.5. (a) Illustration of the Fresnel Zone and its aspects. Modified from Kearey et al. (2002) & Reynolds (2011). (b) Illustration of the required lateral size of objects in the subsurface in order to be recognized as individual events in the seismics. (c) The Fresnel Zone before and after migration of seismic data. Modified from Brown (2001).

## 2.2 Seismic sequence analysis

Precursor to successful interpretation of seismic data, is to properly understand seismic sequences and facies (Brown, 1999). Application of the seismic stratigraphy technique simplifies interpretation of sedimentary structures by subdividing groups of seismic reflections into packages which are coeval, chronostratigraphically constrained genetic depositional intervals (Vail, 1987). This study relies principally on seismic sequence analysis of predominantly clastic materials, however the method can be applied on carbonates as well. Recognizing patterns in seismic data is the basis for understanding sequences and terminations, and is useful to investigate different acoustic properties between layers (Mitchum et al., 1977).

### 2.2.1 Shelf terminology and principles

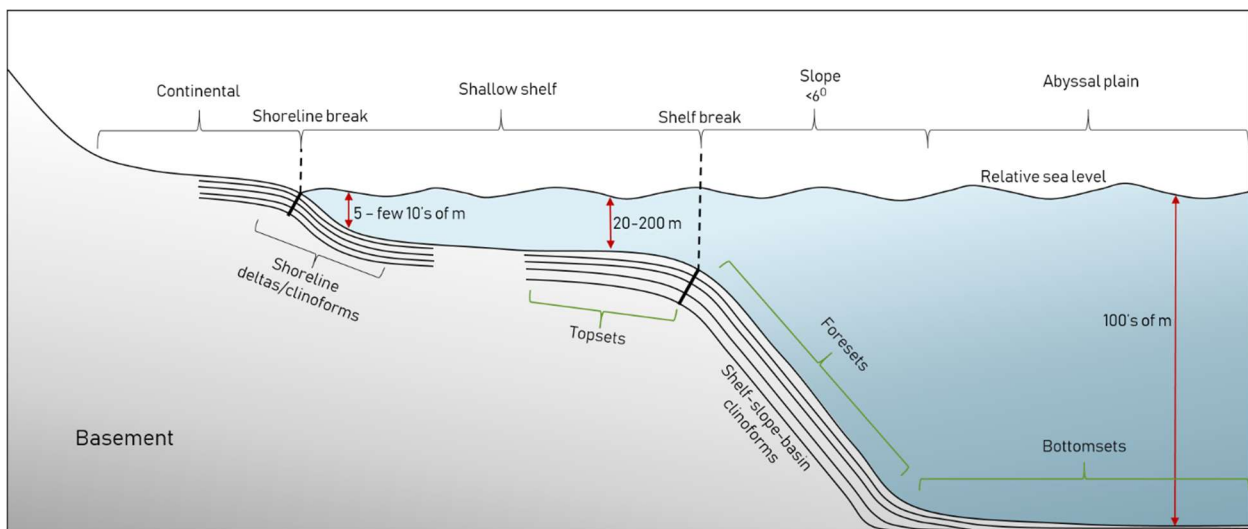


Figure 2.2.1. Illustration of a shelf profile with the adjoining terminology. Shoreline deltas are usually in ten's of meter's scale, whereas shelf-edge clinoforms may be of several kilometers. Clinoforms comprise topsets, foresets (slope) and bottomsets. Note the red arrows indicating the available accommodation space increase towards deeper waters. Modified from Helland-Hansen & Hampson (2009).

A sedimentary basin is an area of the earth's crust that is underlain by a thick sequence of sedimentary rocks where hydrocarbons commonly occur (Selley & Sonnenberg, 2015). The integration of seismic and morphological features such as platform, slope and basin allows the definition of a depositional sequence. One seismic sequence is limited by discontinuities or unconformities defined on the basis of reflection termination patterns (Table 2.2.1) and their lateral continuity. These unconformities represent time-lines and chronostratigraphical surfaces, called sequence boundaries (SB). However the term sequence boundary is commonly used regarding the "top" of a regressional event, and marks a degree of change within the sedimentary regime, basin tectonics, sediment source, rate of sedimentation or amount of erosion across the surface (Figure 2.2.2). A maximum flooding surface (MFS) on the contrary

represents the surface of deposition corresponding to the most transgressive and/or distal configuration of a stratigraphic architecture, at the same time as the shoreline is at its maximum landward position (Posamentier et al., 1988; Homewood et al., 2000). The distal configuration is recognized as fine-grained sediments within a clastic transgressive deposit. Furthermore, the transgressive stratigraphic representation theoretically shows a fining upwards trend (Figure 2.2.2.a). The system tracts are the relatively conformable successions of genetically related strata deposited during a specific phase of the relative sea level cycle (Figure 2.2.2.b) bounded by stratigraphic surfaces such as e.g. SB and MFS (Posamentier et al., 1988).

Seismic sequence stratigraphy is useful within petroleum exploration as it allows the prediction and localization of reservoirs and seals (such as e.g. MFS), in addition to estimating the lateral extent and variation of reservoir units (Bonin, 2018).

A clinoform is defined as the entire sigmoid profile comprising the topset, foreset and bottomset of a depositional sequence (Steel & Olsen, 2002; Helland-Hansen & Hampson, 2009). The outbuilding of sigmoid, oblique, complex, shingled and hummocky progradational patterns form through progressive lateral development of gently sloping depositional processes (Mitchum et al., 1977). Shelf-edge clinoforms are commonly in a larger scale compared to shoreline deltas. The topset-bottomset configuration however is common for both. Shelf-edge clinoforms and slopes commonly display low angles, varying between two to seven degrees (Steel and Olsen, 2002; Johannessen & Steel, 2005). The foreset patterns can be practiced to interpret paleowater depths during deposition, by analyzing the height of the prograding clinoforms (Figure 2.2.1; Vail, 1987).

#### **2.2.1.1 Controls on the stratigraphic pattern**

Variations in stratigraphic patterns has four major controls. First, tectonic subsidence which creates *accommodation space*. The space between the sediment surface (seabed), and the relative sea level available to store sediments, defines the accommodation space (Coe et al., 2002). As illustrated in Figure 2.2.1, the accommodation space is often controlled by the water depth, e.g. it increases from the shallow shelf towards the deeper basins. Hence, the shelf morphology along with changes in eustatic sea-level are major controls.

The second one is the *eustatic changes in sea level*, which comprises both the regional and global changes, and is considered to be the major control on stratal patterns and lithofacies distribution (Vail, 1987). The different stages through the sea level fluctuations is referred to as system tracts.

The third control is the *volume of sediments available* in the depositional system. Precipitation and run-off through river systems are thus important factors regarding the third control, as most sediments in offshore environments depend on sediment supply from elevated continental regions (Bonin, 2018). The fourth and last control is *climate*. The variations in climate, e.g. from arid to cold, are the major controls on sediment types and thus the different lithofacies deposited (Vail, 1987).

## 2.2.2 System tracts

The system tracts represent different stages within the relative sea level cycle (Figure 2.2.2) superimposed on a depositional system resulting in different depositional structures and geometries.

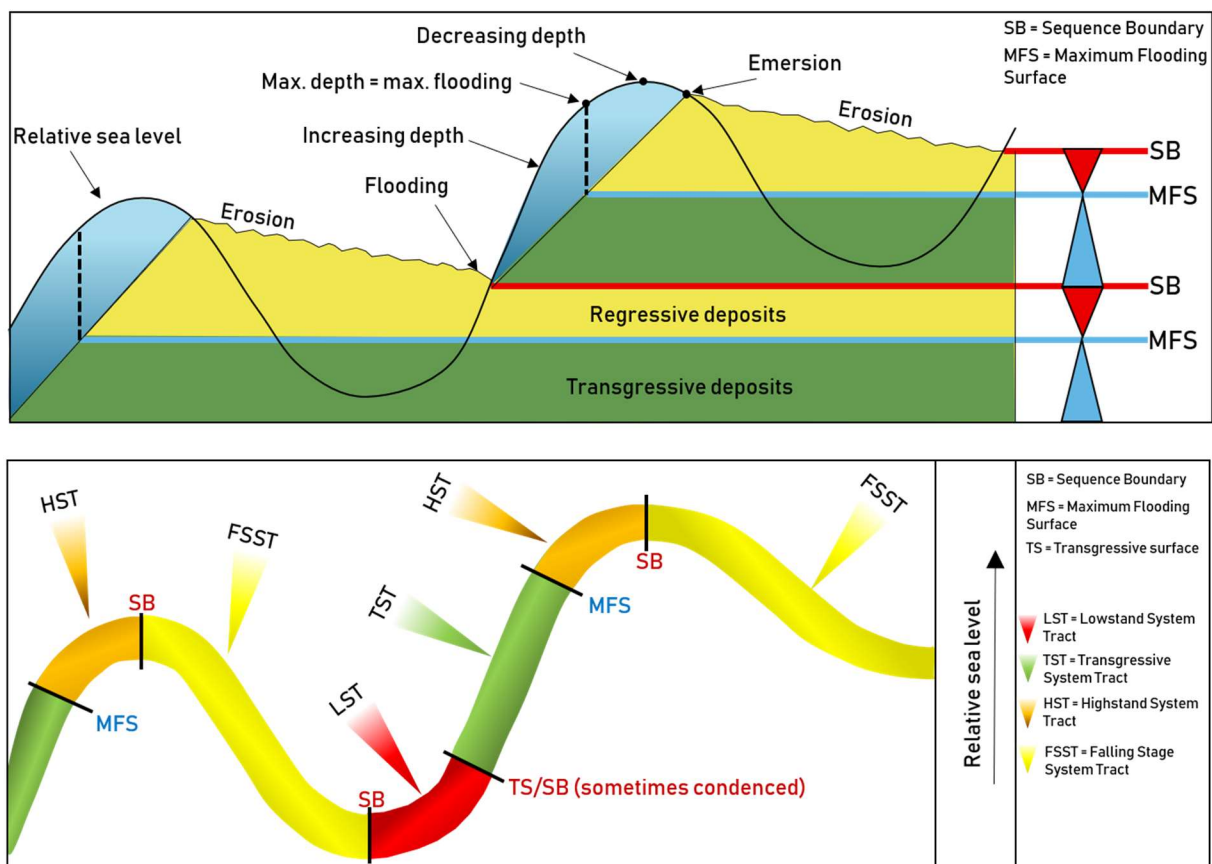


Figure 2.2.2. (a) Relation between the relative sea level in a cyclic manner and impact on the sedimentary depositional system. Note the deepening/fining upwards trend in the transgressive deposits, and the shallowing/coarsening upwards on the contrary for the regressive deposits. (b) The relative sea level and correlating different system tracts. Constructed from Homewood et al. (2000) & Bonin (2018).

The Falling Stage System Tract (FSST) is formed by regressive deposits that accumulate in the distal areas after the onset of a relative sea level *fall*, in advance of the next relative sea level rise. FSST is commonly characterized by a flat or descending shelf edge progradation pathway, represented by the *trajectory* (Figure 2.2.4). The trajectory records the pathway of a progressive



shelf-edge, during the development of accreting clinoforms (Figure 2.2.4; Johannessen & Steel, 2005). The Lowstand System Tract (LST) is defined by the sediments which accumulated after the onset of relative sea level rise (Bonin, 2018). The LST is commonly characterized in clastic systems by exposure and erosion of the shelf, incised valleys and channelized slope systems progressively building out on the in the proximal parts (Coe et al., 2002).

A transgressive surface begins to form at the start of relative rise in sea level, and migrates landward during the transgression (Bonin, 2018). The Transgressive System Tract (TST) is formed by sediments accumulating from the onset of the relative sea rise until the time of maximum transgression (e.g. Maximum Flooding Surface), prior to the sea level fall of the sea level cycle. The sediment record is often characterized by deposition of marine shales forming blanket paleotopography with high sedimentation rate on the shelf (Coe et al., 2002). Lastly, the Highstand System Tract (HST) includes the progradational deposits that form when sediment accumulation rates exceed the rate of increasing accommodation space during the late stages of relative sea level rise. The shoreline progressively steps landward, whereas the shelf-edge progressively builds out basinwards, recognized as clinoform architecture and rising trajectories are common (Vail, 1987; Schlager, 1992; Coe et al., 2002). Several of the best coastal sand reservoirs in the world has formed during a transgressive high stand, when deposition was characterized by rapidly increasing accommodation space. The sandy sediments are mostly trapped in coastal plains and nearshore deltas during highstands, progressively buried by shales. The fine grained sediments of the upper transgressive system tract forms sealing lithologies, and keep the trapped hydrocarbons in place within the sands (Vail, 1987).

### ***2.2.2.1 Reflection terminations***

The sequence boundaries and flooding surfaces discussed are often displayed in seismic data as reflection terminations. A reflection termination occurs where two reflectors in the seismic converge or otherwise disappear along the dip direction (Mitchum et al., 1977; Vail, 1987). A seismic truncation/termination, implies that the reflection is cut by an unconformity (Catuneanu, 2011).

The different reflection terminations (Table 2.2.1, Figure 2.2.3) result from both changes in the depositional environment, and the subsequently removal of rock or applied change along an unconformity. Sediments deposited during episodes of active rifting, known as syn-rift sediments, normally show horizontal strata terminating progressively against another surface of different angle. The younger strata progressively overstep one another (Veeken, 2007). This

is recognized in seismics as an *onlap* termination. Toplap indicates termination of e.g. clinoforms against an overlying unconformity, as a result of sedimentary bypass where there is no deposition, in addition to minor erosional events (Catuneanu, 2011). On the contrary, downlap is represented by a *downwards* termination of inclined strata, and usually occur at the base of clinoforms; the bottomsets.

*Table 2.2.1. Overview of the different reflection terminations. Modified from Veeken (2007).*

Reflection terminations (separating sequences at boundaries)
<ul style="list-style-type: none"><li>• Downlap</li><li>• Toplap</li><li>• Onlap</li><li>• Erosional truncation</li><li>• Angular unconformity</li></ul>

# Seismic stratigraphy

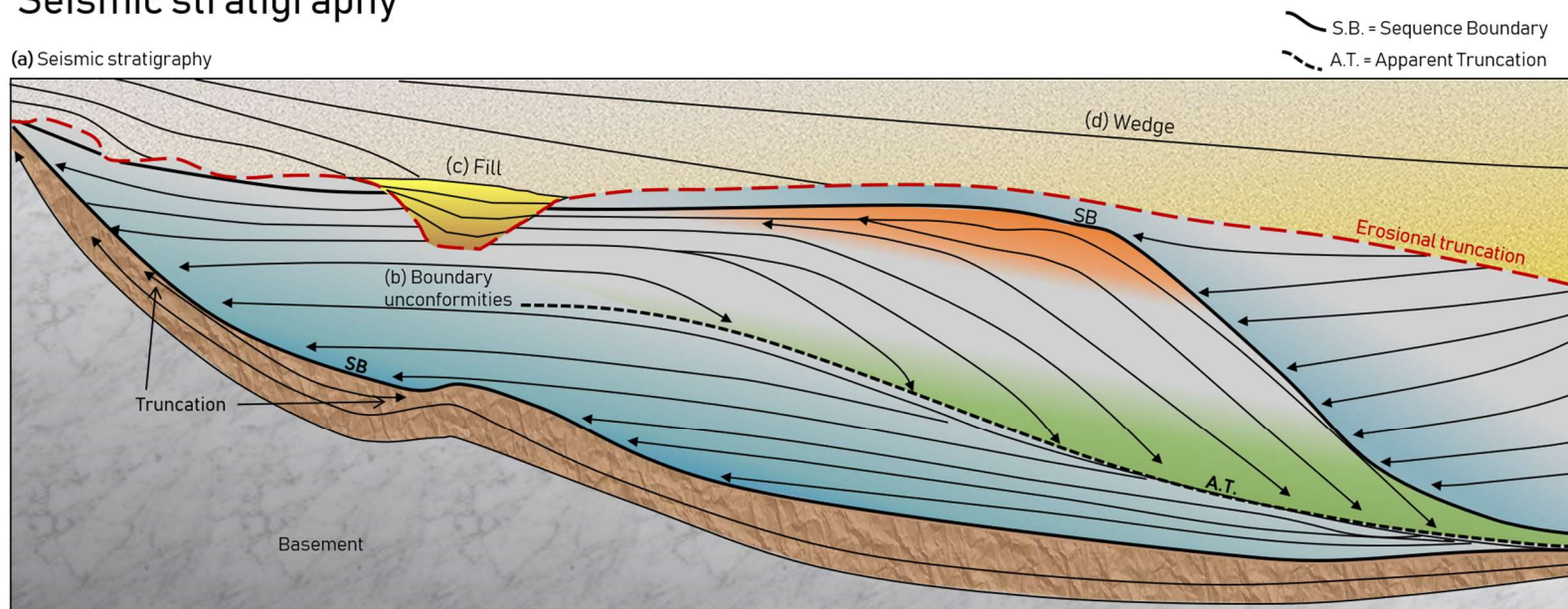
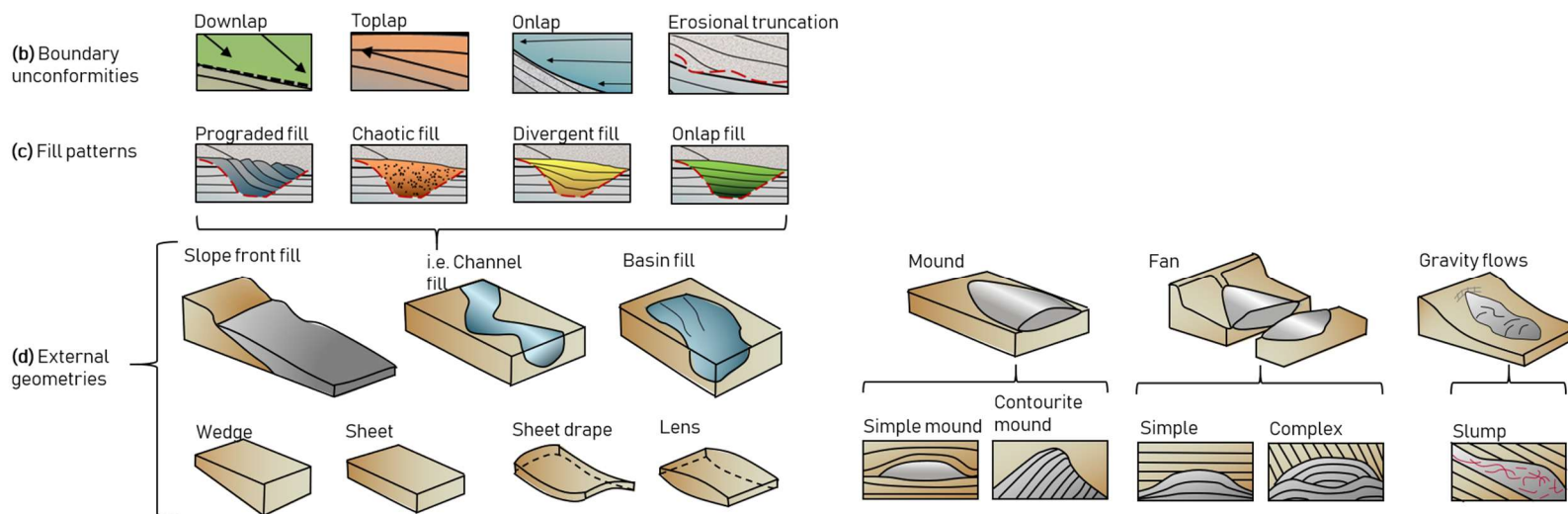
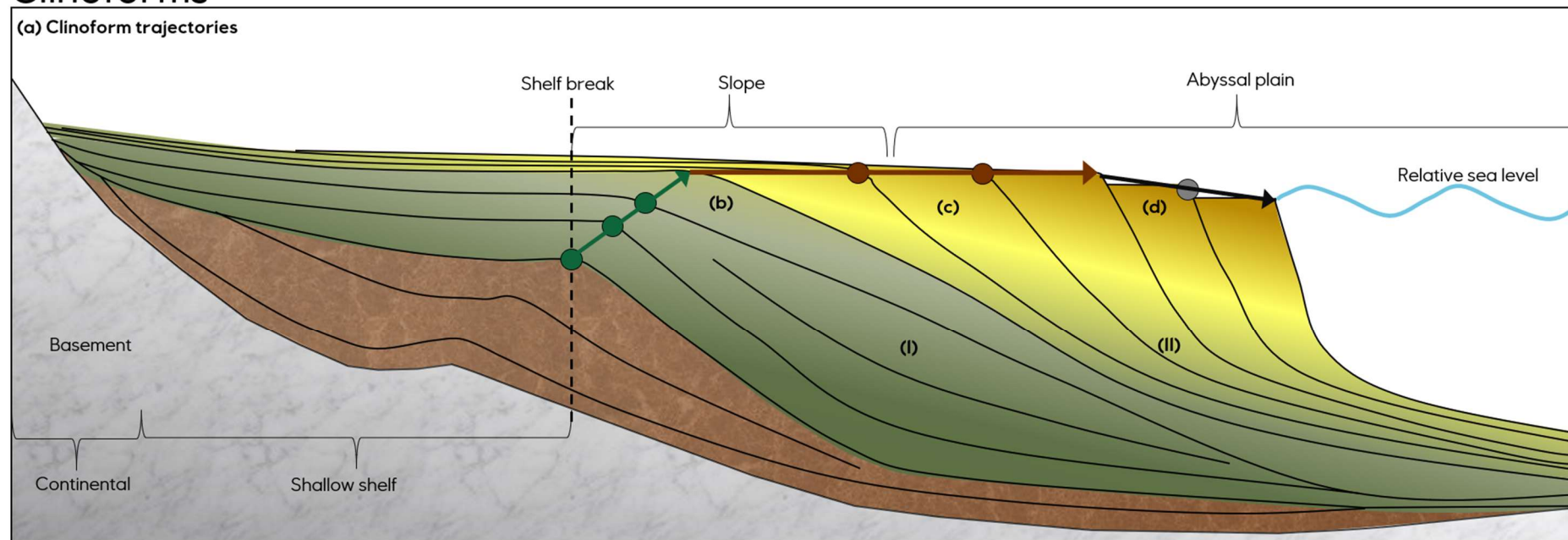


Figure 2.2.3. Overview of the different elements counting within seismic stratigraphy such as boundary unconformities, fill patterns and external geometries. Constructed based on theory from Mitchum et al. (1977), Vail (1987) & Brown (1999).



# Clinoforms

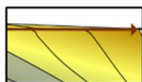


## Trajectories

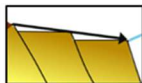
(b) Ascending/rising trajectories



(c) Flat trajectories



(d) Descending trajectories



## Prograding clinoform geometries

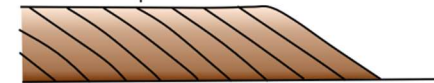
(I) Sigmoidal



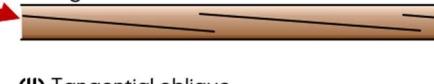
Complex sigmoidal/oblique



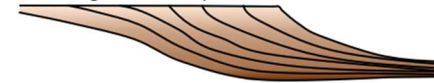
Parallel oblique



Shingled



(II) Tangential oblique



● = Break of slope

Figure 2.2.4. Clinoform geometries and trajectories. Note that ascending trajectories are common for a sigmoidal geometry, whilst flat and descending trajectories are common for oblique geometries. Based on theory from Mitchum et al. (1977) and Helland-Hansen & Hampson (2009).

## 2.3 Seismic facies parameters

Following the establishment of seismic sequences, lithofacies and environments within the sequences are interpreted from seismic data through facies analysis (Mitchum et al., 1977). The objective of seismic facies analysis is to quantify and interpret seismic parameter variations within the sequences and system tracts, caused by geological changes during deposition (Vail, 1987). Seismic facies analysis include description of reflection parameters such as reflection configuration, continuity, amplitude, frequency and interval velocity. The different parameters and their correlative geological interpretations are presented in Table 2.3.1 and Table 2.3.3. The ability to identify particular sedimentary environments and predict lithofacies is of great value for petroleum exploration, by providing a pointer to the location of a potential source, reservoir and seal rocks (Kearey et al., 2002).

Table 2.3.1. The different reflection parameters taken into account when evaluating and interpreting seismic facies. Modified from Mitchum et al. (1977).

Internal reflection parameter	Geological interpretation	Seismic examples	
Configuration	<ul style="list-style-type: none"> <li>• Bedding patterns</li> <li>• Depositional processes</li> <li>• Erosion and paleotopography</li> <li>• Fluid contacts</li> </ul>	Parallel	Chaotic
Continuity	<ul style="list-style-type: none"> <li>• Later continuity of strata</li> <li>• Depositional process</li> </ul>	Continuous	Discontinuous
Amplitude	<ul style="list-style-type: none"> <li>• Velocity and density contrasts of interfaces</li> <li>• Bed spacing</li> <li>• Fluid content</li> </ul>	Strong	Weak
Frequency	<ul style="list-style-type: none"> <li>• Bed thickness</li> <li>• Fluid content</li> </ul>	High	Low
Interval velocity	<ul style="list-style-type: none"> <li>• Lithology estimations</li> <li>• Porosity estimations</li> <li>• Fluid content</li> </ul>	From high to low Vp	From low to high Vp
External forms & areal association of seismic facies units	<ul style="list-style-type: none"> <li>• Gross depositional environment</li> <li>• Sediment source</li> <li>• Geological setting</li> </ul>		


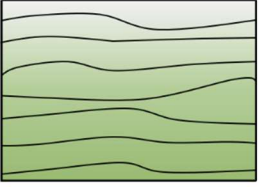
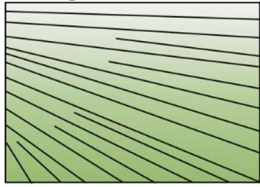
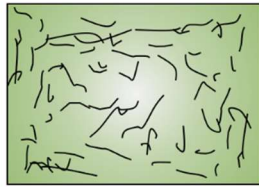
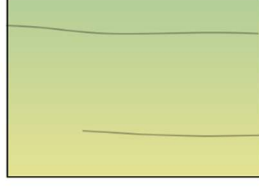
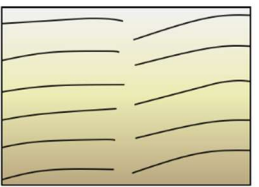
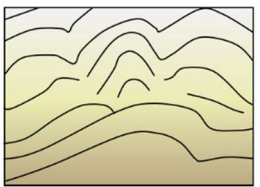
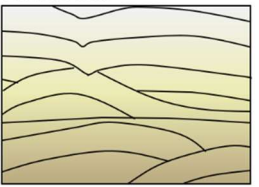
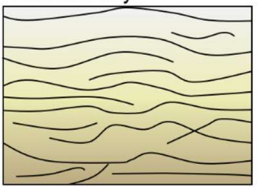
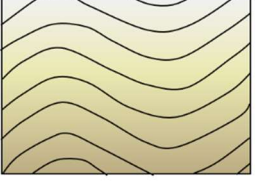
The internal reflection configurations are defined within seismic sequences (Table 2.3.3). Parallel or subparallel reflection configurations suggest uniform rates of deposition on a uniformly subsiding shelf or stable basin setting (Mitchum et al., 1977). These configurations often characterize shallow-water shelf environments (Figure 2.2.1), whilst sigmoidal or oblique cross-bedded units often mark deeper-water shelf edge (Figure 2.3.1) (Kearey et al., 2002). The divergent reflection configuration is frequently caused by lateral variations in the rate of deposition, or a progressive tilting of the depositional surface. The chaotic reflection configuration displays discontinuous, discordant reflections suggesting a disordered and chaotic arrangement of reflection surfaces. It may be indicative of slump structures, channel fill complexes, or highly faulted and folded zones of rock (Figure 2.3.1, Mitchum et al., 1977). Lastly, the reflection free areas indicate e.g. homogenous strata deposited during prevailing, stable depositional conditions (Veeken, 2007).

Seismic facies units are three-dimensional seismic sequences, composed of groups of reflections with parameters differentiating from the adjacent and encompassing facies units (Randen et al., 1998). The internal reflection configurations are important to identify, yet external geometries of seismic facies units ought to be described in context with the internal. This parallel evaluation of internal and external geometries is done in order to understand and comprehend the holistic understanding of units' reflection configurations (Table 2.2.1 & Figure 2.2.3). Seismic facies are foremost interpreted in terms of sedimentary processes and lithologies, energy regime, and lastly the environmental setting.

Table 2.3.2. Overview of the most common external reflection configurations, sub-divided by fill-patterns, mound-configurations and other. The table is complementary with Figure 2.2.3.

<b>External reflection configurations (seismic facies units)</b>		
<b>Fill patterns</b>	<b>Other</b>	<b>Mounds etc.</b>
<ul style="list-style-type: none"> <li>• Basin fill</li> <li>• Slope front fill</li> <li>• Channel fill</li> <li>- Prograded fill</li> <li>- Chaotic fill</li> <li>- Divergent fill</li> <li>- Onlap fill</li> </ul>	<p>Other external geometries:</p> <ul style="list-style-type: none"> <li>• Wedge</li> <li>• Sheet</li> <li>• Sheet drape</li> <li>• Lens</li> </ul>	<p>Mound</p> <ul style="list-style-type: none"> <li>• Simple mound</li> <li>• Contourite mound</li> </ul> <p>Fan</p> <ul style="list-style-type: none"> <li>• Simple</li> <li>• Complex</li> </ul> <p>Gravity flows</p> <ul style="list-style-type: none"> <li>• Slump</li> </ul>

Table 2.3.3. Internal reflection configurations (within sequences). Note that the table is linked to Figure 2.3.1., 2.2.3 and 2.2.4.. Modified from Mitchum et al. (1977) and Kearey et al. (2002)..

Internal Reflection configurations (within sequences)	
Most common:	Other:
<ul style="list-style-type: none"> <li>• Parallel (Figure 2.3.1)</li> <li>• Subparallel</li> <li>• Divergent</li> <li>• Chaotic</li> <li>• Reflection-free</li> <li>• Prograding clinoforms (Figure 2.2.4)                             <ul style="list-style-type: none"> <li>- Sigmoid</li> <li>- Oblique</li> <li>- Complex sigmoid-oblique</li> <li>- Shingled</li> <li>- Tangential oblique</li> </ul> </li> </ul>	<ul style="list-style-type: none"> <li>• Disrupted/discontinuous</li> <li>• Contorted</li> <li>• Lenticular</li> <li>• Hummocky</li> <li>• Wavy</li> <li>• (Even)</li> <li>• (Regular)</li> <li>• (Irregular)</li> <li>• (Uniform variable)</li> </ul>
<div style="display: flex; flex-wrap: wrap;"> <div style="width: 50%;"> <p>Parallel</p>  </div> <div style="width: 50%;"> <p>Subparallel</p>  </div> <div style="width: 50%;"> <p>Divergent</p>  </div> <div style="width: 50%;"> <p>Chaotic</p>  </div> <div style="width: 50%;"> <p>Reflection free</p>  </div> </div>	<div style="display: flex; flex-wrap: wrap;"> <div style="width: 50%;"> <p>Disrupted/ discontinuous</p>  </div> <div style="width: 50%;"> <p>Contorted</p>  </div> <div style="width: 50%;"> <p>Lenticular</p>  </div> <div style="width: 50%;"> <p>Hummocky</p>  </div> <div style="width: 50%;"> <p>Wavy</p>  </div> </div>
<p>Figure 2.3.1. The most common reflection configurations and other modifying terms, following the configurations outlined in Table 2.3.2. Modified after Kearey et al. (2002).</p>	

## 2.4 Sedimentary structures from core observations

Seismic data enables interpretation of structures and lithologies on a regional scale, however the more detailed observations of lithologies and smaller scale sedimentary structures can be seen from cores. Cores from the offshore exploration areas are gathered during drilling operations, where a vertical section of the rock-record is sampled. Variations in grainsize, colour and density of a rock, coupled with sedimentary structures, reflects the depositional energy regime and environment during deposition of the sediments (Collinson et al., 2006).

In a fluvial setting, ripples with asymmetric shapes occur in unidirectional currents, e.g. at the beds of rivers. Irregularities on the riverbed cause localized regions of high flow rate, resulting in erosion and deposition. Furthermore, where the sand input is high, and there is no net erosion, climbing ripples form. The formation of ripples occur in the lowermost part of the flow regime. Towards the upper flow regime, where the flow power increases, ripples are replaced by dunes, of much larger scale. In the upper flow regime, plane bed or antidunes form (Collinson et al., 2006; Koller et al., 2017).

For marine depositional environments, the observed structures are often related to tidal influence, wave-currents, animal activity on the seafloor etc. Wave-ripples form on the seafloor, where regular back-and-forth movement of the waves build symmetrical ripples, in elongated shapes on the seabed. Tidal deposits are often characterized by e.g. double mud-drapes, from the flood- and ebb-water stand (Collinson et al., 2006).

Soft sediment deformation structures form in response to unstable density contrast or lateral variations in load, where the sediments liquidizes or loses strength. Sand sinking into an underlying mud is a classic example, and is often triggered by earthquakes, breaking waves, or rapid deposition of sand (Figure 2.4.1). The down-dropped load casts are the synforms, which often appear along with antiforms, such as flame-structures of mud pushed upwards into the sand layer (Owen, 2003).

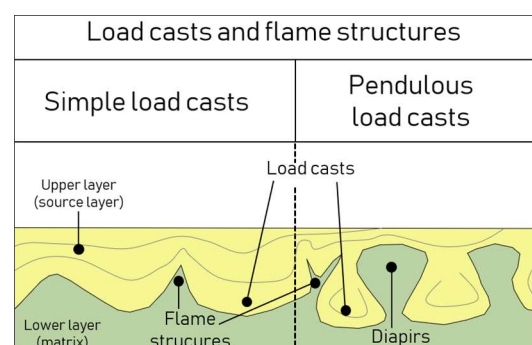


Figure 2.4.1. Examples of soft sediment deformation structures. Modified from Owen (2003).



## 2.5 Fault configurations and seismic imaging

Extensional tectonic regimes often result in breaking of the earth crust, and the resulting structure is a mosaic pattern of horsts (highs) and grabens (lows) bounded by normal faults (Gawthorpe & Leeder, 2000). The Norwegian continental shelf constitutes several rift basins, and the present day configuration of the North Sea Basin is no exception. The growth of normal faults initiates a sedimentary response as accommodation space (depocenters) is created within the basin and erosion usually occur at the flanks and highs. Faults appear on seismic data as vertical line-ups of discontinuous reflections.

Normal faults are constructed in extensional tectonic regimes where down-dropping of hanging wall blocks cause a vertical/lateral displacement of lithological layers (Twiss & Moores, 2007).

Reverse faults, on the contrary, form in compressional tectonic settings where an opposite displacement of lithologies is caused by an upward movement of the hanging wall relative to the footwall (Figure 2.5.1). Faults act as migration pathways for hydrocarbons, or as sealing features in depth depending on the juxtaposed lithologies and constitute an important aspect of petroleum exploration. The most common fault configurations is presented in Figure 2.5.1. The reconstruction of fault activity in a region can roughly be determined based on pattern recognition on both sides of a fault zone in seismic data (Gawthorpe & Leeder, 2000).

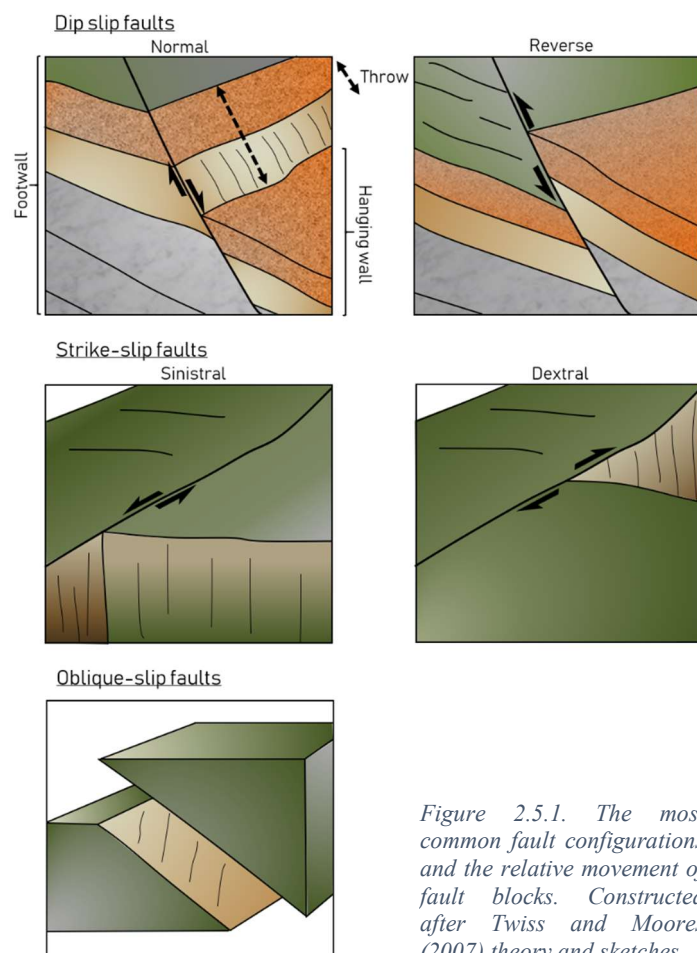


Figure 2.5.1. The most common fault configurations and the relative movement of fault blocks. Constructed after Twiss and Moores (2007) theory and sketches.

## **2.6 The petroleum system**

The petroleum system is a unifying concept that encompasses all the elements and processes necessary to generate and store hydrocarbons (Magoon & Beaumont, 2003; Metwalli & Pigott, 2005). The elements include the following; source rock, a migration pathway through permeable layers upward, a reservoir rock with sufficient porosity and permeability, a trap, and lastly, a seal. The elements must be placed in time and space in such a manner that organic matter in a source rock can be converted into a petroleum accumulation and preserved (Magoon & Dow, 1994). The different elements and processes are presented in Figure 2.6.1. Oil is generally occurring in unmetamorphosed sedimentary characterized rocks, of continental, shallow- and deep-marine water origin (Pratt, 1942; Selley & Sonnenberg, 2015).

A source rock can be broadly defined as any fine-grained, organic-rich rock capable of generating and expelling hydrocarbons, given however, that sufficient exposure to heat and pressure is in place (McCarthy et al., 2011). Following deposition of organic-rich sediments, microbial processes convert some of the organic matter into biogenic methane gas which is commonly identified within shallow sequences. The successive infill of e.g. basins, results in greater depths of burial which is accompanied by increased heat in accordance with the basin's geothermal gradient. The applied heat causes the organic matter to gradually transform into an insoluble organic matter known as kerogen. There is mainly three types of kerogen, determined using a combination of organic petrography, pyrolysis and other geochemical evaluations. The different kerogen and corresponding depositional environment was presented earlier (Figure 1.5.1).

In general, temperatures increase towards earth's center in depth yet with local and regional thermal variations. The heat flow through layers fluctuates as the thermal conductivity of various sediments differs, and thus the geothermal gradient is specific and defined within each petroleum province (Selley & Sonnenberg, 2015). For the Central Graben in the North Sea, the geothermal gradient has been manifested as 40°C/km from drill-stem tests and reservoir temperature measurements (Cornford, 1994). Commonly, the temperature (as discussed), rock density, salinity and pressure increases with depth, whereas porosity decreased. The relationship between temperature and pressure in depth governs the behavior of fluids in the subsurface, including water and hydrocarbons within the pore-space of a rock (Archer & Wall, 1986; Selley & Sonnenberg, 2015).

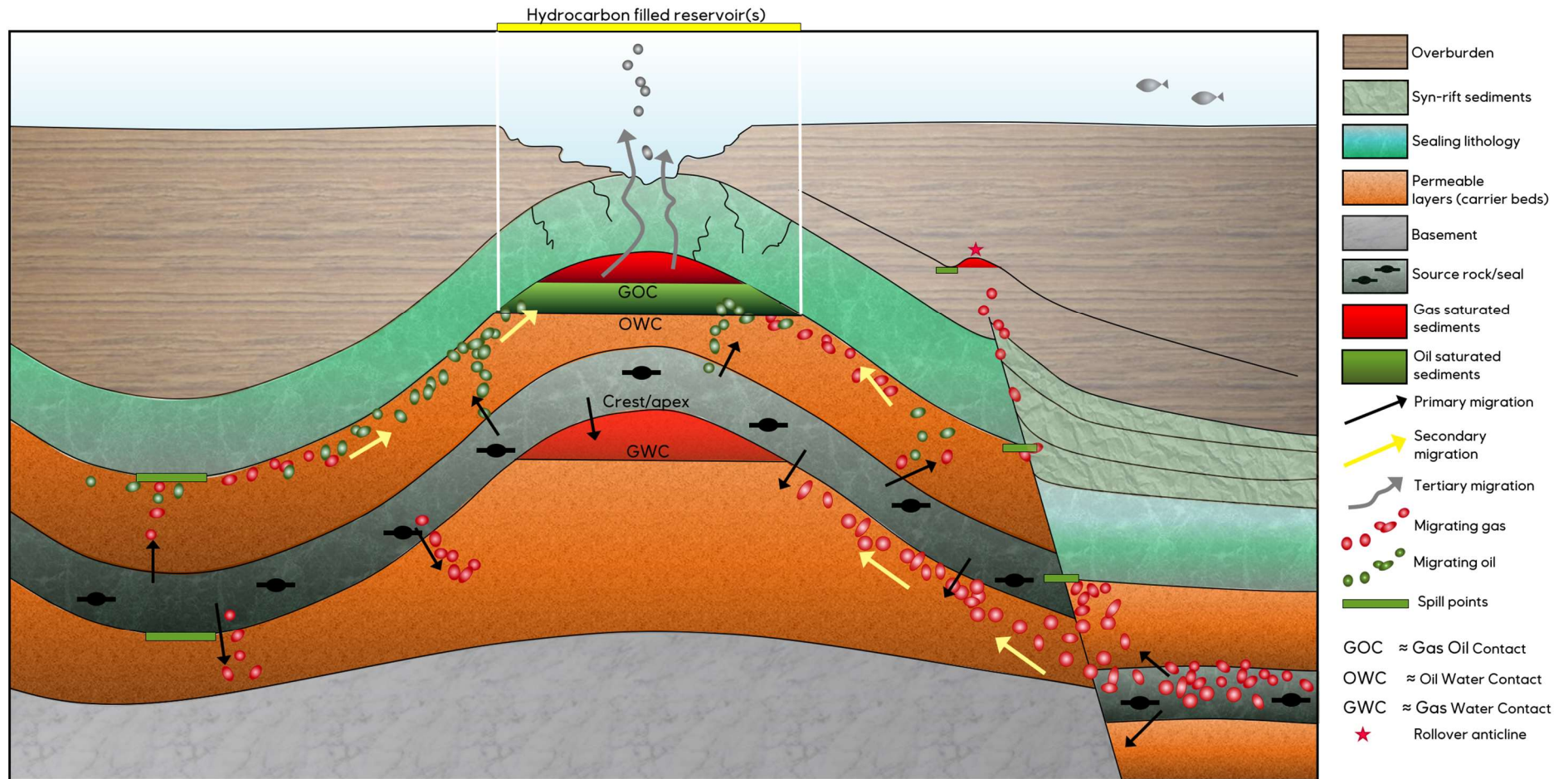


Figure 2.6.1. Illustration of the petroleum system and the different elements/processes, showing a classic anticlinal fold trap with hydrocarbon accumulations in permeable layers at different levels. Note that only oil has accumulated in the shallowest trap, with migrated hydrocarbons from the source rock directly below. The down-faulted block to the right is included to exemplify that oil and gas is generated at different temperature/pressure gradients, oil first- followed by wet- and dry-gas, and that the source rock additionally can work as a seal for the lowermost trap.

### 2.6.1 *Primary/secondary/tertiary migration*

The burial of a source rock initiates cracking and thus expulsion of hydrocarbons (Henriet et al., 1991). The expelled hydrocarbons causes a great pressure increase, resulting in movement and migration of hydrocarbons from source (e.g. clay/shale) into permeable carrier beds (e.g. sands or carbonates). This process is referred to as the *primary* migration (Price, 1981). The subsequent movement of hydrocarbons within permeable carrier beds and reservoirs is termed as *secondary* migration, where the movement direction is principally a response to differential pressures in the subsurface. However there is consensus that the interplay between subsurface pressure and buoyancy, the latter caused by the different densities of the respective fluids, is the dominant factor controlling shallow gas and fluid migration (Schowalter, 1979; England, 1994; Selley & Sonnenberg, 2015). The relationship between these two factors forces subsurface fluids and gases to take advantage of both vertical and favorably laterally dipping subsurface pathways.

Reservoir rocks are characterized by high permeability and porosity allowing fluids to flow and pass through the host rocks, however a reservoir system cannot function as efficient lateral drains unless it is continuously overlain by unbreached sealing lithologies (Demaison & Huizinga, 1994; Magoon & Dow, 1994). Leaking and outflow of hydrocarbons from a well-defined trap nevertheless is almost inevitably within a petroleum system, despite the low permeability properties of the sealing layer. This leakage has been termed *tertiary migration* (Figure 2.6.1, Cartwright et al., 2007).

Although the general pattern in migration of hydrocarbons is primarily understood by pressure gradients and buoyancy in depths, the overall drainage of a petroleum system can be subdivided into laterally and vertically migration (Demaison & Huizinga, 1994). The vertically drained systems are generally found where faults and fractures compose the greatest controls (Rajan et al., 2012). Although, there is some dispute as to the exact nature by which faults permit fluid flow (Judd & Hovland, 2009). Whether faults act as sealing structures or migration pathways depend on, among other factors, the juxtaposed lithologies (Figure 2.6.3, Selley & Sonnenberg, 2015). Vertically drained petroleum systems are generally characterized by the occurrence of hydrocarbon accumulations above or near the top of the active source rock, with small horizontal offsets, indicating that lateral migration distances are short. Stacked accumulations could be expected to contain the same genetic oil, where the presence of fault

and fractures limit the size of the fetch area, leading to zones with numbers of small- and medium-sized accumulations (Demaison & Huizinga, 1994; Magoon & Beaumont, 2003).

Despite the nature of vertical, upwards migration initiated by pressure gradients and buoyancy, lateral migration occurs. This may be e.g. along a horizontally continuous regional seal resting on a widespread carrier bed/reservoir (permeable) unit, where a significant dip is present (Demaison & Huizinga, 1994; Judd & Hovland, 2009). Such features can include channels and clinofolds (Rajan et al., 2012). Laterally drained petroleum systems usually have a couplet of continuous seals overlying a laterally continuous reservoir. The structural deformation in such regions is usually low to moderate. Faults and fractures are less controlling factors, in comparison to the vertically drained petroleum systems. Tectonic stability is critical in order to maintain seal integrity (Demaison & Huizinga, 1994). The lateral migration accounts for occurrences of oil accumulations in thermally immature strata located far from the pod of active source rock (Magoon & Beaumont, 2003). Large amounts of the expelled hydrocarbons is considered to be “lost” by circumventing traps.

The occurrences of oil, gas and water in a stratified manner according to their relative densities within porous permeable reservoir rock entrapments, imply that the fluids are free to migrate vertically and laterally within the reservoir (Selley & Sonnenberg, 2015).

## 2.6.2 Traps

The existence of petroleum accumulations requires migrating hydrocarbons to be focused from a much larger volume of mature source rock into a much smaller volume of entrapment (Demaison & Huizinga, 1994). Oil and gas are trapped in the uppermost structural culmination, or the highest point of a stratigraphic pinchout trap of a permeable rock unit, where they are stored if a sufficient seal is in place (Selley & Sonnenberg, 2015).

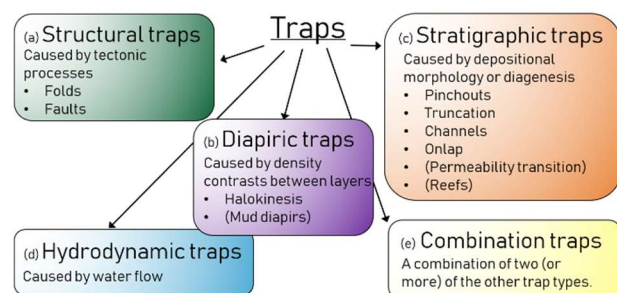


Figure 2.6.2. Overview of the different trap types, presented in Figure 2.6.3, Figure 2.6.4, Figure 2.6.5, Figure 2.6.6 & Figure 2.6.7.

The different trap configurations are presented in Figure 2.6.2 to Figure 2.6.7. Trap configurations may comprise a dip closure, fault-bounded dip closure, stratigraphic pinch out, or combinational traps (Veeken, 2007). Structural traps are characterized by the presence of mainly faults and folds altering the subsurface stratigraphy into ideal storage settings for hydrocarbons, such as dip and fault-bounded closures. Fault juxtaposed traps placing reservoir rocks against low-permeable layers providing a structural closure have been discussed by

numerous authors since the early 20th century (Clapp, 1910; Hager, 1915; Allan, 1989; Sorkhabi & Tsuji, 2005). Stratigraphic traps are often represented by pinch-outs with no structural closure. Purely stratigraphic traps void of any partial structural control tend to be imperfectly sealed and, consequently, generally smaller in size compared to structural traps (Demaison & Huizinga, 1994). Combination traps could e.g. be a fault-bounded dip closure with lateral truncation and/or pinch out (Figure 2.6.7).

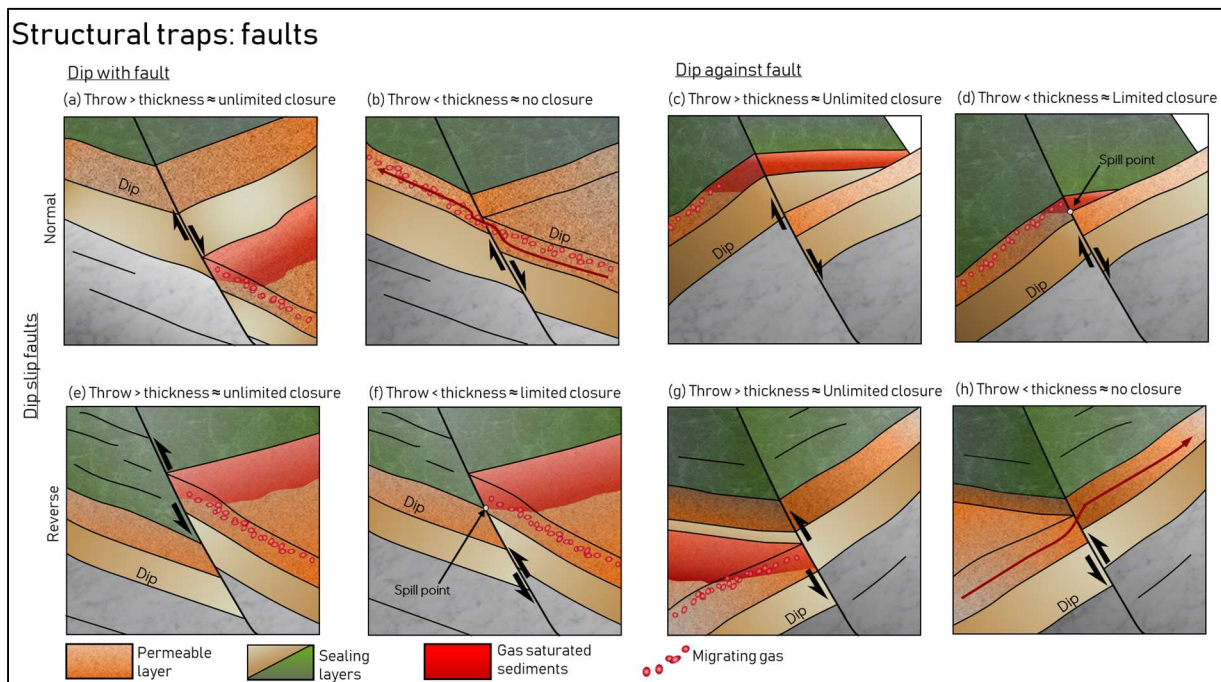


Figure 2.6.3. Structural traps (figure 2.5.3. a): faults. The eight theoretical fault trap configurations. Note how the throw and juxtaposed lithologies affects the closure and trap potential, i.e. (a) where a carrier bed/reservoir rocks is resting against a low-permeability rock and thus a structural closure is in place. Compiled based on theory from Sorkhabi & Tsuji (2005).

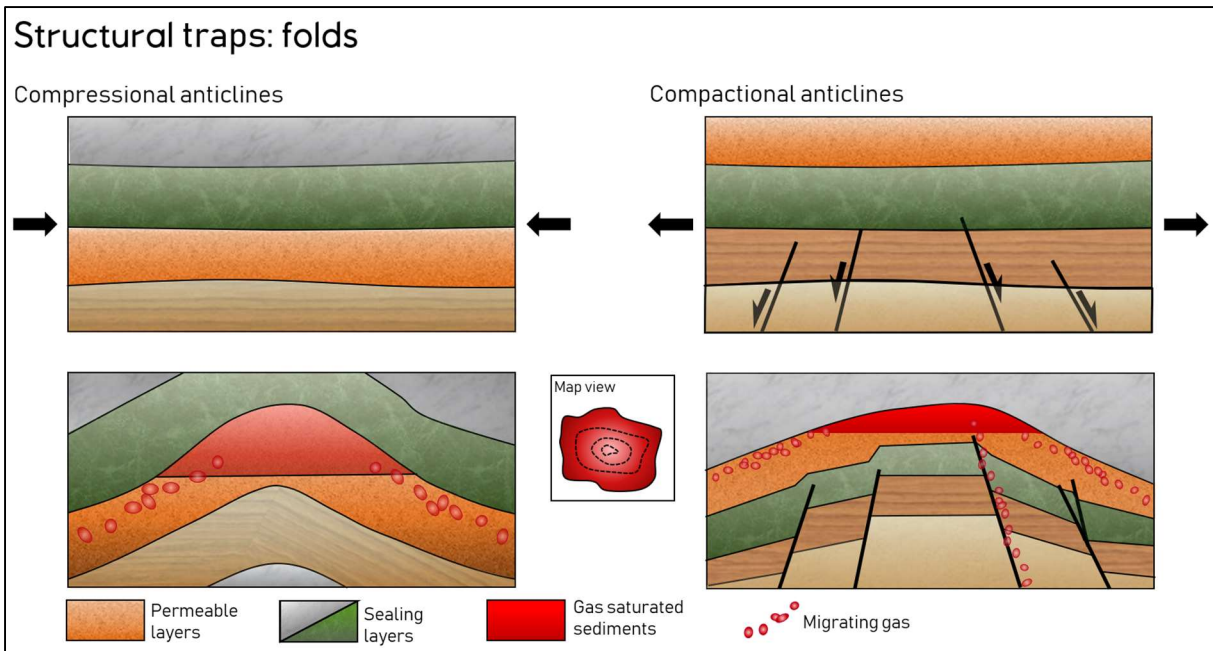


Figure 2.6.4. Structural traps (figure 2.5.3. a): folds. The up-dip of layers connects and shape anticlines which are ideal for accumulating and storing of hydrocarbons. Anticlines form in several ways, such as during compressional- or compactional-regimes. Modified from Selley & Sonnenberg (2015).

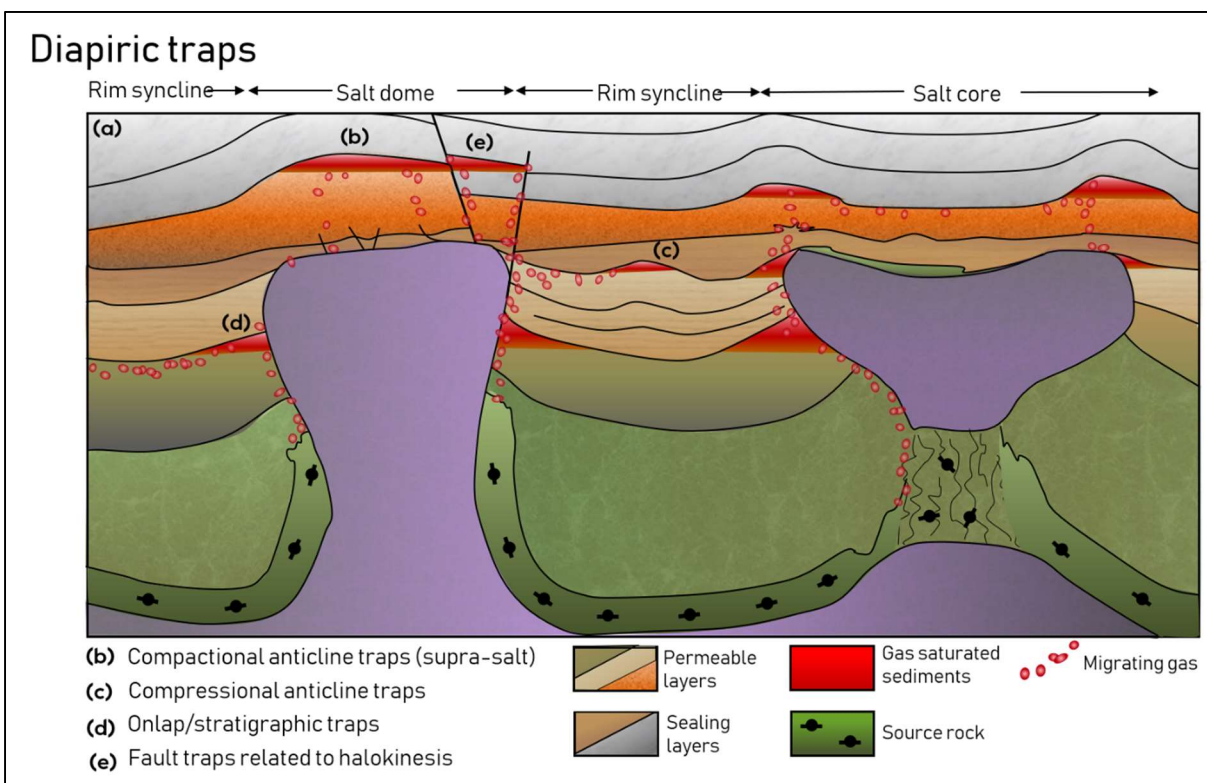


Figure 2.6.5. Diapiric traps (figure 2.5.3. b). Traps related to halokinesis where salt intrudes the overlying layers, folding and compressing the sediments thus creating pinchouts, truncations, anticlines and faults. Modified from Selley & Sonnenberg (2015).

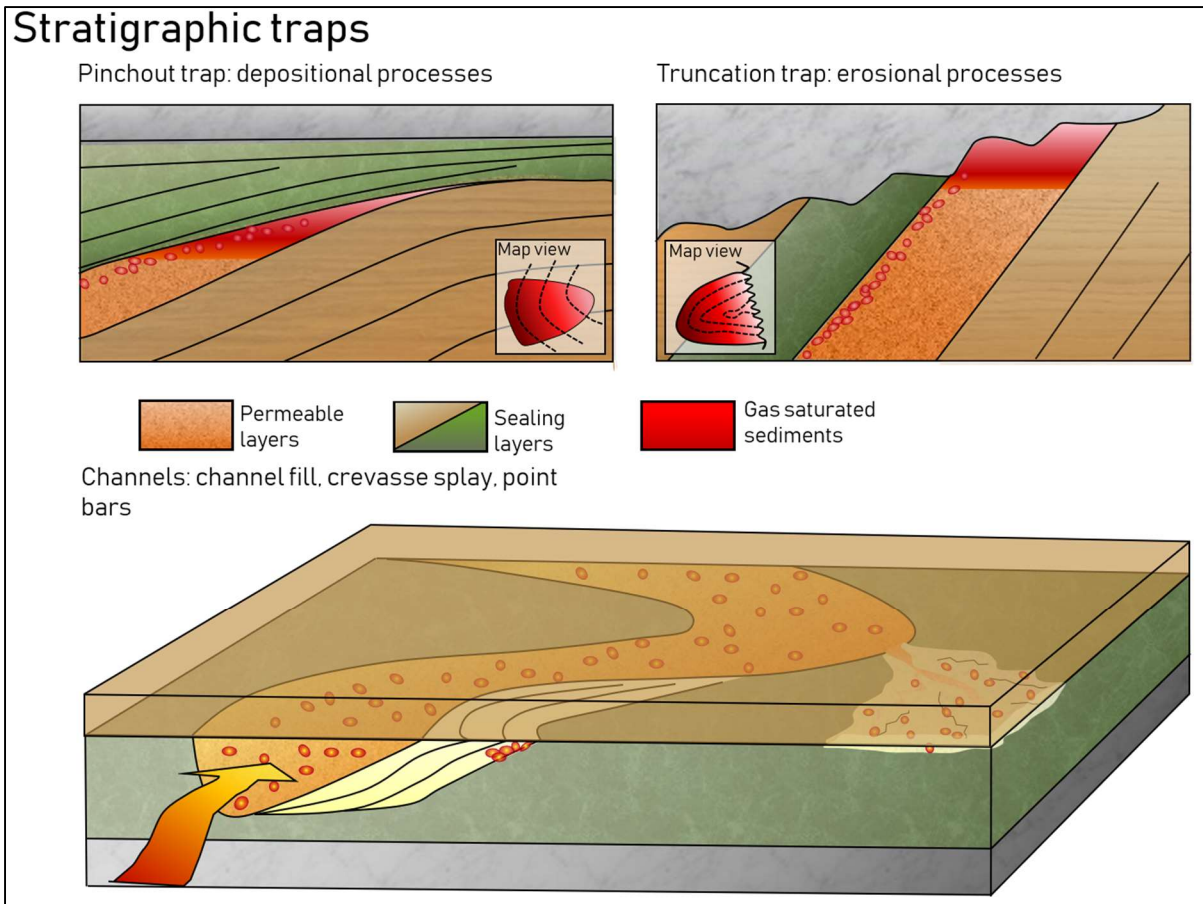


Figure 2.6.6. Stratigraphic traps (figure 2.5.3. c). Pinchout traps formed from depositional processes, truncation traps formed from i.e. erosion of sediments, and lastly channel related traps such as channel fill, crevasse splays and point bars composed of sandy sediments in an otherwise homogenous shaly/fine grained environment. Modified from Selley & Sonnenberg (2015).

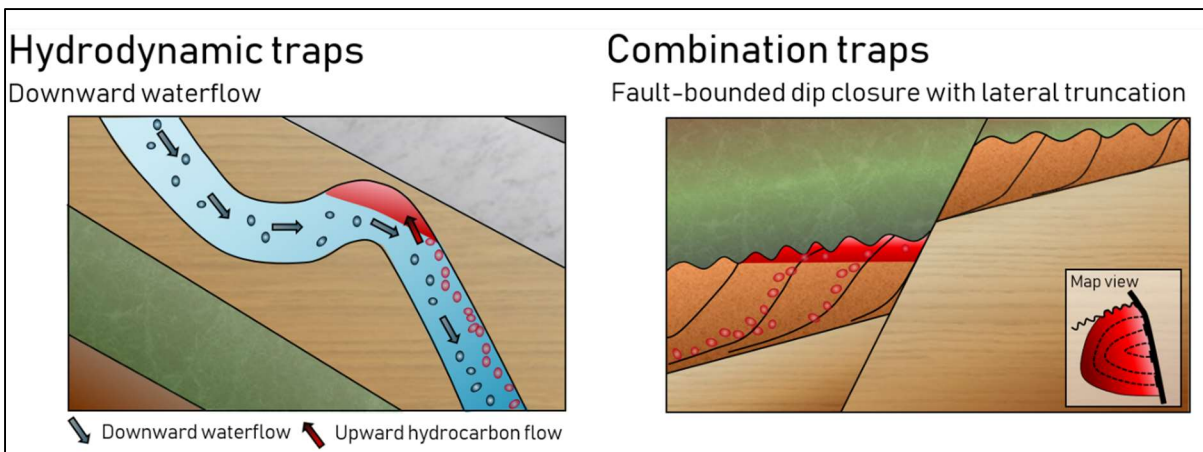


Figure 2.6.7. Hydrodynamic and combination traps (figure 2.5.3. d & e). Hydrodynamic traps are less abundant than i.e. structural/stratigraphic traps, but appear where a downward waterflow exceeds the upwards buoyancy effect of hydrocarbons. Combination traps may be a conjunction of two or more, of the abovementioned traps. Modified from Selley & Sonnenberg (2015).



## 2.7 Direct hydrocarbon indicators

Shallow gas accumulations have been recognized from acoustic datasets since the late 1950s. The importance as a research topic has intensified recently (Garcia-Gil et al., 2002). 3D seismic data makes it possible to map the spatial distribution of leakage-related seismic anomalies, even though establishing the relation between migration/leakage processes and their corresponding seismic expression is challenging (Arntsen et al., 2007; Løseth et al., 2009). The existence of shallow gas is often associated with, and related to, deeper situated petroleum systems and therefore a comprehensive understanding of the origin and migration of these features is extremely valuable in petroleum exploration (Chand et al., 2014).

### 2.7.1 Seismic response of gas

The presence of free gas occupying the pore space of sediments induces a profound effect on the host rocks' geoacoustic and geophysical properties. Gas substituting the normal water occupation in sediments results in a prominent reduction primarily in the seismic velocity, but additionally in the density of the gas-saturated rock (Figure 2.7.1; Andreassen et al., 2007). The change in geophysical properties is manifested and revealed directly in seismic data as an abnormally high amplitude with reversed polarity (phase reversal) commonly referred to as a *bright spot*. Bright spots are recognized at the interface between water- and gas-saturated sediments (high to low velocity). The drastic reduction in velocity causes an expression in the seismic data similar to when harder rocks overlie softer rocks (Figure 2.1.2). This seismic response is expressed by a reversed polarity. Dim spots likewise occur because of a decrease in amplitude on the top reservoir reflection, indicative of a change in fluids within the porespace (Veecken, 2007). In the seismic data, dim spots simply appear dimmer or more transparent than the surrounding reflectors amplitudes.

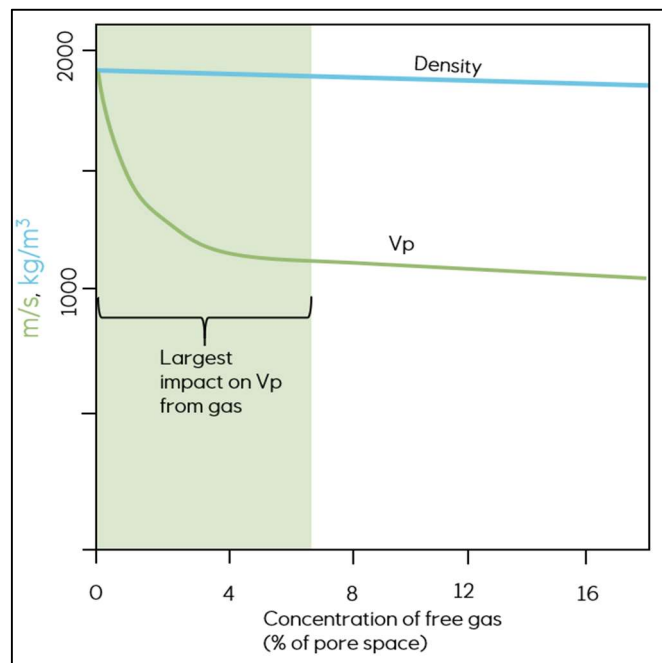


Figure 2.7.1. Illustration of the change in wave velocity ( $V_p$ , m/s) and density ( $\text{kg/m}^3$ ) calculated as a function of gas saturation within the free pore space of sediments (i.e. sandstone) with porosity=0.4 and  $V_p=1,900\text{m/s}$ . The equation assumes a uniform distribution of gas in the sediments. Modified from Andreassen et al. (2007).

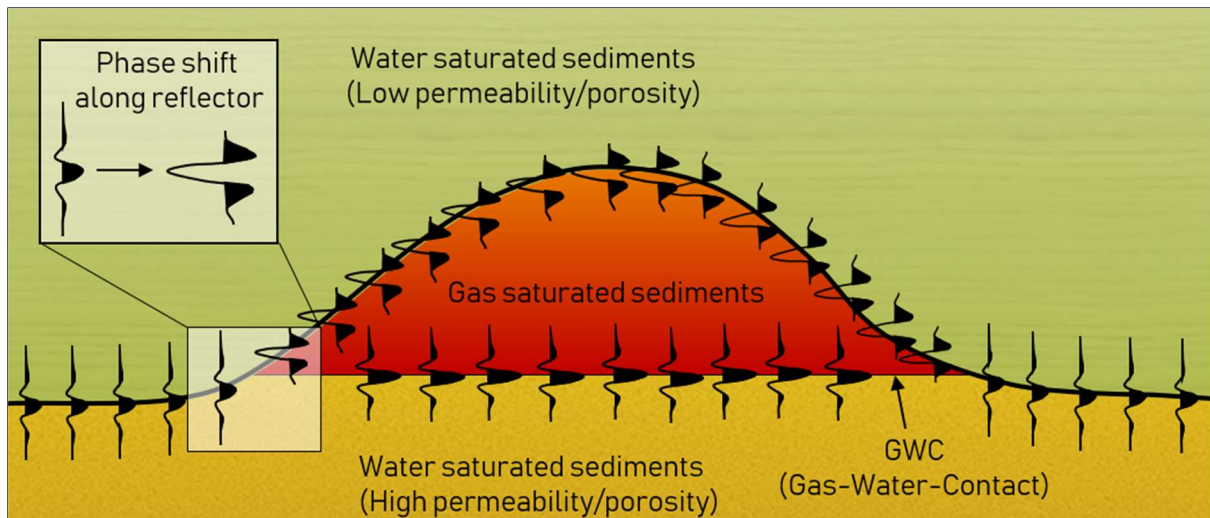


Figure 2.7.2. Illustration of gas-filled anticlinal trap with the corresponding seismic response (zero-phase, normal polarity data). Note how the phase of wavelet changes along the reflector, moving from water-saturated sediments to gas-saturated sediments. The lower gas-water-contact (GWC) has a normal phase, and is recognized as a flat spot in the seismic data. Constructed from Andreassen et al. (2007) & Løseth et al. (2009).

In the absence of bright spots, fluid contacts nonetheless can be recognized by *flat spots* in the seismic data as horizontal reflection events discordant to the local geological dip (Kearey et al, 2002). These two occurrences in the seismic are attributable to the large reflection coefficient at the top and bottom of gas-filled reservoirs, however the flat spots display a normal polarity, meaning that there is no phase reversal present (Kearey et al., 2002; Veeken, 2007). This is due to the increasing velocity and density when the seismic wave moves from the gas- to water-filled pore space in sediments, which induces a positive reflection coefficient. There are ideally three fluid contacts: the gas-oil-contact (GOC), the oil-water-contact (OWC) and lastly the gas-water-contact (GWC) if there is no oil present in the reservoir. Flat spots are easily identified on account of the flat nature of the fluid contact, but also because they are unconformable with adjacent reflectors (Brown, 1999). The horizontal orientation is caused by the buoyancy effect, and the fact that gas is lighter than water and floats above. The seismic responses of bright- and flat-spots are exemplified in Figure 2.7.2.

Furthermore, gas accumulations and fluid migration in the subsurface may display a number of other characteristic seismic responses, such as acoustic columns, pull-down effects and gas chimneys (Løseth et al., 2009; Vardar & Alpar, 2016).

### 3 Data and methods

#### 3.1 Data

Details of the datasets utilized in this study are described in the next chapter, followed by the methods and the approach used to achieve the objectives of this study. The study relies principally on an extensive database of 3D and 2D seismic data. The 3D data is a merge comprising 16 seismic cubes, the location and extent of which is shown in Figure 3.1.1. The position of the core logged in the study is indicated in Figure 3.1.1.c.

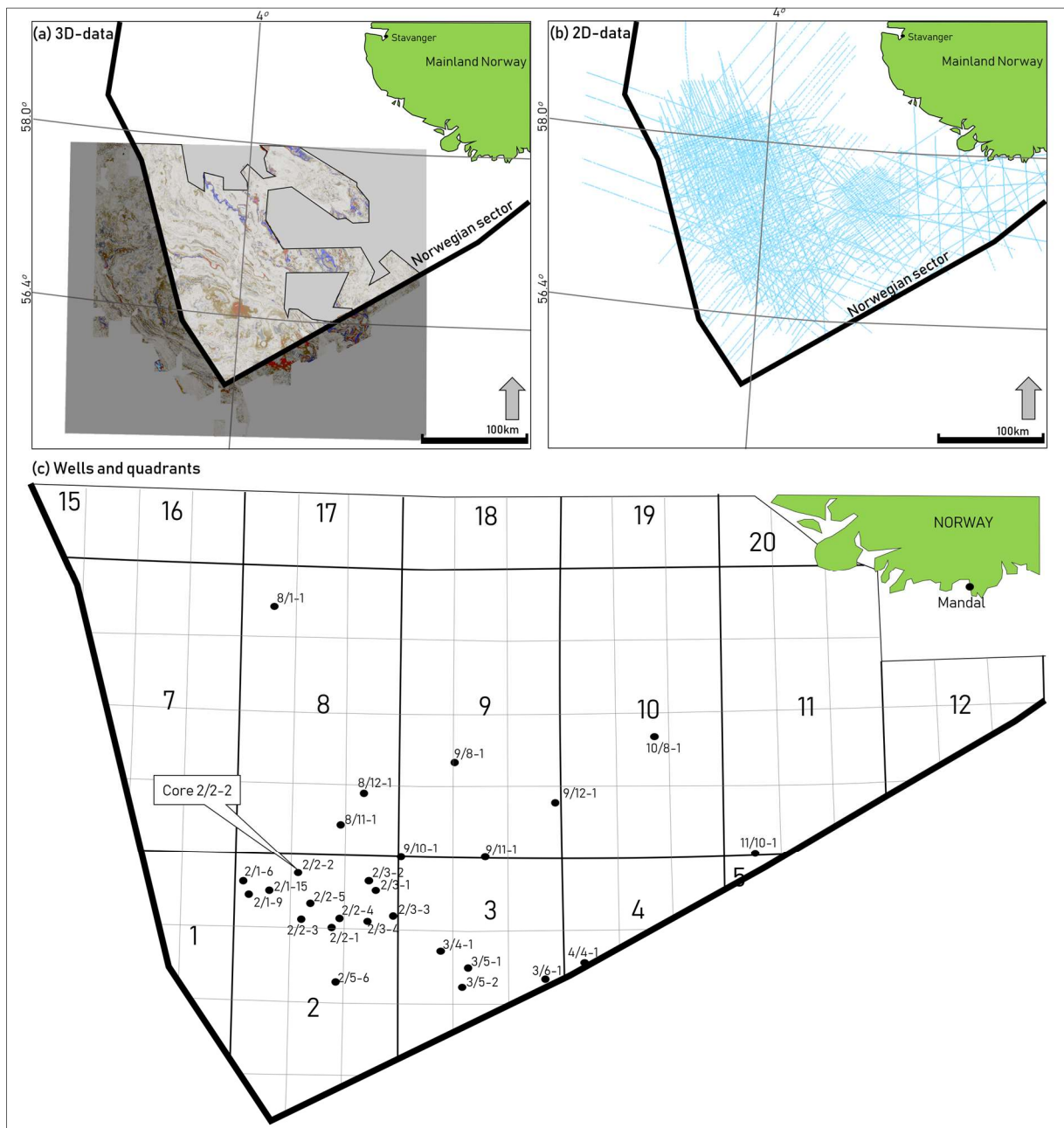


Figure 3.1.1. The location and extent of the (a) 3D-merge, (b) 2D-data in blue lines, (c) wells available in this study.

Eight 2D-seismic surveys are also included. An overview of all the available seismic data and wells is given in Appendix 9.2. The advantage of utilizing large amounts of 3D-seismic data in correlation with 2D-lines, is that the data cover large parts of the southern North Sea, and thus reflects and comprises the full depositional structures and migration pathways for hydrocarbons. The 3D-merge covers 400x275km of the North Sea, with varying quality and presence. Seismic 3D-data lacks in some areas between the 16 originally merged cubes, these are however covered and filled in by 2D-lines.

One core from well 2/2-2, the Desmond discovery well, located in the central part of the study area, was correlated with the interpretations from the seismic data and information from well logs in order to better reconstruct and suggest a paleo-environment. The core was accessed through Lundin's Weatherford laboratory in Stavanger. An overview of the different wells and where the well-information (completion logs and reports) was obtained is given in Appendix 9.3. The Norwegian Petroleum Directorate (NPD) Factpages were used frequently for well-information, and is not further referred to in the text.

## **3.2 Methods**

### **3.2.1 *Software***

Seismic analysis and interpretation was performed in the seismic software Schlumberger's Petrel E&P Platform 2017. The software was primarily used for interpreting reflectors, generate surfaces, volume and surface attributes, and 3D-views of sequences and structures identified.

### **3.2.2 *Workflow***

The approach adopted for this study is outlined in Figure 3.2.1 and divided into seven key stages, with the complementary logic and aims described successively. The following sub-chapters outlines this workflow and are noted correspondingly; 3.2.2 a – g.

#### **3.2.2.a. Preparation of data**

Firstly, the seismic- and well-data available for interpretation was configured in Petrel and both the polarity convention (Figure 2.1.1) and frequencies for the different datasets were determined.

The frequency at different depths is possible to approximate by examining the frequency spectrum (Appendix 9.4), available through the inspector tool in Petrel. By combining the different sequences with the velocity log from nearby wells, an approximation of the seismic

velocity for an isolated seismic interval can be suggested. The wavelengths were derived from Equation 2.1, and the resolution was calculated based on Equations 2.2 and 2.3, presented in Appendix 9.1. The results of the frequency calculations are presented in Table 3.2.1. The resolution of the data is important to be aware of for the following interpretation of the seismic data, as it provides information about the scale of the observed objects.

Table 3.2.1. The estimated and calculated frequencies, wavelength, vertical- and horizontal resolutions for the defined sequences used in the study. Note that the calculated horizontal resolution is estimated for migrated data. The vertical and horizontal resolution thus equals one another.

ZONE 1 (deeper, southern part)					ZONE 2+3 (shallower, northern part)			
Sequence	Velocity (Well 2/4-11)	Average Frequency	Wavelength (v/f)	Resolution	Velocity (Well 8/10-2)	Average Frequency	Wavelength (v/f)	Resolution
Upper Miocene	2005m/s	30 Hz	66.8m	16,70m	1648m/s	45 Hz	36.6m	9,15m
Lower Miocene	2117m/s	25 Hz	84.6m	21,17m	1742m/s	42 Hz	41.4m	10,36m
Upper Oligocene	2225m/s	20 Hz	111.2m	27,81m	2032m/s	35 Hz	58.0m	14,51m
Lower Oligocene	2540m/s	17 Hz	149.4m	37,35m	2498m/s	25 Hz	99.9m	24,9m

Several wells were tied to the different parts of the merged seismic 3D-cube using an in-house synthetic seismogram from Lundin. Picks from the NPD and Lundin were used to identify three important surfaces; the Base Oligocene, the Mid-Miocene Unconformity and the Top Miocene, which binds the stratigraphic interval used in this study. The picks chosen by the NPD were consistently weighted especially for mapping the Mid-Miocene Unconformity (MMU). The horizon mapping was done manually and partly by 2D- and 3D-autotracking at an increment of 32 inlines/crosslines throughout the available data. A summary of the different horizons and picks is presented in Appendix 9.5. The naming convention applied throughout the study for the Oligocene-Miocene sequences have been updated accordingly to chronostratigraphic work available in the literature (Deegan & Scull, 1977; Rundberg & Eidvin, 2005).

### 3.2.2.b: Establish seismic sequence framework

A seismic stratigraphic framework was established by subdividing the Oligocene-Miocene interval into sequences, based on reflection configurations, possible flooding surfaces and sequence boundaries. Horizons were chosen in a manner that would best distinguish zones of different sedimentological character. After establishing a series of horizons, a reference cross-section was chosen in order to indicate the vertical position of surfaces and attributes relative to each other throughout the presentation of the results. Surfaces were then generated based on

the picked horizons. A minimum curvate interpolation was applied during the gridding process to enhance the smoothness of the subsequent generated surfaces.

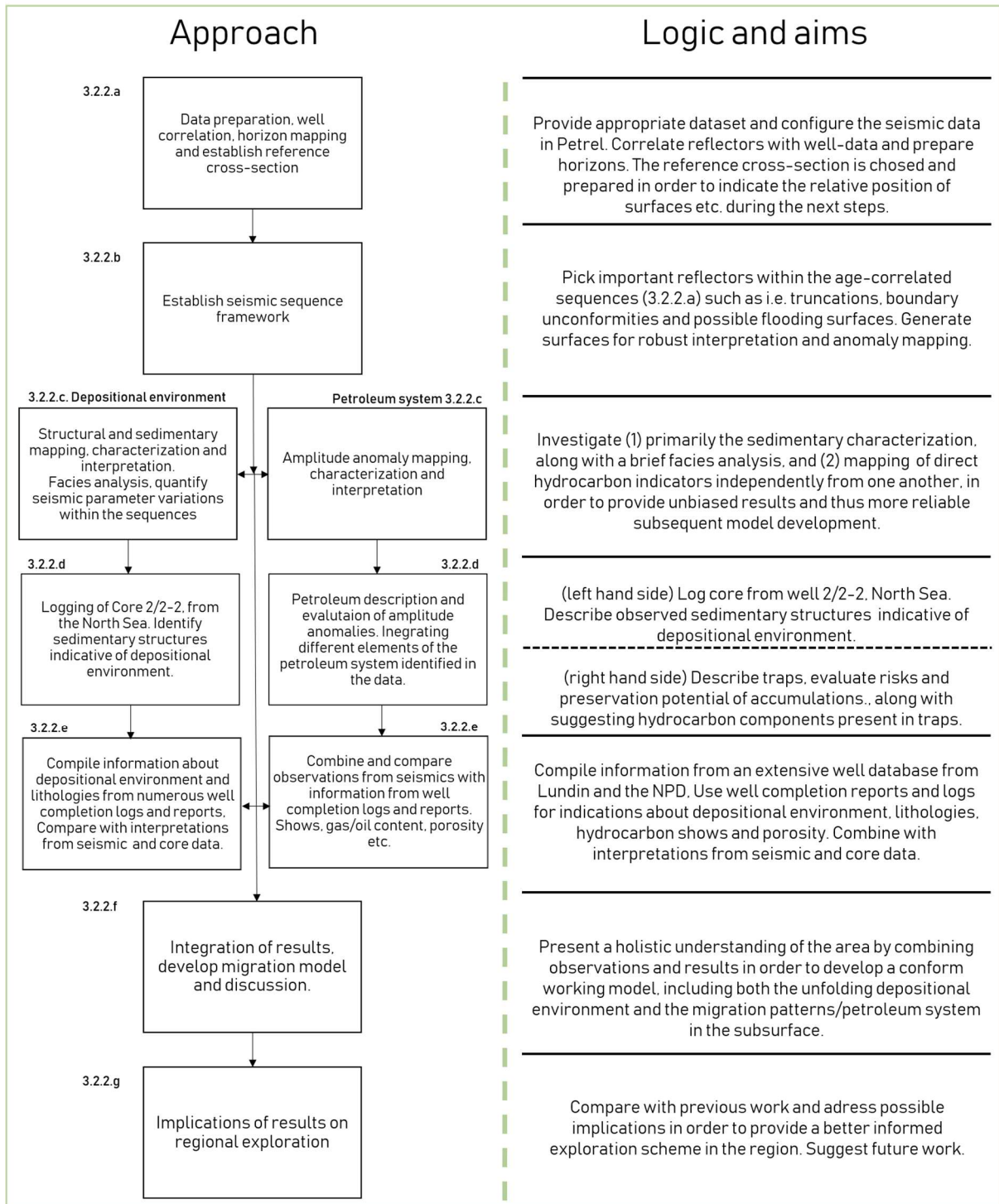


Figure 3.2.1. Flowchart displaying the outline of the seven key stages/approaches, with the coherent logic and aims.

### 3.2.2.c Left hand side: Structural and sedimentary mapping

During the presentation of the identified structures, the region was divided into three zones in order to keep track on the position of the observed features. The cube was screened for structural features which were mapped out in three dimensions through cross-sections, allowing a holistic understanding and extent of the different dominating elements, such as salt diapirs and related faults, horsts and grabens, clinoforms, channels etc.

Following the gridding and surface generation process a variance cube (*attribute*) of the seismic 3D-merge was used to demonstrate the overall structural character and geomorphological features, ensued by surface attribute (value extraction) extractions completed along the previously established reflection framework (surfaces) at various offsets and search windows. Structural elements such as faults, salt diapirs and channel systems were easily detected through the variance cube and mapped out at different levels/depths. The results from this approach are mostly presented by attribute maps and 3D-visualizations.

Attributes represent different ways of presenting basic, however complex, information by extracting measurements along surfaces through simple mathematical manipulation and are valuable for gaining insight from the data particularly when displayed spatially over interpreted horizons (Brown, 2001; Chopra & Marfurt, 2005; Carpenter, 2013). They are frequently used throughout the study with the aim to simplify and ameliorate the interpretation process of seismic data.

Emphasis was given to sequence boundaries, transgressive surfaces, clinoform geometries and shelf-edge trajectories during the description of the seismic sequences. Paleo-water depths were calculated for four periods, using the vertical height (TWT) of clinoforms by converting two-way-traveltime to meters. The equation (Equation 3.1) used is presented in Appendix 9.1. An overview of the calculated depths are given in Table 3.2.2. The velocities are picked from well 2/4-11 and 8/10-2, similar to the frequency estimates.

Table 3.2.2. Calculated paleo-water depths.

Sequence	Velocity (Well 2/4-11 or Well 8/10-2)	Average clinoform heights (TWT)	Water depth
Upper Miocene	1648ms	300ms (at most)	<250m
Upper Oligocene/Middle Miocene	2117m/s	280-330ms	300-350m
Upper Oligocene	2032m/s	150-200ms	150-200m
Lower Oligocene	2540m/s	200ms	250m

A brief facies analysis was applied to the formerly established seismic sequences and system tracts, in order to quantify and interpret both lateral and vertical facies variations. The analysis was carried out by evaluating the different parameters outlined in Table 2.3.1 and the internal reflection configurations listed in Table 2.3.3. The inferred geological variations during deposition from the facies analysis were then applied to the depositional patterns from the sequence analysis.

#### **3.2.2.d. Left hand side: Core logging and observation**

Two cores were cut from well 2/2-2 in Quadrant 2 of the southern North Sea, and the shallowest one was logged and integrated with the seismic data. The core was accessed through Lundin. The variations in rock colour and grain size were logged on a centimeter scale. The core comprised approximately 15m of sediments. Small-scale structures such as ripples and soft sediment deformation structures were noted, along with other features such as organic rich layers, plant fragments, bioturbation, and shell fragments. The observations were combined into one well-log, with all the observations included. The findings were later on incorporated and combined with the seismic data.

#### **3.2.2.d. Left hand side: Compile information from wells**

Information from numerous well completion logs and reports was compiled and correlated to findings from seismic data and core observations. The well information was gathered through published wells from the Norwegian Petroleum Directorate Factpages, and also from well-logs provided by Lundin (Appendix 9.3). Some wells are not yet published. Indications of depositional environment from biostratigraphy and fossil assemblages were collected for the Oligocene-Miocene periods, as well as descriptions of strata alongside indications of lithologies from gamma-ray logs.

#### **3.2.2.c. Right hand side: Direct hydrocarbon indicators**

Packages of sediments with seismic character indicative of fluid fill in the pore-space differentiating from water, such as gas- and oil-accumulations, were mapped so that zones of amplitude anomalies in the study area could be distinguished and quantified. By consequently generating several minimum amplitude (min-amp) surface attributes throughout the seismic volume within the established sequence framework, mapping of bright spots in the study area was conducted in an efficient manner. The bright spot identification relies on the principle that



host rocks filled with gas or oil in the pore-space express a high amplitude as a results of the hydrocarbon-initiated reduction in seismic velocity, as discussed in chapter 2.7.1.

The mapping of bright spots was completed throughout the seismic volume using varying attribute windows and offsets from the different surfaces enveloping or lying in the vicinity of the anomalous reflectors. The mapped high amplitudes may nevertheless represent dissimilar features in the subsurface deviating from gas accumulations, such as gas filled sand or mineral-contacts dependent on pressure/depth. A transparency filter was applied to isolate and visualize only the brightest anomalies, most likely to represent hydrocarbons. Flat-spots were attempted localized in relation to bright spots, through cross-sections and manually screening of the data.

Migration pathways were investigated by mapping of zones with weakened seismic amplitude deviating from the surrounding and otherwise conform sediments, known as masking zones. Structural features such as faults, along with the overall external geometry and dip of layers were evaluated as potential migration pathways, as described in chapter 2.6.1.

#### **3.2.2.d+e. Right hand side: Petroleum potential**

Near-by wells and well-logs adjacent to the hydrocarbon indicators were screened in order to evaluate whether or not it is likely that the seismic anomalies represent gas or oil, and if so, of what origin (e.g. kerogen types and age). By combining the anomalies, migration pathways and well-logs, an overall evaluation of the probability to whether oil is present, and/or gas, was established. A short evaluation of some particular hydrocarbon filled traps were done to consider the potential of oil and/or gas in place, along with the different risks related to the trap geometry and seal.

#### **3.2.2.f. Integration of results and development of models**

The process and approach outlined in the foregoing sections provided an unbiased characterization and interpretation of the stratigraphic elements in the study area, as well as the distribution of direct hydrocarbon indicators. An independent reconstruction of the depositional environment was suggested based on the observed seismic features, such as clinoform geometries and progradation patterns, channels, canyons, etc. in combination with the depositional indications obtained from the core-log. Source areas, depocenters and other important features were evaluated from external and internal reflection geometries and attribute maps. Paleo-geographic maps for the changing depositional environments during Oligocene-Miocene were suggested based on the results from sequence analysis, and especially the paleo

shelf-breaks, along with information from core and well completion reports- and logs. The suggested location of e.g. paleo shelf-breaks and the depositional environment was compared to previous work in the area.

Furthermore, integration of the results from the sedimentary mapping and the hydrocarbon-indications, was performed by combining surfaces, variance maps and Min-Amp maps through transparency filters. This allowed the amplitude anomalies to be related visually to both structural and geomorphological features, with the aim of developing an integrated hydrocarbon-migration model in the area. The inferred lithologies suggested from system tracts and well logs were evaluated as potential reservoirs and seal-rocks. An overall evaluation of the petroleum system and the different elements it comprises was done.

### 3.2.2.g. Evaluate artefacts, risk and confidence of the seismic interpretation

Sheriff (2002) defined artefacts as acquisition footprints recognized as “*patterns in the data caused by the acquisition method*”. Such phenomena must be disregarded in order to circumvent misinterpretation and wrong conception of the seismic data, as it is not related to the true geology in the subsurface (Badley, 1985). In this case, artefacts related to the processing method as well as the acquisition are present. Several lateral, regular occurrences of elongated depressions occur in the eastern part of the 3D-merge. The same goes for sporadic occurrences of vertical chimneys where seismic data is suddenly lacking or disrupted (Figure 3.2.2). However, it is important to evaluate apparent artefacts and geological structures individually in order to establish the true origin of the observed feature.

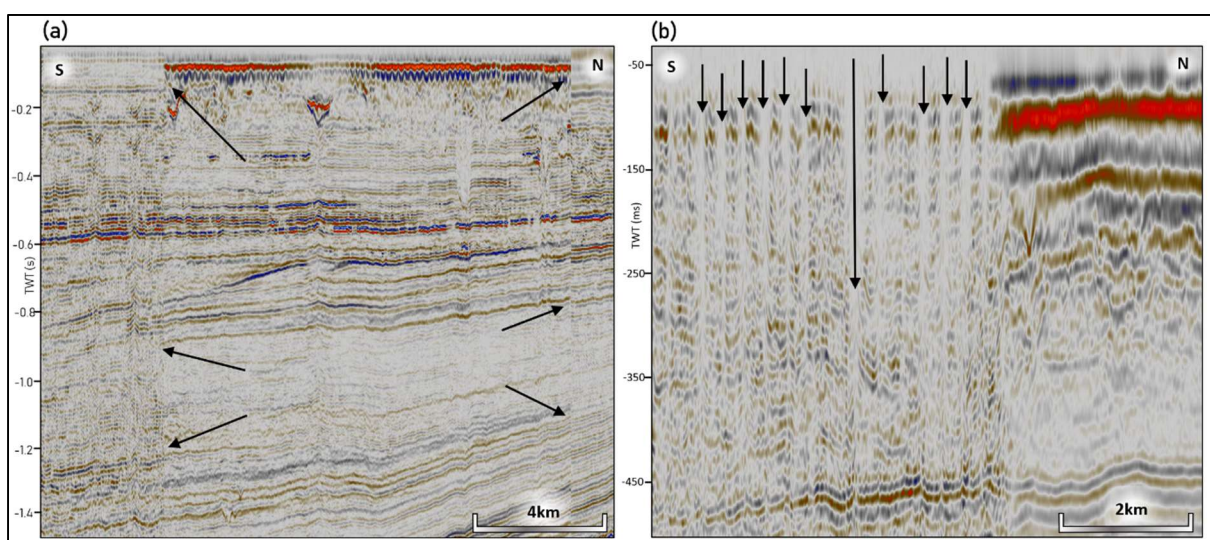


Figure 3.2.2. (a) Vertical zones where the seismic data is merged and reflectors are slightly displaced. (b) Lines of wiped out data, stretching both vertically and horizontally.

## 4 Results

### 4.1 Presentation of results

The following chapter includes the seismic and core observations of the Oligocene and Miocene sequences, which forms the basis for the reconstruction of the geological depositional environment and the petroleum system of the southern North Sea. The results are presented in a chronological order, beginning with an overview of the seismic framework and geological setting, followed by a description of the reflection terminations and sequences. The position and orientation of the respective cross-section presented are indicated by a yellow arrow on a miniature map (Figure 4.1.1) of the southern North Sea, and surfaces/attribute maps on a miniature reference-cross section (Figure 4.1.2). The southern North Sea has been divided into three zones which are also used to indicate the relative position of identified features (Figure 4.1.1). These zones roughly display the proximal (Zone 3) to distal (Zone 1) setting.

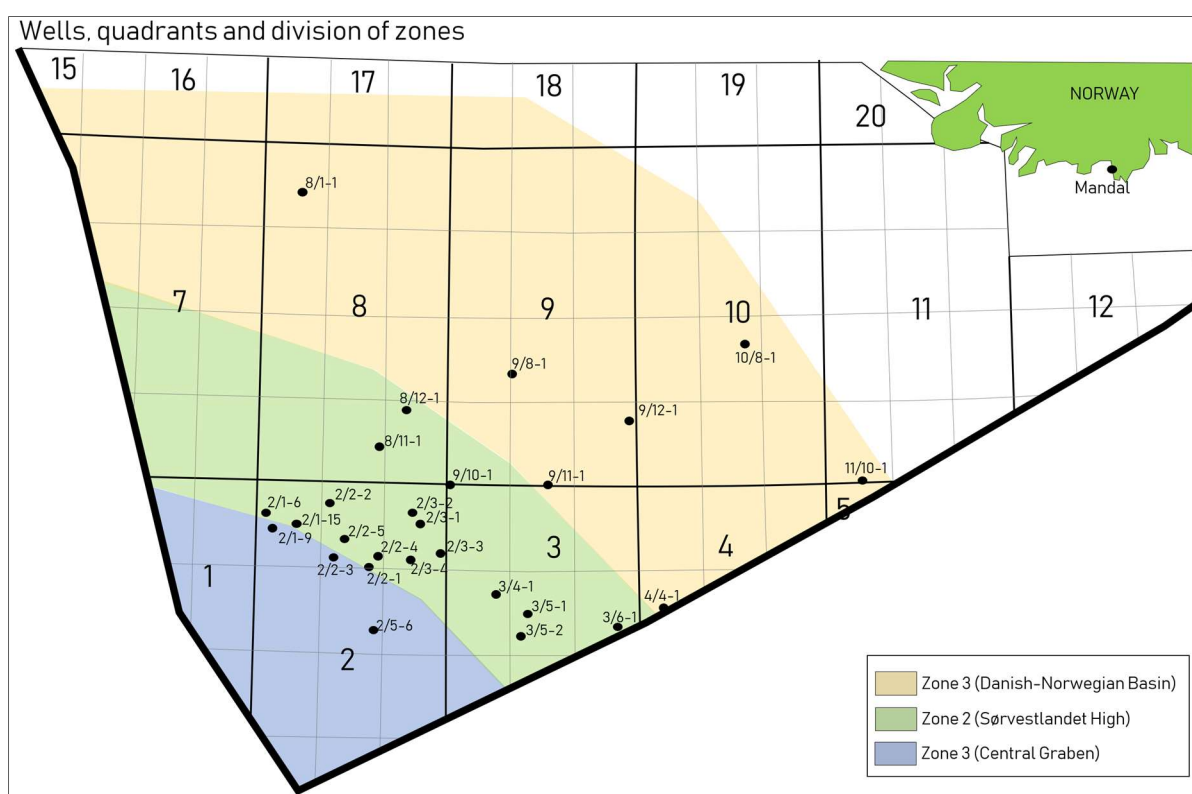


Figure 4.1.1. Overview of Quadrants, most frequently used wells and division of zones used for the presentation of the results in this study.

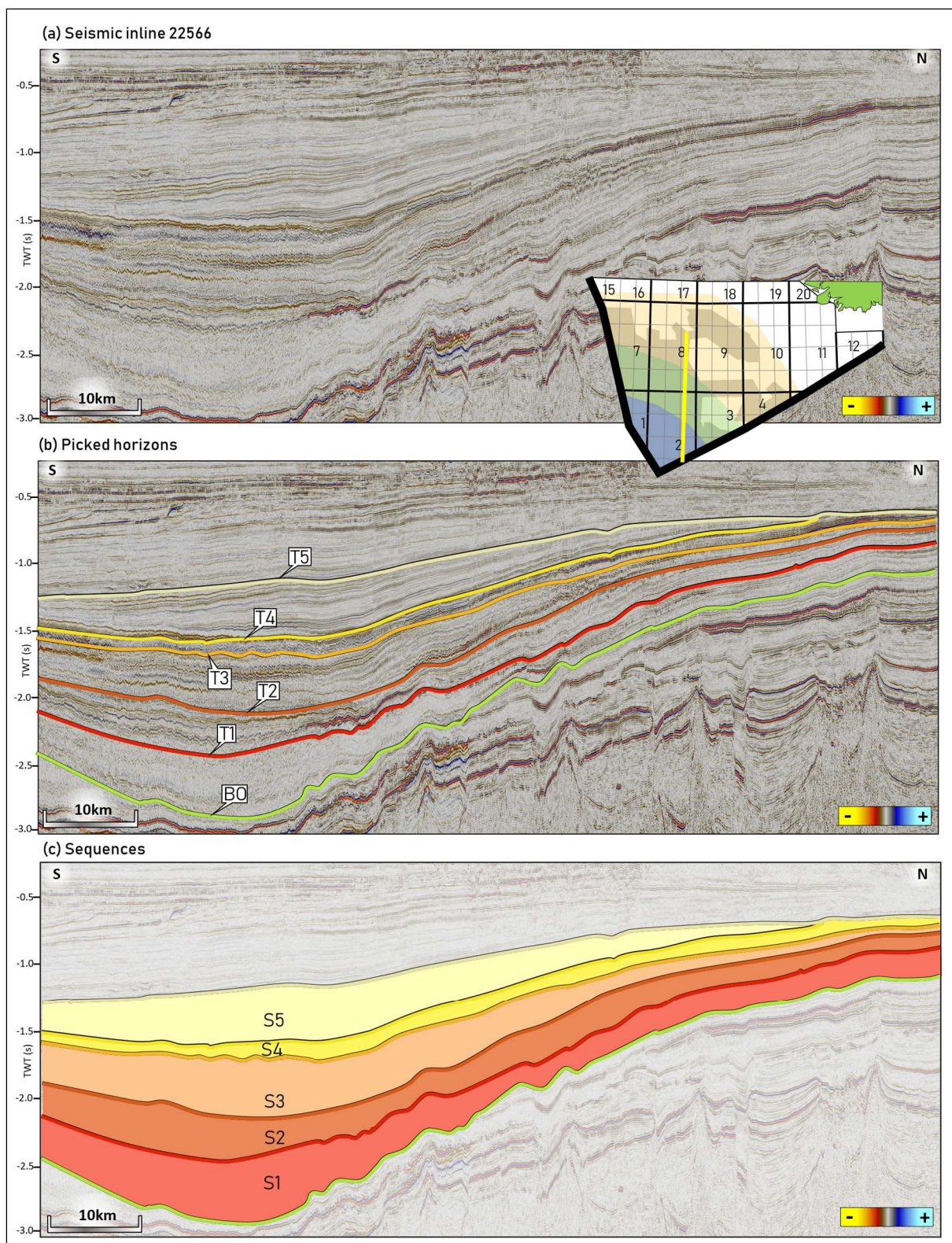


Figure 4.1.2. Reference cross-section (inline 22566). (b) Shows the seismic sequence boundaries (Base Oligocene-Top 5), and (c) shows the seismic sequences. The position of the cross-section is indicated in the small box, where mainland Norway is coloured in green and the divided zones for the study is indicated.

Five sequences with six sequence boundaries have been mapped and described (Figure 4.1.2 & Figure 4.1.3). Sequence 1 (S1) is bounded by the base Oligocene reflector, and the Top 1 (T1)

reflector, and is the lowermost sequence, hence, the oldest one (relatively). The Mid-Miocene Unconformity (MMU) was correlated to several wells, which are presented in Appendix 9.5.

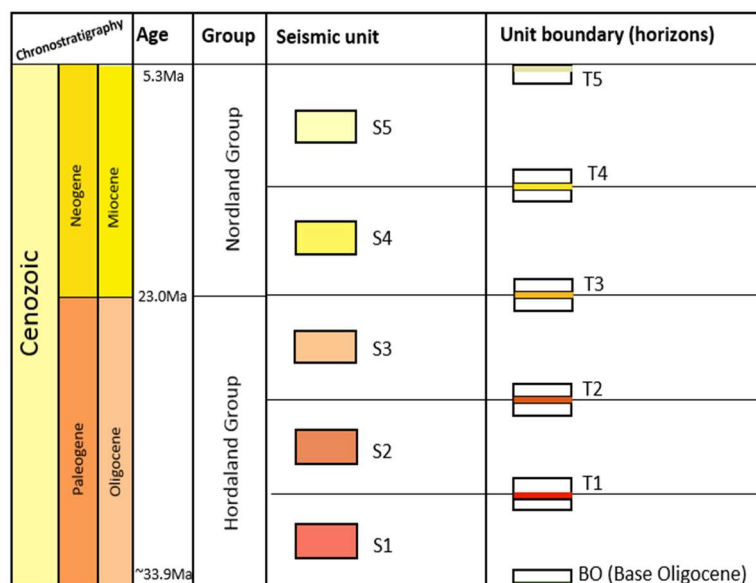


Figure 4.1.3. Stratigraphic colour chart for the seismic sequence framework. The ages are correlative to the NPD’s geological time scale (2014).

## 4.2 Seismic facies

Six seismic facies are characteristic of the Miocene-Oligocene sequences within the study area, and these are named SF1-SF6. A short description of the different facies and a short interpretation of these are shown in Figure 4.2.1. SF1-SF4 are most common in the seismic sequence description, while SF6 is abundant where the direct hydrocarbon indicators are discussed. SF5 is common around salt diapirs.

Seismic facies	Description	Geological interpretation	Example
SF1	Low to high amplitudes, parallel to subparallel reflection configuration	Uniform depositional setting, however high amplitudes may also represent lithological contrasts.	
SF2	Dipping layers, moderate to high amplitudes and frequencies, parallel/subparallel/divergent reflection configurations.	Prograding sets of clinoforms/sediments deposited onto shelf.	
SF3	Low to high amplitudes and frequencies, disrupted and low connectivity reflectors, however parallel arranged.	Polygonal faults as a result of soft sediment deposition.	
SF4	Reflection free zones with low amplitudes and frequencies. Reflection configuration difficult to determine.	Homogeneous units. Sediment infill in a subsiding basin	
SF5	High amplitude and frequencies in a chaotic reflection pattern. External dome or diapir geometry.	Salt diapirs	
SF6	Disrupted seismic reflectors with weakend amplitudes and frequencies	Gas chimneys or wipe out zones from strong (bright spots) amplitudes above.	

Figure 4.2.1. The classified seismic facies used throughout the study.

## 4.3 General characterization of the sequences

### 4.3.1 Reflection terminations

The reflection terminations are observed at the outermost extent of seismic reflectors, e.g. when they are terminated. They are however presented through the study by colour codes grading towards the respective termination of the reflectors. The reflection terminations of the S1-S3 sequences interpreted in this study show an external synclinal shape of the reflectors within Zone 1, which in general onlaps towards the layers dipping down from northeast. Onlaps occur on the southern part of synclinal shape as well, at the UK side of the offshore area. These onlapping, synclinal reflectors (shaded in blue; Figure 4.3.1), onlapping towards both north and south, forms the deeper basin parts, where the margins are defined by the onlaps. Within Zone 2 & 3, the layers show a dipping trend from northeast towards southwest, with downlaps toward the underlying reflectors. Some of the units are eroded and disappears towards the north. Some are cut by unconformities whereas others are thinning or pinching out. The S4 & S5 sequences situated above the Mid-Miocene Unconformity (MMU) deviates from the other sequences in terms of reflection terminations, as the synclinal shaped reflectors with onlaps along the basin margin is not present.

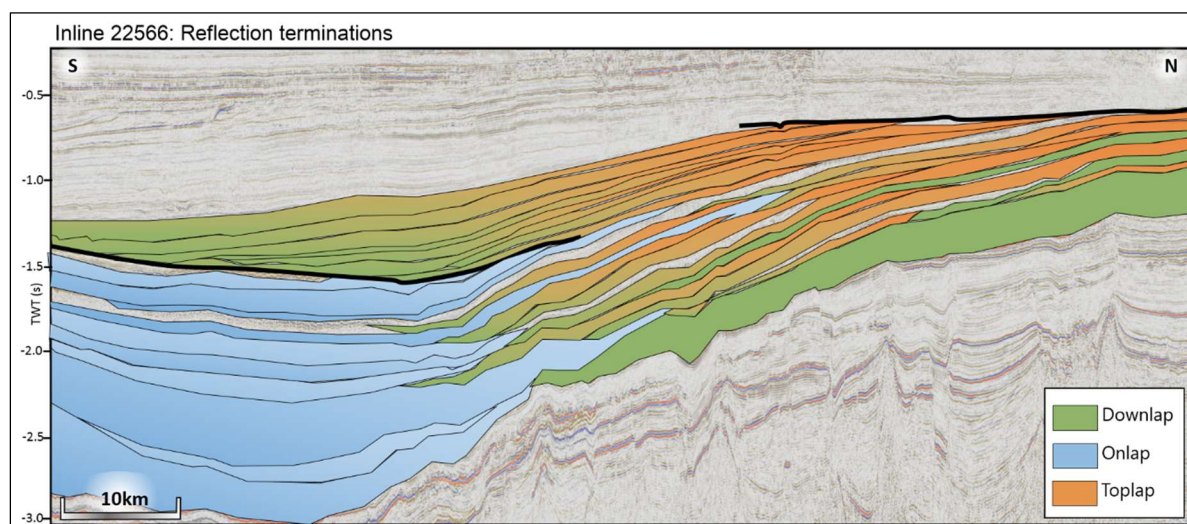


Figure 4.3.1. The figure display the reference cross-section with the overall trend of reflection configurations, roughly within the picked sequences. The colour configuration correlates with Figure 2.2.3 from the theory chapter. The exact reflection termination occurs at the very “end” of the units, but are here indicated by grading colours.

### 4.3.2 *Structural characterization*

The Oligocene-Miocene sequences overlie down-faulted blocks, where normal faults dominate. The vertical displacement of reflectors along these fault zones are largest in the underlying Mesozoic sediments, however some of the fault breach through the Oligocene-Miocene sediments. The displacement of sediments at the Oligocene-Miocene level is far less compared to the Mesozoic offset. The Oligocene-Miocene sequences show equal unit thicknesses on both sides of the fault zones. The shallowest vertical extent of the fault zones are commonly below the T3 surface.

Within the previously described basin margins, zones of heavily faulted reflectors occur in the seismic data. The faults show small vertical offset, but are closely spaced and abundant within the S1, S2 and S3 sequences. Viewed from above, the fault zones show curved shapes, oriented randomly. These zones are attributed to polygonal faults throughout the presentation of the results.

The attribute maps reveal several semi-circular zones of high chaotic reflection patterns and diapiric shaped structures in the cross-sections. These features have been attributed to Seismic Facies 5. By suggesting that the diapirs are related to salt and halokinesis, some examples of cross-sections have been included in order to time the events of salt movement. Firstly, reflectors overlapping towards the chaotic reflection pattern within the diapiric shaped structures, show a synclinal shape where the layers bend downwards in a curve. Such curves occurring adjacent to salt diapirs are typically rim synclines, and considered as such further on. Above the diapir, some layers vary in thicknesses laterally; thinning towards the top of the diapir structure, and increasing in vertical thickness towards the sides. These layers with varying vertical thicknesses occur on several vertical levels, and are identified in order to determine episodes of salt movement. As seen from Figure 4.3.2, layers coloured in yellow are folded upwards in an anticlinal shape above the diapiric structure. The thickness of the units remains constant. Lastly, the shallowest sediments show no trends of either varying unit thicknesses nor anticlinal folds above the diapiric structure. These units are continuous and do not seem to have any relation to the underlying diapir. Such mapping of unit variations above and adjacent to the diapiric structures are applied in order to establish a halokinetic time-event chart.

Figure 4.3.2 and Figure 4.3.3 display the same diapir however observed from a different angle and orientation. One well has been drilled above this diapir, 2/3-1, and is classified as a gas discovery (the Løven discovery). A normal fault is situated above the diapiric salt structure.

The vertical extent reaches from the top of the diapir through S4. The S5 sequence however does not show a vertical displacement of the layers, and is thus not affected by the underlying diapir or the related fault. The S1 sequence show increasing thickness at the northeastern side of the fault, where the strata is down-faulted.

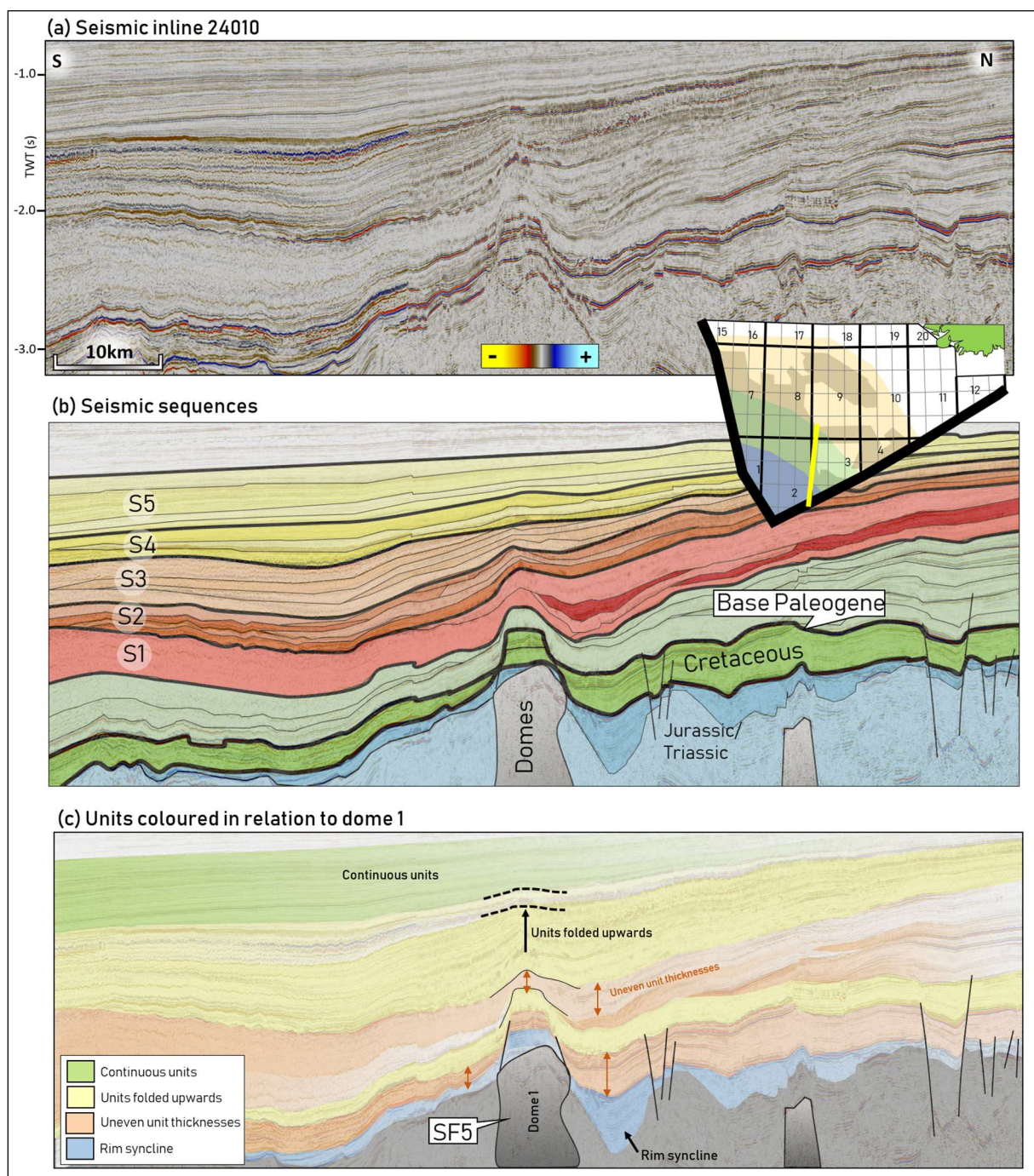


Figure 4.3.2 Inline 24010, with the (b) seismic sequences, and (c) units classified based on thickness variations and folding in relation to the identified diapir. Note the Seismic Facies 5 annotation. The units show variations between uneven unit thicknesses adjacent and above the diapir, homogenous thickness regardless of the diapir, and lastly units folded upwards above the diapir. The highest level of doming influence is suggested to be within S3. Overlying the halokinetic altered units are continuous reflectors which seems not to have been altered or somehow affected during and after deposition by the diapir.



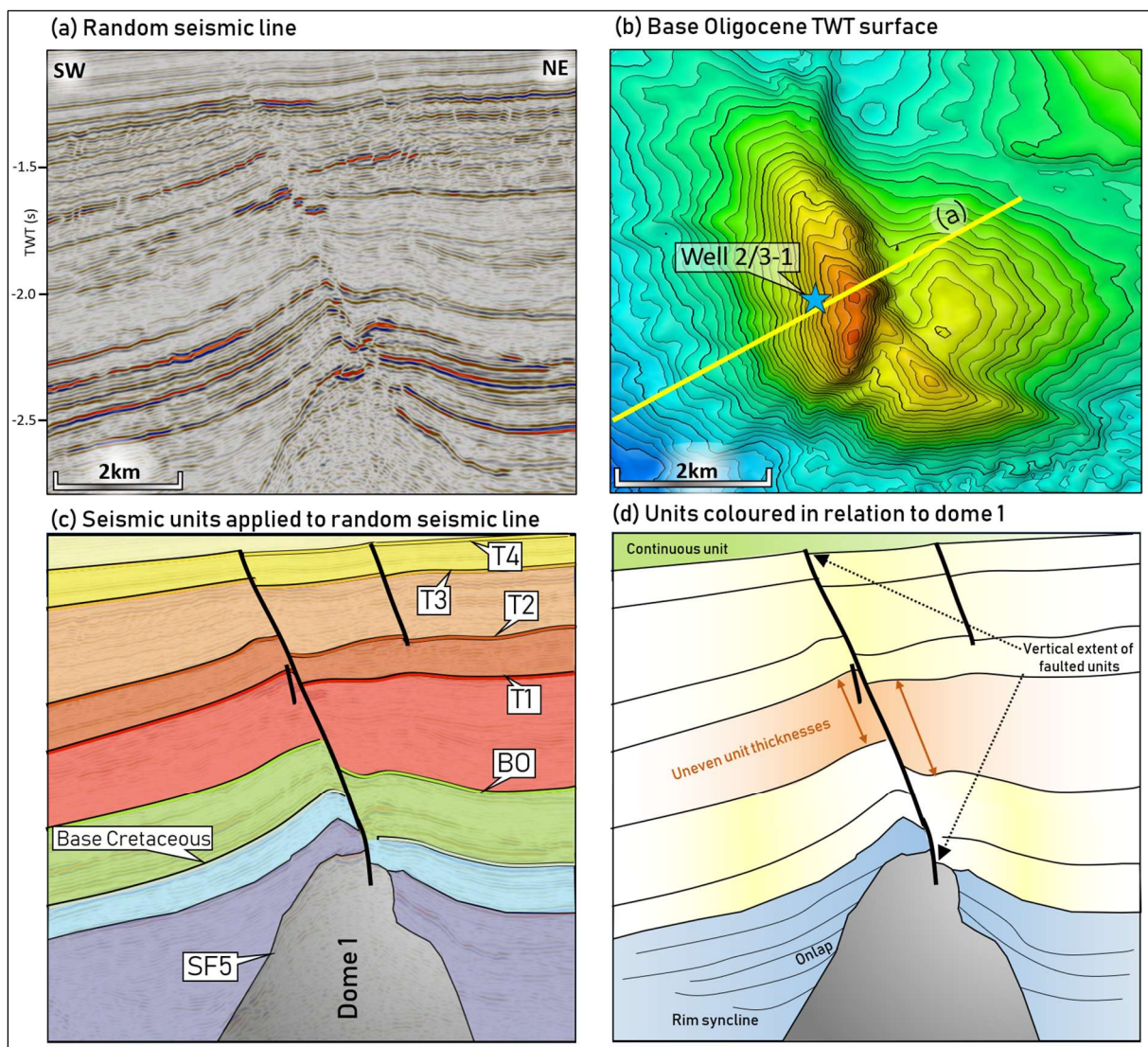


Figure 4.3.3. The figure display the same diapir as in Figure 4.3.2, but seen from a different angle (b). The variation in unit thicknesses follows the same colour-code as in the previous figure. Several onlaps were observed towards the diapir and are coloured in blue. This zone has been attributed to a rim syncline.

## 4.4 Sequence 1

The lowermost sequence, S1, is bounded by the Base Oligocene reflector below and T1 (Top 1) above. The Base Oligocene reflector was mainly interpreted along a peak with a strong amplitude, however the horizon truncates underlying strata and is thus an angular unconformity, so occasionally it was interpreted and interpolated along line-ups where reflectors below disappear (Figure 4.4.3). Surfaces interpreted along line-ups of disappearing reflectors were considered as erosive unconformities. The T1 surface was interpreted along a peak with high amplitude. The reflector showed good lateral continuity, covering the larger parts of the study area.

A summary of the facies description, reflection terminations, external geometries and observed structures for the respective sequence, is given in Figure 4.4.1. All the listed elements in the table are presented throughout the sequence chapter.

S1	Zone 1 (South)	Zone 2	Zone 3 (North)
<b>Seismic facies description</b>	Parallel, medium to high frequencies and medium amplitudes, however disrupted by polygonal faults.	Diffuse divergent reflection configurations.	Medium to high frequencies, continuous reflectors.
<b>Reflection terminations</b>	Onlaps/truncates towards northeast onto shallower units in the north, and similarly towards the southwest.	S2 downlaps unconformably towards underlying Eocene deposits (Base Oligocene reflector). The BO reflector cuts the underlying Eocene strata.	The internal S1 units thin towards the northeast.
<b>External geometries</b>	Basin with margins defined by onlaps.	Sigmoidal clinoform geometries with low-angle foresets, dipping towards the southwest. Rising shelf-break trajectories.	Climoform topsets with a very gentle dip towards the southwest.
<b>Structures</b>	Polygonal faults abundant.	Reflectors occasionally disrupted by deep-seated, normal faults, salt diapirs and salt-related faults.	System of braided elongated depressions, orientated east-west.

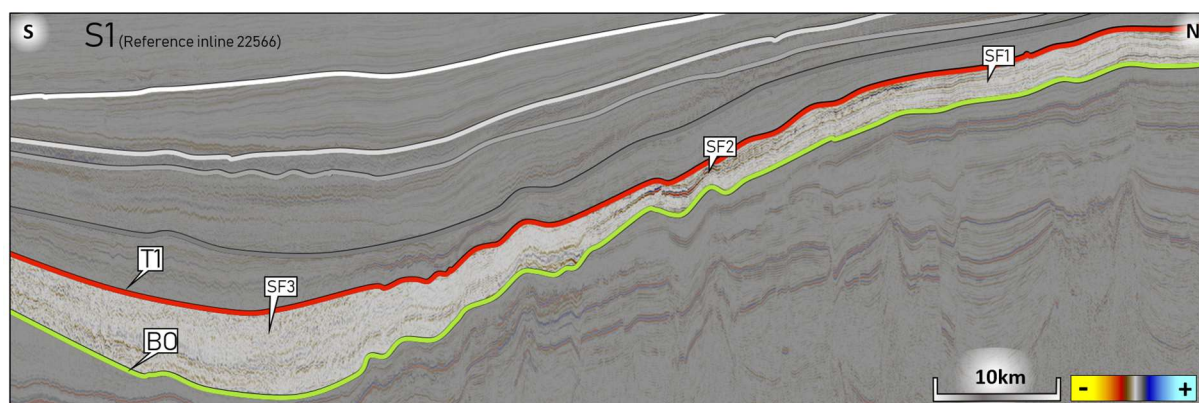


Figure 4.4.1. The table describes the general trends of the sequence throughout the study area (Zone 1 – 3). The recognized seismic facies (classified in Figure 4.2.1) shown on the reference cross-section; SF3 in the deeper parts (Zone 1), SF2 and SF1 towards the northeast.

The Base Oligocene (BO) surface shows an external basin geometry, with a clear dip towards the southwest (Figure 4.4.2). The S1 sequence comprises reflectors arranged in a synclinal external shape in the southwestern part (Zone 1), with medium to high frequencies and

amplitudes. Polygonal faults are abundant in the parts bounded by the onlapping basin margins (Figure 4.4.5.c). The faults occur randomly relative to each other, with curved geometries in map view, and no clear trend in orientation (Seismic Facies 3). The continuity of the reflectors when observed, excluding the faults, are good and subparallel. Patterns occur similarly on both sides of the polygonal fault zones. The reflectors within S1 rests unconformably on the underlying Base Oligocene and Eocene sediments (Figure 4.4.7). The Eocene sediments are dominantly orientated west-east, with a dip towards the east. The S1 units on the contrary, dips towards the southwest.

Adjacent to the basin fill, a southwesterly dipping slope is present towards the northeast. The surface is partly interrupted by diapirs (SF5) and salt-related faults (Figure 4.4.2.b. & Figure 4.4.5.d). The faults occur between zones of chaotic reflection patterns, called salt diapirs.

Towards northeast, within Zone 3, a distinct elongated elevation occurs (Figure 4.4.2.b). The ridge cuts through several of the sequences and is further investigated in chapter 4.9.

The sequence (S1) comprises several smaller units with combined external geometries showing the characteristic shelf-slope-basin configuration. These units are attributed to prograding clinoforms, with sigmoidal geometries, and gently dipping foresets. A distinct break in the angular configuration of the clinoform reflectors, is attributed to the paleo-shelf-break (Figure 4.4.6). This break separates the gently dipping, northeastern shelf (Seismic Facies 1) from the southwestern, steeper dipping foresets (Seismic Facies 2). The tracked progressive displacement of the shelf-break shows an ascending (rising) trajectory. The average vertical height of the foresets of the clinoforms are approximately 200ms (TWT), however varying. The foresets commonly downlaps onto the Base Oligocene within Zone 2 (Figure 4.4.7), where the reflectors interfingers with the onlapping sequences from the basin (Figure 4.3.1).

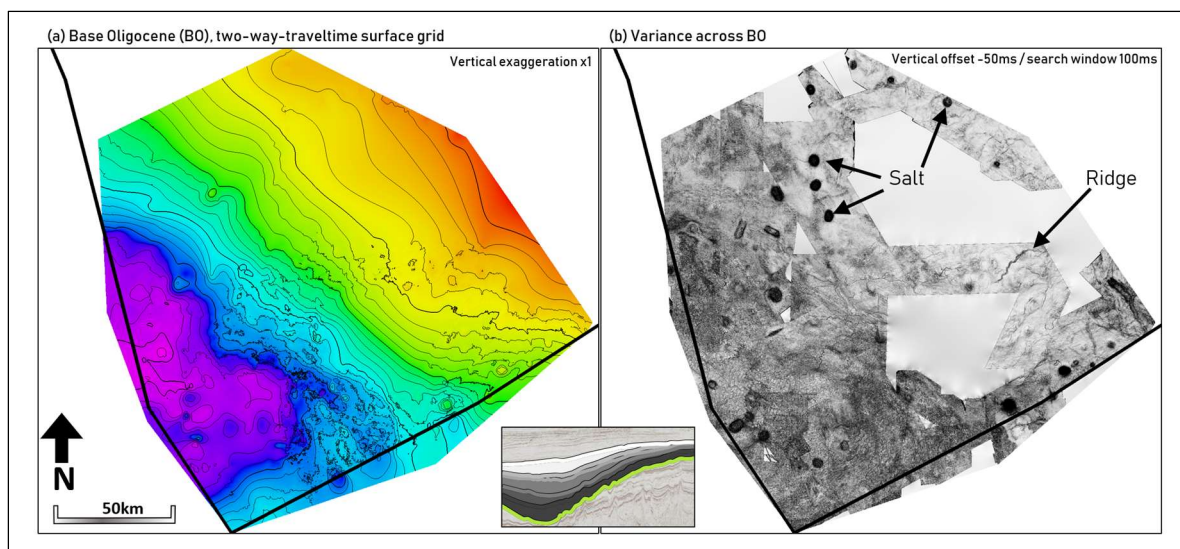


Figure 4.4.2. (a) Shows the Base Oligocene (BO) surface, where a clear dip towards southwest is observed. (b) Shows a variance surface attribute across the BO surface. The dark black semi-circular zones have been related to salt diapirs.

Towards the northeast in Zone 3, areas with elongated depressions in otherwise structure-free zones appear on variance maps within the sequence (Figure 4.4.4). The depressions are up to 500m wide, with a lateral extent exceeding 30km. The orientation is primarily arranged in a east/northeast – west/southwest direction.

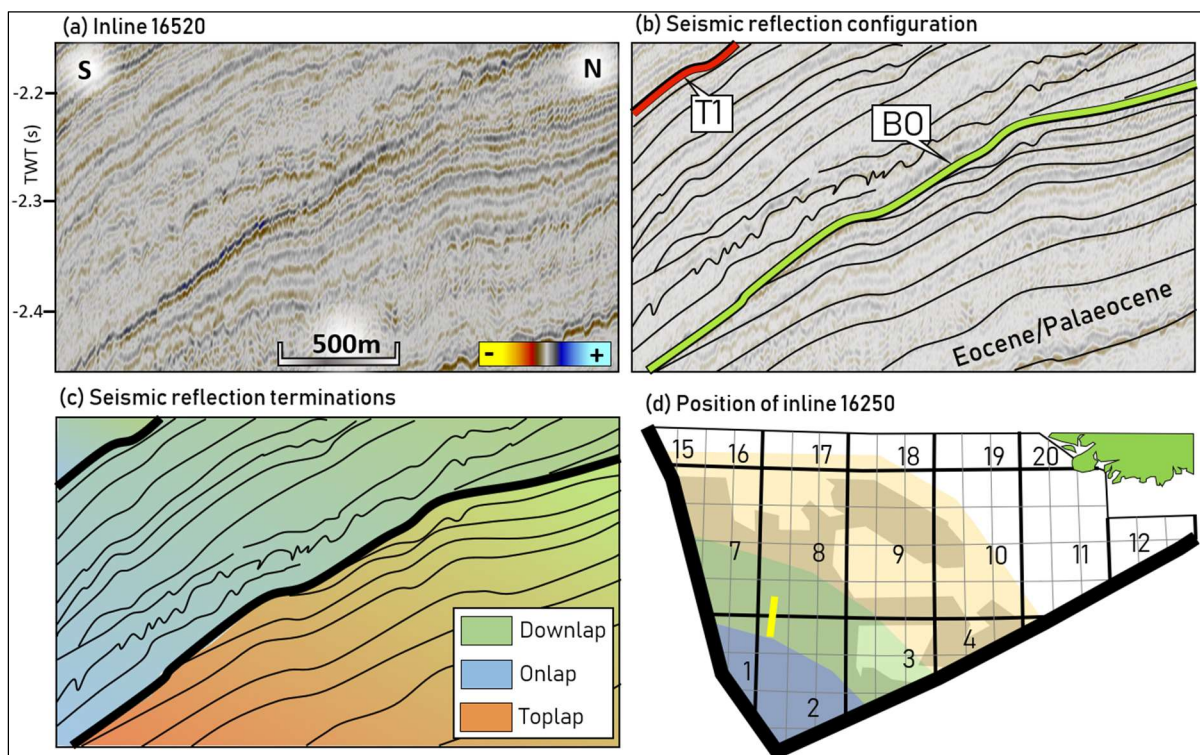


Figure 4.4.3. (a) Seismic inline 16520, where (b) the seismic sequence boundaries are shown. (c) is coloured based on the reflection terminations classification as used previously. The BO reflectors cuts the underlying Eocene unit, and an angular unconformity is thus present.

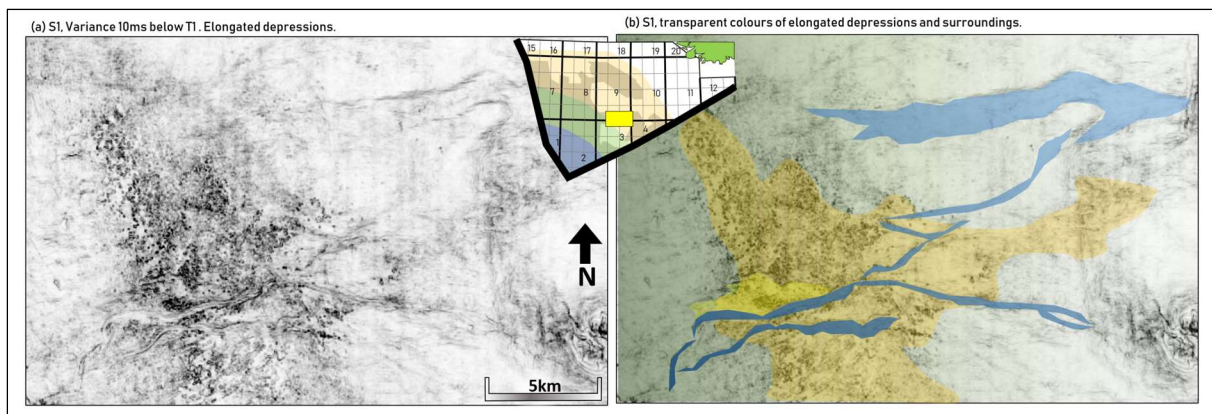


Figure 4.4.4. (a) Variance within S1 with (b) coloured shades/structures, the blue colour indicated elongated depressions within Zone 3 of the study area.

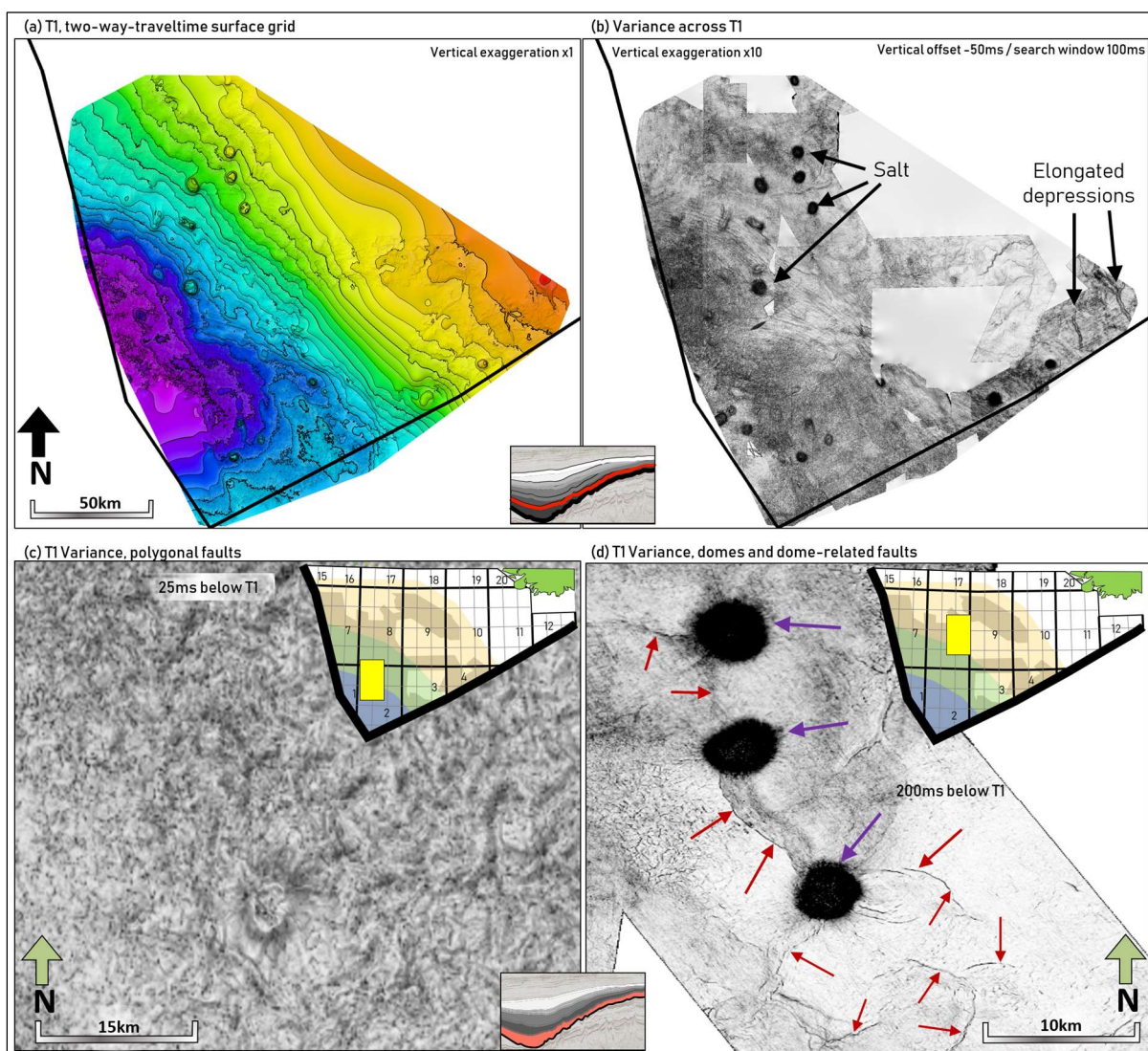


Figure 4.4.5. (a) The Top of S1 (T1) TWT surface. (b) Variance surface attribute across T1. (c) Polygonal faults shown from above, in the deeper part of the sequence. (d) Diapirs (purple arrow) with adjacent faults (red arrows) shown by variance within S1.

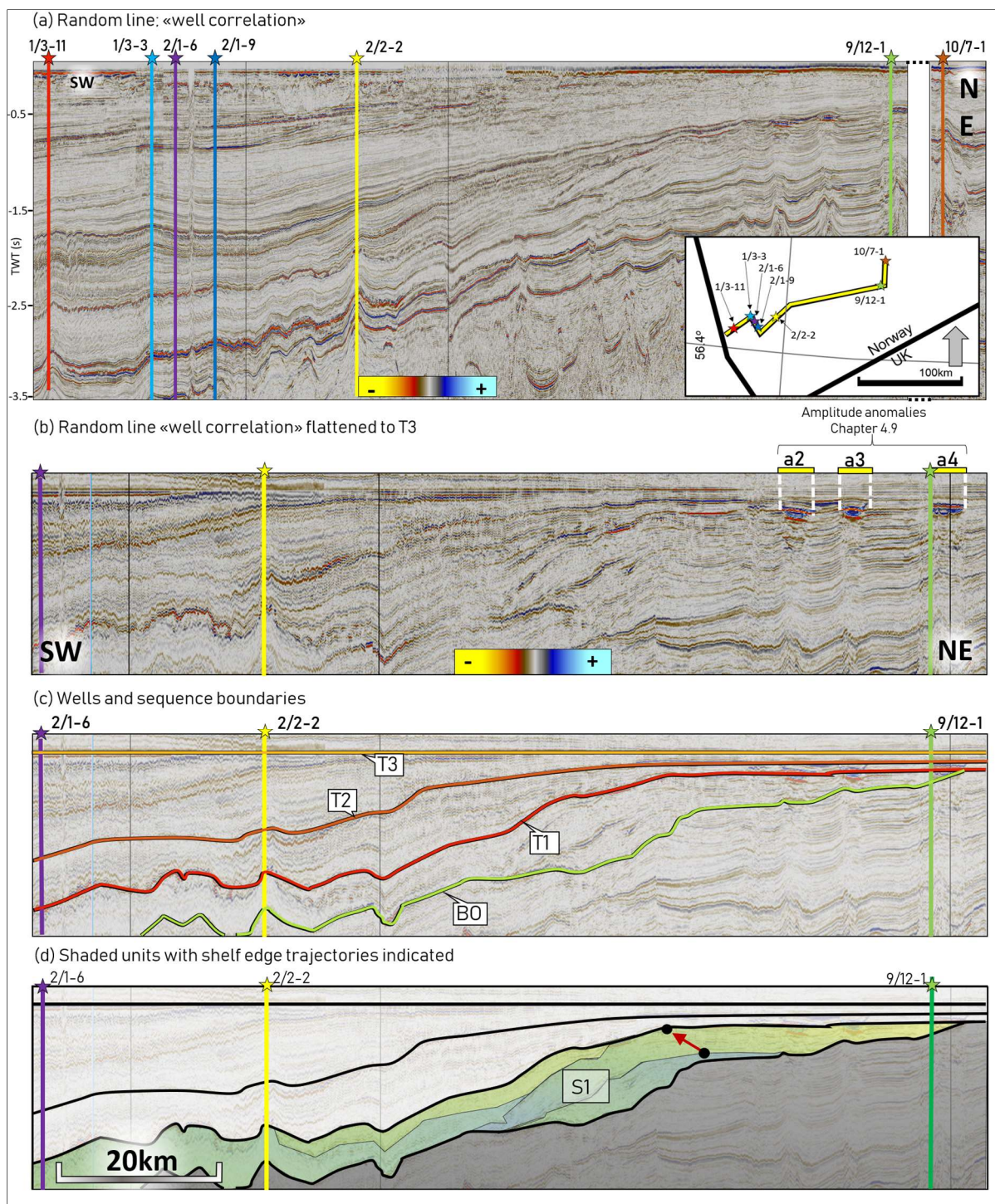


Figure 4.4.6. (a) Random seismic line, (b) flattened to the T3 reflector. (c) Wells and sequences applied. (d) The overall geometry of S1, where the progressive displacement of the shelf is indicated by ascending trajectories (red arrow).

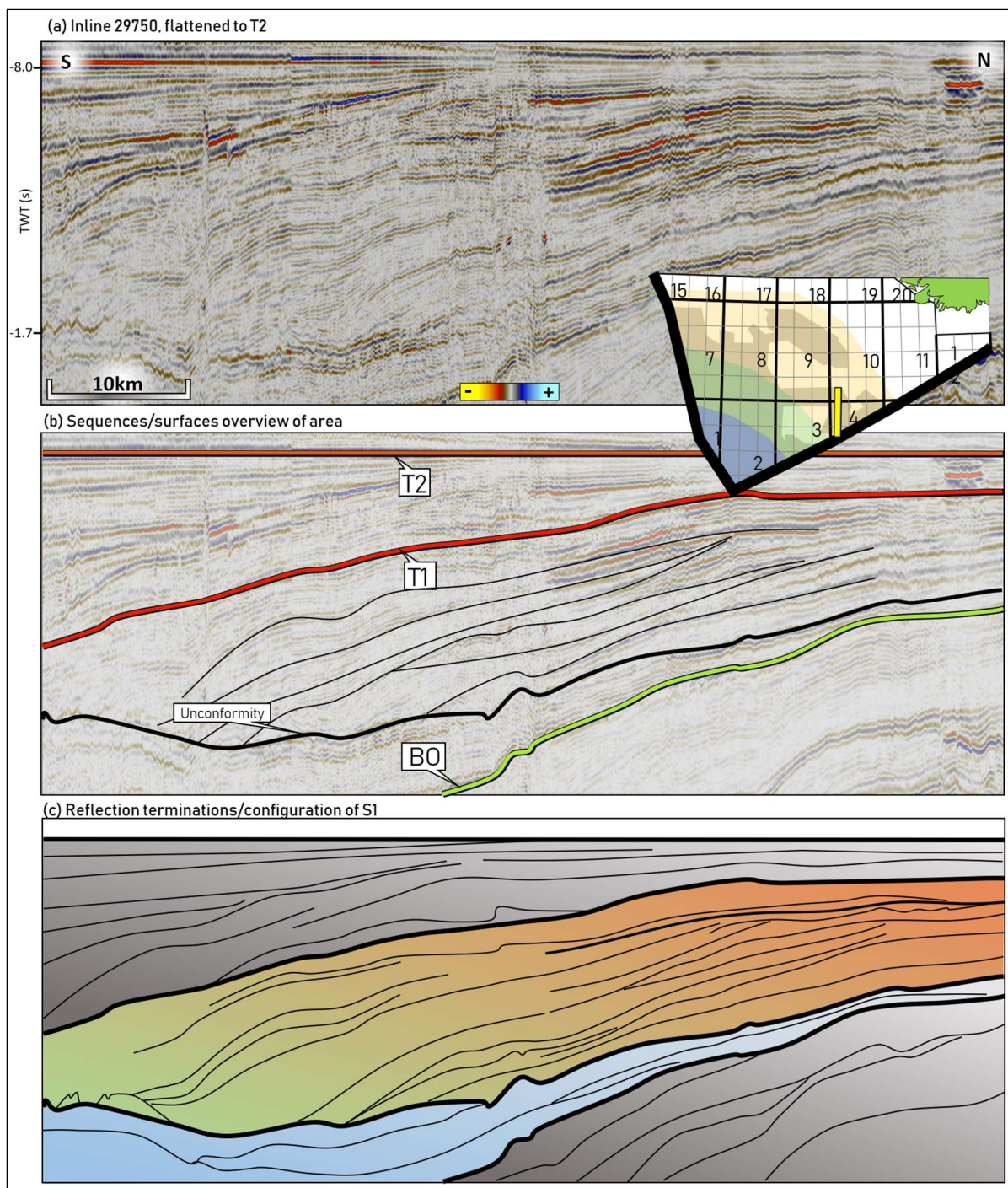


Figure 4.4.7. (a) Inline 29750 within Zone 2 of the study area, flattened to the T2 horizon. (b) displays the seismic sequence boundaries and one unconformity identified within S1. (c) The S1 sequence coloured based on the reflection termination classification. The upper part of the sequence shows downlap towards the unconformity, separating it from an underlying unit which onlaps towards the north.

## 4.5 Sequence 2

S2	Zone 1 (South)	Zone 2	Zone 3 (North)
<b>Seismic facies description</b>	Parallel, medium to high frequencies and medium amplitudes, however disrupted by polygonal faults.	Dipping layers and subparallel reflection configurations. Medium to high amplitudes.	Reflectors dipping slightly towards southwest. Parallel/subparallel reflection configuration of high amplitudes and good continuity.
<b>Reflection terminations</b>	Onlaps/truncates towards northeast and southwest.	Downlap towards T1.	Cut by an erosive unconformity (T3) in the shallower parts towards the northeast.
<b>External geometries</b>	Basin infill, units show increased thicknesses towards the central part Zone 1.	Clinoforms with oblique geometries, steep foresets and descending shelf-break trajectory.	Topsets slightly dipping towards southwest.
<b>Structures</b>	Polygonal faults abundant.	Salt related diapirs and faults.	Elongated depressions with chaotic/divergent fill in the northeast.

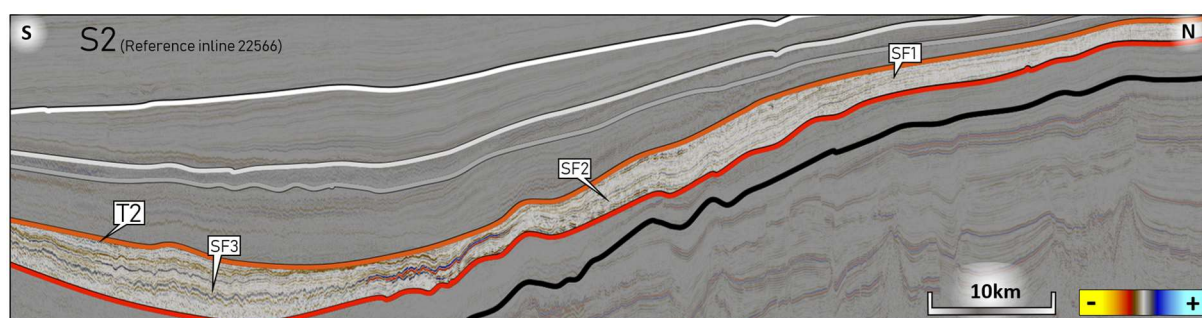


Figure 4.5.1. The table describes the general trends of the sequence throughout the study area (Zone 1 – 3). The recognized seismic facies (classified in Figure 4.2.1) shown on the reference cross-section; SF3 in the deeper parts (Zone) 1, SF2 and SF1 towards the northeast.

The S2 sequence is firstly described by use the seismic data (Figure 4.5.1), followed by a well and core correlation, and core description. The sequence shows reflectors with southwestward dip in Zone 2, which partly downlaps onto the underlying T1-reflector in the deepest parts (Zone 1, Figure 4.5.3). Towards northeast, the T2 reflector is truncated by the overlying T3 reflector. Similar to S1, the reflectors within Zone 1 comprises abundant occurrences of polygonal faults. Salt diapirs occurs frequently on the variance map for T2 (Figure 4.5.2).

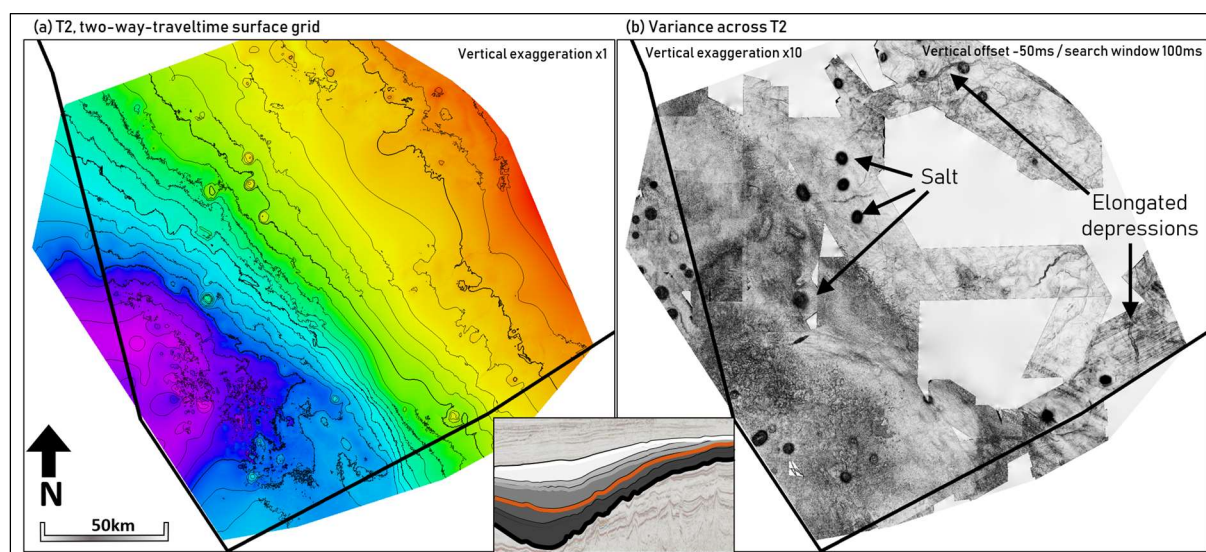


Figure 4.5.2. (a) The Top of S2 (T2) TWT surface. (b) Variance surface attribute across T2.



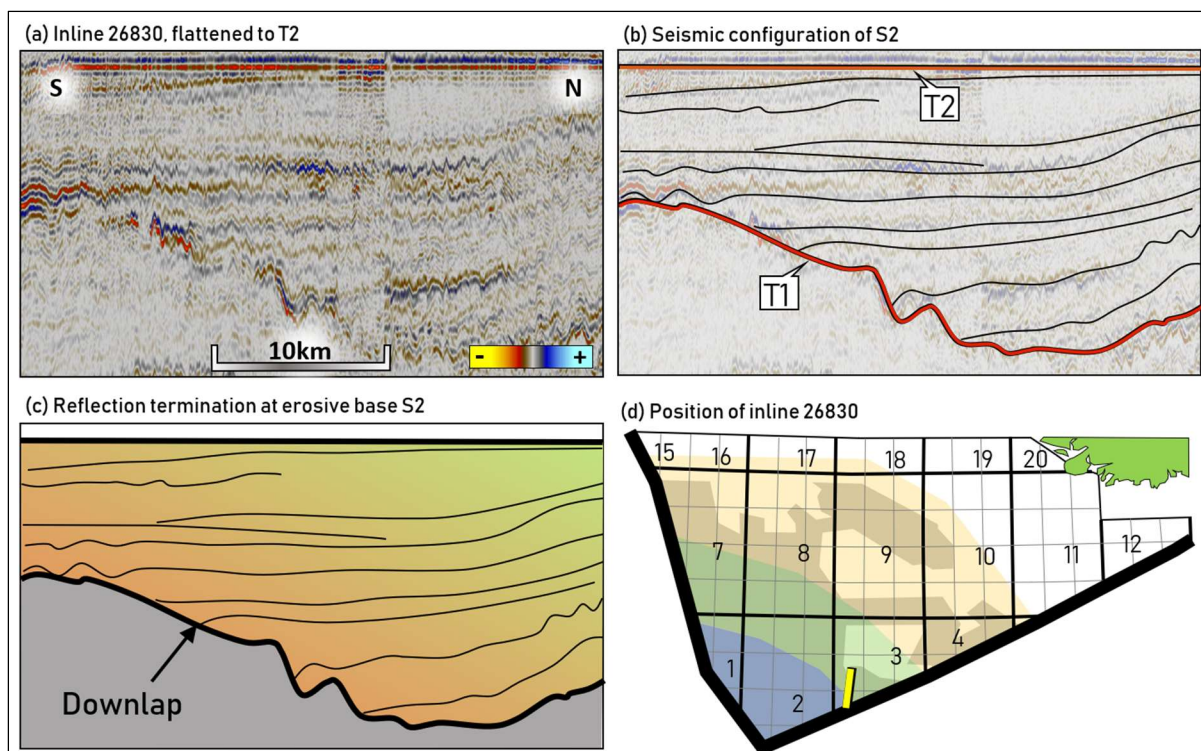


Figure 4.5.3. The figure shows the reflection terminations within Zone 1 of the study area for S2, flattened to T2. The sequence downlaps towards T1.

The S2 sequence comprises several units with parallel, almost horizontal reflectors towards the northeast, in Zone 3 and partly 2. The dip changes to a steeper configuration within Zone 2, where the break in dip is attributed to the paleo-shelf break. The shelf break separates the northeastern, horizontal reflectors, from the southwesterly, steeper dipping foresets. The external configuration is characterized by complex oblique clinoform geometries. The average height of the clinoforms is ranging from 150 to 200ms (TWT). The progressive displacement of the shelf-break is identified along the break of angle for each respective unit, which progressively overlaps each other towards the southwest. The trajectories along the identified shelf-breaks are slightly descending. The position of the logged core is shown in Figure 4.5.4, with the corresponding gamma ray log from well 2/2-2. The gamma ray log shows low values in the S2 interval, and higher values for the overlying and underlying sediments of S1 and S3.

In the northeastern part (Zone 2 & 3), at least two, very distinct elongated depressions occur on variance maps and in cross-sections. The depressions are made up by steep sides cutting through the underlying seismic reflections. High amplitudes occur both at the base of the erosive contact, as well as along internal infill reflectors (Figure 4.5.5). The depressions range from 400 – 1000m in width, and are up to ten kilometers long. The horizontal extent of the depressions may be restricted by the resolution and appearance on the seismic data. They may therefore exceed the mapped horizontal extent.

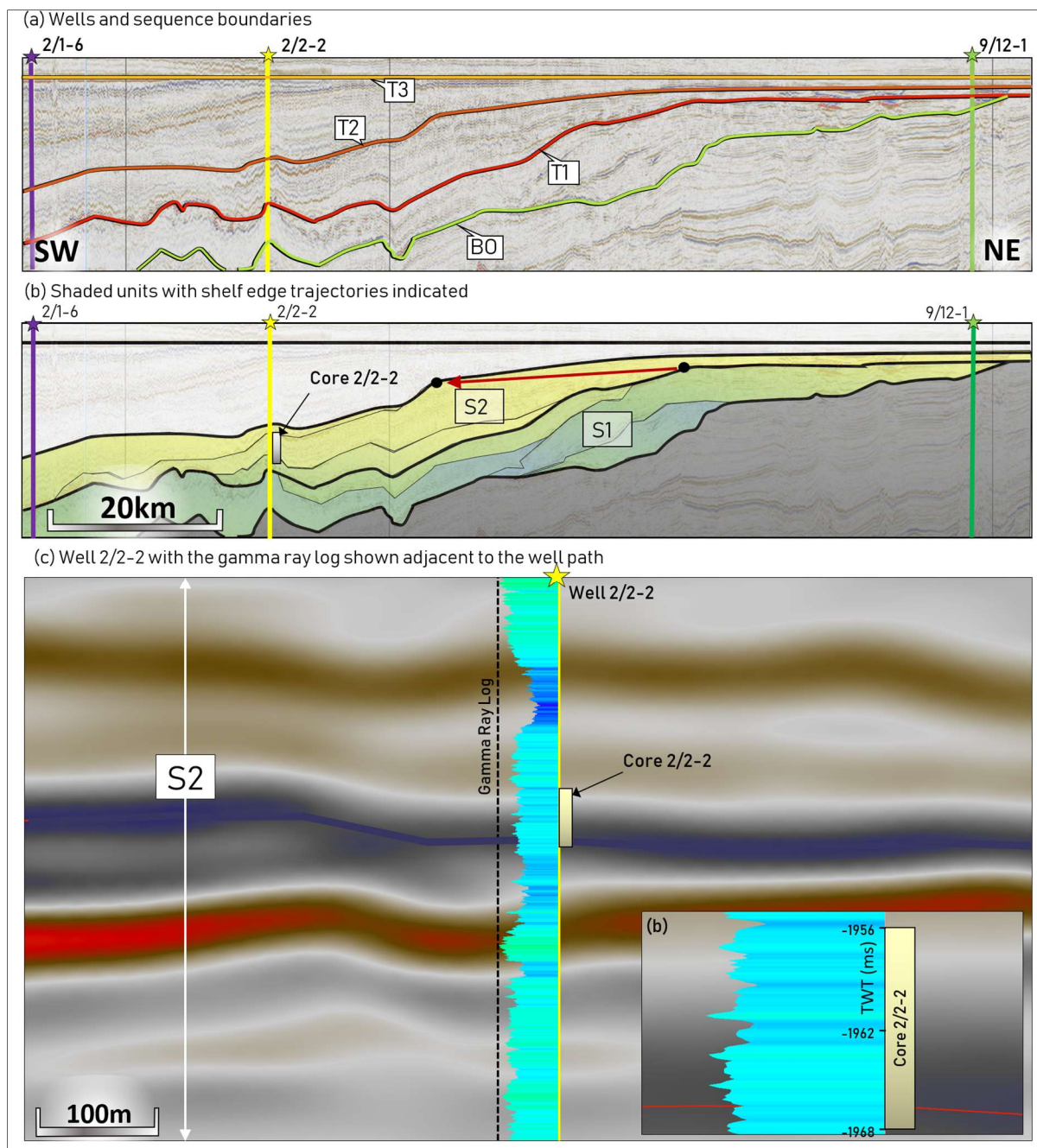


Figure 4.5.4. (a) Random seismic line flattened to the T3 reflector with wells and sequences shown. (b) The overall geometry of S2, where the progressive displacement of the shelf is indicated by slightly descending trajectories (red arrow). (c) The core-interval (TWT interval minus 1956-1968ms) shown to the corresponding gamma ray log from well 2/2-2. Blue colour = low gamma ray values, green = high gamma ray values.

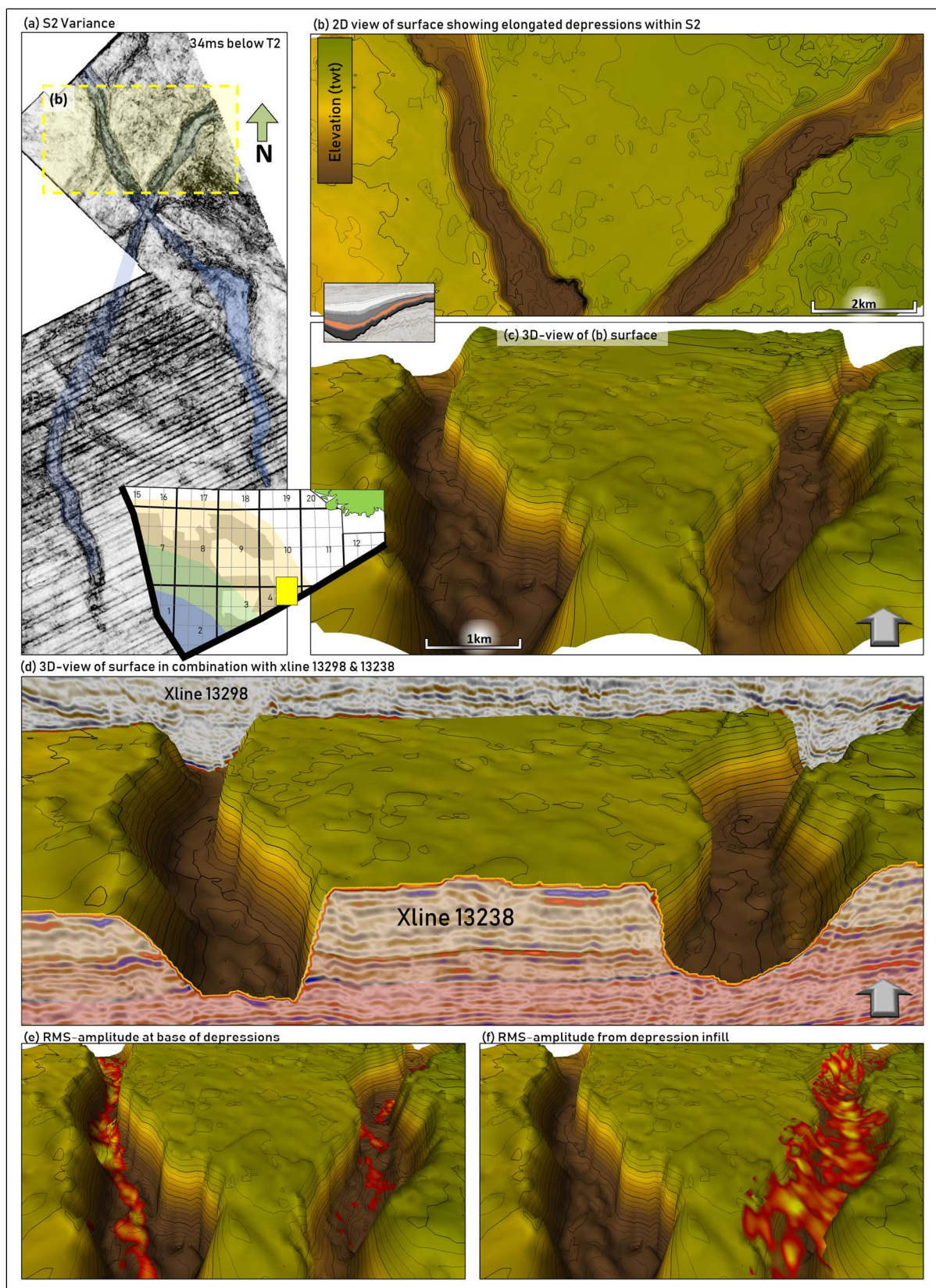


Figure 4.5.5. (a) Variance within S2 in the northeastern part of the study area (Zone 2), where elongated depressions are shaded in blue. (b) Map view of surface (TWT) interpreted along the erosive base and top of the elongated depressions. Position indicated in (a). (c) 3D view of the same surface as in (b). (d) 3D view with seismic cross-sections shown. Sequences applied with transparency below the erosive base. (e) RMS surface attribute along the erosive base. (f) RMS attribute along and intra-fill reflector.

#### 4.5.1 Core observations

The measured depth of the core from well 2/2-2 was 1980-1994m. It was converted into TWT (1956-1968ms) through the well-top spreadsheet, using a pre-defined well-velocity model from Lundin. The core is situated within the S2 sequence, in Quadrant 2, and the relative position in the basin is indicated in Figure 4.5.4.

The core consisted in general very fine to fine, yellow-grey in colour, micaceous sand layers altering with reddish-brown silt layers and partly dark grey mud. The visible porosity of the sand layer was poor. Several cross laminations such as unidirectional and climbing ripples were observed. Occasionally, pinch and swell structures similar to wave ripples were present, along with double drapes, organic layers with plant fragments and sporadic occurrences of broken shells. Soft sediment deformation structures such as flames and load casts were abundant in bed contacts between sand (on top) and mud (below) (Figure 2.4.1 & Figure 4.5.7). The layers were bioturbated both vertically and horizontally, varying from being sparse to intense in the degree of deformation.

The lower part of the core is relatively coarse compared to the middle part, which was quite fine grained and dark in colour. The upper part shows a coarsening upward trend, buried by a blue/grey calcite layer. The calcite layer showed some isolated closed pores, and cul-de-sac pores. Pictures of the entire core are presented in Appendix 9.6.

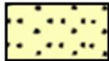










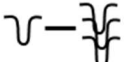

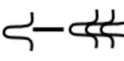

	Sandstone		Calcite limestone
	Shale		Siderite
	Unidirectional ripples		Shell/shell fragments
	Climbing ripples		Plants/organic material
	Wave ripples		Pyrite
	Convolute lamination		Sparse-intense vertical bioturbation
	Double drapes		Sparse-intense horizontal bioturbation
	Soft sediment deformation (e.g. flame structures, loads/casts)		

Figure 4.5.6. Legend for core log presented in the next figure.

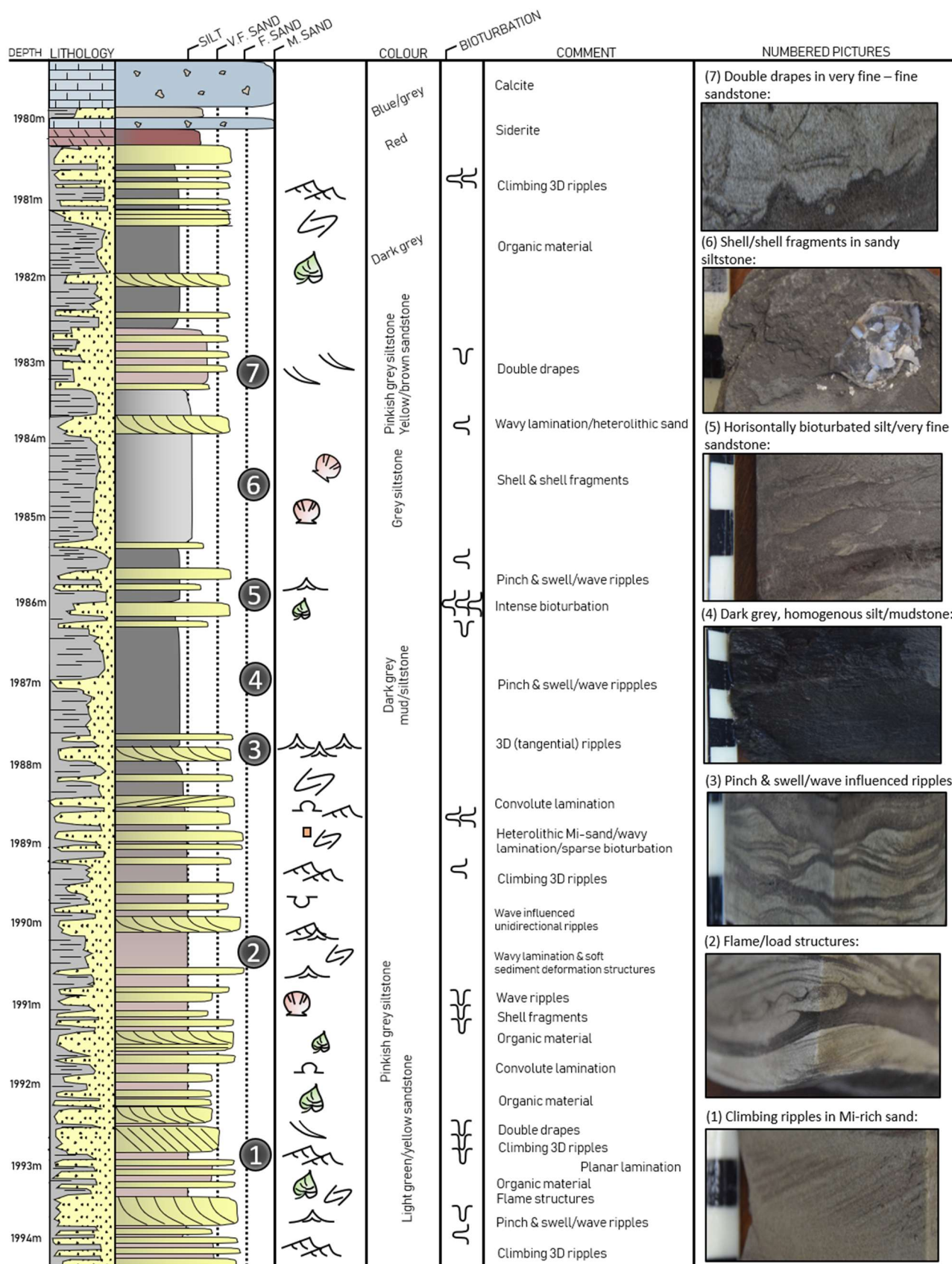


Figure 4.5.7. Log of core 1 from well 2/2-2. The entire core is approximately 15m. Note the position of the pictures indicated in grey circles, numbered 1-7.

## 4.6 Sequence 3

S3	Zone 1 (South)	Zone 2	Zone 3 (North)
<b>Seismic facies description</b>	Subparallel reflection configuration, with amplitudes ranging from low to high in a disrupted, high frequency region.	Divergent and parallel reflection configuration dominates, with medium-high amplitudes and frequencies.	Strong amplitudes and high frequencies dominate in the northern part. Parallel, close to horizontal reflectors.
<b>Reflection terminations</b>	T3 reflector continues beyond study area. S3 however downlaps onto the underlying T2 reflector.	The upper part of the sequence is truncated by an angular unconformity, T3.	The sequence is truncated by the T3 angular unconformity in north/northwest
<b>External geometries</b>	Synclinal external geometry of reflectors within Zone 1.	Sigmoidal clinoform geometries, with rising shelf-break trajectory. Foresets show a clear dip towards southwest.	Above the suggested shelf-break, topsets show a very gentle/almost horizontal dip towards southwest.
<b>Structures</b>	Polygonal faults dominate within this zone.	Zones of salt diapirs and related faults cutting through the sequence.	Depressions in north and northeast, with chaotic fill, orientated north/northeast – south/southwest.

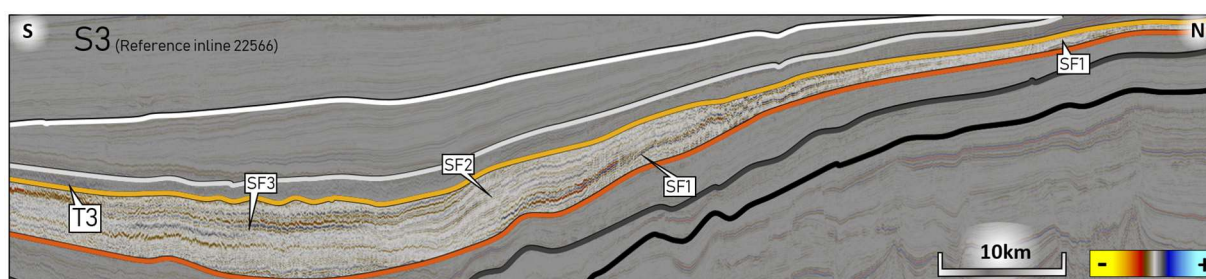


Figure 4.6.1. The table describes the general trends of the sequence throughout the study area (Zone 1 – 3). The recognized seismic facies (classified in Figure 4.2.1) shown on the reference cross-section; SF3 in the deeper parts/Zone 1, SF2 and SF1 towards the northeast.

The T3 reflector was tied to well 1/3-11 in the southern part (Zone 1) and 9/12-1 in the northeastern part (Zone 2 & 3) by the regional Mid-Miocene Unconformity (MMU; Appendix 9.5). The surface along with T2 encompasses S3. In the northeastern part of the study area (Zone 2 & 3), the surface was placed where the underlying reflectors (including the T2) disappear, or toplap towards the T3. The T3 is thus considered an unconformity. However in the basin parts (Zone 1), the surface was interpreted along a peak. In this area, the underlying continuity of the reflectors were intact.

The sequence is expressed by southwestward dipping reflectors where the SF1 facies dominates in the northeastern part (Figure 4.6.1). Polygonal faults are abundant in the southern part, Zone 1 (Figure 4.6.2), similar to the two previously described sequences. Parallel continuous reflectors horizontally covers Zone 2 & 3, and are further on attributed to the topsets of identified clinoforms. The change in dip which is termed as the paleo shelf-break is successively displaced towards the southeast, compared to the T2 shelf-break. The shelf-break for T3 is roughly orientated northwest-southeast, perpendicular to the basin axis. The progressive displacement of the shelf-break is tracked through the trajectory, which is flat in the lowermost part of the sequence (Figure 4.6.5), and ascending in the upper part (Figure 4.6.6). The inferred

shelf-break is placed between the suggested topset and foresets of clinoform units recognized within the sequence. The external geometry of the clinoform units combined show a sigmoidal configuration. The foresets are gently dipping, and less steep compared to the underlying T2 clinoforms. The vertical thickness of the clinoforms are ranging between 280 and 330m. Furthermore, the S3 show internal reflection configurations classified as divergent (Figure 4.6.3). The thicknesses of the internal units increases towards the southwest, and comprises reflectors with good continuity and medium amplitudes.

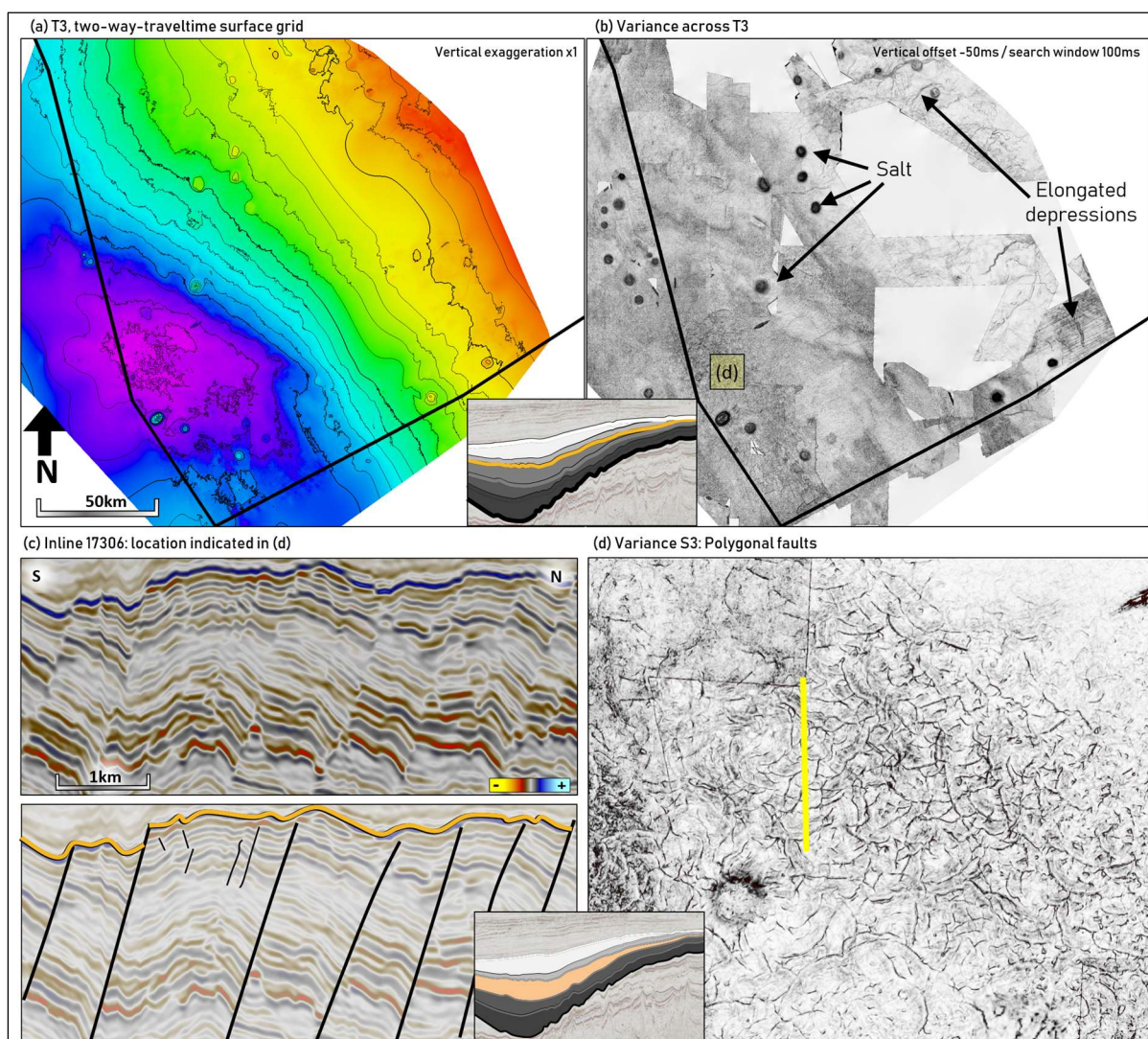


Figure 4.6.2. (a) The Top of S3 (T3) TWT surface. (b) Variance surface attribute across T3. (c) Vertical line ups of disconnected reflectors ~ polygonal faults, below T3. (d) Map view of variance surface attribute within T3 ~ polygonal faults.

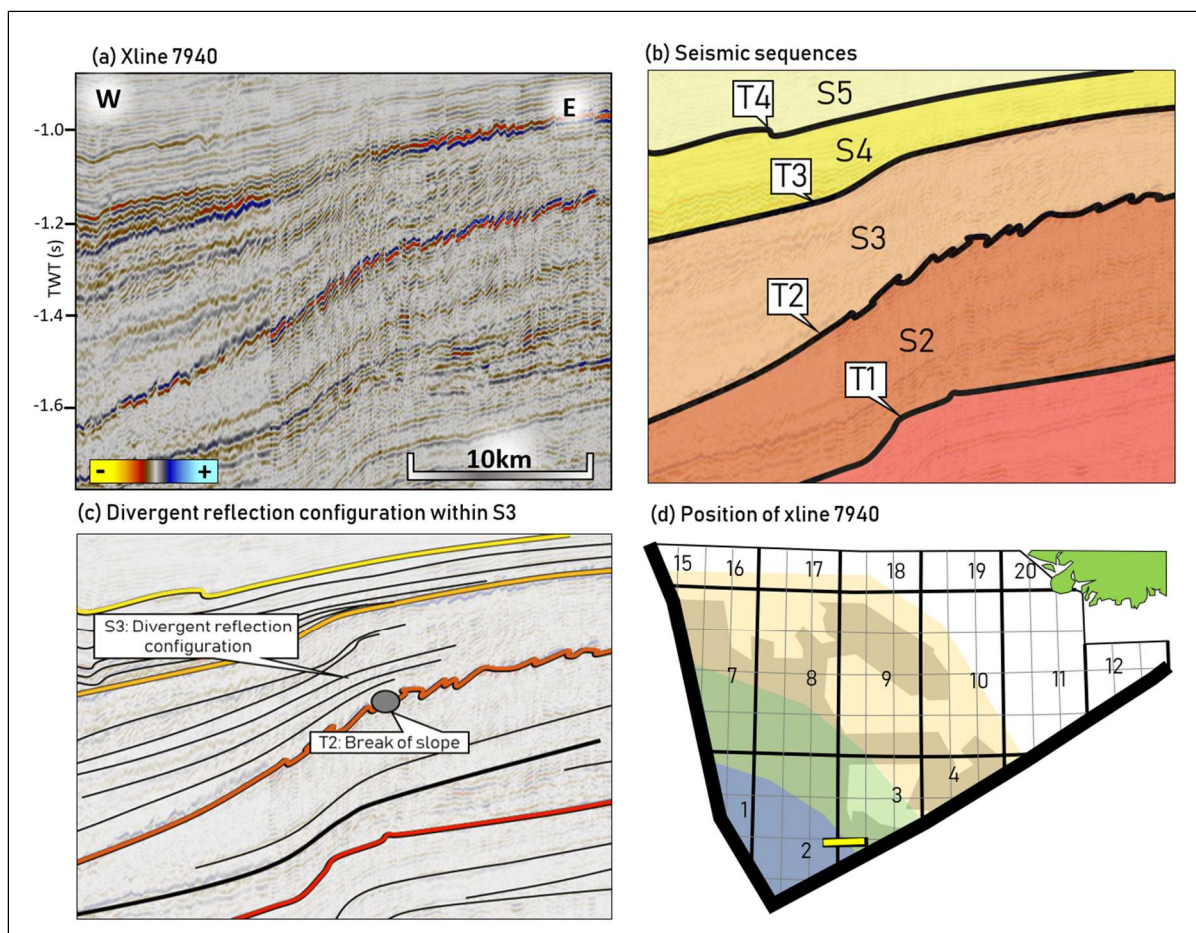


Figure 4.6.3. The figure display the divergent reflection configuration of the S3 sequence, where the thickness of the internal-units increases westwards. The divergent pattern is also present in a north-south direction. The break of slope from T2 is also included.

Complex patterns of depressions occur in variance maps in the northern part of Quadrant 9 (Zone 3). When observed in cross-sections, the depressions cuts through otherwise lateral, continuous reflectors. The fill in the depressions have a chaotic seismic character. The cross-sections also show that the filled depressions occur at several vertical levels as isolated features. The depressions are orientated roughly northeast – southwest at the T3 level, however the geometry of the depressions changes through the layers upwards. These depressions are shown during the S4 description (Figure 4.7.3).

Elongated depressions also occur in the northwestern corner of Quadrant 4, within Zone 3 on the border to Zone 2 (Figure 4.6.4). The average orientation of the depression is varying from north – south. The depressions overlap across one another, bifurcates and converge. Some display a meandering geometry.



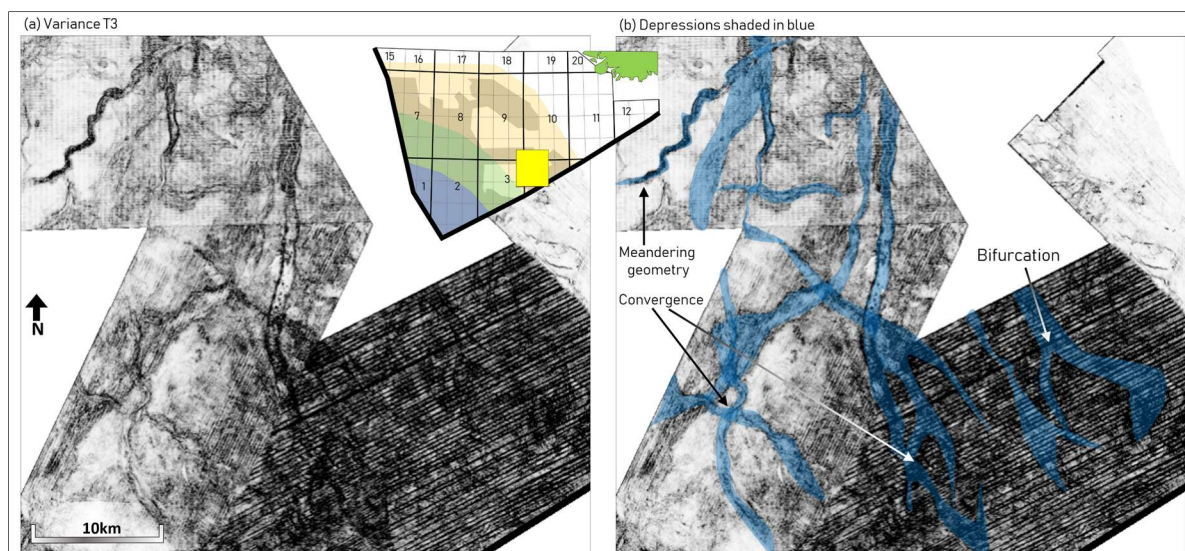


Figure 4.6.4. (a) Variance map across T3 (MMU) in the northwestern corner of Quadrant 4. (b) Shaded depressions in blue.

The gamma ray log from three wells is shown in Figure 4.6.6. The gamma ray log is included to evaluate the probability of sand-rich or clay-rich sediments within the prograding sequences, S1-S3. Well 2/1-6 shows that the S2 sequences has lower gamma ray values compared to the underlying S1 and overlying S3. The same goes for well 2/2-2, with the exception of a small zone with low gamma ray values occurring around the MMU. In well 9/12-1, low gamma ray values occur for the S2 interval. The low gamma rays around S2 is repeated through all of the three logs, and is thus correlated. The low gamma ray occurring around the MMU in well 2/2-2 is not recognized in the two other wells.

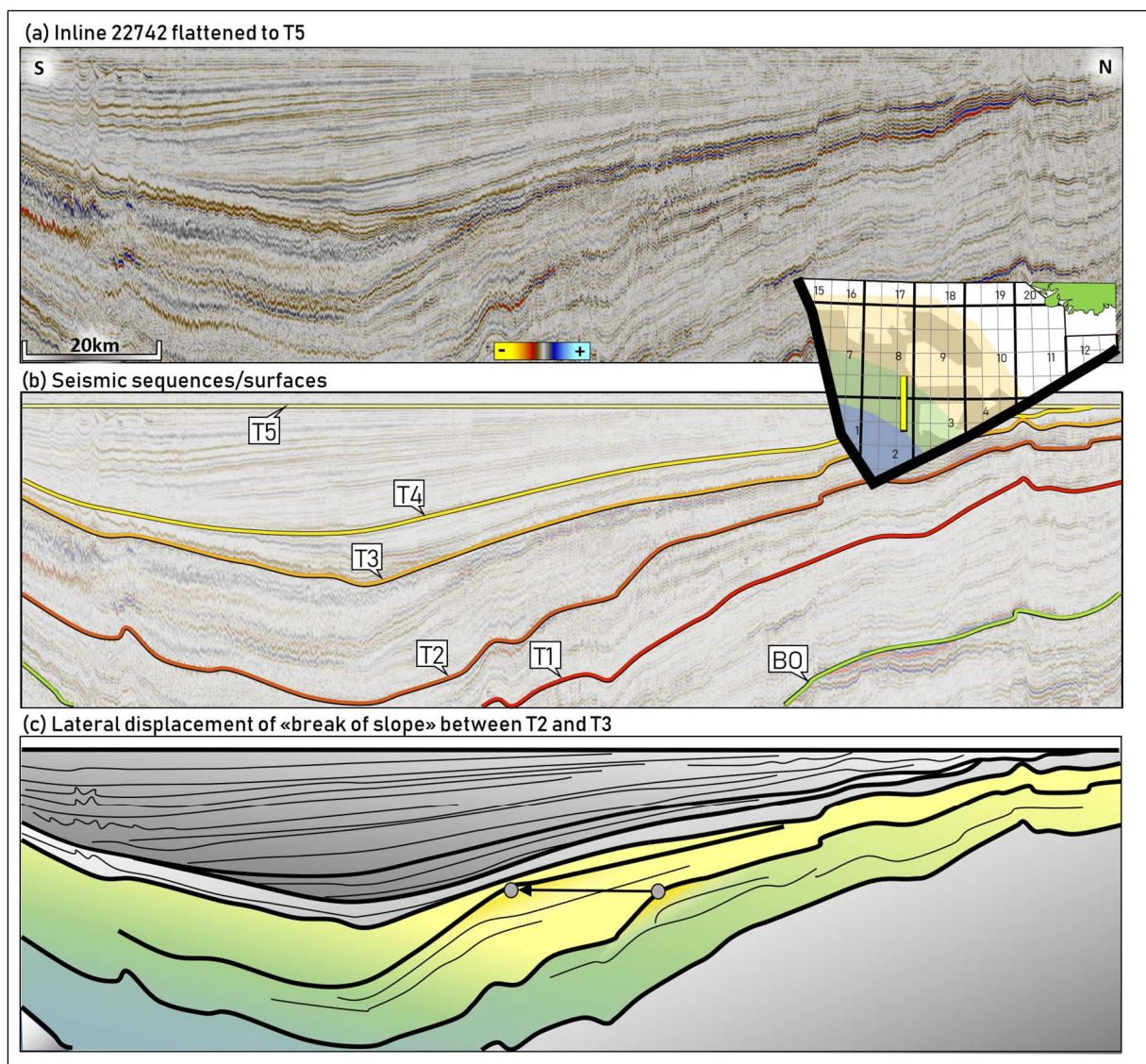


Figure 4.6.5. (a) Inline 22742 flattened to T5. (b) The seismic sequence boundaries. (c) shows the suggested location of two paleo-shelf breaks, with the shelf-edge trajectory slightly ascending from T2 to an intra S3-reflector.

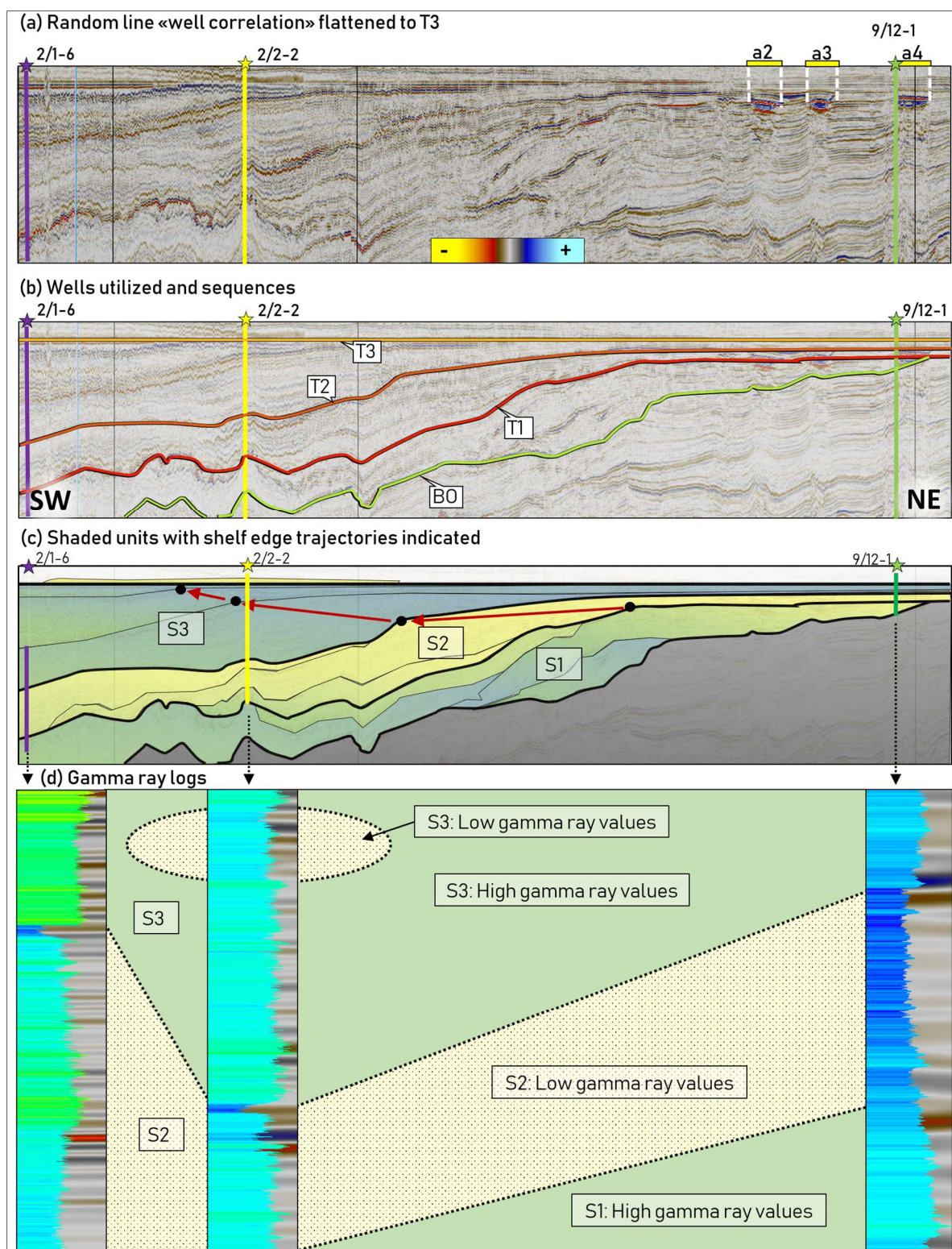


Figure 4.6.6. Showing the (c) gently ascending shelf edge trajectories, and sigmoidal clinoform geometries. (d) shows correlation of gamma ray logs for the well interval indicated in (c), with low gamma-ray values indicated by blue colour.

## 4.7 Sequence 4

S4	Zone 1 (South)	Zone 2	Zone 3 (North)
General description	S4 internal reflectors downlap unconformably onto the underlying T3 (MMU) reflector.	T4 shows a southwesterly dipping, high amplitude reflector with good connectivity.  Few external structures observed.	Cut by T5 in the northernmost parts. Sequence thins towards the northeast.  System of elongated depressions in the northern part of Quadrant 9, orientated northeast-southwest.

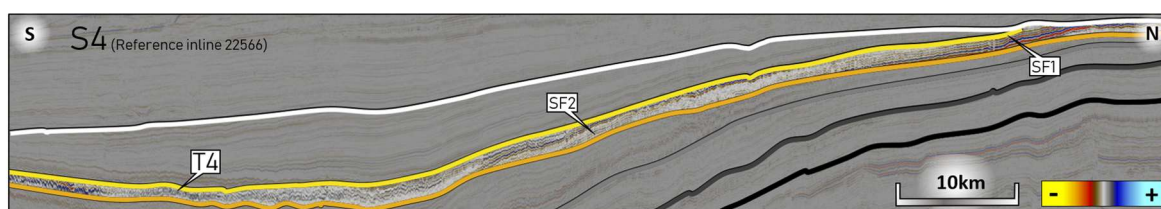


Figure 4.7.1. The table describes the general trends of the sequence throughout the study area (Zone 1 – 3). The recognized seismic facies (classified in Figure 4.2.1) are shown on the reference cross-section.

Sequence 4 is bounded by the T4 reflector on top, interpreted along a regional, high amplitude peak, and the T3 reflector at the base. The sequence onlaps unconformably towards the underlying T3 (MMU) reflector within Zone 1. Towards the north, the sequence is cut and truncated by the overlying T5 reflector. The thickness of the sequence is quite thin compared to the previously described sequences and thus fewer observations are included. The surface shows a southwestward dip, where several diapirs cuts through the sequence (Figure 4.7.2). The large system of elongated depressions described briefly for the T3 were observed at both the S4 and S5 level as well. Some of the depressions are curved back and forth, in a meandering shape (Figure 4.7.3). Towards the S5 level, the orientation of the depression changes from being dominantly northeast-southwest, to a more north/south configuration.

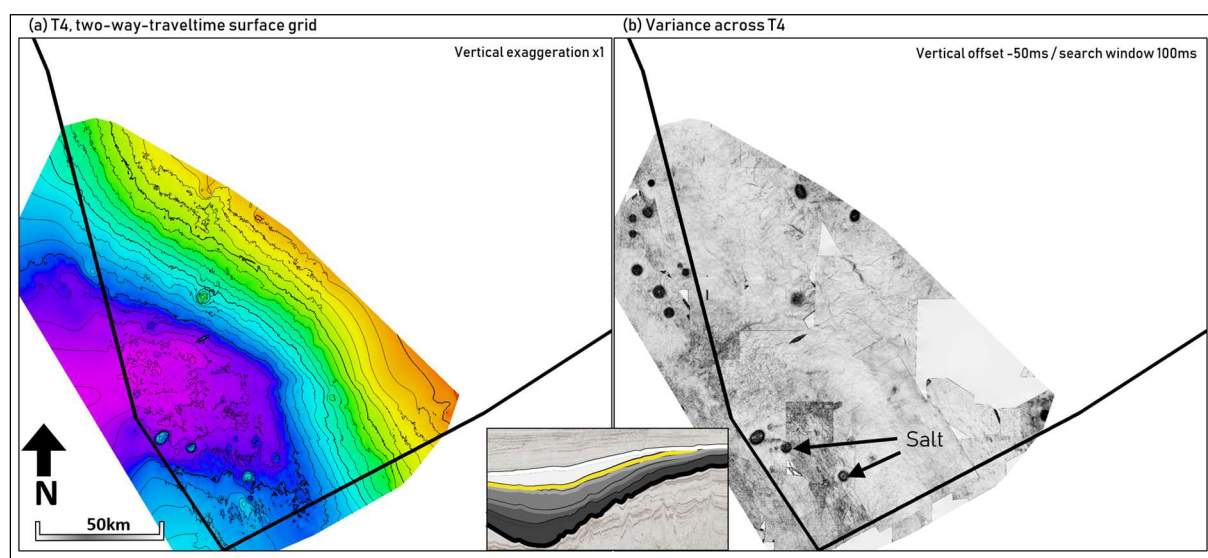


Figure 4.7.2. a) The Top of S4 (T4) TWT surface. (b) Variance surface attribute across T4.

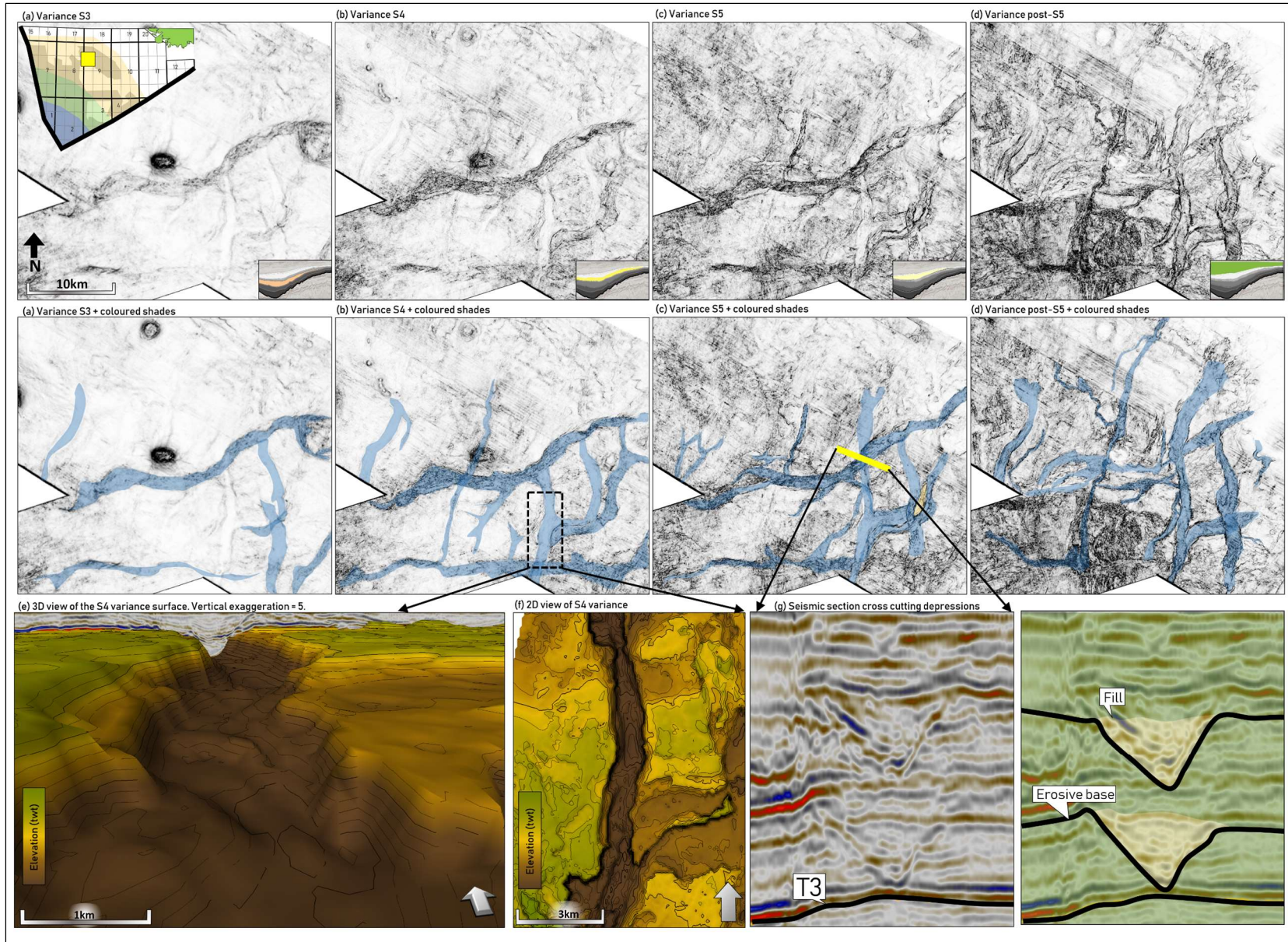


Figure 4.7.3. The figure displays elongated depressions recognized within Zone 3 of the study area, in the northern part as indicated in (a). The evolution and changing pattern of the depressions is shown through sequence 3 to post-5.

## 4.8 Sequence 5

S5	Zone 1 (South)	Zone 2	Zone 3 (North)
<b>Facies description/ reflection terminations</b>	Dipping, continuous, low-high frequency and amplitude reflectors. Downlap towards southwest, onto underlying T4 and T3.	Dipping, continuous, low-high frequency and amplitude reflectors.	Toplaps towards T5.
<b>Other</b>	Basin infill.	Gently dipping foresets, sigmoidal clinoforms with rising trajectories.	Systems of elongated depressions in north (Quadrant 9) and northeast. Orientated roughly north-south.



Figure 4.8.1. The table describes the general trends of the sequence throughout the study area (Zone 1 – 3). The recognized seismic facies (classified in Figure 4.2.1) shown on the reference cross-section; SF1 and SF2 dominating.

The last sequence, S5, shows a slightly different reflection configuration and degree of continuity compared to the first three sequences, S1-S3. The sequence consists of continuous reflectors reaching from the shallower part (Zone 3), across Zone 2, and beyond the deeper parts (Zone 1) of the seismic data. Towards the southwestern margin of the previously described basin geometry (Zone 1), the sequence downlaps towards S4 and T3. The onlap towards northeast and southwest which was common for the S1-S3 sequences, is not present here. This is illustrated by the reflection terminations (Figure 4.3.1). The T5 reflector makes out the upper boundary of the sequence, and cuts the underlying T4 reflector towards the north (Figure 4.8.2).

The internal units encompassed within the S5 sequence show increasing vertical thicknesses towards the south, and decreasing thicknesses towards the north. The units show sigmoidal external geometries, where the foresets show a very gently dip towards the south (Figure 4.8.1 & Figure 4.8.4). The vertical height of the internal units are approximately 300ms (TWT) at the most. The reflectors show a modest change in dip within Zone 1, which may be attributed to a paleo-shelf break. However the break is not as clear as for the S1, S2 and S3 sequences. A rising trajectory is suggested based on the sigmoidal shape and southwestward propagating direction on the internal units.

In the northern part of Quadrant 9, elongated depressions occur above those described at the T3 and S4 levels. The orientation of the depressions are organized dominantly north-south. The variance maps around these depressions also show parallel, horizontal lines, which are disregarded from the geological interpretation and considered as artefacts. Furthermore, elongated depressions with adjacent mounds are recognized in the seismic data in the

northeastern corner of Quadrant 3. These depressions also show a north-south orientation, and are up to 1km wide and ten's of kilometers in length (Figure 4.8.3).

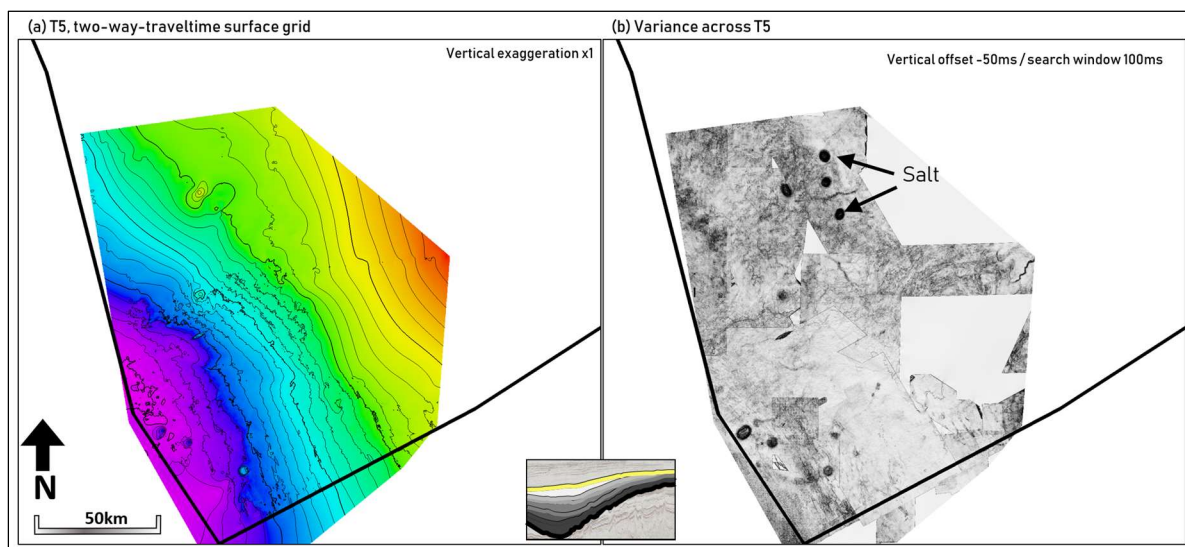


Figure 4.8.2. The Top of S5 (T5) TWT surface. (b) Variance surface attribute across T5.

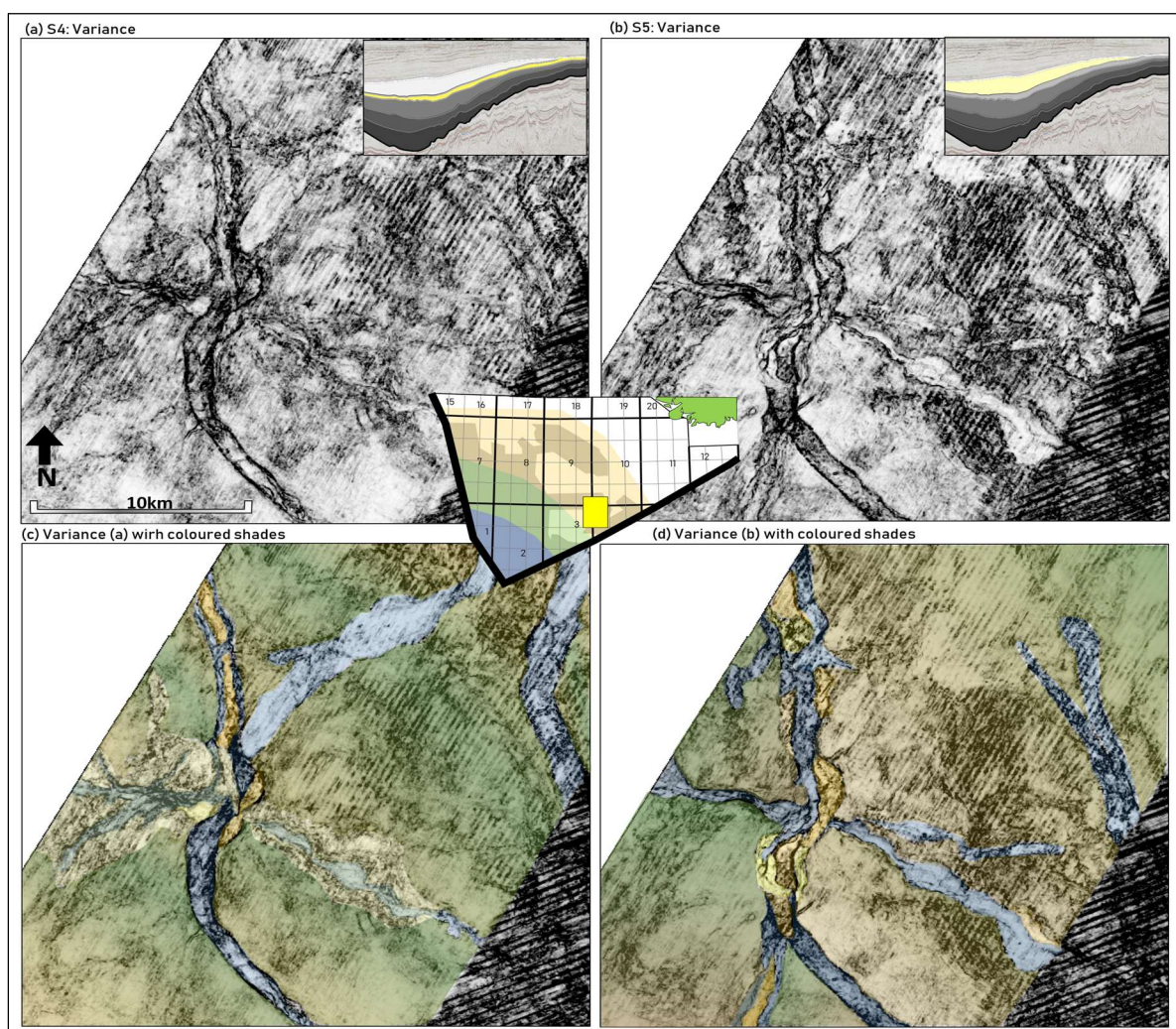


Figure 4.8.3. The figure shows the vertical evolution and change of a system comprising several elongated depressions. (a) Variance within S4 with the correlating (c) coloured shades. (b) Variance within S5 with the correlating (d) coloured shades.

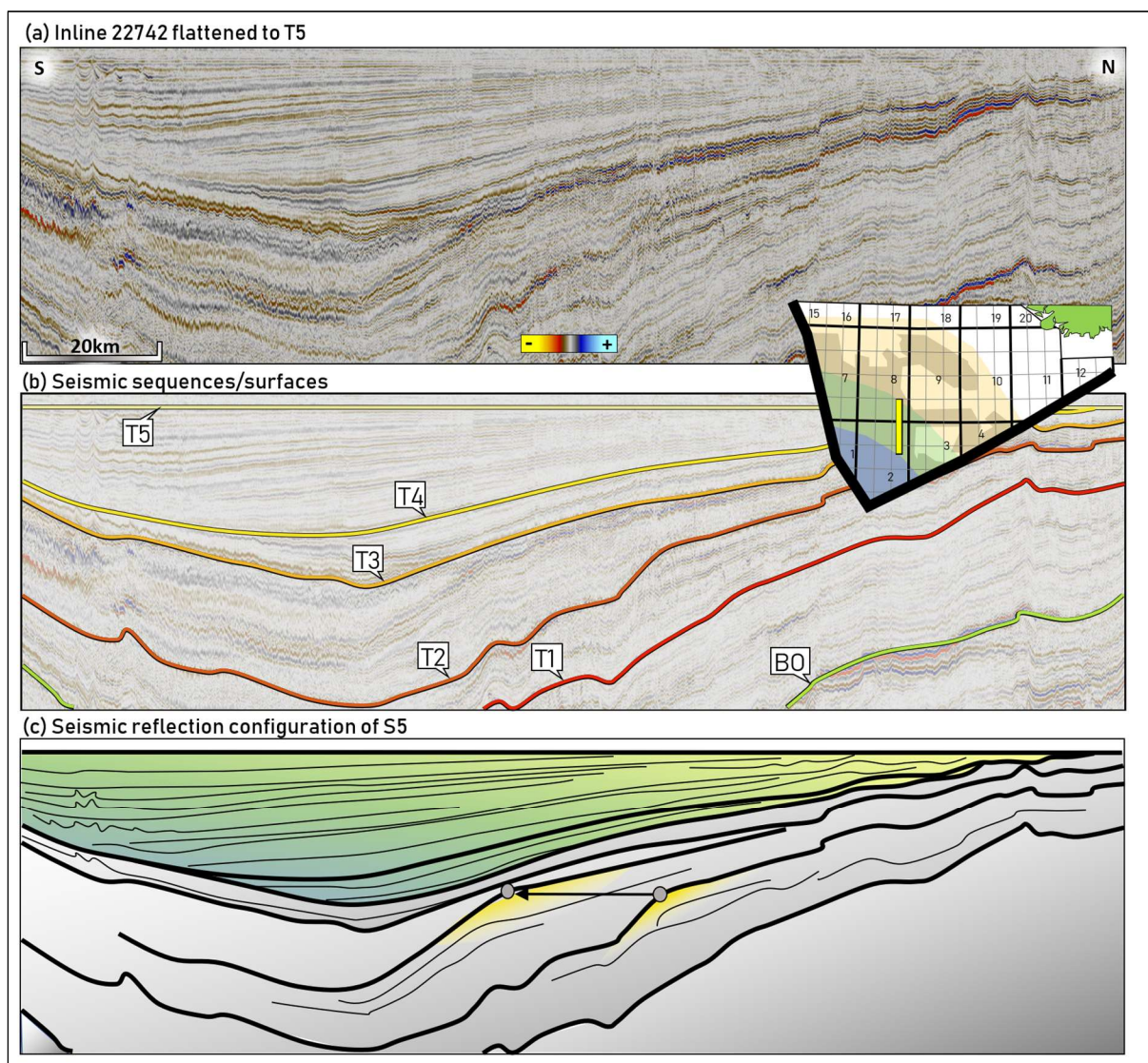


Figure 4.8.4. (a) Seismic inline, the same as used in Figure 4.6.5. (b) The seismic sequence boundaries marked, and (c) S5 coloured accordingly to the reflection termination classification used throughout the study. The unit shows downlapping reflection terminations towards T4/T3. The sequence is cut/toplaps in the north.

## 4.9 Seismic hydrocarbon indicators

Several direct hydrocarbon indicators (DHI's) are present in the seismic data. To begin with, amplitude anomalies within Zone 1 is presented, subsequently followed by Zone 2 and Zone 3 amplitudes.

### 4.9.1 Zone 1

In the southern part (Zone 1), the brightest amplitude anomalies (bright spots) with a reversed phase polarity occur commonly above zones of wiped-out reflection patterns, similar to Seismic Facies 6 (Figure 4.9.1). These zones may be caused by noise, considering the amount of energy absorbed by the bright spots above. Nevertheless, they may also be caused by fluid variations



within the pore space. The bright spots in this region are commonly situated above deeper-seated diapiric salt structures, attributed to Seismic Facies 5. The S1-S3 sediments in this area are heavily faulted, where polygonal faults dominate. However some fault zones extend all the way from the underlying Mesozoic sediments through the T3 reflector. The deepest bright spots are situated below anticlinal folds, similar to structural traps. At the T5 level, bright spots also occur laterally displaced relative to one another, along the up-dip of the reflectors towards northeast (Figure 4.9.1).

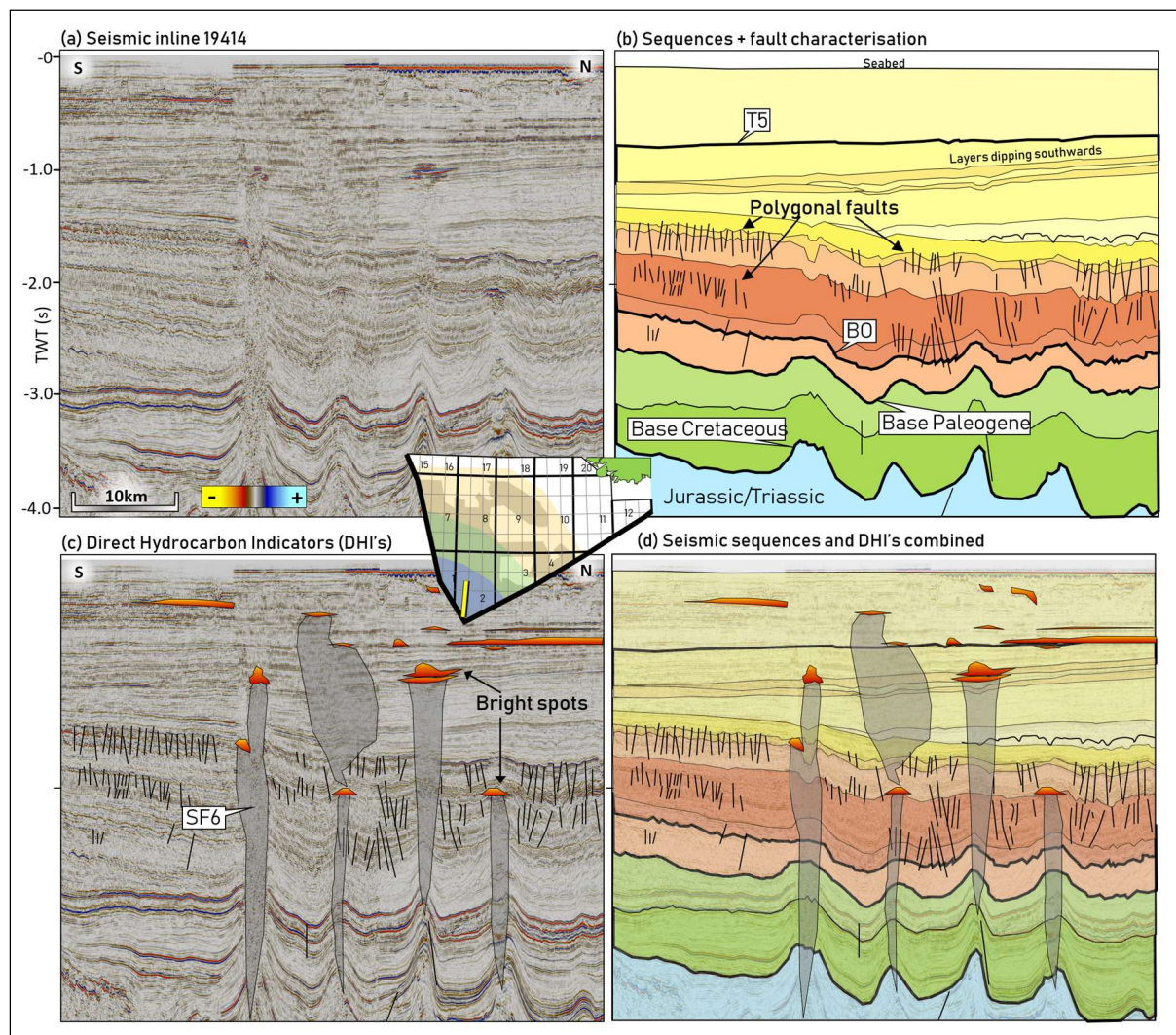


Figure 4.9.1. (a) Seismic inline 19414 located in Zone 1. (b) Seismic sequences applied to inline 19414, with faults and dip of layers annotated. (c) Direct hydrocarbon indicators such as bright spots, as well as Seismic Facies 6. Several of the bright spots occur roughly above the suggested SF6. (d) Seismic sequences and direct hydrocarbon indicators combined.

## 4.9.2 Zone 2

Towards Zone 2, a complex pattern of bright spots appear adjacent and above the diapiric structure previously described close to the well 2/3-1 (Figure 4.9.2). The bright spots in this area have been divided into three levels. The first, and deepest level, show a bright spot along a reflector dipping gently towards the southwest. The horizontal extent of the bright spot is

shown through a minimum amplitude (MinAmp) surface attribute, and exceeds the normal fault situated above the diapir. Hence, it is present on both sides of the fault – on the same vertical level (Figure 4.9.3). The reflector where the bright spot is situated is identified on both sides of the fault zone from patterns and packages of reflectors similar on both sides.

For Level 2, the bright spots are bounded by the fault zone towards the northeast, along the up-dip of the reflector. Towards southwest, where the reflector dips downward, the bright spot disappear approximately at a given vertical level, following the height-contour of the structure. This horizontal extent is illustrated by the MinAmp map. The shallowest levels of bright spots appear below the T3 reflector, where a sequence of parallel and laterally continuous reflectors are in place above. Several amplitudes appear below the T3 reflector further up-dip, towards the north (Figure 4.9.2.b).

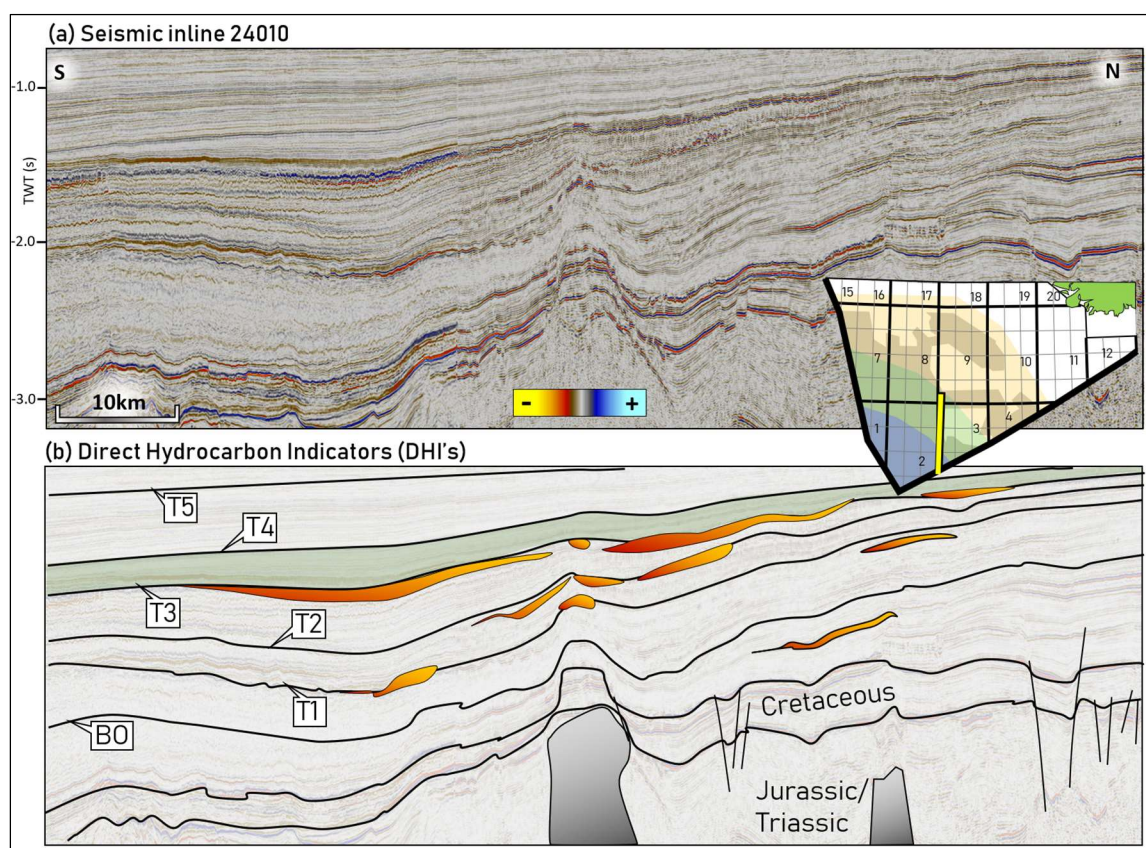


Figure 4.9.2. Inline 24010 (same as Figure 4.3.2) within Zone 1 & 2, with (b) DHI's such as bright spots indicated in red/orange. The shaded green marks a unit with parallel, continuous reflections. Note that all the bright spots occur below the shaded green unit, in a laterally up-dip displaced way.

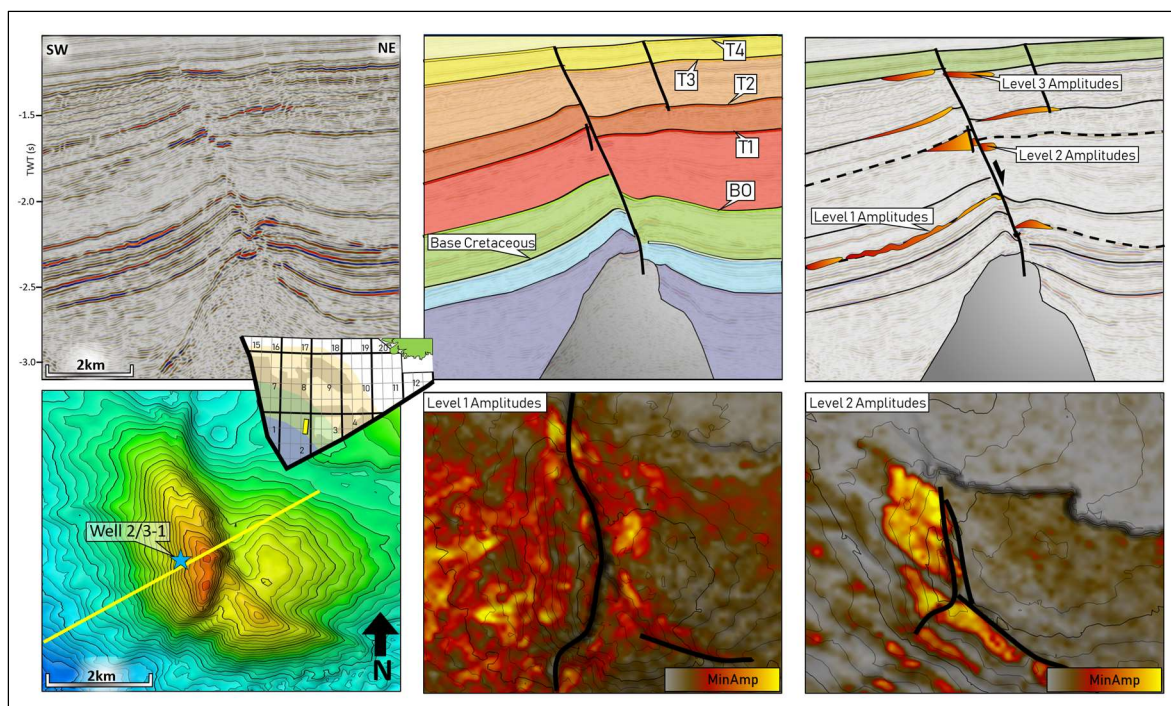


Figure 4.9.3. (a) The same diapir structure as in the previous figure, as well as in Figure 4.3.3. The DHI's occur adjacent to a fault located above the diapir, at different vertical levels. At Level 1, the amplitude anomalies occur in a further horizontal extent compared to Level 2 amplitudes. Level 2 amplitudes seem to be restricted by the dip and fault, and Level 3 by a sealing layer.

Towards the eastern margin of the Norwegian southern North Sea, close to well 4/4-4, bright spots occur similarly to those observed around well 2/3-1. The amplitude anomalies in this area is termed a8, and is divided into three stratigraphic vertical levels. The anomalies are situated close to a anticlinal, faulted dome. At the first (deepest) vertical level, a wide bright spot is present with a horizontal extent and geometry similar a stratigraphic pinch-out trap. Towards the southeast, the bright spot disappear from the first level as a fault zone cuts through the seismic layer. A new bright spot occur at a shallower level, Level 2, towards the apex of the anticlinal structure. A clear phase shift is observed along the reflector and is attributed to hydrocarbon-initiated reduction in seismic velocity. The bright spots at this level are bounded both by the dip of the strata, as well as by the faults. Such trap configuration is similar to a structural and combination trap. The horizontal extent and boundaries of the fault spot is illustrated by the MinAmp attribute map view (Figure 4.9.4).

Furthermore, a bright spot occur approximately above the fault zone (Level 3). The horizontal extent of the bright spot show an elongated depression, which is also visible through variance (structural) maps. The bright spots is restricted to the base of the elongated depression. The trap configuration is similar to stratigraphic channel traps.

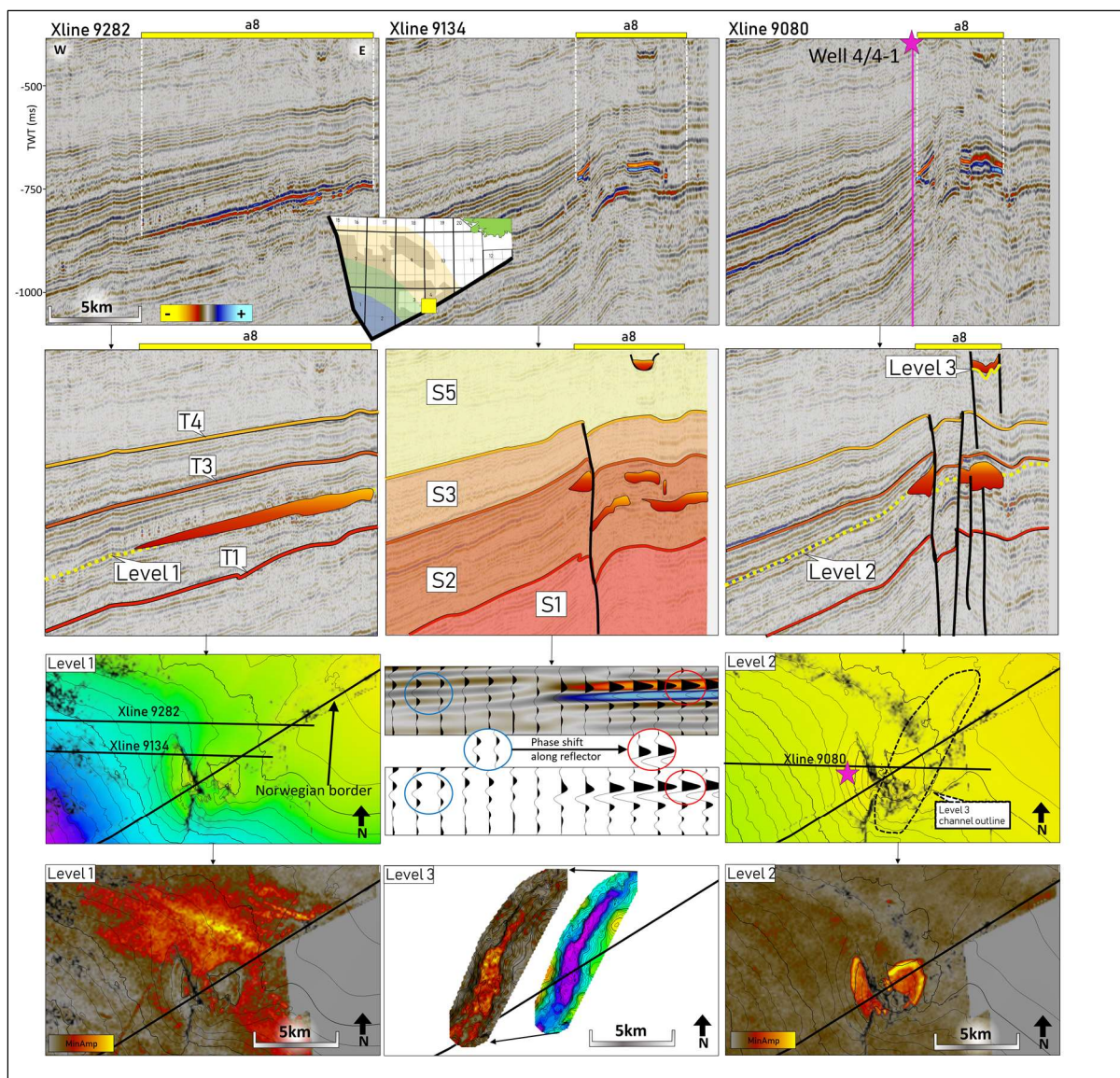


Figure 4.9.4. The figure display three seismic cross-sections cutting through a zone of bright spots (a8) at different places. From the first one (xline 9282), a bright spot with apparently a relative large horizontal extent is present (level 1). When investigating it further towards a faulted zone, the bright spot changes and is only appearing close to the fault and at different levels above (level 2 & 3). The bright spot in the uppermost level appear at the base of an elongated depression, resembling a channel. In the center of the figure, the phase shift along the reflector occurring when entering the amplitude anomaly is shown through wiggle display.

### 4.9.3 Zone 3

Towards northeast in the study area, within Zone 3, bright spots are abundant in anticlinal traps. The amplitude anomalies in this area were numbered as a1-a6, in addition to one zone of smaller bright spots (z7) (Figure 4.9.5). The anomalies are situated above seismic wipe-out zones (SF6), which again are underlain by diapiric structures (SF5). All of the bright spots occur below the same stratigraphic level and reflector, the T3 (Figure 4.9.6).

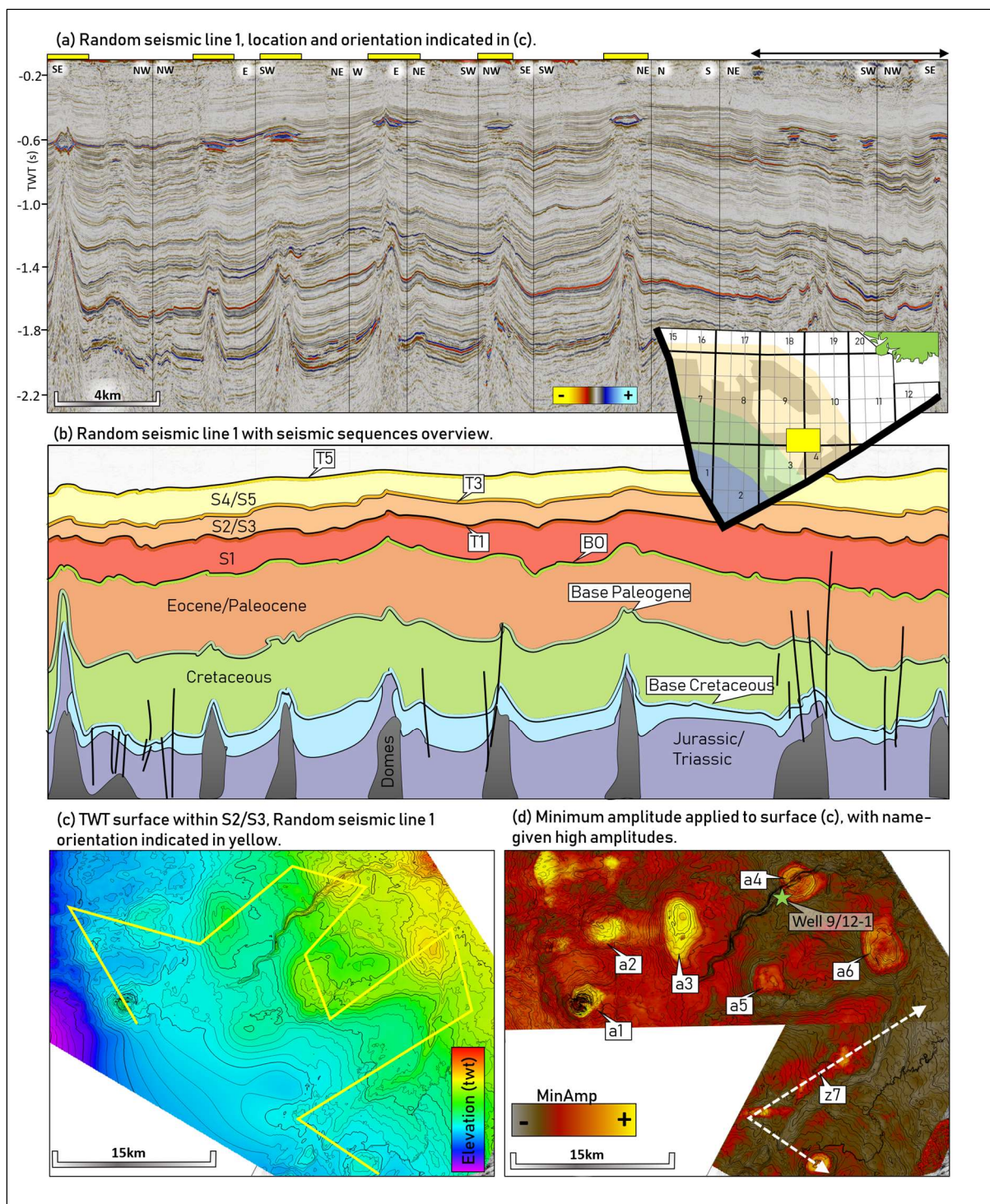


Figure 4.9.5. (a) Random seismic line 1, position indicated in right corner (Zone 3). (b) Sequences and sequence boundaries, along with faults and diapirs. (c) Precise position and orientation of Random seismic line 1, shown by TWT surface grid. (d) Minimum amplitude surface attribute across grid in (c), displaying numbered bright spots.

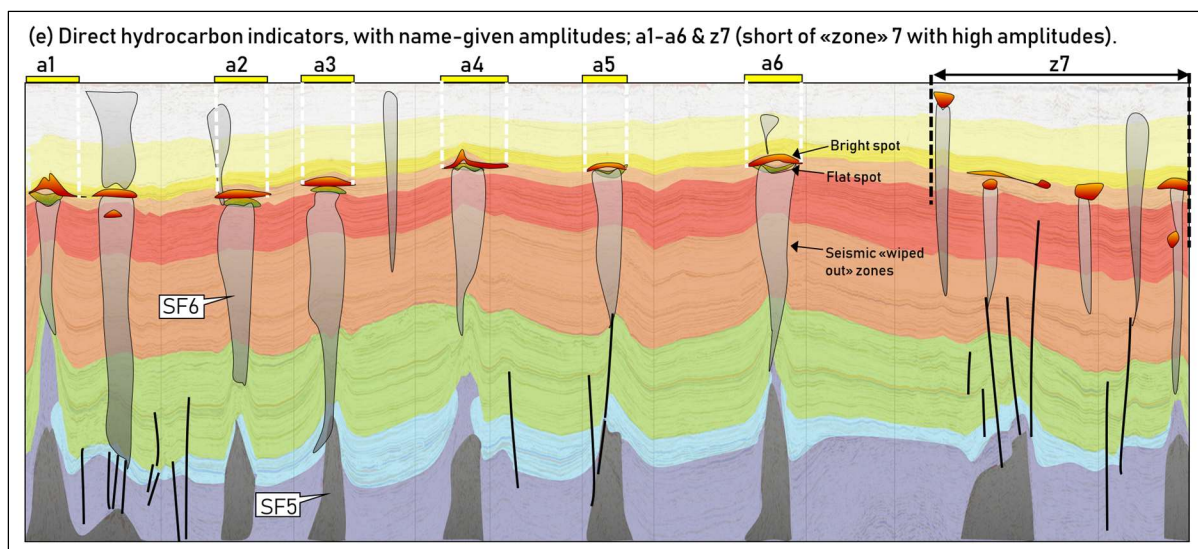


Figure 4.9.6. Continuation of Figure 4.9.5, (e), showing seismic sequences combined with direct hydrocarbon indicators. Note Seismic Facies 6 in the upper part, and Seismic Facies 5 in the lower part. Bright spots numbered Anomaly 1 – Anomaly 6 (a1-a6). Z7 = zone of high amplitudes.

Zone 7 is presented to demonstrate the precision of the bright spot occurrences below a specific reflector at the T2 level. In contrast to the a1-a6 anomalies, few of these bright spots occur in correlation to or above wipe out zones (Figure 4.9.7). The reflectors above the T2 are characterized by continuous, sub-parallel facies. These reflectors are within the S3 sequence.

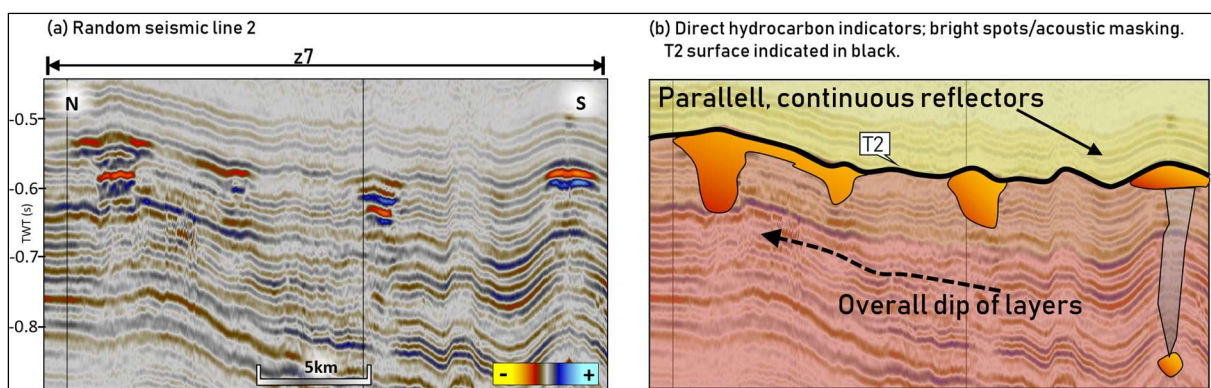


Figure 4.9.7. Zone 7 (z7) from Figure 4.9.5. (a) Random seismic line 2 and (b) shaded sequences and coloured direct hydrocarbon indicators. Note that all the bright spots occur below T2, and are buried by layers of continuous, parallel reflectors.

Well 9/12-1 is situated very close to the a4 amplitude anomaly, at the down-flank outer boundary. The amplitude anomaly is interrupted by a ridge, briefly described in S1, and one fault towards the southwest. The fault zone separates the anomaly into two separate bright spots. The overlying, parallel reflectors are recognized on both sides of the fault, and the southwestern part is displaced upwards (Figure 4.9.8). The vertical extent of the bright spot, from the apex to the bottom, is approximately 100ms (TWT). The a3 amplitude anomaly is situated a slightly deeper stratigraphic level, and comprises two bright spots separated by a flat-spot. The

overlying reflectors are parallel, continuous, and are not disrupted by faults or any other structural features.

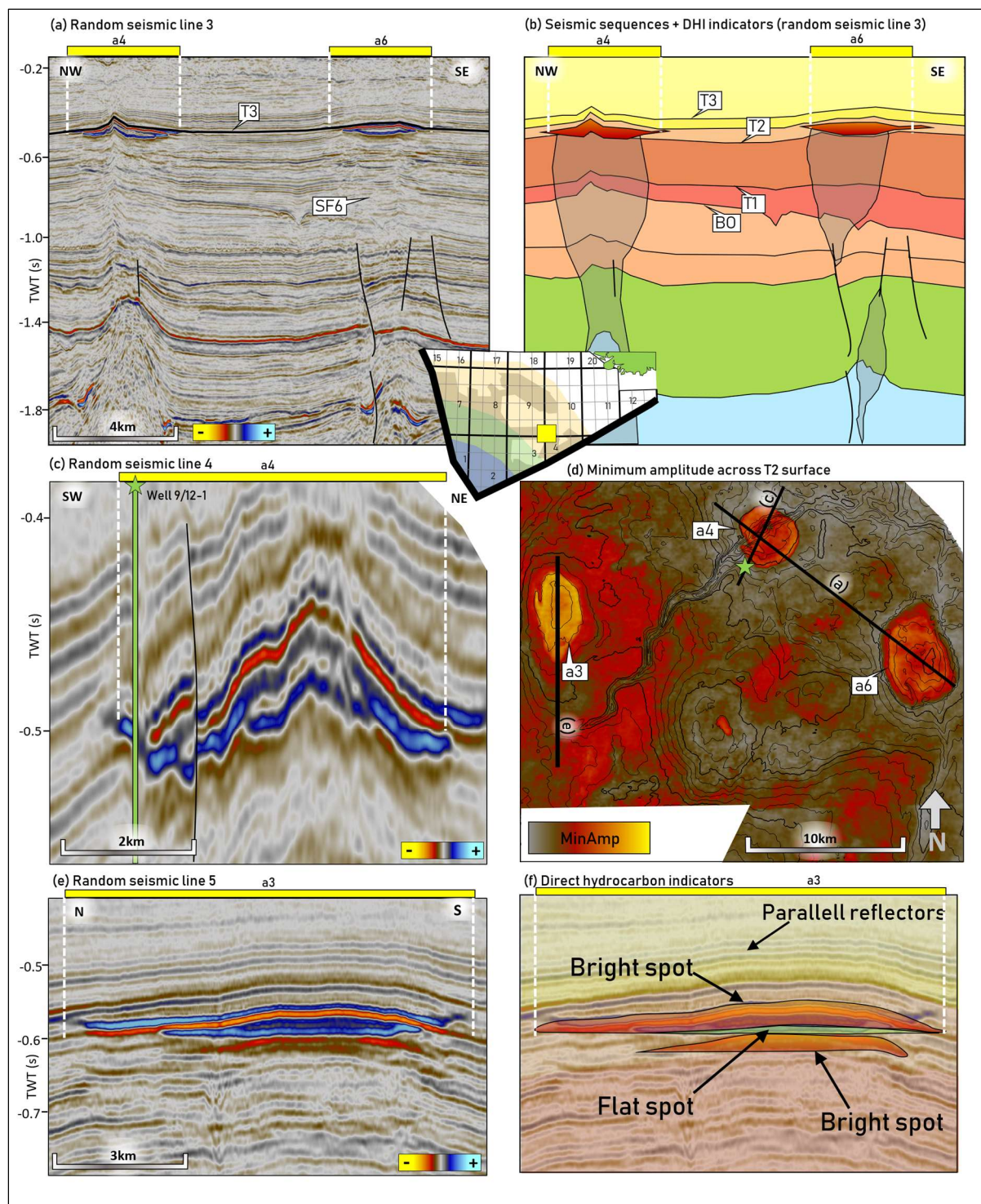


Figure 4.9.8. Amplitude anomalies a4 & a5 from Figure 4.9.5. (a) shows seismic random line 3, position indicated in (d) map. (b) Sequences and sequence boundaries. (c) Focused section on a4 with well 9/12-1 indicated in green. (d) Minimum amplitude surface attribute across the T2 surface. (e) Focused seismic cross-section on a3, position indicated in (d). (f) Random seismic line 5 coloured with respect to sequences and DHI's.





## 5 Discussion

The current chapter aims to evaluate and integrate the key observations and findings from the seismic data, the core logging results of well 2/2-2 and also regional well data. The chapter is divided into four parts, beginning initially with a summary of the chapter in Figure 4.9.1 presented to serve as an overview of the tectonic and depositional setting. The figure schematically provides an integrated overview of the discussed interpretations from the seismic data, core, and well data (Appendix 9.1) in the region. The summary is ensued by a description of the general characterization of the shelf. With this setting in mind, the paleo-environmental conditions that prevailed during deposition of the S1-S5 sequence are discussed, and finally the petroleum system indicators at the Oligocene-Miocene level are considered.

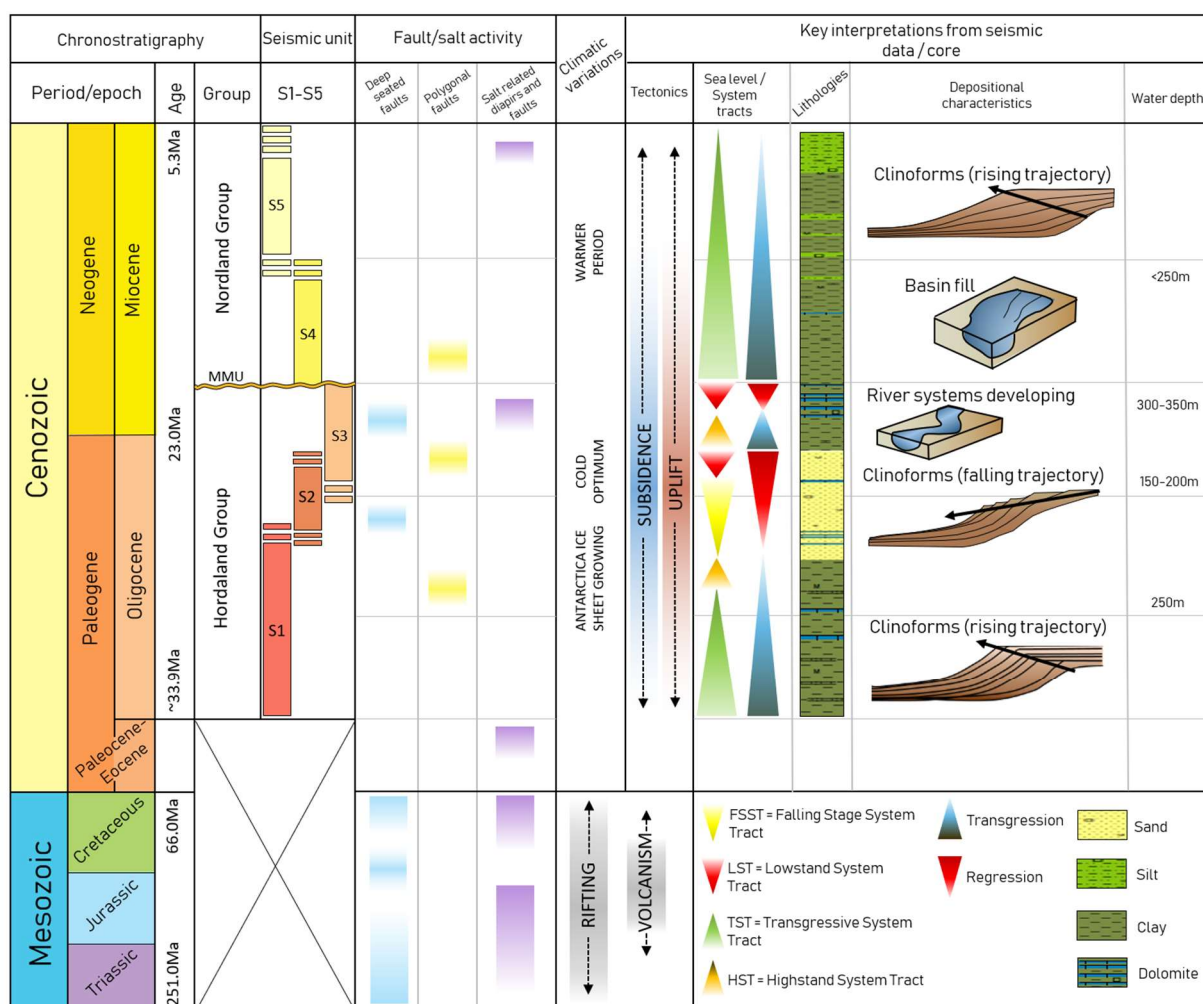


Figure 4.9.1. Summary of chapter 5.1 and 5.2. The timing of faults, salt diapirs and tectonic events, along with the external geometries characteristic for the respective sequences, the main lithologies (from well 2/1-15), system tracts and estimated water depths.

## **5.1 A general characterization of the shelf**

The seismic configuration of the Oligocene-Miocene sequences shows an overall trend of progradational units dipping southwestwards, with a topset-foreset geometry (Zone 2 & 3), symptomatic of clinoforms and shelf-progradation (Figure 4.3.1 & Figure 4.3.2). The deeper parts (Zone 1) comprises polygonally faulted sediments deposited in a distal basin setting, onlapping towards the prograding units sourced from northeast. The source and depocenters are further discussed in the reconstruction of the depositional environments (5.2).

The underlying sediments of early Cenozoic and Mesozoic age are represented by down-faulted blocks, where fault zones locally breach the overlying the Oligocene-Miocene sequences. The down-faulted pattern coupled with the prograding clinoforms, reflects a shelf of combined structural and sedimentary evolution (Figure 5.1.1; Helland-Hansen et al., 2012). Such shelves have a direct structural shelf-break, which is in turn blanketed and propagated by sediments retaining a break-of-slope geometry, with displacement occurring according to the structural heritage (Helland-Hansen et al., 2012). The overall tectonic setting at the transition to the Cenozoic after the Mesozoic rifting stages was characterized by passive subsidence, where accommodation space was continuously created. The Fennoscandian Platform, which provided the source of the units prograding into the basin, was contemporaneously uplifted (Eidvin et al., 2013; Gibbard & Lewin, 2014). Sedimentary shelves are often characterized by deep frontal waters (the subsiding basin in the area), a hinterland (Fennoscandian Platform) that can deliver enough sediments such that the margin is able to prograde, and transgressions that periodically flood back across the low-gradient coastal and alluvial plains (Helland-Hansen, 2012).

Interpreted faults in the study area are divided into two groups. The first one is represented by patterns and zones of polygonal faults which occur pervasively and distinctly in the deeper parts of sequence 1-3, within Zone 1. Some are disturbed by noise, nonetheless the displacement of reflectors is quite clear on the seismic data. Polygonal faults are traditionally an indication of sediment contraction and fluid expulsion, caused by rapid burial and applied pressure onto water saturated sediments (Berndt et al., 2003). The water escapes vertically upwards, fracturing and faulting the sediments. The end product is a series of near vertical faults orientated in polygonal shapes. They can thus be an indication that fine-grained sediments are present within this deeper zone (S1-S3).

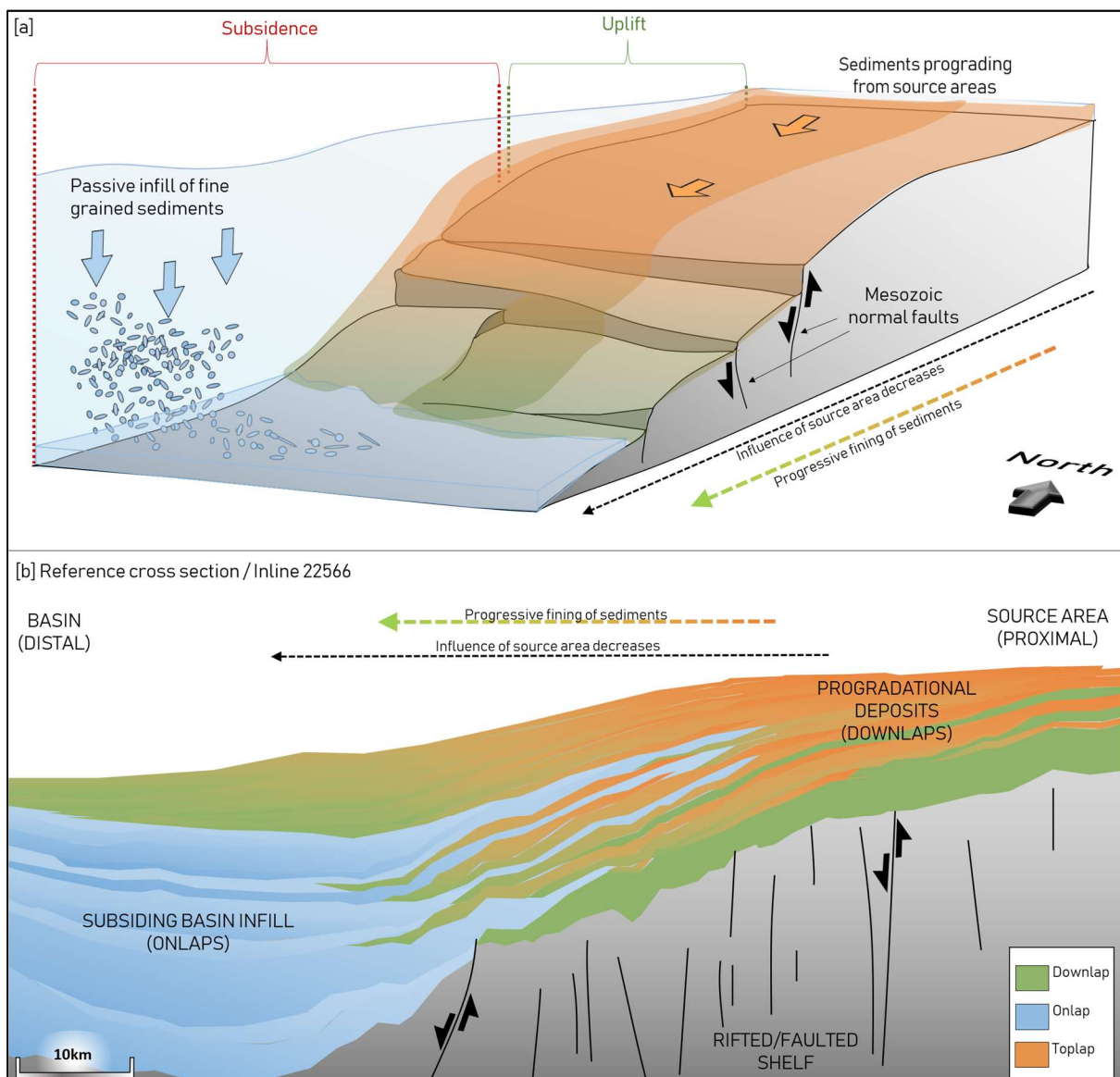


Figure 5.1.1. (a) Combined structural (Mesozoic faulted) and sedimentary (Cenozoic prograding sediments) shelf. (b) The shelf characteristics from the seismic data.

The second group of faults consists mainly of deep-seated faults related to Mesozoic rifting (Ziegler, 1975), and the vertical extent of these faults can locally be observed offsetting the Oligocene-Miocene strata. These faults follow the Mesozoic rift patterns. The vertical offset at the Oligocene-Miocene level is much less extensive than the displacement of the Mesozoic strata, and the units commonly show equal thicknesses on both sides of the fault zones. It is therefore suggested that the reactivation of faults occurred after the deposition of the Oligocene-Miocene sequences. However, the shallowest vertical extent of these faults constrains the faulting to have occurred before the overlying sediments were deposited, which are commonly below the T3 reflector in this study. The faulting thus took place after deposition of S1-S3, at the onset of S4.

Vertical movement of salt diapirs usually occur as a response to density differences between salt-layers and overlying sediments (Selley & Sonnenberg, 2015). A suggested timing of halokinetic movements (Figure 4.9.1) is presented by observing the varying thicknesses and occurrences of faults around the salt diapirs (Figure 4.3.2 & Figure 4.3.3). When salt migrates upward, accommodation space is created adjacent to the salt diapir as a result of salt withdrawal from the salt layer below. This results in a rim syncline, identified by onlapping reflection terminations towards the salt body and a synclinal shape of the reflection pattern. During episodes of halokinesis, the accommodation space above the salt body decreases as it moves upwards, resulting in a thinning of layers deposited while the salt moved vertically upwards (Lewis et al., 2013; Selley & Sonnenberg, 2015). Units that have the same thickness above and adjacent to the salt diapir are suggested to have deposited during quiescent times, during intermissions in halokinesis. Lastly, units folded upwards (anticlinal) vertically above the salt diapir are suggested to have formed during a late stage of halokinesis, occurring after the sediments were deposited (Figure 5.1.2). Such anticlinal shapes are abundant in the study area, working as hydrocarbon traps. The salt present in the region is attributed to the Zechstein salt deposits of Permian age (Ziegler, 1975).

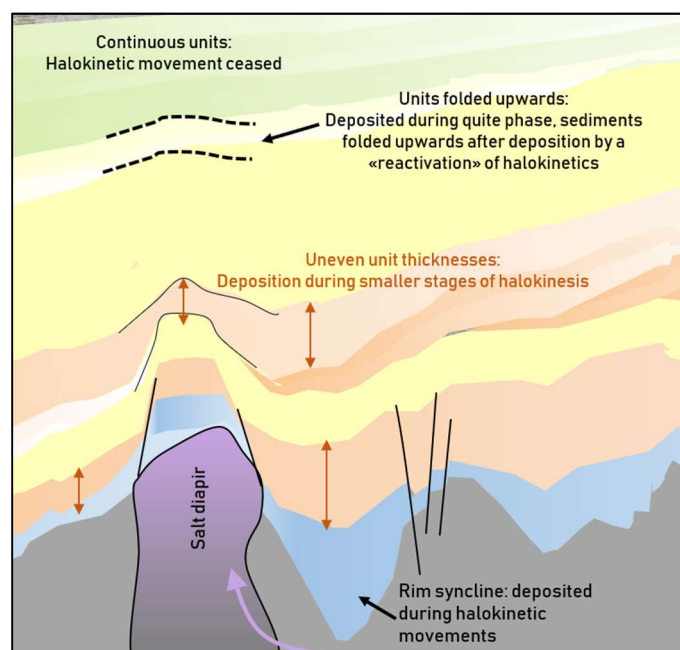


Figure 5.1.2. Reconstruction of salt movements suggested from differential thicknesses of layers and/or folding above salt diapir.

## 5.2 Reconstructing the paleoenvironments

### 5.2.1 *Early Oligocene (Rupelian) - S1*

The Lower Oligocene sequence (S1) rests unconformably on the older Eocene deposits with an angular discordance, downlapping southwestwards (Figure 4.4.3). Eocene deposits are roughly orientated with a dip towards the east. The topset-foreset configuration, orientated with the proximal parts towards the northeast, and the distal parts towards southwest, is interpreted to represent the paleo-shelf and slope. The distal parts of the paleo-shelf environment are attributed to Zone 1, where polygonal faults are abundant. The reflection configurations in the basin parts are otherwise, excluding the polygonal faults, quite continuous and parallel, and onlaps towards the prograding clinoforms from northeast. Polygonal faults do not form in response to a tectonic event, but rather from deformation of soft sediments (Lonergan et al., 1997). The parallel seismic facies, along with the polygonal faults, are both strong indications of fine-grained material, laid down at a stable deposition rate, distal to the sediments source. The fine-grained material may have been transported by suspension in the water-column, in a low-energy, deep-water regime (Figure 5.2.1).

The proximal areas towards northeast include several elongated erosional depressions, suggested to represent channel systems (Figure 4.4.4). The channels cut through and overlaps one another, resembling a braided river system.

A suggested position of the shelf-break for the Lower Oligocene period is orientated northwest-southeast, perpendicular to the Norwegian-Danish Basin and depocenter axis. The shelf-break was identified from the seismic data where a change in the angular configuration of the reflection pattern was observed (Figure 5.2.2). The external clinoform geometries showed a sigmoidal profile, where the stacking of clinoform units resulted in a climbing stacking pattern (Figure 4.4.7). These are shown by rising trajectories, and are common in high-stand system tracts. The top of the unit (T1) is considered a transgressive surface, represented by a strong amplitude. The water depths have been calculated by the volume of sediments, between the upper and lower bounding surfaces for each suggested clinoform unit. The vertical thickness of the clinoforms were measured after flattening overlying reflectors, such as the Mid-Miocene Unconformity (T3), in order to exclude later tilting or otherwise post-depositional altering of the sediments. The water depth during the Early Oligocene was estimated to be approximately 250m, where the average clinoform heights were 200ms (Table 3.2.2 & Figure 4.9.1).

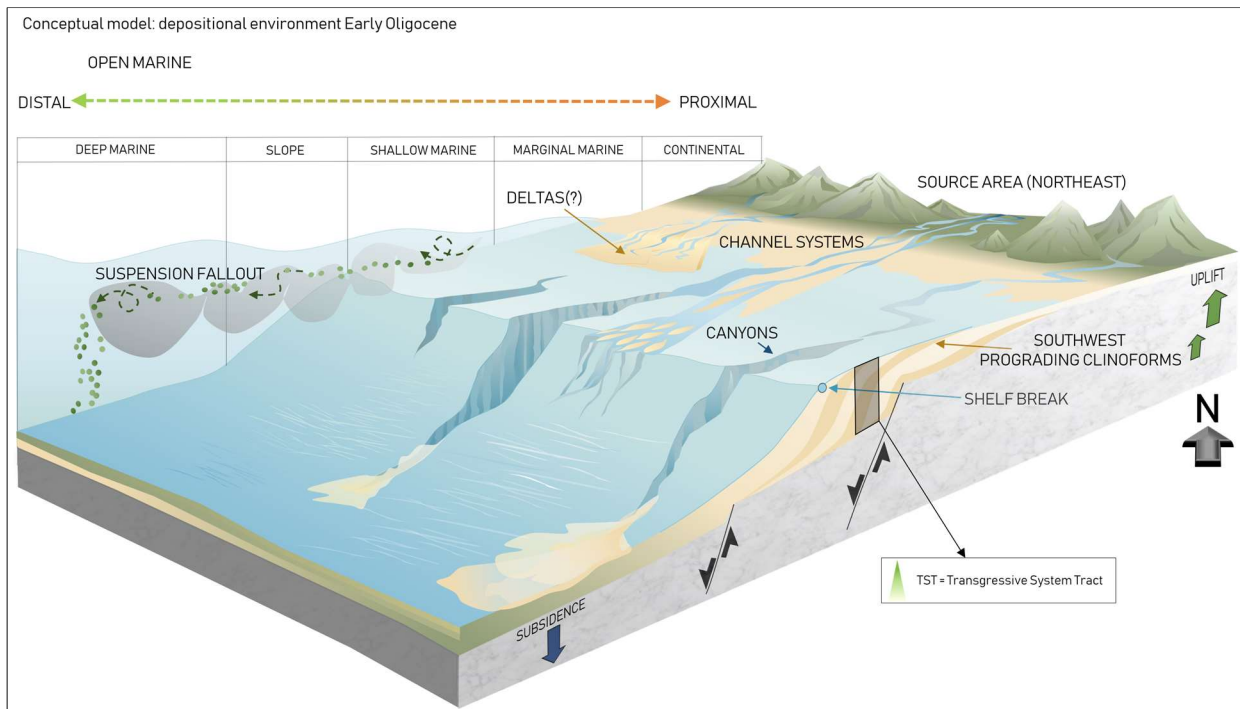


Figure 5.2.1. Conceptual model for the depositional environment during the Early Oligocene. Fine-grained deposits dominate on the shelf, and coarser-grained material was restricted to the marginal marine inner part of the system.

During the Early Eocene period, crustal separation began, resulting in inversion of the Mid-Norway margin at the Late Eocene-Early Oligocene transition (Gibbard & Lewin, 2014). The profound change in sedimentary pattern from the underlying Eocene to the overlying Oligocene units marks a change in the tectonic regime in the area. The sediments were mainly sourced from the northeast, as seen from the dip in the seismic, in contrast to the Eocene when sediments were principally derived from the west (Clausen et al., 2000). The southwestward tilting of the Oligocene sediments indicates progradation into the basin from areas to the north that were exposed to erosion. The erosion was a result of uplift and southward tilting of the Fennoscandian Platform, related to the break-up of the northeast Atlantic and mantle processes (Knott et al., 1993; Faleide et al., 2002; Knox et al., 2010; Gibbard & Lewin, 2014).

The transition from the Eocene-Oligocene is suggested to have occurred during a phase of transgression (Gibbard & Lewin 2014), where the waters were ventilated and gradually became deeper. Earth's climate experienced a critical turning point, switching from the greenhouse which prevailed during the Mesozoic era, towards a cooler icehouse condition in the Early Oligocene period. The change was a result of large-scale tectonics, oceanic and climatic processes. The southern North Sea therefore experienced major eustatic sea-level fluctuations as a result of both tectonics and also the growth and melting of icesheets, especially in the Antarctic region (Vandenberghe et al., 2003). Later on in the Early Oligocene, the prevailing climate was generally seasonally wet, hot and tropical (Gibbard & Lewin, 2014).

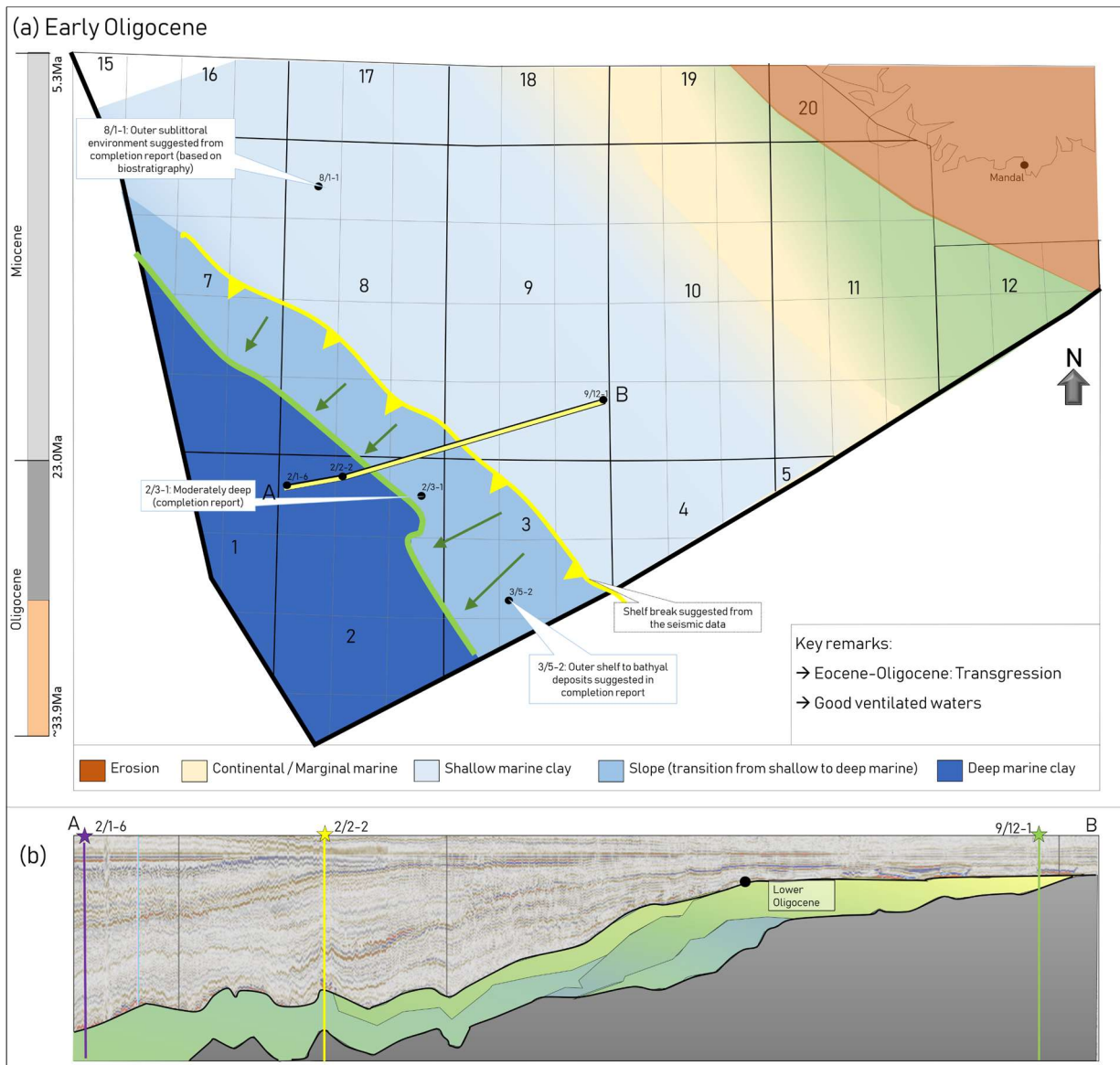


Figure 5.2.2. (a) Paleo-map of the Early Oligocene. Shelf-break and slope identified from seismic data. (b) Seismic geo-section (the same as presented in Figure 4.7.2., results) showing the unit's reflection configuration and correlation with wells.

Contemporaneously to the uplift of the Fennoscandian Platform, the deepest part of the Norwegian-Danish Basin and the Central Graben were subsiding. The creation of accommodation space through basin subsidence was out of phase relative to eustatic sea-level changes, and mainly controlled by regional-scale differential vertical movements. The fine-grained sediments were deposited continuously in a uniform depositional setting as described earlier. Uplift and exposure of landmasses from the hinterland (southernmost Norway) occurred concurrently with basin subsidence (Jarsve et al., 2014).

The lower parts of the Hordaland Group are consistent with the suggested fine-grained lithologies based on polygonal faults and the overall distal setting in the deeper (southwest) part of the basin. Observations from well 2/3-1, located close to the transition of the suggested slope-basin from the seismic data, suggest a moderately deep marine environment for the Early

Oligocene period. This corresponds to the suggested water depth based on the evaluation of clinoform heights in the area. Furthermore, the completion report from well 8/1-1 showed biostratigraphy indicating an outer sublittoral environment for the same period, where shallower marine strata were observed. The identified shelf break from cross-sections is located in between these wells, and to a certain extent correlates to the paleomaps presented by Gibbard & Lewin (2014). The study area was located in the north/northeastern part of the Norwegian-Danish Basin during the Early Oligocene, surrounded by the Fennoscandian Platform in the north, the Polish Platform to the east and the Shetland platform to the west (Figure 5.2.3; Vandenberghe et al., 2003).

Eidvin et al. (2013) implied that the Scandinavian platform has been an important sediment source for the Norwegian continental shelf since the Paleocene, including the southern North Sea. They divided the Scandes mountains into two major culminations, one in the central South Norway, and one in the northern Nordland, Troms and Sweden, further on referred to as the southern and northern Scandes domes. The southern Scandes Dome is likely to have been the most important source for the deposits examined within the study area.

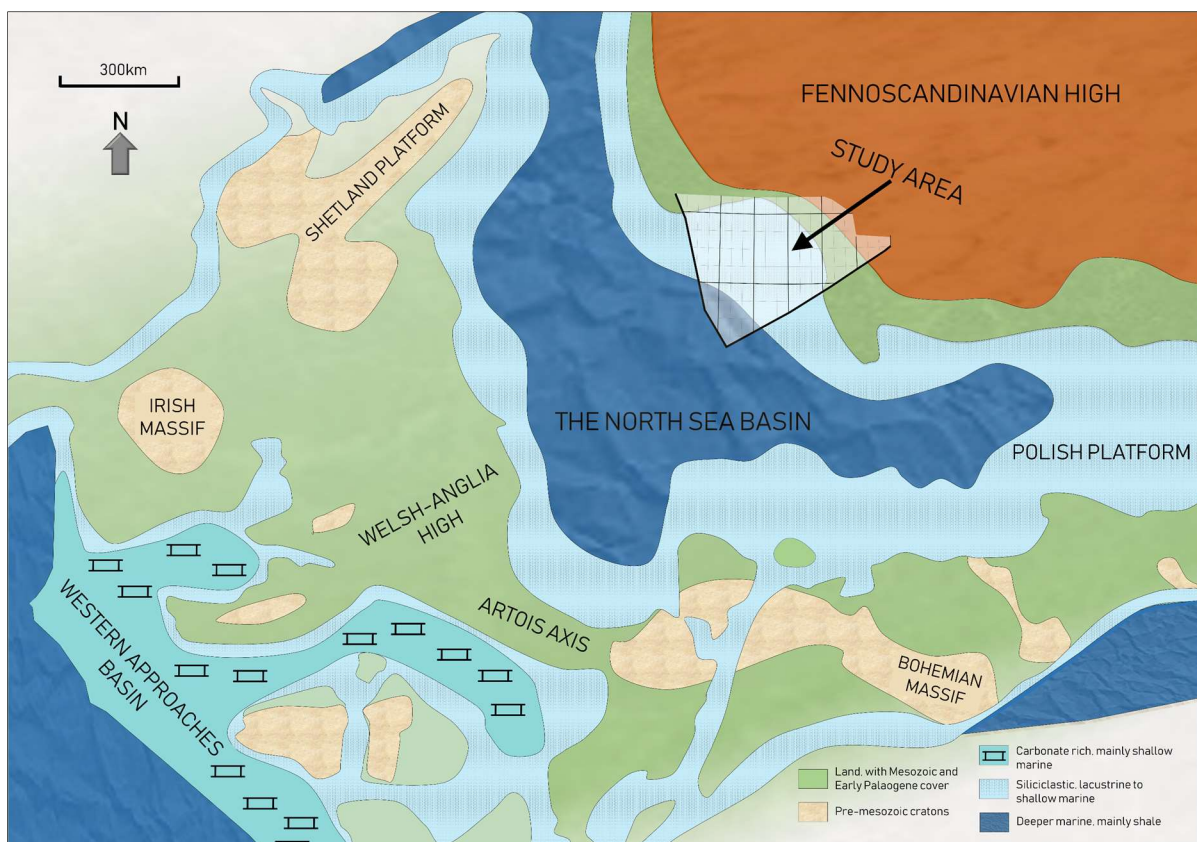


Figure 5.2.3. Regional paleo-map with the study area indicated, and the outline of the North Sea Basin during the Early Oligocene shown. Map correlated with Figure 5.2.1. and modified from Knott et al. (1993) & Vandenberghe et al. (2003).



## 5.2.2 Late Oligocene (Chattian) – S1/S2

The upper part of S1 and the S2 sequence have been ascribed to the Upper Oligocene Chattian period. This chronostratigraphic correlation is based primarily on the core observations, but also the overall geometries of the deposited units.

In general, the sequences can be internally subdivided into several units which are interpreted as sets of clinofolds prograding towards the southwest. The geometries vary between oblique and complex-oblique, with relatively steep foresets and short slopes. The identified progressively southwestward displaced shelf-breaks suggest a descending (falling) trajectory, which is common in regression sea-level cycles. Hence the lithological column may be represented by Falling Stage System Tracts (FSST) or Lowstand System Tracts (LST), and is thus grain size expected to coarsen upwards. A higher energy depositional regime is expected to have dominated further out on the shelf, and was no longer restricted to deltaic deposits in the most proximal parts, as was the case for the Early Oligocene depositional setting (Figure 5.2.4). The units mark a shift from a relative sea-level highstand, towards a progressive shallowing of the basin. The depth of the basin was estimated to be approximately 150-200m (Table 3.2.2 & Figure 4.9.1), which reflects the progressive shallowing of the basin.

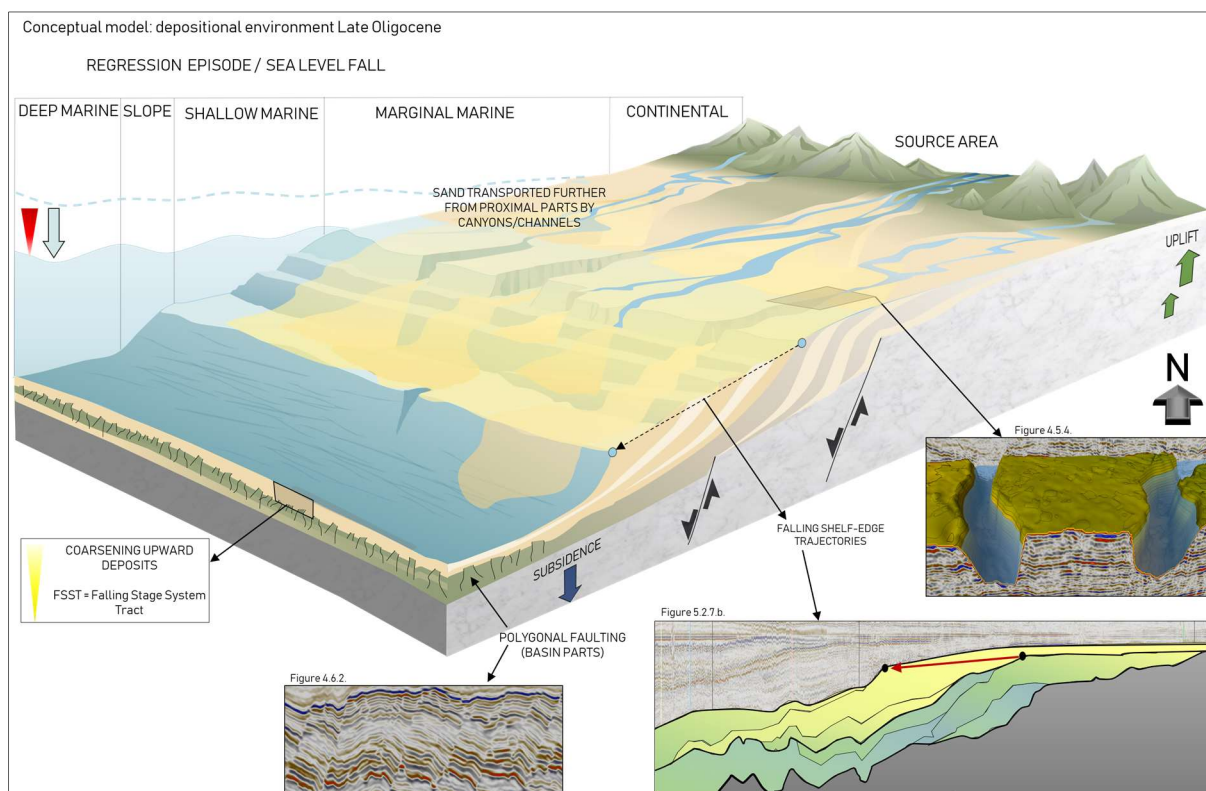


Figure 5.2.4. Conceptual depositional model for the Late Oligocene, where a fall in sea-level caused a progressive shallowing of the basin. Sand-material deposited further on to the shelf.

Several large depressions with steep sides, up to 100's meters in width, have been interpreted as canyons cutting through the underlying deposits. As shown in Figure 4.5.5 from the results, the base of the canyons as well as internal layers showed strong amplitudes, which may either be caused by gas saturation in the sediments, or from differential sand content compared to the surrounding shale-dominated lithologies (Haavik & Landrø, 2014).

The orientation of the prograding units, where the proximal parts are situated in the northeast and the distal parts towards the southwest, indicates a source of sediments located roughly further northeast of the observed units. Eidvin et al. (2013) also suggested sediment progradation from Scandinavia towards the south/southwest in the Late Oligocene (Figure 5.2.4).

#### ***5.2.2.1 Core interpretation***

The observation from core 2/2-2 provides the most intimate and thorough evaluation of the depositional environment during the Late Oligocene (Chattian). The observed asymmetrical ripples are attributed to fluvial deposits, forming at the base of channels (Figure 5.2.5). Climbing ripples were quite abundant in the sand-rich sediments of the core, suggesting a high input of sediments (Collinson et al., 2006). The soft sediment deformation flame – and load cast structures may have formed as a response to rapid deposition of sand. The sediment supply is thus suggested to have been high (Owen, 2003).

In addition to fluvial deposits, double mud drapes were present in between sand layers, along with bioturbation and wave ripples. The mud drapes are strong indicators of tidal influence (Collinson et al., 2006). The upper part of the core was a blue-grey calcite, which may have formed from colonies of molluscs. Shell fragments, such as nacre, occurred sporadically as well. All of these structures indicate a marginal marine depositional environment, with tidal and fluvial influence, possible in an foreshore (beach) or upper shoreface setting (Figure 5.2.5). These zones may fluctuate up and down, depending on the tide and overall sea-level. This supports the argument that shallower marine conditions dominated far out on the shelf, compared to the Early Oligocene period.

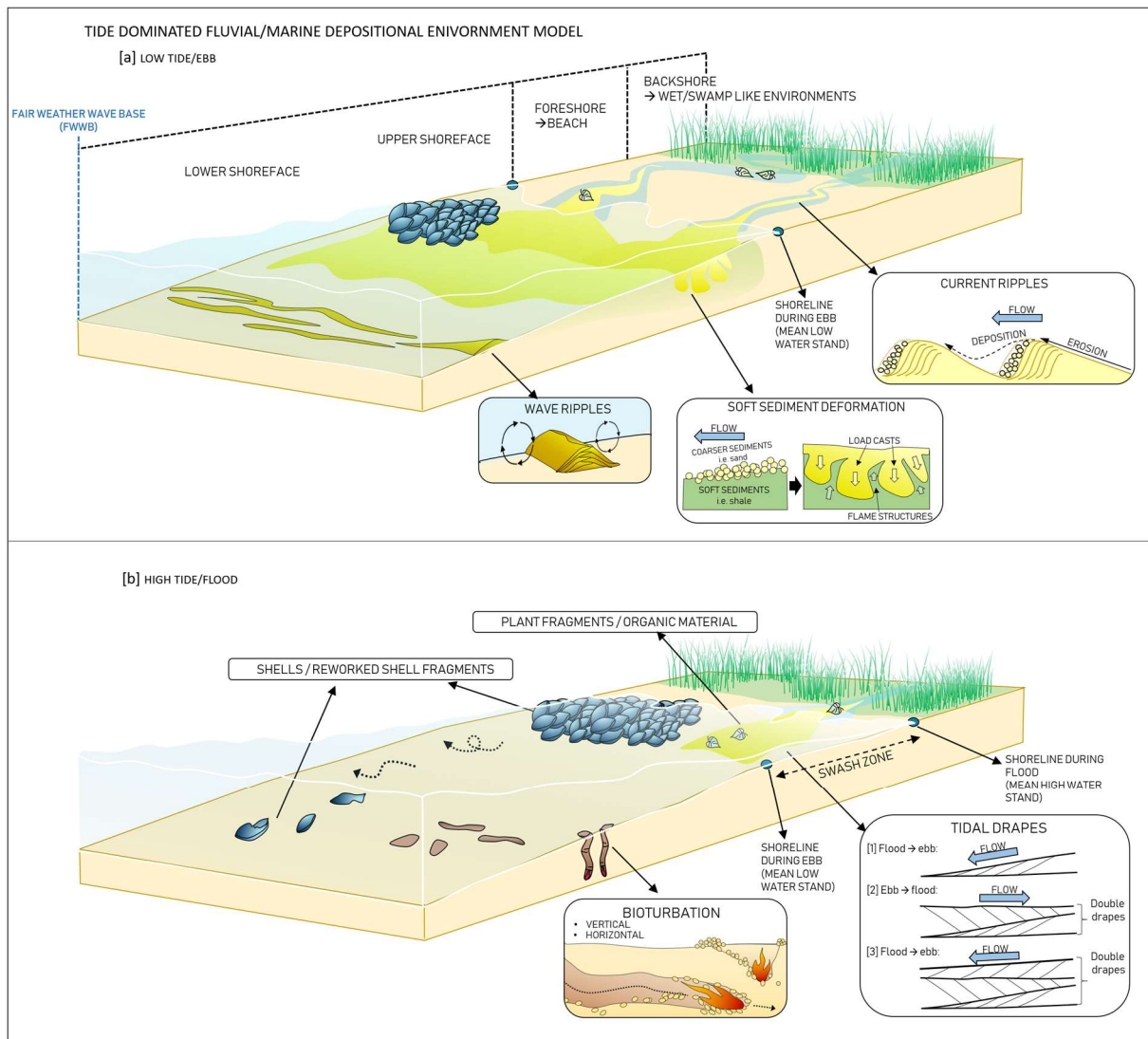


Figure 5.2.5. Conceptual model demonstrating the depositional environment dominating during deposition of the sediments identified in core 2/2-2, and the formation of the different structures observed, such as ripples, soft sediment deformation etc. (a) During low-stand water (ebb), and (b) during high-stand water (flood).

### 5.2.2.2 The Vade Formation

The sand unit recognized in the core is termed the Vade Formation, and was first recognized by Isaksen & Tonstad (1989). The seismic interpretation suggested deposition of coarser sand-rich sediments further onto the shelf, based on system tracts and trajectories (Figure 5.2.6.b), which corresponds to the suggested extent of shallow marine environment and deposition of coarser material from the logged core (Figure 5.2.6.a). The extent of the Vade Formation according to Isaksen & Tonstad (1989) has previously been restricted principally to Quadrant 2 on the Norwegian continental shelf (Figure 5.2.6.c). Nevertheless, the sand occurs in several well logs outside the original margins of the formation, within Quadrant 8, 4, 9, 10 and 11, as demonstrated in Figure 5.2.6.

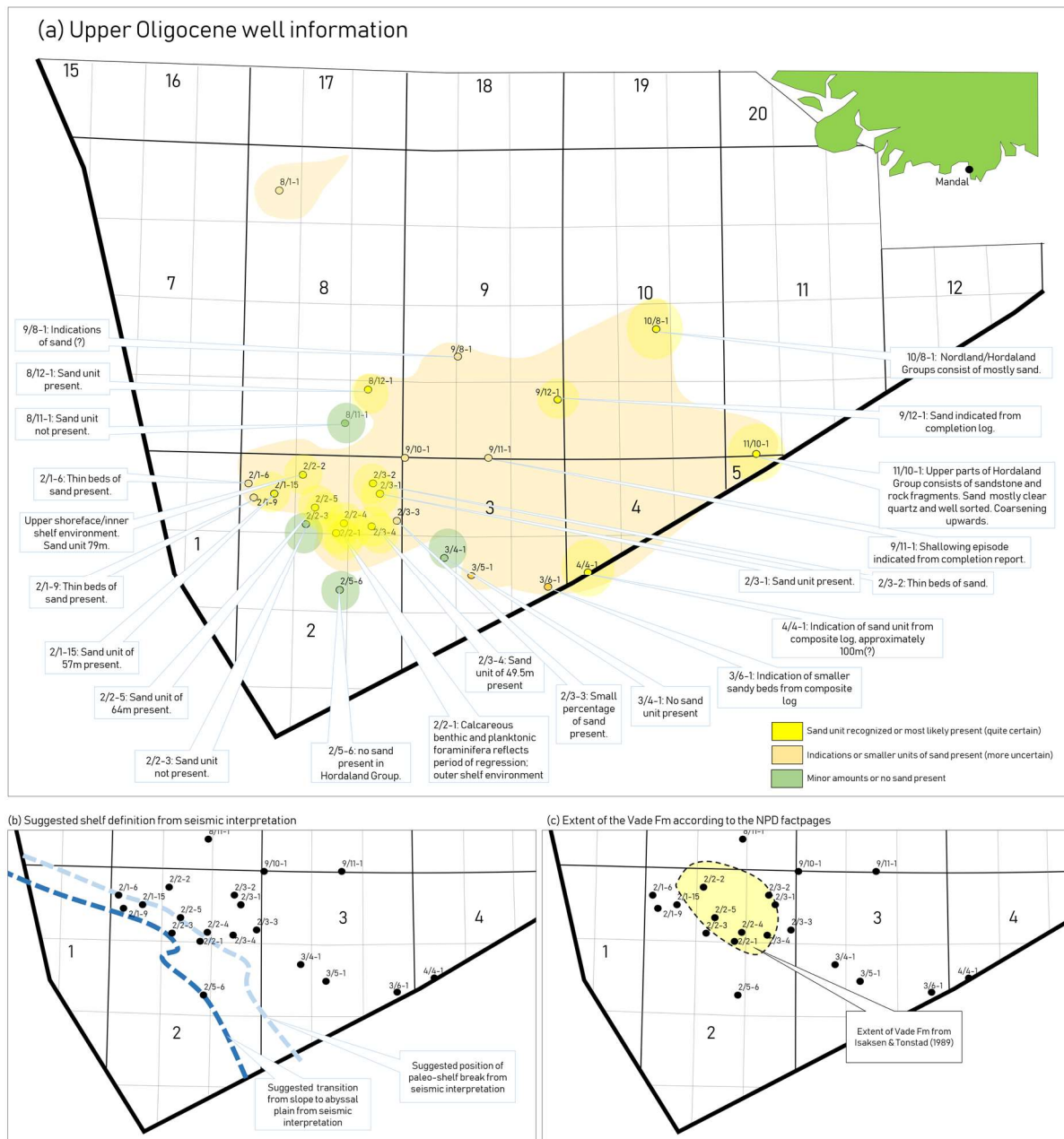


Figure 5.2.6. (a) Correlation of well information from the region, with regard to sand-content in the Upper Oligocene sediments, forming the basis of the new suggested extent of the Vade Formation. (b) Suggested position of shelf-slope-basin from seismic interpretation. (c) Extent of Vade Formation from Isaksen & Tonstad (1989).

By combining the suggested position of the shelf break from seismic data, with a sediment source located in the north/northeast, alongside well and core log information, a new expanded horizontal reach of the formation is suggested (Figure 5.2.7). The extent comprises hydrocarbon indicators around well 9/12-1 and 4/4-1, further discussed in section 5.3.

### 5.2.2.3 Correlation with regional geology

The suggested regression from the seismic data and core log can be attributed to a relative fall in sea level, occurring contemporaneously with a continued uplift of the Fennoscandian Platform, which caused further exposure and erosion of the previously deposited Oligocene

sediments (Eidvin et al., 2013). The regression was superimposed on a longer stage of transgression, where the basin in general became deeper. The suggested fall in sea-level, based on the seismic interpretation, could be related to a cold climate that prevailed early in the Late Oligocene. The Antarctic continental ice sheet began a build-up phase in the Early Oligocene, which persisted until Late Oligocene (27Ma to 26Ma) (Eidvin et al., 2013). During periods of low-stand sea-level, extension of river systems across the previously submerged marginal areas may occur (Gibbard & Lewin, 2014) as identified in the seismic data. The orientation of the observed canyon and river systems in the area affirms the suggested northeast-southwest progradation of sediments (Figure 5.2.4).

The completion report for well 2/2-1 interpreted the Vade Formation to represent outer shelf environment for the deposition of the formation, based on the presence of calcareous benthic and planktonic foraminifera. Eidvin et al. (2013) suggested that the unit was deposited in a deep-marine setting beyond the deltaic slope, and that in well 2/2-2, the sand is present but not dominating, and probably deposited by gravity flows. The observed sedimentary structures from core 2/2-2 logged in this study are well preserved, which is not expected if the sand was deposited by gravity flows. Gravity flows often occur at low-gradient slopes where the slope gradients are maximum 2°, and usually 1° (Canals et al., 2004). The slope observed in the seismic is relatively short and steep, which in general does not favour gravity flow environments.

The basin parts however may have continued to subside independently of the shallowing episode, similar to the tectonic setting suggested for the Early Oligocene. Fine grained material is suggested to have been deposited in the deepest part of the basin, endorsing the post depositional polygonal faulting, similar to the Lower Oligocene sediments. Well-logs showing the lithostratigraphy of the Upper Oligocene interval display the discussed Vade Formation, otherwise surrounded by claystone and thin strings of limestone and dolomite. Dolomite forms in warm, shallow marine environments and therefore provides additional support of a shallow marine environment prevailing during the Oligocene (Collinson et al., 2006).

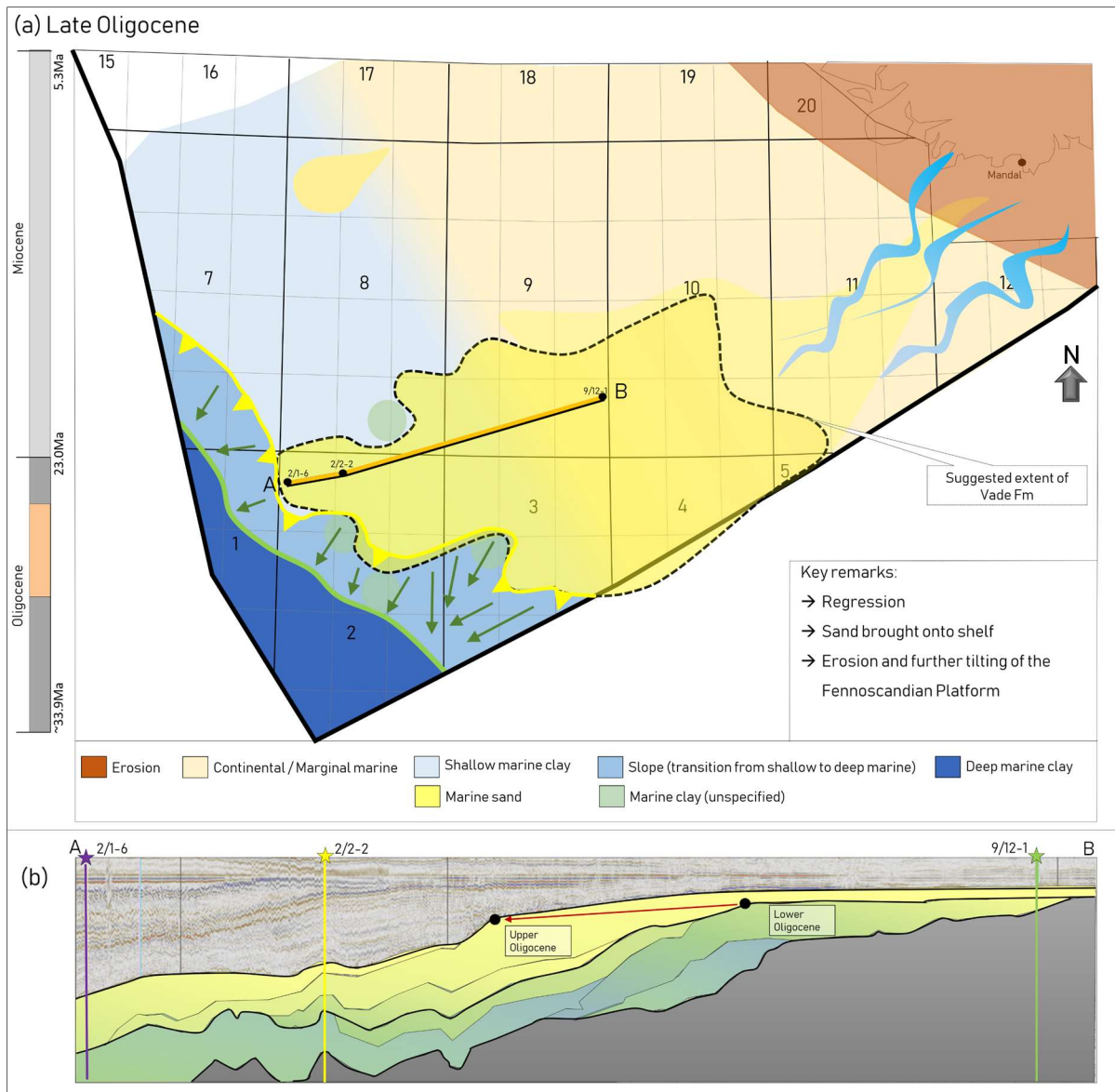


Figure 5.2.7. (a) The paleo-environment for the Late Oligocene shallow-water period. The suggested extent of Vade Formation indicated, along with shelf-break positioned based on seismic interpretation combined with well-data and biostratigraphy.

### 5.2.3 *Late Oligocene (Late Chattian) - Middle Miocene (Serravalian)*

The S3 sequence is bounded by the underlying T2 sequence boundary, and the overlying Mid-Miocene Unconformity (MMU). The sequence overlies the regressive, sand-rich sediments deposited in early Chattian times, and is attributed to the latest part of the Oligocene period, and the Early – Middle Miocene.

The unit shows less well-defined clinoform progradation structures compared to the underlying units, with more lateral continuous reflection configurations. The overall external geometries, however, are more similar to sigmoidal prograding clinoforms. These are mainly low-angle, with flat trajectories for the lower part of S3 and rising trajectories in the upper part. Some internal reflectors are arranged in divergent patterns, which may indicate deposition during a progressive tilting of the depositional surface (Figure 4.6.3; Mitchum et al., 1977; Veeken, 2007). Furthermore, the basin part is dominated by polygonal faults towards the southwest, indicating fine-grained lithologies as interpreted in the previous sequences.

During the latest Oligocene and Early-Middle Miocene, the whole area progressively deepened, and a transgression drowned the exposed shelf from early Late Oligocene times (S2). The shoreline progressively moved towards the proximal, northeastern parts of the shelf, where the previously channel and canyons were buried by fine-grained deposits (Figure 5.2.8). Deltaic deposits are thus expected to have been restricted to the inner parts of the shelf, close to the source area, where the energy regime is still relatively high (Figure 5.2.9). The majority of the shelf was dominated by a low-energy regime, where fine-grained deposits were transported through suspension or slow infill from the prograding sigmoidal clinoforms (Figure 5.2.9). The expected fine-grained, deep-water deposits are confirmed by several well logs, such as 2/1-6, 2/2-2, 9/12-1 (Figure 4.6.6) and 2/1-15, where high gamma ray values surround the identified Vade Formation (Sequence 2; low gamma ray interval). A thinner low gamma ray interval also occurs in the shallower part of well 2/2-2, at a vertical level corresponding to the MMU. The rising shelf-edge trajectories observed in the seismic data indicate a rising sea-level, where accommodation space was thus created (Figure 5.2.8.b). The water depth was estimated from an average clinoform height ranging between 280-339ms (TWT), and is suggested to have been as deep as 300-350m (Table 3.2.2 & Figure 4.9.1). This interpretation corresponds well to Jarsve et al. (2014) who suggested a water depth of 300m in the Late Oligocene (Chattian) period.

The climatic conditions shifted towards a warmer environment which, in combination with glacial melt, can be related to the increasing sea level trend observed in this period as indicated by the rising shelf-edge trajectories. The warmer climate might correlate with the global Late Oligocene Warming Event (LOWE) discussed by Simaey (2004). Contemporaneously to the transgression, the Fennoscandian Platform was exposed to further tilting, which is recorded by the observed divergent reflection configurations (Figure 5.2.8).

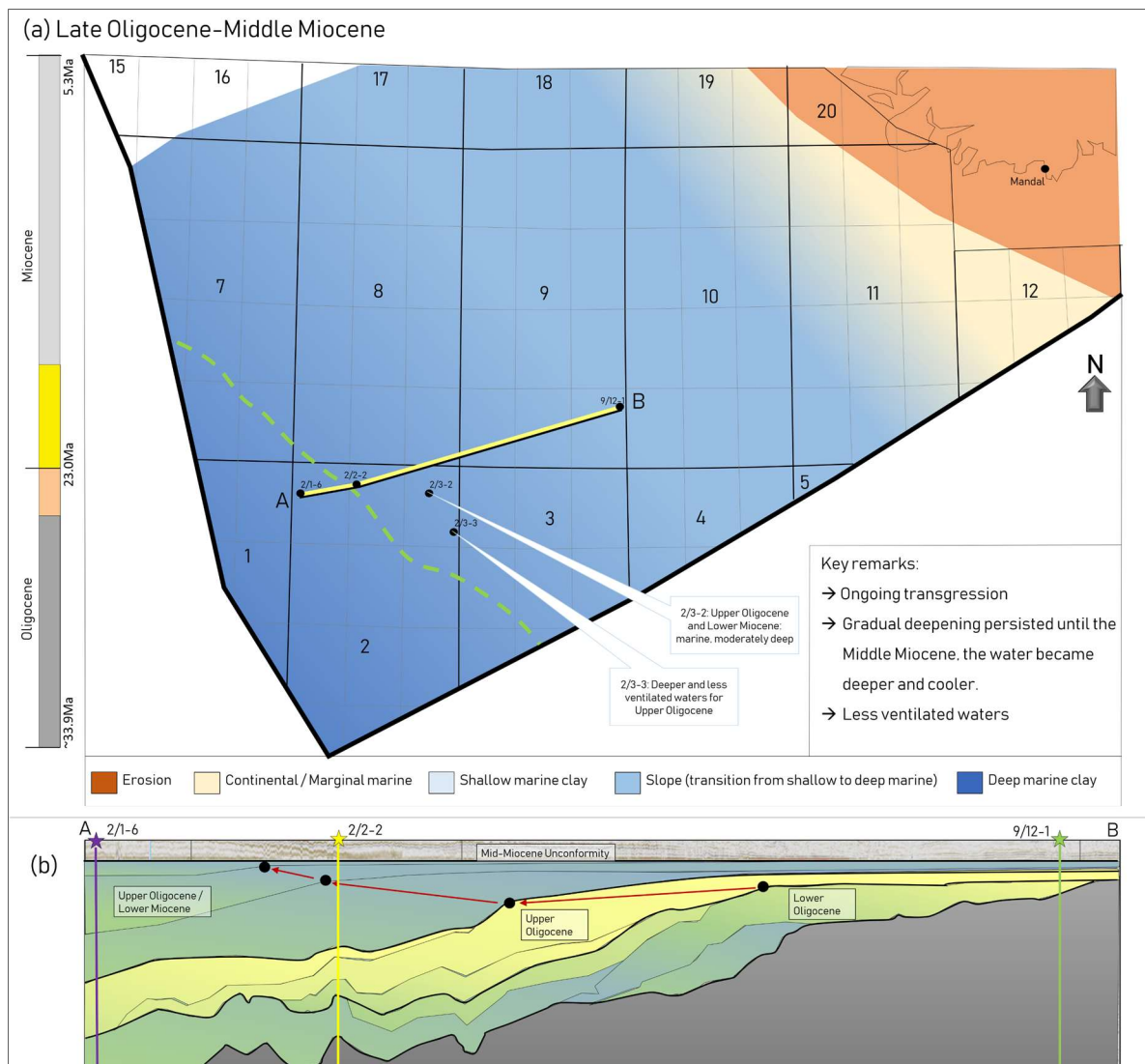


Figure 5.2.8. a) The paleo-environment for the Late Oligocene-Middle Miocene period. Continued subsidence and a relative increase in sea-level caused a progressive deepening of the Norwegian-Danish Basin, with water depths ranging between 300 – 350 meters (suggested from clinoform heights). (b) Geoseismic cross-section showing the shelf-edge trajectories, and the relative content of clay (green/blue) vs. sand (yellow) – rich sediments.

The Mid-Miocene Unconformity (MMU) was correlated through several wells (Appendix 9.5), and mapped regionally through the study area. Line ups of truncations of the underlying sediments occur most frequently in the shallower parts of the basin at this level, however the surface was tracked partly along a peak in the deeper parts of the basin. This may indicate that erosion was most efficient in the shallower parts which is likely to have been most exposed,



whereas the basin remained relatively protected and unaltered during the erosional episode (Figure 5.2.10).

Deltas restricted to the inner parts of the shelf that developed during sea-level highstands (Highstand System Tracts=HST, Figure 5.2.9), are not observed in the seismic data. However it is assumed that they have formed as HST progradational deposits when sediment accumulation rates exceeded the rate of increasing accommodation space during the late stages of transgression (Coe et al., 2002). The deltaic deposits are suggested to have been exposed to erosion and reworking during a more brief shallowing episode resulting in the MMU. The sand-rich deposits are likely to have been transported further out on the shelf, towards the southwest (Figure 5.2.10). The shorter interval of observed low gamma ray values at MMU level from well 2/2-2 may be attributed to sand-rich sediments deposited during the erosional event observed in the strata as the MMU.

The Early Miocene is suggested to have been accompanied by inversion resulting in widespread deltaic progradation from central Sweden and southern Norway, where large parts of the Norwegian-Danish Basin became terrestrial in the Early Miocene (Eidvin et al., 2013). Eidvin et al. (2013) described a delta system sourced from the southern Scandes in Norway and central Sweden, towards the Norwegian-Danish Basin. The same authors suggested that the deposition of the delta may have been the result of continued inversion of the basin and corresponding uplift of the hinterland source area.

Along with the MMU, several channel systems are recognized in the seismic data. Channels in the upper part of Quadrant 9 (Figure 4.7.3) are orientated in a northeast-southwest manner, where the source is located towards the northeast (up-dip). These channels overlap one another on several vertical levels, occurring in the uppermost part of S3, S4 and S5. The vertically stacked, isolated, channels are consistent with the development of a braided river system through time (Figure 4.7.3). In the northwestern corner of Quadrant 4 (Figure 4.6.4), similar braided river systems and also meandering channels are observed. The channel systems are suggested to have formed as a response to falling sea level coupled with a continued uplift of the Southern Scandes Dome. The shelf was exposed to erosion and channels progressed further out onto the shelf (Figure 5.2.10). These channels are suggested to have contributed to the transport of coarser-grained sediments from the previously discussed Miocene delta (Eidvin et al., 2013) of the Norwegian-Danish Basin towards the deeper parts of the basin, where thin strings of sand are recognized at MMU-level in the gamma ray log from well 2/2-2.

The MMU suggests a rotation of the inner shelf, which may coincide with the tectonic uplift of the Fennoscandian Platform, and especially the South Scandes Dome, located in southern Norway (Eidvin et al., 2013). The uplift of the Fennoscandian Platform culminated at the Early to Middle Miocene transition, and the deposition of the Skade Formation northwest of the study area was caused by a large fall in relative sea level (Eidvin et al., 2013). The massive erosion resulting in the MMU is thus suggested to have occurred as a result of a relative sea level fall, where Highstand System Tracts (HST, deltaic deposits) were subject to erosion and redeposition further onto the shelf (Figure 5.2.10).

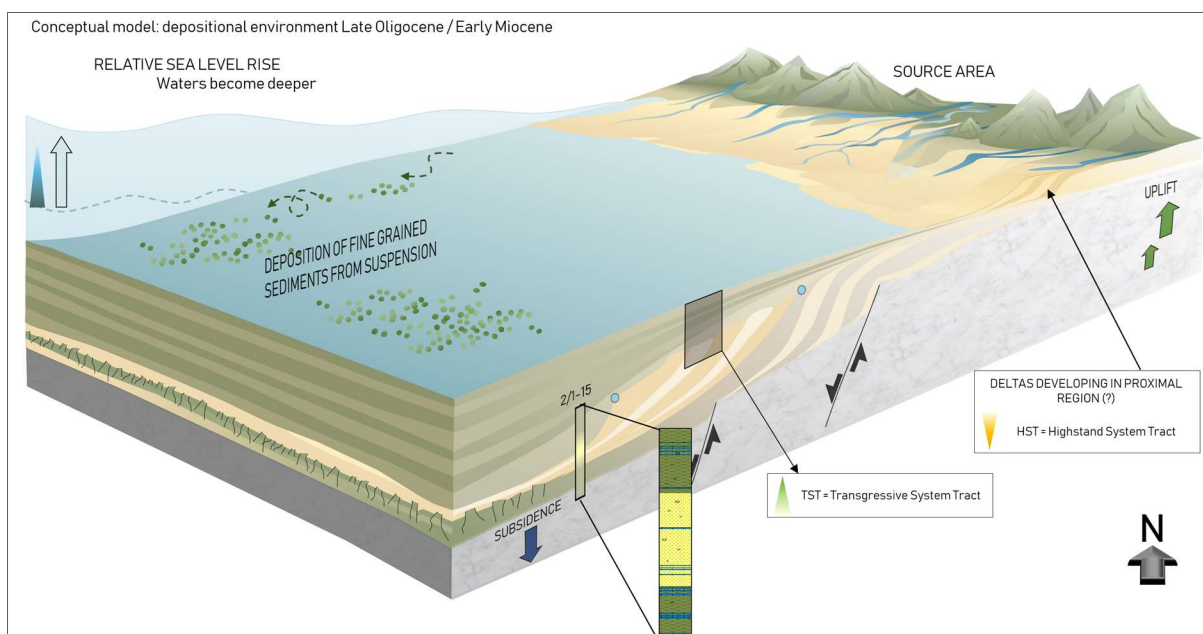


Figure 5.2.9. Conceptual model for the depositional environment persisting during the Late Oligocene – Early Miocene. The sandy sediments of the Vade Formation was successively buried by fine-grained material, as indicated from well logs. Lithology log from well 2/1-15 indicated, where Transgressive System Tracts are observed. The shoreline retreated northeastwards, restricting deltas and deposition of coarse-grained material to the inner parts of the shelf.

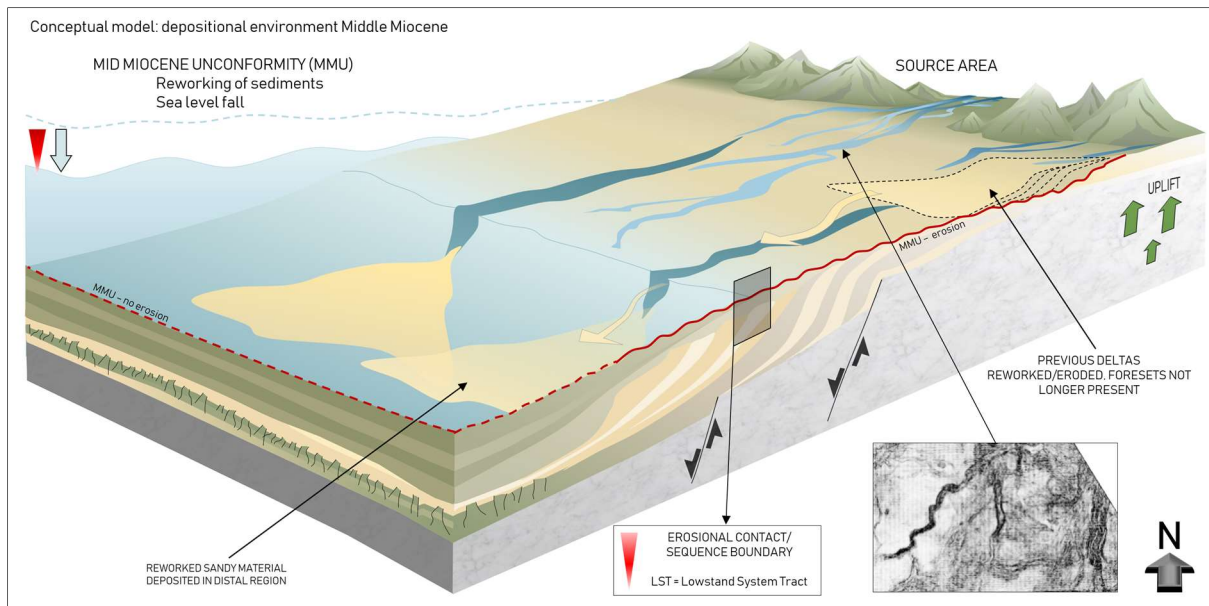


Figure 5.2.10. Conceptual model of the depositional environment suggested from the Mid-Miocene Unconformity (MMU). Sediments deposited during Highstand System Tracts (HST) were reworked and thus no longer visible in the proximal parts of the shelf. River and canyon systems developed across the shelf. The MMU is considered a regional unconformity, however not observed in the deepest basin parts in the seismic data.

#### 5.2.4 *Late Miocene (Tortonian/Messinian)*

The S4 and S5 sequences overlying the MMU downlap onto the sequence boundary partly towards the basin (southwest). The upper boundary of the S4 shows a high amplitude which is suggested to represent a flooding surface, from a shorter period of rising sea level which drowned the exposed and eroded Mid-Miocene shelf.

S5 shows an overall external geometry similar to sigmoidal clinoforms. The foresets are very gently dipping towards southwest, where a depocenter is suggested to have been in place (Figure 5.2.11). The location of the depocenter is also consistent with increasing thickness of the unit towards southwest. The deepest parts of the basin, located approximately above the Cretaceous Central Graben, provided greater accommodation space and thus the thickest part of the unit was deposited here. A possible shelf-break is suggested towards the southwest, orientated northwest-southeast, however the expected change in dip along reflectors, where a break-of-slope could be placed, is not as clear as for the S1-S3 sequences. There is therefore more uncertainty related to the exact suggested position of the shelf-break. Nevertheless, a slightly rising shelf-break trajectory is suggested for the sequence, which is common in transgressive episodes.

The internal reflectors of the sequence show good lateral continuity, which indicates that the sediments were deposited in uniform depositional conditions (Veeken, 2007). Fine-grained sediments are suggested to have been deposited in an open marine system through the slow infill of a subsiding basin towards the southwest. The basin progressively became shallower, as the Upper Miocene sediments were deposited and filled up the basin. The estimated water depth at the onset of the Late Miocene have been calculated to 250m (Table 3.2.2 & Figure 4.9.1), and decreasing rapidly with the ongoing sedimentation.

As the basin became shallower, channel systems are suggested to have developed in the proximal parts of the shelf. These systems are observed in the northern part of Quadrant 9, in the same area for those described at the Mid-Miocene Unconformity. The channels at the MMU level were roughly orientated northeast-southwest, however in the upper parts of S5, the channels are orientated in a more directly north-south manner. Elongated channels in the northwestern corner of Quadrant 4 are similarly orientated north-south for the upper parts of S5. The channels cut through the underlying S4 sequence, and are therefore observed in variance extractions at this level. The progressive shallowing and channel system development in the proximal parts of S5 are not suggested to have formed primarily as a response to falling

sea level, which was the case for the channel systems at the MMU level. They are instead attributed to a shallowing of the basin caused by a progressive infill and increased sediment supply (Figure 5.2.11).

Eidvin et al. (2013) correspondingly suggested that the open marine system was shallower than previous periods during the Cenozoic. The Fennoscandian Platform was still a positive relief feature in the region, and uplift continued. The orientation of the gently-dipping, sigmoidal prograding clinoforms along with the north-south orientation of channels, suggest that deposition was sourced primarily from the north. The synclinal geometry indicates that subsidence continued in the deeper parts of the basin. The sigmoidal shape of the clinoforms are common where fine-grained sediments dominate the shelf. Eidvin et al. (2013) suggested fine grained deposition towards the basin through the drainage system on the shelf established in the Oligocene and Early Miocene. This drainage system is represented by the previously established and described channels (Figure 5.2.12.c; Figure 4.6.4 & Figure 4.7.3).

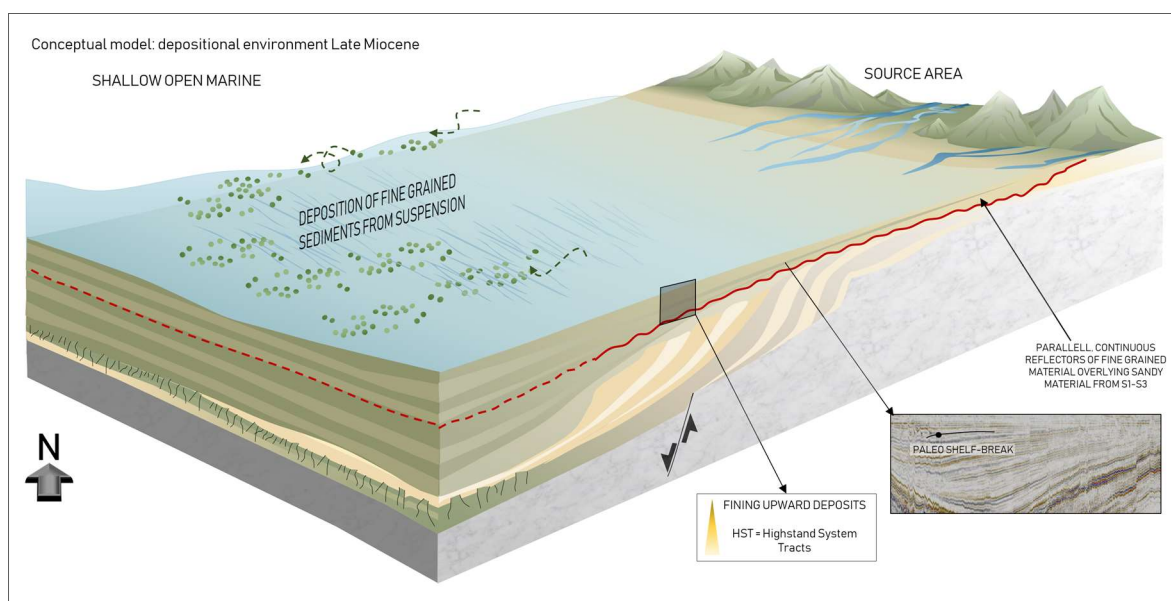


Figure 5.2.11. Conceptual model for the depositional environment persisting during the Late Miocene. Fine-grained sediments were deposited into the subsiding basin in the southwest through suspension and progressive development of gently-dipping sigmoidal clinoforms.

A common feature of the well logs in the area is fine-grained, clay-rich material. Well 2/2-1 suggested olive gray clay deposited in an inner shelf environment, which indicates that shallow marine conditions stretched far out on the shelf. The completion report for well 2/3-2 suggested a shallow marine depositional environment with open sea connections for the Late Miocene period. Well 2/3-1 completion report suggested even lagoonal environments based on the biostratigraphy, however little indications of barrier island etc. have been observed in the seismic data. Information about the depositional environment from well logs, coupled with a

suggested gently-dipping slope situated in the distal parts of the shelf, places a modest shelf-break orientated roughly northwest-southeast, in the southeastern-most part of the study area (Figure 5.2.12).

The recognized flooding surface (S4) is correlated to a warmer climate dominating the Mid-Late Miocene. The climatic optimum occurred during the Mid-Miocene (~17Ma to 14Ma) inducing a eustatic sea-level rise (Zachos, 2001), which drowned the exposed shelf. The transgression in the area appears to have been enhanced by the continued subsidence in the southern part of the basin, coupled with increased tilting of the Fennoscandian Platform (Eidvin et al., 2013; Gibbard & Lewin, 2014). The uplift of the Fennoscandian Platform accelerated in the late Mid-Miocene, and sediment supply to the southeastern embayment of the North Sea increased through the input from Baltic River located in the northwest. The sediments, though, did not reach the southern North Sea until the Late Miocene (Knox et al., 2010). The tectonic regime causing the uplift of the Fennoscandian Platform, north of the study area, which began earlier in the Oligocene, culminated during the early Late Miocene. Cloetingh et al. (2005) suggested that the uplift possibly was driven by mantle processes and the opening of the Northeast Atlantic Ocean.

Rasmussen (2005) suggested that the shoreline prograded as far as the Central Graben at the end of the Late Miocene. The suggested location of the shelf-break is correlated with Gibbard & Lewin (2014), who indicated that shallow marine waters dominated larger parts of the southern North Sea (Figure 5.2.12). A distinct tilting of the Norwegian-Danish Basin commenced in the Late Neogene, and was succeeded by marked erosion of the marginal areas of the Norwegian-Danish Basin (Eidvin et al., 2013). This erosion is corroborated by the observed channel systems. The Late Miocene was characterized by a cooling of the warmer climate that had persisted earlier in the Late Miocene, at the onset of major Northern Hemisphere glaciations which occurred around approximately 2.6Ma (Eidvin et al., 2013).

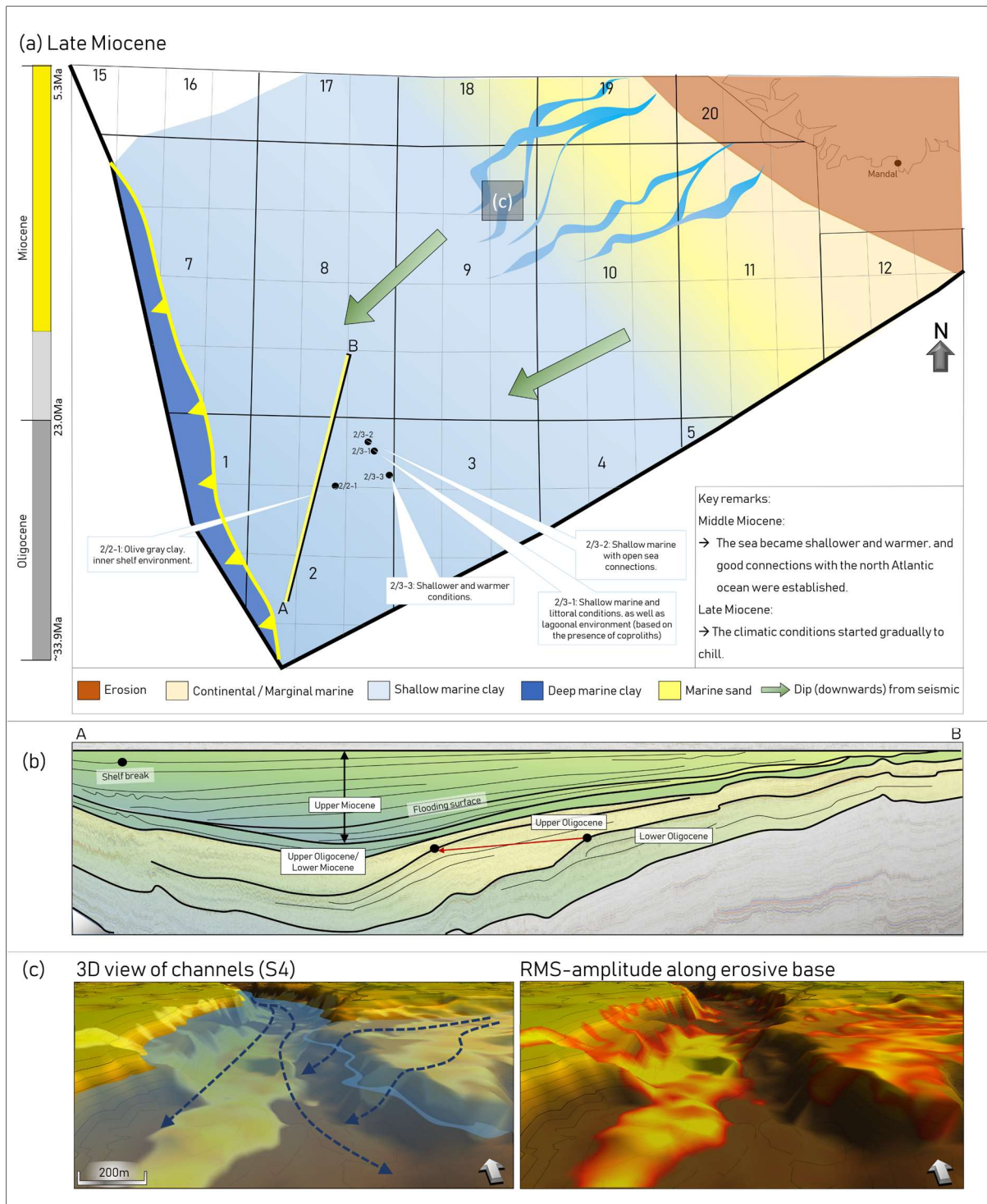


Figure 5.2.12. (a) The paleo-environment for the Late Miocene period. Shallow marine conditions dominated on the shelf, with a shelf-break positioned towards the southwest. Shelf-break is placed based on the seismic interpretation, well-logs, and Gibbart & Lewin (2014). (b) Geoseismic cross-section showing the fine-grained sediments deposited into the subsiding basin. The T4 flooding surface indicated. (c) 3D view of channels from the northern part of Quadrant 9.

### 5.3 Petroleum system indicators

The clearest hydrocarbon indicators observed in the seismic data are discussed for each zone, with emphasis to potential migration pathways in the subsurface. The seismic data have been used to interpret and suggest migration models related to the respective amplitude anomalies, and additionally the trap type and horizontal extent. Some of the named amplitude anomalies, a1-a8, are further discussed with regards to the potential hydrocarbon content filling the traps (origin, gas vs. oil, leakage). Alongside the seismic data, wells are used to better understand the petroleum system. Table 5.3.1 is presented as a summary of the hydrocarbon shows in the Oligocene strata noted in the wells, along with the recognized Vade Formation and mapped amplitude anomalies. Well 2/3-1, 4/4-1 and 9/12-1 are all located adjacent and down-flank of the identified bright spot.

Table 5.3.1. Overview of the emphasized hydrocarbon indicators from seismic data and well logs.

Well	Seismic amplitude anomaly	Sand unit present (Vade Fm)	Hydrocarbon shows (from wells)	Position of well
2/2-1		Yes (71m)	Gas	
2/2-2		Yes (79m)	Gas	
2/2-4		Yes (98m)	Dual gas discoveries	
2/3-1	Løven discovery (several levels of amplitude anomalies)	Yes	Dual gas discoveries	Down-flank
4/4-1	a8	Yes (suggested in this study)	Unknown/no well report published	Down-flank
9/12-1	a1-a6	Yes (indicated from well log)	No	Down-flank

#### 5.3.1 Subsurface drainage system

##### 5.3.1.1 Zone 1 – vertically, structurally controlled migration

The bright spots recognized within Zone 1, situated vertically above the Central Graben, occur above seismic wipe-out zones where reflection amplitudes are generally weakened. The wipe-out zones may represent migration pathways of hydrocarbons, however they may also occur as a result of noise from the overlying bright spots which attenuate a significant portion of the seismic energy (Figure 4.9.1). It is possible that these zones do indeed represent migration pathways, as the Jurassic source rock is situated vertically below. The extent of the Jurassic



source rock is adapted from Cornford (1994), and is shown in relation to the discussed hydrocarbon indicators towards the end of the chapter (Figure 5.3.7). The Oligocene sediments in this area consist mainly of fine-grained sediments laid down in a distal depositional setting, which are polygonally faulted. The polygonal faults, along with some deeper seated Mesozoic faults, are suggested to feed the overlying layers with hydrocarbons migrating upwards according to density and following pressure differences in the subsurface (Figure 5.3.1). Towards the uppermost parts of the Miocene, the lateral distribution of bright spots towards the north indicates a shift from vertical to lateral migration, following sub-horizontal pathways within permeable layers.

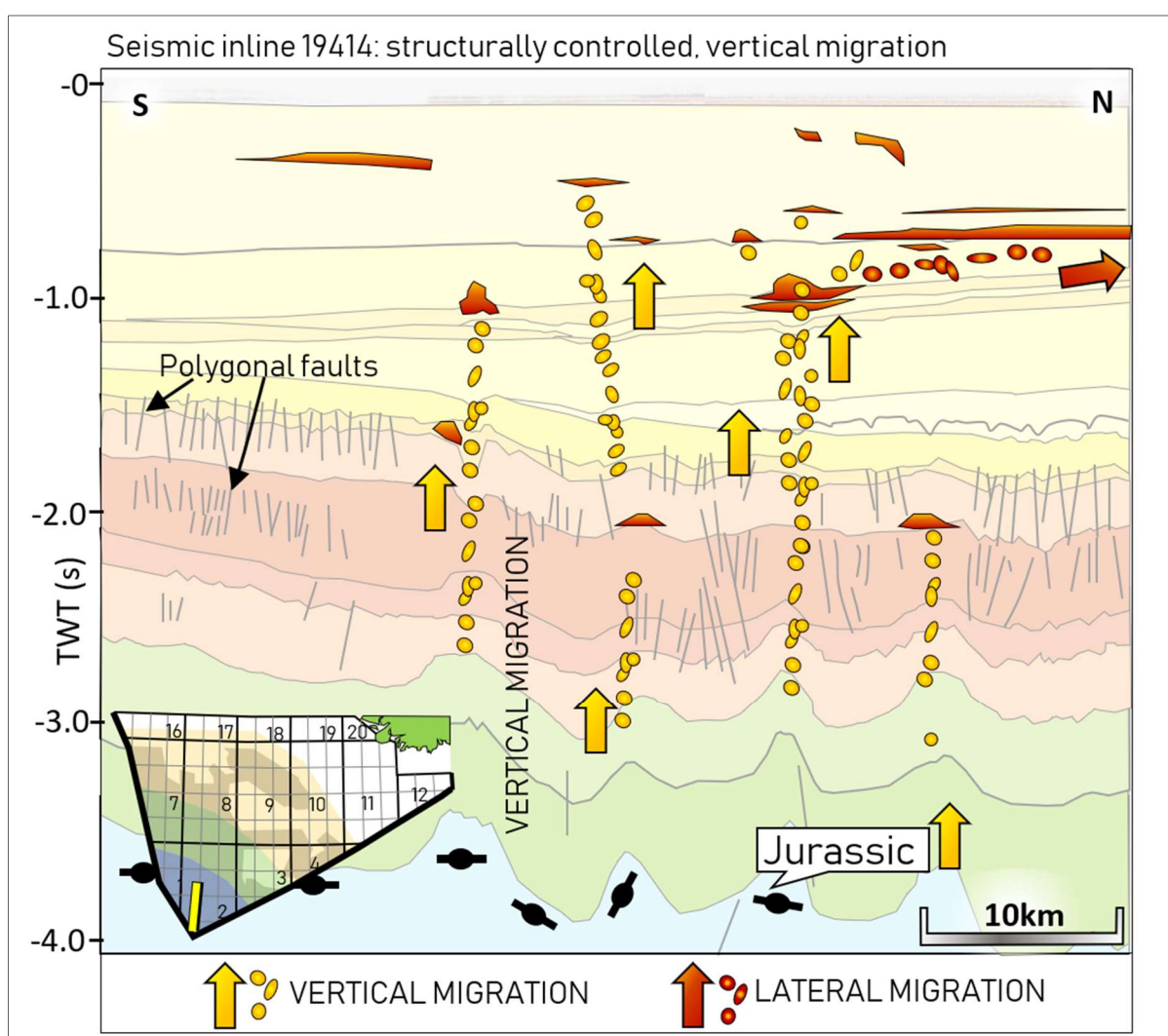


Figure 5.3.1. Bright spots and migration patterns within Zone 1, above the Jurassic Central Graben. Polygonal faulted Oligocene units allowing the upwards migration of hydrocarbons. Some indications of lateral migration in the uppermost Miocene.

### 5.3.1.2 Zone 2 – Well 2/3-1, The Løven discovery

The bright spots observed in the vicinity of well 2/3-1 (the Løven discovery) occur at several vertical levels along an interpreted salt-initiated normal fault. The amplitude anomalies were not

named, but rather included to describe the migration pattern in the area. The horizontal extent of the Level 1 bright spots in this area is greater than the extent of the bright spots at Level 2, and reaches beyond the normal fault. The possible hydrocarbons indicated by these amplitude anomalies are suggested to be contained in a stratigraphic trap, and were in place before the normal faulting episode occurred at an early stage of salt development (Figure 5.3.2a).

The Level 2 bright spots are bound by a normal fault towards the northeast, and pinches out southwestwards, and a combination trap is suggested. The bright spots are vertically limited to the shallowest extents of the fault, and are suggested to be structurally controlled by salt movement and a salt-related normal fault in this area. Normal faulting, induced by the salt movement below, interrupts the Level 1 amplitudes, and forms both a trapping feature, as well as a vertical migration pathway. The migration pattern changed from being primarily lateral at the early stage salt-development, to vertically dominated at a later stage of halokinesis. Hence, both stratigraphic and structural elements controls the migration in this area.

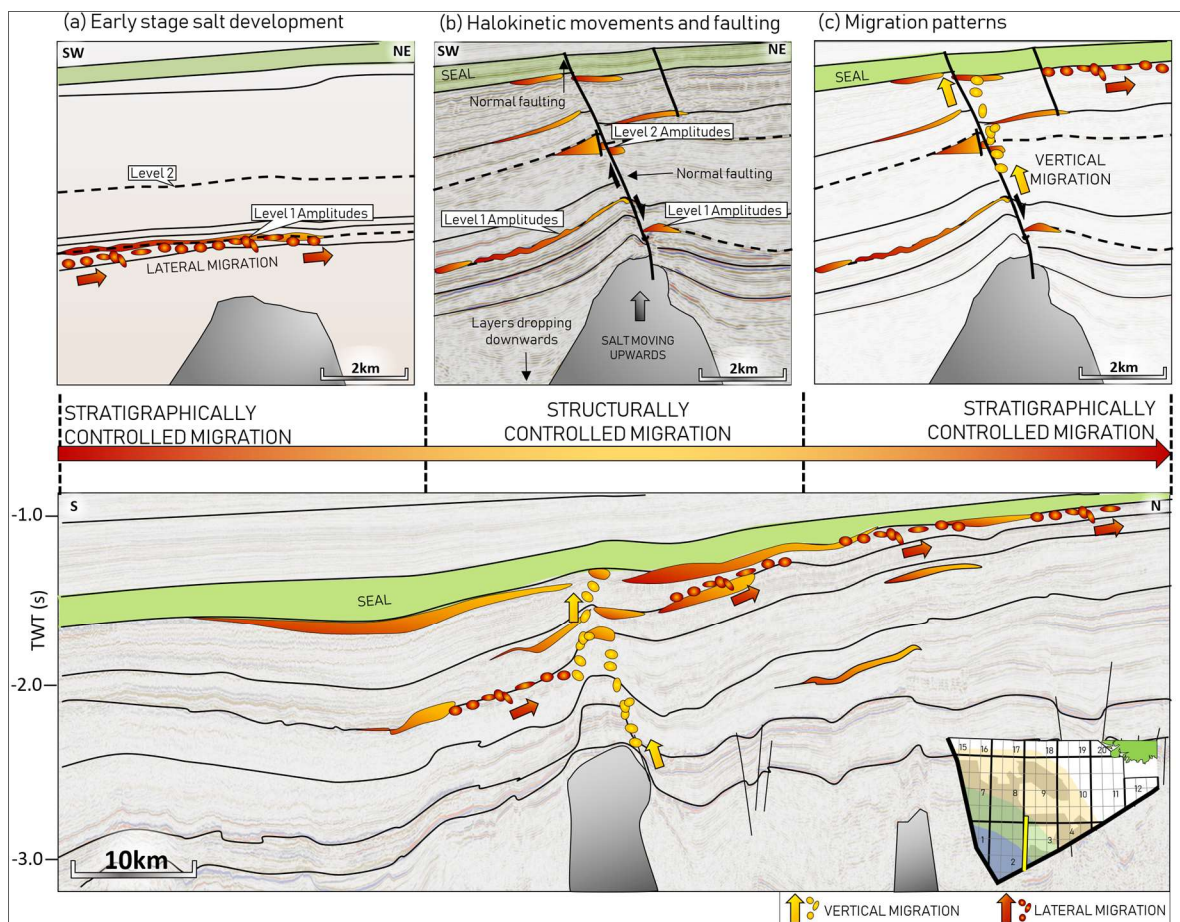


Figure 5.3.2. (a) Early stage salt development where lateral migration, up-dip, along stratigraphic interfaces dominate. The hydrocarbons were stored in a stratigraphic trap. (b & c) Vertical migration induced by salt movement and normal faulting. Hydrocarbons occurring vertically along fault-zone. Lateral migration again occurring along the stratigraphic interface between a permeable layer and the overlying seal (seal formed from the Upper Oligocene/Lower Miocene transgression), up-dip. (d) Larger scale overview of alternating migration pattern around the salt diapir.

Other bright spots occur further northeast from the vertically shallowest level of bright spots around the salt-related fault. These laterally situated bright spots occur at the same stratigraphic level, up-dip, and are underlain by parallel reflectors which represent deposits attributed to the Late Oligocene/Early Miocene transgression event. Fine-grained, low-porosity and permeability lithologies are therefore likely and the composite log from well 2/3-1 suggest the same fine grained lithologies.

### 5.3.1.3 Zone 2 – Well 4/4-1

The  $a_8$  amplitude anomalies situated close to well 4/4-1 show similar trends as those close to 2/3-1. Bright spots occur at three different vertical levels, all with different horizontal extent and trap geometry, however all termed  $a_8$ . At the deepest vertical level, the Level 1 bright spot occurs below an intra S2 reflector, with a horizontal extent and geometry which suggests a stratigraphic pinch-out trap (Figure 5.3.3 & Figure 2.6.6). The boundaries are not confined by faults or other structural elements, and the migration is primarily stratigraphically controlled by subsurface interfaces between layers of different porosity and permeability.

The bright spot at Level 1 is disrupted by faults towards the southeast and subdivided into smaller amplitude anomalies occurring at a shallower vertical level, along the fault zones. The hydrocarbons represented by bright spots are fault-bound up-dip, towards the center of the fault blocks, but are otherwise generally depth conformant in the down-dip area. The hydrocarbons are therefore suggested to be stored in 3-way fault bound dip closure, combination traps (Figure 5.3.3 b & c). Considering the vertical displacement of bright spots from Level 1 to Level 2, it is likely that structural controls (faulting) allowed vertical migration of hydrocarbons. Furthermore, the Level 3 bright spots of the  $a_8$  amplitude anomaly occur above the fault zone. The strong negative amplitude shows a horizontal extent similar to a channel (Figure 5.3.3 & Figure 4.9.4), and a stratigraphic trap is therefore suggested for this level. The migration pattern may have shifted from the vertical, structurally controlled trend, to a more lateral manner again when the hydrocarbons reached the porous channel deposits. The migration pathway around the  $a_8$  anomaly is thus a combination of firstly lateral migration, subsequently followed by structural altering of the sediments, enabling new vertical routes of migration, and lastly lateral migration through a channel system. Fluvial deposits filled with hydrocarbons may also be the case for the observed high amplitudes in the canyon/river system observed within the S2 sequence, towards the eastern area of the Norwegian continental shelf (Figure 4.5.5), and the high amplitudes identified within fluvial beds in the northern part of Quadrant 9. This suggests

that stratigraphic channels contribute significantly to hydrocarbon flow patterns and traps in the study area within the Oligocene-Miocene sequences.

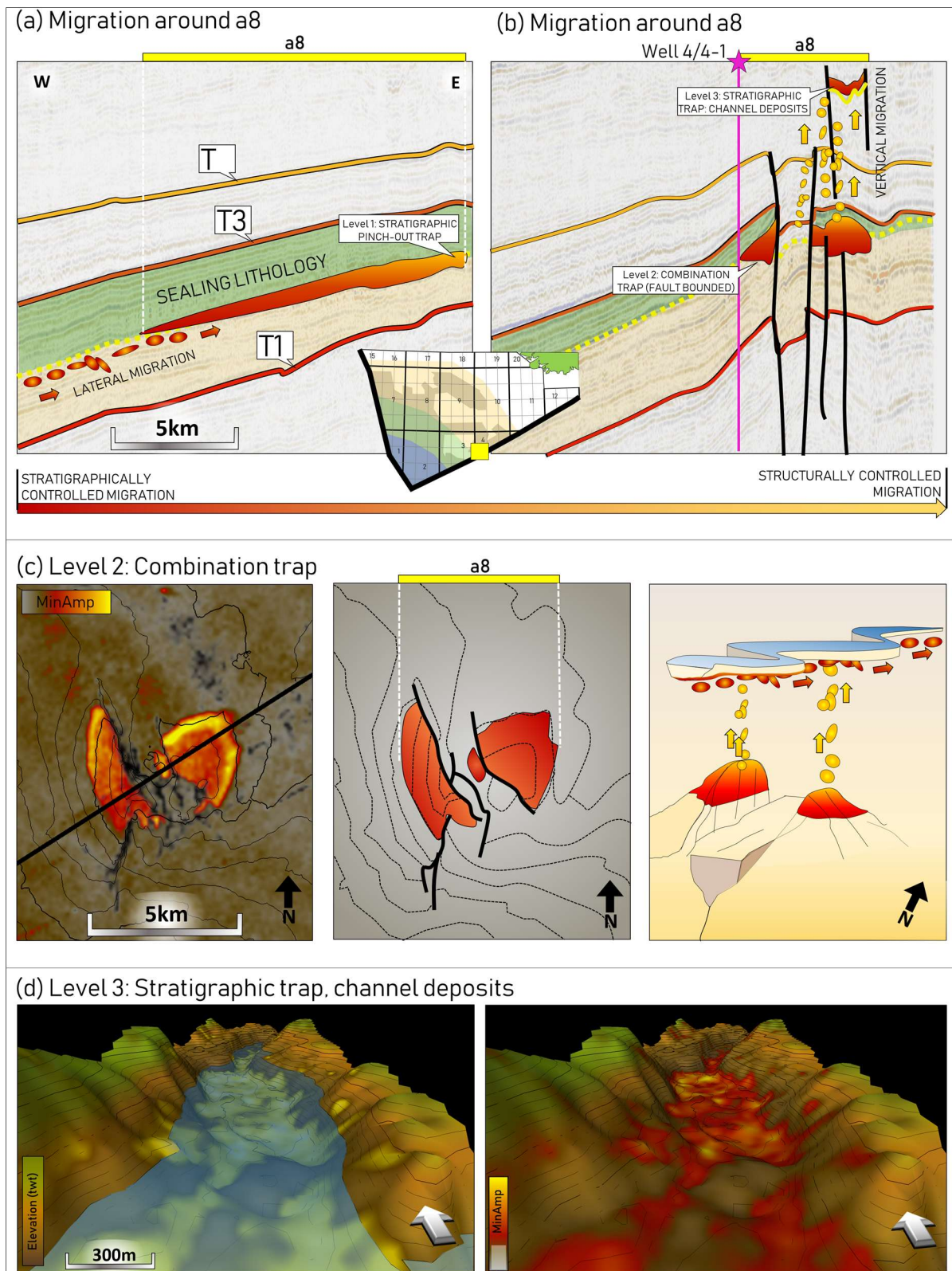


Figure 5.3.3. (a) Lateral migration and filling of hydrocarbons into a stratigraphic pinch out-trap at Level 1, turning into (b) vertical migration induced by faulting (structurally controlled). (c) The Level 2 mapped hydrocarbon filled combinational traps, seen from above. (d) Level 3, 3D-view of the interpreted stratigraphic channel trap, with high-amplitudes at the base of the erosive channel.

### 5.3.1.4 Zone 3 – migration and petroleum potential

The amplitude anomalies a1-a6 located in the southeastern part of Quadrant 9, along with a zone (z7) of smaller bright spots are all situated at the same stratigraphic level in the subsurface. The amplitudes are located well within the suggested extent of the Vade Formation (Figure 5.3.7), and occur below the T2 reflector, separating the permeable and porous Vade Formation from the overlying parallel, continuous reflectors attributed to fine-grained clay and shales deposited during the transgressive event of the Late Oligocene and Early Miocene (Figure 5.3.4).

Below each of the amplitude anomalies, several salt diapiric structures are present (Figure 4.9.6), which may have folded the overlying sediments causing the anticlinal shape of the traps. The traps are thus suggested to have formed after the Vade formation was deposited, around Mid-Miocene times, as suggested initially (Figure 4.9.1). The trap formation is thus a combination of structural altering of the sediments, combined with a lateral migration controlled by the lithologies in the subsurface.

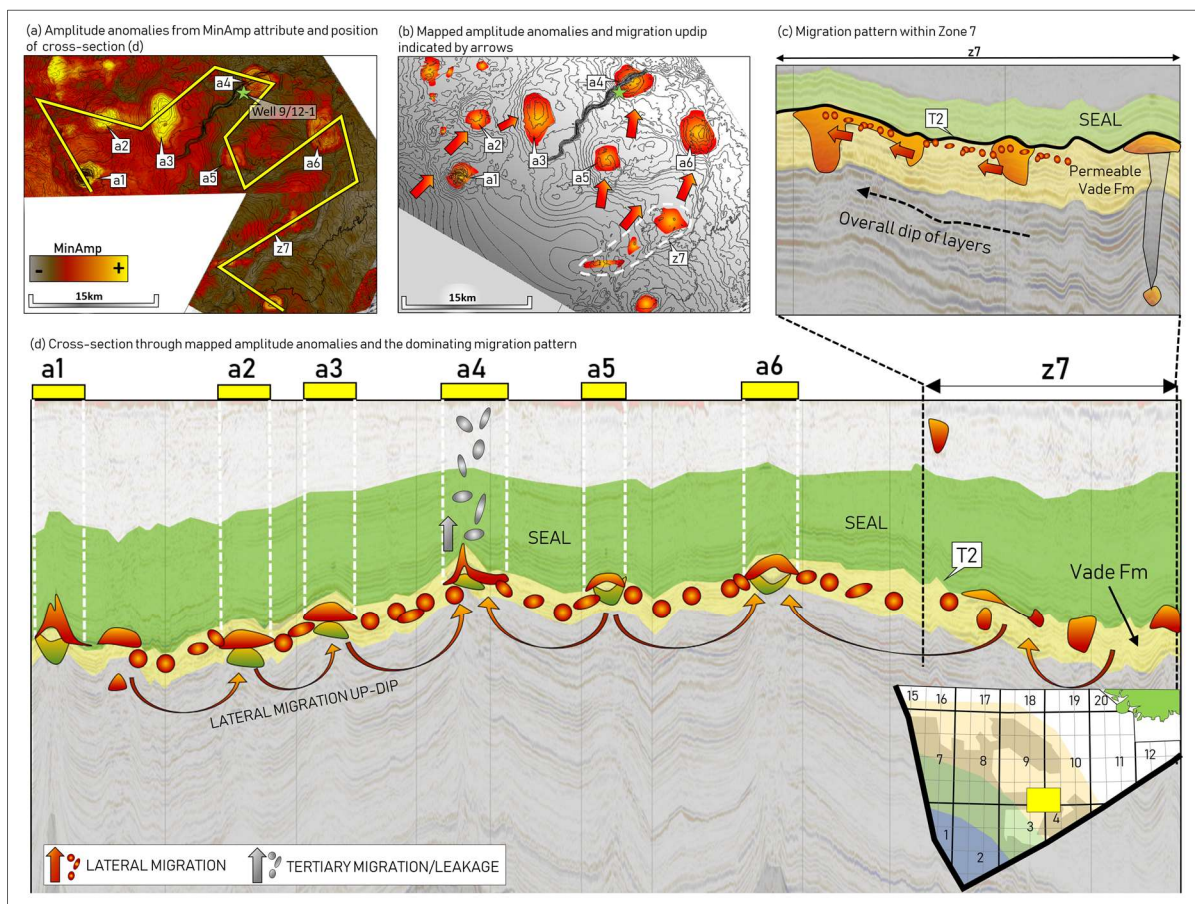


Figure 5.3.4. (a) Amplitude anomalies displayed by Minimum-Amplitude attribute, and the orientation of (d) cross-section. (b) The mapped extent of the amplitude anomalies a1-a6 and z7. (c) Stratigraphically controlled lateral migration within z7. (d) Cross-section through the a1-a6 and z7 amplitude anomalies, with the suggested migration pattern.

### ***5.3.1.5 Reservoir potential of the Vade Formation***

As seen from Figure 5.3.4, the amplitude anomalies all occur below the T2 reflector, in a seismic sequence coeval to the Vade Formation. The mapped porosities and sand content of the Vade Formation (Figure 5.3.5) shows modest lateral variation but in general fair to very good reservoir properties are observed.

The a8 and a3-a4 amplitude anomalies are located in the northeastern, and eastern, part of the recognized sand interval. This location corresponds to the proximal parts of deposition, during sea level lowstand. Sandy-sediments were laid down in a higher energy environment compared to the distal setting. High-energy depositional regimes are often reflected by deposition of coarser-grained, sand-rich sediments. Such sediments are likely to have higher initial porosity, and thus good quality secondary porosity. The dominating porosities from the more distal setting of the Vade Formation, within Quadrant 2, are derived from well completion reports and logs (NPD & Lundin, Appendix 9.3). The observed porosity from core 2/2-2 was poor, however the completion log suggested a very good measured porosity of the sand. Information about the permeability of the Vade Formation was more restricted in the well completion reports, and is not further discussed.

The summarized porosities of the formation were primarily measured in the distal part of the formation, towards the southwest. It is assumed that the porosities dominating in the proximal area, towards the northeast, are as good or better than those recorded in the southwest. The sand-rich sediments deposited in the proximal area are likely to have been deposited in a high-energy environment, where the initial porosity is good (Magoon & Dow, 1994; Selley & Sonnenberg, 2015). Information about the porosities around the a1-a8 were not obtained, but the porosities in this area are assumed to be fairly good.

The Vade Formation represents the Lowstand System Tracts deposited during a sea-level lowstand, which was flooded by the Late Oligocene-Middle Miocene transgressional event. The fine-grained sediments deposited during this time are likely to have poor porosity and low permeability, which is suitable for a sealing rock in a petroleum system (Selley & Sonnenberg, 2015).

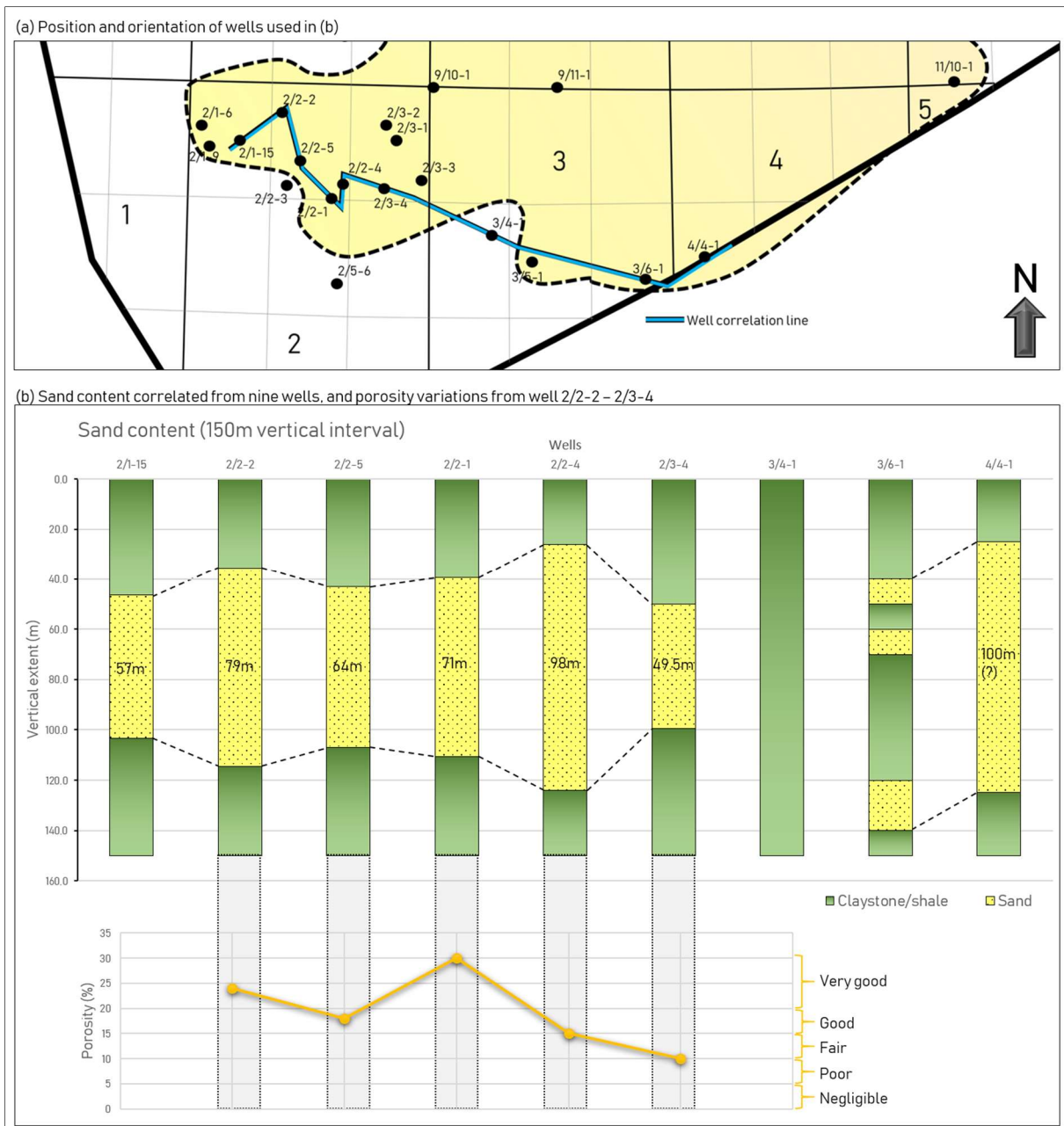


Figure 5.3.5. (a) Overview of wells used in correlation, (b) showing the variations in vertical thicknesses of the Vade Formation. Note that the vertical thickness of the Vade Formation in well 4/4-1 is a rough suggestion based on the gamma ray log. Porosity variations from wells (2/2-2 – 2/3-4) completion logs and reports. Source of information given in Appendix 9.3.

### 5.3.2 Petroleum potential

This sub-chapter aims to provide a more detailed evaluation of the migration routes and petroleum systems in the area with particular focus on the a2, a3 and a4 amplitude anomalies.

Vertical chimneys occurring below the a1-a6 amplitude anomalies, as presented in the results, could indicate a vertical migration pattern in the area. Nevertheless, noise and wipe-out is normal below bright spots, since they absorb much of the energy from the seismic waves, and weaken the amplitude of the underlying reflectors. Furthermore, the 9/12-1 well penetrated the

Jurassic source rock below the observed amplitude anomalies, which was not mature. It is thus unlikely that the hydrocarbons have originated and migrated vertically from an immature source rock directly below. The chimneys of wipe out zones are therefore disregarded as migration pathways, and rather considered as wakened amplitude zones, caused by the attenuation from the overlying bright spots.

A distinct ridge briefly described in the results and one fault cut through the a4 amplitude anomaly (Figure 4.9.4 & Figure 5.3.6). This amplitude is at the shallowest level of all the amplitude anomalies in this area. The fault zone is recognized by the displaced reflectors observed above the anomaly, towards the southwest. A fault cutting through a hydrocarbon filled trap may initiate leakage (tertiary migration). Well 9/12-1 located at the outer boundary of the bright spot, down-flank, did not encounter any hydrocarbons at this level (Table 5.3.1 & Figure 5.3.6). If the trap is subjected to leakage, it is likely that the structure is no longer filled to spill, which provides a reasonable explanation for the dry well.

The amplitude anomaly on the northeastern side of the fault may also have leaked where the porous sediments of the Vade Formation are juxtaposed across fault zone. A new spill point is thus suggested, at the shallowest intersect of the porous layers. Furthermore, the hydrocarbon volume located above the spill point is capped by the fine-grained lithologies from Upper Oligocene/Middle Miocene. The reflectors are quite continuous, which suggests that the seal is working, and the hydrocarbons below are intact. A well situated further up-flank would therefore be more likely to encounter hydrocarbons. The same principle of leakage through faults goes for the a8 amplitude anomaly, previously discussed (Figure 5.3.3.b). A well located further up-flank would be more likely here as well to encounter hydrocarbons.

The other amplitude anomalies, a1-a3 & a5-a6, occur below continuous, parallel seismic reflections marking the fine-grained seal of Late Oligocene/Miocene age, where no faults exceeding the vertical resolution are observed in the seismic data. Leakage is therefore only likely to occur only when the trap is filled to spill.

#### ***5.3.2.1 Gussow's principle***

The a1-a6 traps are likely to have been filled by hydrocarbons successively, with the deepest trap filled to spill first. Hydrocarbons migrating into the lower traps (e.g. a2), segregate into two layers above the water-saturated sediments, in accordance with the law of gravity and density (Gussow, 1953). Gas overlies oil in the trap. When the trap is filled to spill the oil-water-contact is pushed down until the spill point is reached. The lowermost oil within the trap



will begin a migration up-dip, pass the spill point, until a new trap is reached. Any additional oil entering the trap would be forced to continue pass the spill point. This means that a gas-filled trap is no longer a potential storage for oil (Figure 5.3.6). Gas will not begin to migrate from the trap until the trap is completely filled with gas, and all the oil is displaced. Then, when the gas-oil-contact becomes a gas-water-contact, leveled with the spill point, gas can flow further upwards to the second trap, where oil already is in place. Any additional gas or oil will bypass the first trap and continue up-dip.

The second trap (e.g. a3; Figure 5.3.6), situated at a shallower vertical level, is similarly filled to spill. Oil enters the trap first, as explained by the successive filling to spill for the first trap. Any additional oil will continue pass the spill point. An oil-filled trap though is still a potential storage for gas, as gas can infiltrate and accumulate above the oil – successively displacing the oil from the trap. The oil is then pushed out of the second trap, similar to the process described for the first trap, and continues up-dip to fill a shallower situated trap (a4 & a6).

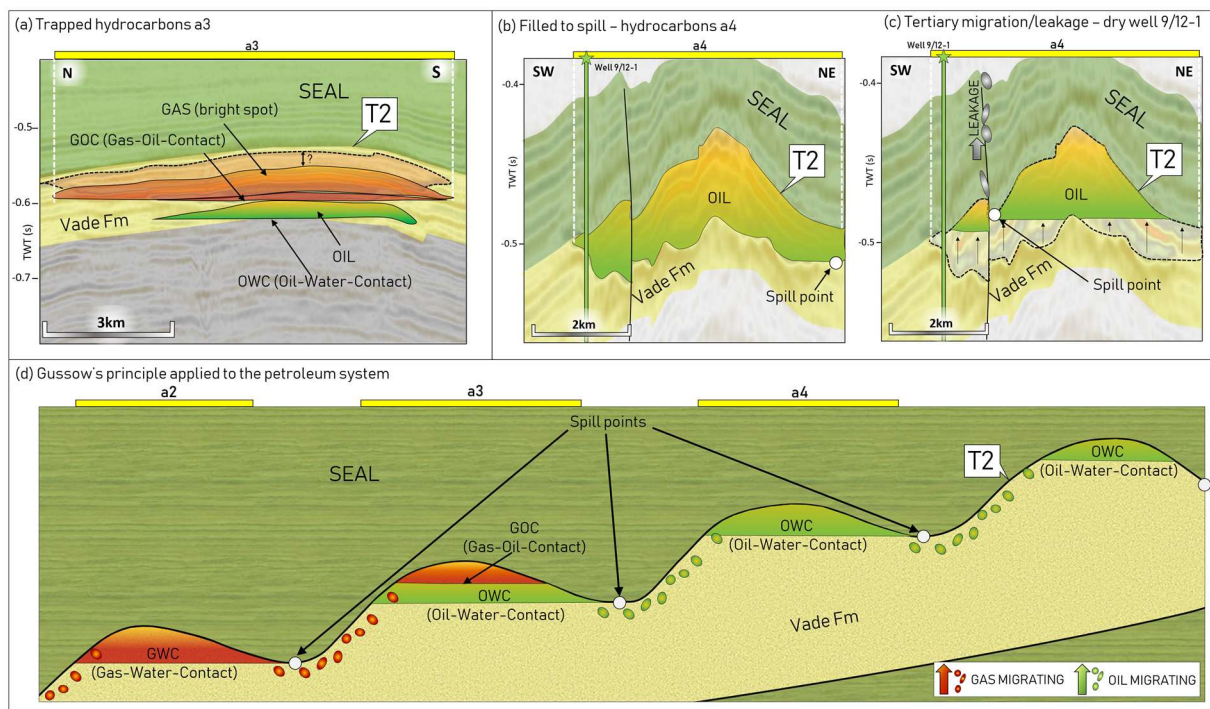


Figure 5.3.6. (a) The a3 amplitude anomaly, and suggested hydrocarbon and petroleum system components. Vade Fm = reservoir rock. Seal = Late Oligocene/Early Miocene. (b) a4 trap filled to spilled, suggested on extent of bright spot(s) from seismic data. Location of well 9/12-1 shown down-flank. (c) Suggested leakage and in-place hydrocarbons, showing a possible explanation of that well 9/12-1 did not encounter hydrocarbons. Note spill-point located at the intersect of fault and the two bright spots. (d) Gussow's principle applied to the petroleum system. Note how the gas fills on top of the oil in a3.

The migration and filling of traps by gas and oil suggests that oil is most likely to be in place in the shallowest traps (a4 & a6), whereas gas, or oil and gas, is filled in the deeper traps. This model for filling of traps is recognized as Gussow's principle (Gussow, 1953). By applying the

principle to the petroleum system in this study, the Vade Formation is likely working as the permeable and porous bed (reservoir) allowing up-dip migration, filling up traps progressively.

The a3 filled trap comprises a double bright spot, where a flat spot was identified between. The upper, high-amplitude, boundary of the shallowest bright spot is attributed to the water-gas interface, where a significant reduction in the seismic velocity is associated with gas in the pore-space. The identified flat spot may represent the gas-oil-contact (GOC), and the lowermost bright spot reflects oil in the pore-space. The presence of both gas and oil suggests that the structure is still working as an oil trap, however it is successively filled with gas, pushing the oil passed the spill point. The traps situated at a shallower level, such as the a4 and a6, are therefore likely to contain oil. The deeper traps relative to the a3 (e.g. the a2 anomaly), are suggested to be gas-filled. The a2 trap is no longer a potential oil trap since any oil reaching the trap will bypass and continue up-dip to shallower traps which are either empty, or not yet filled to spill, as discussed earlier.

The described differential entrapment of hydrocarbons suggests that the a4 and a6 anomalies are more likely to contain primarily oil. The main parts of the a4 has little risk related to leakage, as the trap is buried by thick sequences of fine-grained material. The horizontal extent of the oil-water-contact (OWC), is approximately 3km wide. The vertical column height from the OWC to the apex of the anticlinal fold is approximately 61meters. The estimate assumes a velocity of 2032ms for the Oligocene sequence, as shown in the frequency calculations (Table 3.2.1), and a vertical height in the seismic of 60ms (TWT). Such an extent can contain significant volumes of oil. The a6 trap is buried well below fine-grained, continuous layers of Late Oligocene-Mid Miocene age, and leakage is suggested to only take place pass the spill point. The a8 anomaly, close to well 4/4-1 is, - despite the dry well, suggested to possibly contain oil or oil and gas, considering the proximal, up-dip location of the trap, relative to the source rocks and Vade Formation.

The 2/2-2 well, named the Desmond discovery, along with 2/2-1 and 2/2-4, discovered gas at the Oligocene level in the southern North Sea (Table 5.3.1) (NPD Factpages, Appendix 9.3). Although the presence of gas at the Oligocene stratigraphic level may suggest that this is the most abundant hydrocarbon component at this level, these occurrences of gas are situated further southwest compared to the a4, a6 and a8 anomalies, at a deeper vertical level closer to the source rock (Figure 5.3.7). Following Gussow's principle, the deeper traps are likely to be filled to spill by gas, whereas oil migrates further up-dip to the shallower traps (a4, a6 & a8). The presence of gas thus coincides with the expected differential fill of gas and oil in the area.

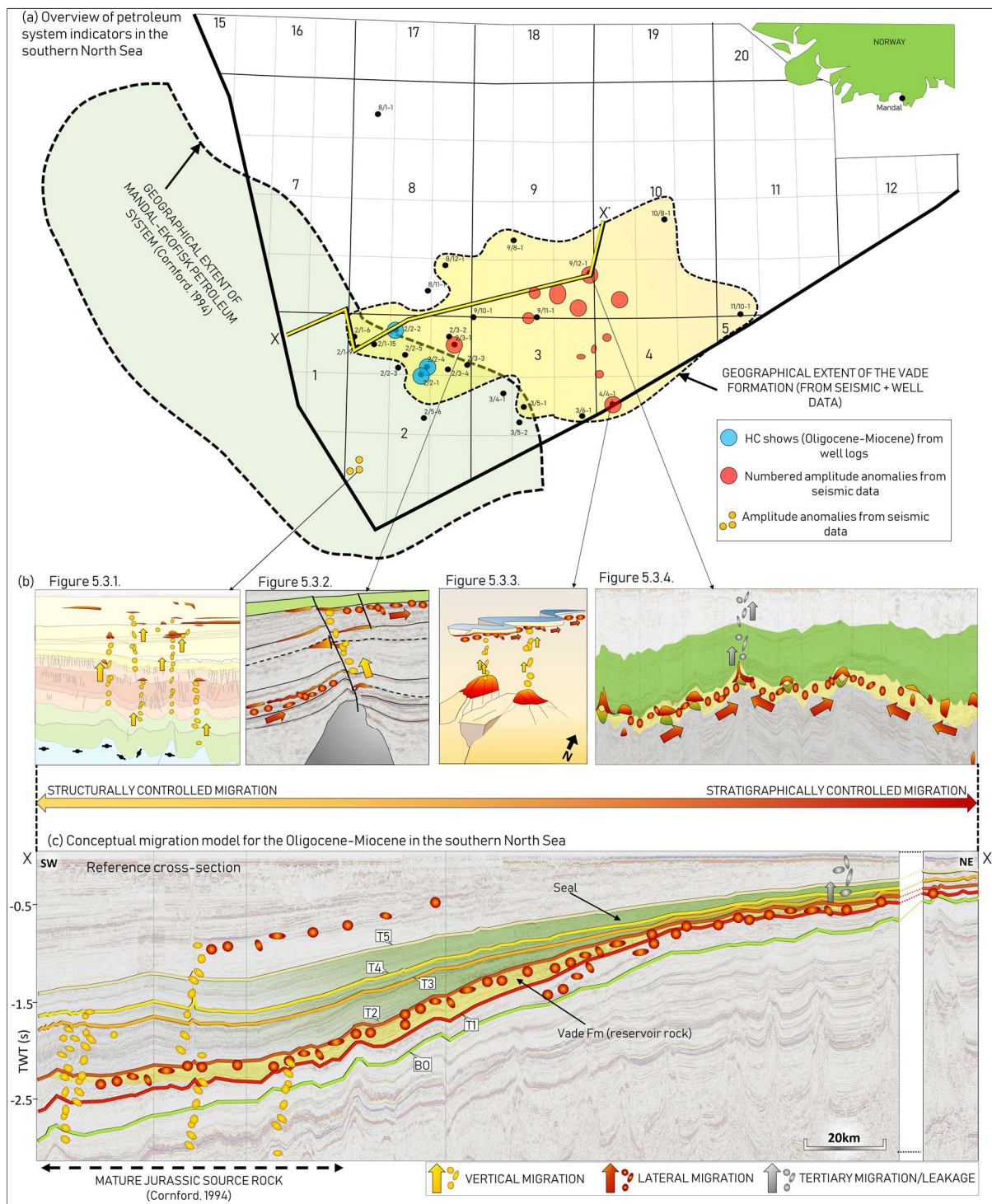


Figure 5.3.7. (a) Overview of the discussed petroleum system indicators in the southern North Sea, with the previously presented figures from the different zones, combined with the horizontal extent of the mature source rock, Mandal Fm (from Cornford, 1994). (c) Conceptual migration model for the Oligocene-Miocene sequences.

The Mandal-Ekofisk petroleum system in the North Sea comprises the Type II source rock, the Mandal Formation of Jurassic age, which is primarily oil-prone. The geographic extent of the oil-prone source rock is preserved in the Central Graben (Cornford, 1994), overlapping with the suggested Vade Formation (Figure 5.3.7). It covers the larger parts of Quadrant 1 and 2 on

the Norwegian continental shelf, an partly Quadrant 3 and 7 (Figure 5.3.7.a). The source rock is mature and oil-generating in the Central Graben. Further northeast, the dark shale of the depositional unit is recognized, however it is immature. This was described by the completion report of well 9/12-1.

Considering the vertical, primary migration above the Central Graben and oil-prone source rock (Zone 1), followed by lateral, secondary migration in the major parts of the Oligocene, it is suggested that the hydrocarbons occurring within the horizontal extent of the Vade Formation constitutes primarily oil in the shallow parts (Zone 2 & 3), and gas closer to the source rock (Zone 1) in the petroleum system. The overall lateral drainage pattern in the subsurface allows hydrocarbon accumulations to occur far from the active petroleum kitchen area (Magoon & Beaumont, 2003). Demaison & Huizinga (1994) suggested a lateral drainage system of the North Sea, which corresponds to the overall suggested migrations pattern of this study (Figure 5.3.7).

## 6 Conclusions

Seismic sequence analysis from primarily 3D seismic data, alongside core observations and well log correlations, has enabled a detailed reconstruction of the paleoenvironments and sea level fluctuations during the Oligocene and Miocene in the southern North Sea. The study highlights petroleum system indicators in the seismic data, and a migration model for the region is demonstrated, along with an evaluation of the potential source rock, differential entrapment of hydrocarbon components, and seal. The main findings of the study are summarized below:

- The shelf is classified as a combined structural-sedimentary shelf, where there is a direct shelf-slope-basin geometry, with faulted segments of Mesozoic age, blanketed and buried by Cenozoic sediments. The Eocene-Oligocene boundary is marked by an angular unconformity, indicating a shift in the progradation pattern, from the western Shetland Platform during the Eocene, towards a northern source during Oligocene-Miocene, the Fennoscandian Platform.
- The reconstructed environments during Oligocene-Miocene show a trend of fluctuating eustatic sea-levels, controlled by basin subsidence in the North Sea Basin concurrently to uplift of the Fennoscandian Platform in the north/northeast, coupled with growth and melt of the Antarctic Ice Sheet.
- Stages of rising sea-level are reflected by low-angle, sigmoidal clinoforms with ascending shelf-break trajectories deposited simultaneously to rapid basin subsidence. Highstand system tracts are characterized by fine-grained, clay-rich material deposited in the basin (Early Oligocene & Mid-Late Miocene). Periods of a relative fall in sea-level are characterized by complex-oblique clinoform stacking patterns, with a distal displacement of the shelf and descending shelf-break trajectories (Late Oligocene). Falling stage system tracts are dominated by the evolution and progradation of complex channel systems and erosion of the exposed shelf. Lowstand system tracts are recognized where coarser, sand-rich material was deposited towards the distal basin margins.
- During a distinct period of regression, the sand-rich Vade Formation was deposited in the distal part of the basin. The findings propose that a shallow environment prevailed during deposition, and a new expanded lateral extent of the identified formation is presented. The mapped porosities and sand content of the Vade Formation shows modest lateral variation but in general good reservoir properties.

- Structural controls on the migration patterns of hydrocarbons are represented by Mesozoic faults, polygonal faults and salt-related diapirs and faults. Halokinetic movement and soft sediment deformation (polygonal faulting) have altered the sequences after deposition and induced the formation of new traps. However observations of hydrocarbon indicators in the Oligocene-Miocene stratigraphy appear to be strongly associated with sedimentary controlled migration according to lithological interfaces in the sub-surface which favour a sub-horizontal up-dip migration. The lateral drainage system is reflected by filled hydrocarbon traps located far from the active source rock, the Jurassic Mandal Formation.
- A differential entrapment model for the migrating hydrocarbons is suggested, where traps located at a deeper vertical level, closer to the source rock, are likely to be filled by gas, and are no longer potential oil-traps. The suggested gas in the deeper levels are confirmed by well 2/2/1, 2/2-2 and 2/2-4, which encountered several gas-pockets within the Oligocene Vade Formation.
- The shallower traps are suggested to contain oil (a4, a6 & a8 amplitude anomalies), based on the differential entrapment principle. Both the a4 and a8 amplitude anomalies have wells placed on the outermost flanks of the closure, nonetheless both encountered only water. The evaluation of potential leakage related to these traps suggests that the traps are no longer filled to the original spill point, and hence the dry wells. With leakage taken into account a new spill point is identified, and a new evaluation of the hydrocarbon accumulations suggests quantities of commercial potential.
- The overall evaluation of the petroleum system in the region suggests that the Vade Formation is working as a well-developed reservoir rock, filled with hydrocarbons of Jurassic age, and capped by a functional seal comprising low-permeability shales deposited during the Late Oligocene-Middle Miocene transgression (Highstand System Tracts).

## **7 Directing future work**

With on-going exploration in this region, it is constructive to highlight areas for future work. The findings in this study have shed new light on the regional development of the Oligocene-Miocene periods, along with a detailed evaluation of petroleum resources in the area. However, the seismic interpretation is primarily based on large-scale observations, and further work should thus focus and go more into detail on the smaller-scale sedimentary patterns, as well as mapping of minor hydrocarbon accumulations. Some recommendations for further work could therefore be as follows:

- Interpretation and mapping of smaller units within the Oligocene-Miocene strata, with emphasis to internal clinoform geometries, variations in dip and the evolution of stacked channels. This could provide a more detailed reconstruction of the variation in source area and progradation pattern of sediment, and thus suggest a more precise reconstruction of the Fennoscandian Platform uplift. Smaller-scale sea-level changes could also be accounted for. Fluvial deposits may also be of particular interest with regards to hydrocarbon storage.
- Identification of smaller bright spots and hydrocarbon indicators in conjunction with a thorough mapping of zones where deep-seated Mesozoic faults breach through the Oligocene-Miocene sequences may reveal an underestimated vertical migration pathway along faults, direct from the source rock below. Smaller hydrocarbon accumulations can be linked to in-place infrastructure of the continental shelf, and might therefore be of great interest to the petroleum industry.
- In order to propose a better reservoir evaluation of the Vade Formation, information about the permeability and lateral permeability-variations should be compiled. Permeability is an important property of every reservoir rock, as it reflects the ability to permit fluid-flow through the layer.

## 8 References

- ALLAN, U. (1989). *Construction fault plane-juxtaposition diagrams (nicknamed «Allan Diagram»)*. AAPG Bulletin, v. 73, p. 803–811.
- ANDREASSEN, K., NILSSEN, E.G. & ØDEGAARD, C.M. (2007). *Analysis of shallow gas and fluid migration within the Plio-Pleistocene sedimentary succession of the SW Barents Sea continental margin using 3D seismic data*. Department of Geology, UiT The Arctic University of Norway. *Geo-Mar Lett* 27:155–171
- ARCHER, J.S. & WALL, C.G. (1986). *Petroleum Engineering Principles and Practice*. Graham & Trotman, London.
- ARNTSEN, B., WENSAAS, L., LØSETH, H. & HERMANRUD, C. (2007). *Seismic modelling of gas chimneys*. *Geophysics*. 72.
- BADLEY, M.E. (1985). *Practical seismic interpretation*. Boston: International Human Resources Development Corporation.
- BERNDT, C., BÜNZ, S. & MIENERT, J. (2003). *Polygonal fault systems on the mid-Norwegian margin: a long-term source for fluid flow*. The Geological Society of London, p. 283-290..
- BONIN, A. (2018). *Sedimentological characterization of carbonate rocks*. European Association of Geoscientists and Engineers, Amsterdam Education Days, 2018.
- BROWN, A. R. (1999). *Interpretation of three-dimensional seismic data*. 5th ed., Vol. 42. Tulsa, Okla: American Association of Petroleum Geologists.
- BROWN, A.R. (2001). *Understanding seismic attributes*. *Geophysics* Vol. 66, p. 47-48.
- BUKOVICS, C. & ZIEGLER, P.A. (1984). *Tectonic development of the Mid-Norway continental margin*. *Marine and Petroleum Geology*, Vol 2, February 1985. Butterworth & Co.
- CANALS, M., LASTRAS, G., URGELES, R., CASAMOR, J.L., MIENERT, J., CATTANEO, A., DE-BATIST, M., HEFLIDASON, H., IMBO, Y., LABERG, J.S., LOCAT, J., LONG, D., LONGVA, O., MASSON, D.G., SULTAN, N., TRINCARDI, F. & BRYN, P. (2004). *Slope failure dynamics and impacts from seafloor and shallow sub-seafloor geophysical data: case studies from the COSTA project*. *Marine Geology*, 213 (1-4). p. 9-72.
- CARPENTER, C. (2013). *Mapping hydrocarbons by integrating seismic with electromagnetic and gravity attributes*. Prepared for the International Petroleum Technology Conference, Beijing.
- CARTWRIGHT, J., HUUSE, M. & APLIN, A. (2007). *Seal bypass systems*. AAPG bulletin, 91 (8), p. 1141-1166
- CATUNEANU, O. (2011). *Principles of Sequence Stratigraphy*. Elsevier Science.
- CHAND, S., KNIES, J., BARANWAL, S., JENSEN, H. & KLUG, M. (2014). *Structural and stratigraphic controls on subsurface fluid flow at Veslemøy High, SW Barents Sea*. *Marine and Petroleum Geology*, 57, p. 494-508.
- CHOPRA, S. & MARFURT, K.J. (2005). *Seismic attributes, a historical perspective*. *Geophysics* vol. 70, no. 5.
- CHOPRA, S., CASTAGNA, J. & PORTNIAGUINE, O. (2006). *Seismic resolution and thin-bed reflectivity inversion*. *CSEG recorder*, 31 (1), p. 19-25
- CLAPP, F. G. (1910). *A proposed classification of petroleum and natural gas fields based on structure*. *Economic Geology*, v. 5, p. 503–521.
- CLAUSEN, O.R., NIELSEN, O.B., HUUSE, M. & MICHELSEN, O. (2000). *Geological indications for Palaeogene uplift in the eastern North Sea Basin*. *Global and Planetary Change*, 24, p. 175-187.



- CLOETINGH, S.A.P.L., ZIEGLER, P.A., BEEKMAN, F. ANDRIESSEN, P.A.M., MATENCO, L., BADA, G., GARCIA-CASTELLANOS, D., HARDEBOL, N., DÉZES, P. & SOKOUTIS, D. (2005). *Lithospheric memory, state of stress and rheology: neotectonics controls on Europe's intraplate continental topography*. *Quaternary Science Reviews*, 24, p. 241-304.
- COE, A., BOSENCE, D., CHURCH, K., FLINT, S., HOWELL, J. & WILSON C. (2002). *The sedimentary record of sea-level change*. The open University, Walton Hall, p. 285.
- COLLINSON, J.D., MOUNTNEY, N. & THOMPSON, D.B. (2006). *Sedimentary structures*. Classic Geology in Europe series, 3rd edition. p. 67-137 & 182-214.
- CORNFORD, C. (1994). *Mandal-Ekofisk(!) Petroleum System in the Central Graben of the North Sea*. Chapter 33 in *The Petroleum System*, Magoon & Dow (1994). AAPG Memoir 60.
- COWARD, M. P., DEWEY, J. F., HEMPTON, M., HOLROYD, J., & MANGE, M. A. (2003). *Tectonic evolution*. Chapter 2, in D. Evans, C. Graham, A. Armour, & P. Bathurst (Eds.), *The Millennium Atlas: Petroleum Geology of the central and northern North Sea* (p. 17-33): The Geological Society of London.
- DEEGAN, C.E. & SCULL, B. (1977). *A proposed standard lithostratigraphic nomenclature for the central and northern North Sea*. Institute for Geological Sciences, London, Rep., 77 (25).
- DEMAISON, G., & HUIZINGA, B.J. (1994). *Genetic classification of petroleum systems using three factors: charge, migration, and entrapment*. In L.B. Magoon and W.G. Dow, eds., *The Petroleum System—From Source to Trap*: AAPG Memoir 60, p. 73–89.
- DORÉ, A.G. (1992). *Synoptic palaeogeography of the Northeast Atlantic seaway: Late Permian to Cretaceous*. In Parnell, J. (ed) *Basins on the Atlantic Seaboard: Petroleum Geology, Sedimentology*.
- EIDVIN, T., RIIS, F., RASMUSSEN, E.S. & RUNDBERG, Y. (2013). *Investigation of Oligocene to Lower Pliocene deposits in the Nordic offshore area and onshore Denmark*. NPD Bulletin no. 10.
- ENGLAND, W.A. (1994). *Secondary migration and accumulation of hydrocarbons*. AAPG Mem. 60, p. 211-217.
- ERIKSEN, O.K., PLANKE, S., MIENERT, J., BÜNZ, S., BERNDT, C., LIE, J. E., & ERIKSEN, F. N. (2010). *P-cable High Resolution Seismic Imaging of Shallow Gas in the Barents Sea*. In 72nd EAGE Conference and Exhibition incorporating SPE EUROPEC 2010.
- FALEIDE, J.I., KYRKJEBØ, R., KJENNERUD, T., GABRIELSEN, R.H., JORDT, H., FANAVOLL, S. & BJERKE, M.D. (2002). *Tectonic impact on sedimentary processes during Cenozoic evolution of the northern North Sea and surrounding areas*. In *Exhumation of the North Atlantic Margin: Timing, mechanisms, and Implications for Petroleum Exploration*. Geological Society of London.
- FYFE, J. A., GREGERSEN, U., JORDT, H., RUNDBERG, Y., EIDVIN, T., EVANS, D., STEWART, D., HOVLAND, M. & ANDREASEN, P. (2003). *Oligocene to Holocene*. Chapter 16, in D. Evans, C. Graham, A. Armour, & P. Bathurst (Eds.), *The Millennium Atlas: Petroleum geology of the central and northern North Sea* (p. 279-287): The Geological Society of London.
- FÆRSETH, R.B. (1996). *Interaction of Permo-Triassic and Jurassic extensional fault-blocks during development of the northern North Sea*. *Journal of the Geological Society*, London. Vol. 153.

- GARCIA-GIL, S., VILAS, F., & GARCIA-GARCIA, A. (2002). *Shallow gas features in incised-valley fills (Ria de Vigo, NW Spain): a case study*. *Continental Shelf Research*, 22(16), p. 2303-2315.
- GAWTHORPE, R. L., & LEEDER, M. R. (2000). *Tectono-sedimentary evolution of active extensional basins*. *Basin Research*, 12(3-4), p. 195-218.
- GIBBARD, P.L. & LEWIN, J. (2014). *Filling of the North Sea Basin: Cenozoic sediment sources and river styles*. *Geological Belgica* (2016), p. 201-217.
- GUSSOW, WM. C., (1953). *Differential trapping of hydrocarbons*. *Alberta Society of Petroleum Geologists*, Vol. 1, No. 6.
- HAAVIK, K.E. & LANDRØ, M. (2014). *Iceberg ploughmarks illuminated by shallow gas in the central North Sea*. *Quaternary Science Reviews*, 103, p. 34-50.
- HAGER, D. (1915). *Practical oil geology*. New York, McGrawHill, p. 150.
- HELLAND-HANSEN, W., & HAMPSON, G. J. (2009). *Trajectory analysis: concepts and applications*. *Basin Research*, 21, p. 454-483.
- HELLAND-HANSEN, W., STEEL, R.J. & SØMME, T.O. (2012). *Shelf genesis revisited*. *Journal of Sedimentary Research*, 2012, v. 82, p.133–148.
- HENRIET, J.P., DE BATIST, M. & VERSCHUREN, M. (1991). *Early fracturing of Palaeogene clays, southernmost North Sea: relevance to mechanisms of primary hydrocarbon migration*. In *Generation, accumulation and production of Europe's hydrocarbons*, ed. A. M. Spencer. The European Association of Petroleum Geoscientists.
- HOMEWOOD P.W., MAURIAUD P. & LAFONT F. (2000). *Best Practices in Sequence Stratigraphy for explorationists and reservoir engineers*. *Bull. Centre of Rech. Elf Explor. Prod. Mem.* 25, p. 81.
- ISAKSEN, D. & TONSTAD, K. (1989). *A revised Cretaceous and Tertiary lithostratigraphic nomenclature for the Norwegian North Sea*. *NPD, Bull.* 5: p. 59.
- JARSVE, E.M., EIDVIN, T., NYSTUEN, J.P. FALEIDE, J.I, GABRIELSEN, R.H. & THYBERG, B.I. (2014). *The Oligocene succession in the eastern North Sea – control mechanisms of basin development and depositional systems*. Cambridge University Press.
- JOHANNESSEN, E. P., & STEEL, R. J. (2005). *Shelf-margin clinoforms and prediction of deepwater sands*. *Basin Research*, p. 521-550.
- JORDT, H., FALEIDE, J.I., BJØRLYKKE, K. & IBRAHIM, M.T. (1995). *Cenozoic sequence stratigraphy of the central and northern North Sea basin: tectonic development, sediment distribution and provenance areas*. *Marine and Petroleum Geology*, Vol. 12, No. 8.
- JUDD, A. & HOVLAND, M. (2009). *Seabed fluid flow: the impact on geology, biology and the marine environment*. Cambridge University Press.
- KEAREY, P., BROOKS, M., & HILL, I. (2002). *An Introduction to Geophysical Exploration*. Third Edition. Blackwell Science Ltd.
- KNOTT, S.D., BURCHELL, M.T., JOLLEY, E.J. & FRASER, A.J. (1993). *Mesozoic to Cenozoic plate reconstructions of the North Atlantic hydrocarbon plays of the Atlantic margins*. From *Petroleum Geology '86 Ltd*. Published by The Geological Society, London. p. 953-974.
- KNOX, R.W.O'B., BOSCH, J.H.A., RASMUSSEN, E.S., HEILMANN-CLAUSEN, C., HISS, M., DE LUGT, I.R., KASINKSI, J., KING, C., KÖTHE, A., SLODKOWSKA, B., STANDKE, G. & VANDENBERGHE, N. (2010). *Cenozoic*. In Doornenbal, J.C. & Stevenson, A.G. (eds), *Petroleum geological atlas of the Southern Permian Basin area*. EAGE Publications, Houten, p. 211-223.

- KOLLER, K.K., BORGES, A.L.D.O. & PUHL, E. (2017). *Prediction of the bedforms generated by density currents based on fluvial phase diagrams*. RBRH Vol. 22, Porto Alegre.
- LEWIS, M.M., JACKSON, C.A.L. & GAWTHORPE, R.L. (2013). *Salt-influenced normal fault growth and forced folding: The Stavanger Fault System, North Sea*. Elsevier, Journal of Structural Geology 54. p. 156-173.
- LONERGAN, L., CARTWRIGHT, J. & JOLLY, R. (1997). *The geometry of fault systems in Tertiary mudrocks of the North Sea*. Journal of Structural Geology, Vol. 20. No. 5, Elsevier Science. p. 529-548.
- LØSETH, H., GADING, M. & WENSAAS, L. (2009). *Hydrocarbon leakage interpreted on seismic data*. Marine and Petroleum Geology 26(7), p. 1304-1319.
- MAGOON, L.B., & DOW, W.G. (1994). *The petroleum system*. In L.B. Magoon and W.G. Dow, eds., *The Petroleum System—From Source to Trap: AAPG Memoir 60*, p. 3–24.
- MAGOON, L.B. & BEAUMONT, E.A. (2003). *Petroleum systems*. In Exploring for Oil and Gas Traps, Edward A. Beaumont and Norman H. Foster, eds., *Treatise of Petroleum Geology, Handbook of Petroleum Geology*, 1999.
- MCCARTHY, K., ROJAS, K., NIEMANN, M., PALMOWSKI, D., PETERS, K. & STANKIEWICZ, A. (2011). *Basic petroleum geochemistry for source rock evaluation*. Oilfield Review Summer 2011: 23, no. 2. Schlumberger.
- METWALLI, F.I. & PIGOTT, J.D. (2005). *Analysis of petroleum system criticals of the Matruh-Shushan Basin, Western Desert, Egypt*. Petroleum Geoscience 11 (2), p. 157–178.
- MITCHUM, R. M., VAIL, P. R., & SANGREE, J. B. (1977). *Seismic Stratigraphy and Global Changes of Sea Level: Part 6. Seismic Stratigraphy - Applications to Hydrocarbon Exploration*. p. 117- 133.
- NPD. (2011). *Factpmaps NPD*. Retrieved from <http://factpages.npd.no/>
- NPD. (2014). *The 2014 NPD lithostratigraphic charts*. Norwegian Petroleum Directorate.
- OWEN, G. (2003). *Load structures: gravity-driven sediment mobilization in the shallow subsurface*. In: *Subsurface Sediment Mobilization* (P. van Rensbergen, R.R. Hillis, A.J. Maltman and C.K. Morley, eds), Spec. Published Geological Society, London, 216, p. 21–34.
- PETERSEN, H.I., NYTOFT, H.P., VOSGERAU, H., ANDERSEN, C., BOJESEN-KOEFOED, J.A. & MATHIESEN, A. (2010). *Source rock quality and maturity and oil types in the NW Danish Central Graben: implications for petroleum prospectivity evaluation in an Upper Jurassic sandstone play area*. In Vining, B.A. & Pickering, S.C. (eds) *Petroleum Geology: From Mature Basins to New Frontiers – Proceedings of the 7th Petroleum Geology Conference*, p. 95–111.
- POSAMENTIER, H.W., JERVEY, M.T. & VAIL, P.R. (1988). *Eustatic controls on clastic deposition I – conceptual framework*. In *Sea Level Changes—An Integrated Approach* (C.K. Wilgus, B.S. Hastings, C.G.St.C. Kendall, H.W. Posamentier, C.A. Ross and J.C. Van Wagoner, Eds.), SEPM Special Publication 42, p.110–124.
- PRATT, W.E. (1942). *Oil in the Earth*. University of Kansas Press, Lawrence.
- PRICE, L.C. (1981). *Primary petroleum migration by molecular solution: Consideration of new data*. J. Pet. Geol. 4, 89-101.
- RAJAN, A., MIENERT, J. & BÜNZ, S. (2012). *Acoustic evidence for a gas migration and release system in Arctic glaciated continental margins offshore NW-Svalbard*. Marine and Petroleum Geology, 32(1), 36-49. Chicago.
- RANDEN, T., REYMOND, B., SJULSTAD, H.I. & SØNNELAND, L. (1998). *New seismic attributes for automated stratigraphic facies boundary detection*. SEG Expanded Abstracts.

- RASMUSSEN, E.S. (2005). *The geology of the upper Middle – Upper Miocene Gram Formation in the Danish area*. Paleontos 7, p. 5-18.
- REYNOLDS, J. M. (2011). *An Introduction to Applied and Environmental Geophysics*. John Wiley & Sons, Ltd.
- RUNDBERG, Y. & EIDVIN, T. (2005). *Controls on depositional history and architecture of the Oligocene-Miocene succession, northern North Sea Basin*. Elsevier, Norwegian Petroleum Society.
- SCHLAGER, W. (1992). *Sedimentology and sequence stratigraphy of reefs and carbonate platforms*. Continuing Education Course Note Series #34, American Association of Petroleum Geologists, p. 71.
- SCHOWALTER, T.T. (1979). *Mechanics of secondary hydrocarbon migration and entrapment*. AAPG Bull. 63, p. 723-760.
- SCLATER, J.G & CHRISTIE, P.A.F. (1980). *Continental stretching: an explanation of the post-mid-Cretaceous subsidence of the central North Sea basin*. Journal of geophysical research, vol. 85.
- SELLEY, R.C. & SONNENBERG, S.A. (2015). *Elements of petroleum geology*. 3rd ed. San Diego, Calif: Academic Press.
- SHERIFF, R.E. (2002). *Encyclopedic dictionary of applied geophysics*. Society of Exploration Geophysicists, Tulsa, OK.
- SIMAEYS, S.V. (2004). *The Rupelian-Chattian boundary in the North Sea Basin and its calibration to the international time-scale*. Netherlands Journal of Geosciences. p. 241-248.
- SORKHABI, R. & TSUJI, Y. (2005). *The Place of Faults in Petroleum Traps*. In R. Sorkhabi and Y. Tsuji, eds, *Faults, Fluid flow, and petroleum traps*: AAPG Memoir 85, p.1-31.
- STEEL, R. J., & OLSEN, T. (2002). *Clinofolds, Clinofold Trajectories and Deepwater Sands*. ResearchGate.
- TWISS, R. J., & MOORES, E. M. (2007). *Structural geology*. Geological Magazine.
- UNDERHILL, J.R. & PARTINGTON, M.A. (1993). *Jurassic thermal doming and deflation in the North Sea: implications of the sequence stratigraphic evidence*. Geological Society, London, Petroleum Geology Conference series 4. p. 337-345.
- VAIL, P. R. (1987). *Seismic stratigraphy interpretation using sequence stratigraphy*. In A. W. Bally (Ed.), *Atlas of Seismic Stratigraphy: AAPG Studies in Geology, Vol. 1*, p. 1-10.
- VANDENBERGHE, N., BRINKUIS, H. & STEURBAUT, E. (2003). *The Eocene/Oligocene boundary in the North Sea area: a sequence stratigraphic approach*. Columbia University Press, New York.
- VARDAR, D. & ALPAR, B. (2016). *High-resolution seismic characterization of shallow gas accumulations in the southern shelf of Marmara Sea, Turkey*. Acta Geophysica, 64, p. 589-609.
- VEEKEN, P. C. H. (2007). *Seismic stratigraphy, basin analysis and reservoir characterization*. Vol. 37, Elsevier.
- WOLD, C.N., 1994. *Cenozoic sediment accumulation on drifts in the northern North Atlantic*. Paleoceanography, 9: p. 917–941.
- WRIGHT, J.D. & MILLER, K.G., 1996. *Control of North-Atlantic deep-water circulation by the Greenland-Scotland Ridge*. Paleoceanography, 11: p. 157–170.
- ZACHOS, J., PAGANI, M., SLOAN, L., THOMAS, E. & BILLUPS, K. (2001). *Trends, rhythms, and aberrations in global climate 65Ma to present*. Science 292, p. 686-693.
- ZIEGLER, P.A. (1975). *Geological evolution of North Sea and its tectonic framework*. The American Association of Petroleum Geologists Bulletin. V.59, No. 7.

## 9 Appendices

### 9.1 Appendix 1 – Equations

*Equation 2.1 – The wavelength of a seismic pulse*

$$\lambda = \frac{v}{f}$$

Approximation of the wavelength of a seismic pulse ( $\lambda$ ), where  $v$  represents the velocity (m/s) and  $f$  represents the frequency (Hz).

*Equation 2.2 – Vertical resolution*

$$Vr = \frac{\lambda}{4}$$

Approximation of the vertical resolution, where  $\lambda$  is the wavelength of a seismic pulse.

*Equation 2.3 – Unmigrated horizontal resolution*

$$Rf_{pre-m} = \frac{v}{2} \sqrt{\frac{t}{f}}$$

Approximation of the unmigrated horizontal resolution, where  $Rf$  is the radius of the Fresnel Zone,  $v$  represents the velocity of the incident wave (m/s),  $t$  equals two-way travel time in seconds (TWT) and lastly  $f$  as the frequency in Hertz

*Equation 2.4 – Migrated horizontal resolution*

$$Rf_{post-mig} = \frac{v}{4f} = \frac{\lambda}{4}$$

Approximation of the post-migrated horizontal resolution, where  $Rf$  is the radius of the Fresnel Zone,  $v$  represents the velocity of the incident wave (m/s) and  $f$  represents the frequency (Hz).

*Equation 3.1 – Converting ms (TWT) to meters*

$$\text{Meters} = \frac{TWT}{2000} * Vp$$

Approximation of the paleo-water in meters, by using the vertical height of clinoforms (TWT, ms), divided by 2 (to get one way traveltime), and again divided by 1000 to convert from ms to s. Lastly, multiply by the seismic velocity (m/s).

## 9.2 Appendix 2 – Overview of all seismic data

Name	Surveys merged	Phase configuration	Provided by	Located (Figure 3.1.1)
3D-merge (16 surveys)	→MC3D- →CGR2015M →PGS MEGA →SURVEY 2013 →LN10M05 south →VGCNS06NQ8 →LN14M01_V6 →RS1001 →LN10M05 north →V61 →EOTWW12 →BG06M01 →MC3D-MOERE →E013003 →ESB2000R08 →LN211M06 →GN1001 →PGS16M01 →PGS16M02	Zero phase, normal polarity	Lundin Norway 2018	Southern North Sea, covering the Norwegian-Danish Basin, Sørvestlandet High & Central Graben.

Name	Survey type	Number of seismic lines	Area covered	Phase configuration	Gathered by/year	Location
UG97	2D	29	145x10km	Minimum phase, normal polarity	1997/Geoteam	North Sea
UG198	2D	45	90x142km	Minimum phase, normal polarity	1998/Geoteam	Nordan
SKAGRE96	2D	16	71x90km	Minimum phase,	1986/Nopec	Skagerrak

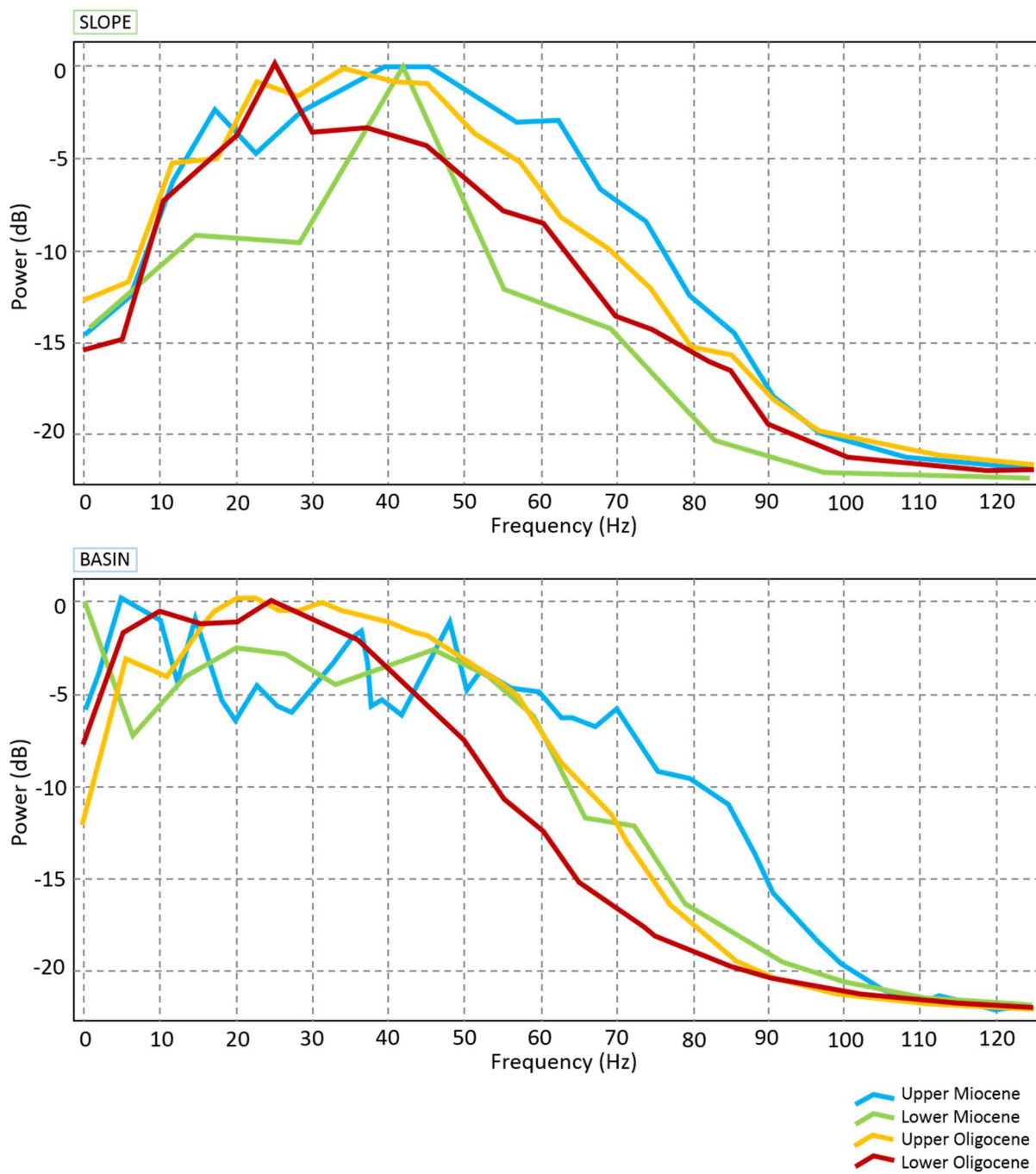
				normal polarity		
SHDE98	2D	56	90x80km	Zero phase, normal polarity	1998/Nopec	Southern North Sea
NSR-04	2D	49	200x140km	Zero phase, normal polarity	2004/TGS	North Sea/Skagerrak
GNSR-01	2D	42	120x76km	Zero phase, normal polarity	1991/Westgec	Southern North Sea
GFR-93	2D	16	69x76km	Minimum phase, normal polarity	1993/Westgec	Southern North Sea
EBS00	2D	70	84x71km	Zero phase, normal polarity	2000/Nopec	Skagerrak
CGME96RE07	2D	182	127x90km		1996/Nopec	Southern North Sea

### 9.3 Appendix 3 – Completion logs and reports from wells

Well	Accessed through	Published at Norwegian Petroleum Directorate Factpages <a href="http://factpages.npd.no/">http://factpages.npd.no/</a>
2/1-6	NPD factpages	Published
2/1-9	Completion log and report from Lundin	Published
2/1-15	Completion log and report from Lundin	Not published
2/2-1	Completion log and report from Lundin	Published
2/2-2	Core, completion log and report from Lundin	Published
2/2-3	Completion log and report from Lundin	Published
2/2-4	Completion log and report from Lundin	Published
2/2-5	Completion log and report from Lundin	Published
2/3-1	Completion log and report from Lundin	Published
2/3-2	Completion log and report from Lundin	Published
2/3-3	Completion log and report from Lundin	Published
2/3-4	Completion log and report from Lundin	Published
2/5-6	NPD factpages	Published
3/4-1	NPD factpages	Published
3/5-1	NPD factpages	Published
3/5-2	NPD factpages	Published
3/6-1	NPD factpages	Published
4/4-1	Completion log from Lundin	Not published
8/1-1	NPD factpages	Published
8/11-1	NPD factpages	Published
8/12-1	NPD factpages	Published
9/8-1	NPD factpages	Published
9/10-1	NPD factpages	Published
9/11-1	NPD factpages	Published
9/12-1	NPD factpages	Published
10/8-1	NPD factpages	Published
11/10-1	NPD factpages	Published



### 9.4 Appendix 4 – Frequency spectrums



### 9.5 Appendix 5 – Well picks Oligocene/Miocene (Lundin)

Epoch	Group	Age	Tops in wells (MD)																	
			1/3-1	1/3-5	1/3-6	1/3-7	1/3-8	1/3-11	2/1-2	2/4-1	2/4-11	3/7-9	7/4-1	7/8-3	7/11-6	7/11-8	8/10-2	9/12-1	9/2-5	
Miocene	Nordland Gp.	Top Messinian	905	1050	1230	1280t	1800	790?	850	954	1228		930	800	880	920	900			
		Top Tortonian											Poor data	1020	1270					
	Hordaland Gp.	Mid-Miocene Unconformity (MMU)	1329	1075	1600	1655	1902	1777	1624		1707	1463	1088	1334	1498	1404	1265	400	414	
		Top Serravalian			1670	1760	1830	1740?	1500	1091			1800	1350	1500	1480				
		Top Langhian						1780		1662										
		Top Burdigalian	1836	1836	1810	1880	1980				1713		1110	1440	1680	1850	1210			
Top Aquitanian					2290						1260	1740								
Oligocene	Hordaland Gp.	Top Chattian/Oligocene	2201	2180	2120	2320	2350		1800		1905	Poor data	1330	1750	1800	2090	1450	426		
		Top Rupelian	2518		2240	2520		2480	2250				1590	2080	2540	2430		750		
		Base Oligocene (BO)	2886	2788	2250?	2880	2830		2300		2701		1810	2520	2820	2643	2000	811		

## 9.6 Appendix 6 - Core 2/2-2



Figure 9.5.1. Core interval 1979,3 (top left) – 1982,3 (bottom right).



Figure 9.6.2. Core interval 1982,3 (top left) - 1985,3 (bottom right).



Figure 9.6.3. Core interval 1985,3 (top left) - 1988,3 (bottom right).



Figure 9.6.4. Core interval 1988,3 (top left) - 1991,3 (bottom right).



Figure 9.6.5. Core interval 1991,3 (top left) - 1994,3 (bottom right).